Universiteit
Leiden
The Netherlands

Chemical tools to modulate endocannabinoid biosynthesis

Deng, H.

Citation
Deng, H. (2017, April 11). *Chemical tools to modulate endocannabinoid biosynthesis*. Retrieved from https://hdl.handle.net/1887/47846

Version:	Not Applicable (or Unknown)
License:	Licence agreement concerning inclusion of doctoral thesis in the Institutional Repository of the University of Leiden
Downloaded from:	https://hdl.handle.net/1887/47846

Note: To cite this publication please use the final published version (if applicable).

Cover Page

Universiteit Leiden

The handle http://hdl.handle.net/1887/47846 holds various files of this Leiden University dissertation

Author: Deng, Hui
Title: Chemical tools to modulate endocannabinoid biosynthesis
Issue Date: 2017-04-11

Chemical Tools to Modulate Endocannabinoid Biosynthesis

PROEFSCHRIFT

ter verkrijging van
de graad van Doctor aan de Universiteit Leiden,
op gezag van Rector Magnificus prof. mr. C.J.J.M. Stolker
volgens het besluit van het College voor Promoties
te verdedigen op 11 april 2017
Klokke 13:45 uur

door

DENG HUI

Geboren te Lanzhou, China in 1987

Promotiecommissie

Promotor	Prof. dr. H.S. Overkleeft
Co-promoter	Dr. M. van der Stelt
Overige leden	Prof. dr. H. Aerts
	Prof. dr. M. Maccarrone
	Prof. dr. J. Brouwer
	Prof. dr. F.J. Dekker
	Dr. L. Heitman
	Dr. P. Pacher

Printed by: Ridderprint BV

Cover design: Hui Deng

You will never be brave if you don't get hurt.

You will never learn if you don't make mistake.

You will never be successful if you don't encounter failure.

所有的失败和成功都是人生经历的偶然和必然。

Table of contents

Chapter 1 **7**
General introduction

Chapter 2 **21**
Discovery of DH376, a 2,4-substituted triazole urea, as a potent and selective inhibitor for diacylglycerol lipases

Chapter 3 **75**
Rapid and profound rewiring of brain lipid signaling networks by acute diacylglycerol lipase inhibition

Chapter 4 **123**
Diacylglycerol lipase inhibitors prevent fasting-induced refeeding in mice

Chapter 5 **139**
[^{18}F]DH439, a positron emission tomography tracer for in vivo imaging of diacylglycerol lipases

Chapter 6 **159**
Chiral disubstituted piperidinyl ureas: a class of dual diacylglycerol lipase-α and ABHD6 inhibitors

Chapter 7 **193**
Activity-based protein profiling reveals the mitochondrial localization of monoacylglycerol lipase

Chapter 8 **219**
Summary and future prospects

List of publications **233**

Summary in Chinese **235**

Curriculum Vitae **237**

1

General Introduction

Endocannabinoids

Extracts of the plant *Cannabis sativa*, also known as marijuana*,* have been used for recreational and medical purposes for thousands of years.[1,2] Marijuana affects multiple physiological processes, including pain sensation, memory, mood, sleep and appetite.[3] In 1964, the structure of Δ^9-tetrahydrocannabinol (Δ^9-THC, Figure 1) the principal psychoactive component of *Cannabis sativa,* was reported.[4] It took almost 30 years to identify the target protein (termed cannabinoid CB1 receptor) that is activated by Δ^9-THC.[5] The CB_1 receptor belongs to the family of G-protein-coupled receptors and is expressed in neurons, astrocytes and microglial cells in various brain regions, including cerebellum, hippocampus, basal ganglia, cortex, amygdala, hypothalamus, thalamus and brainstem.[6] In neurons, the cannabinoid CB_1 receptor is often located at pre-synaptic membranes, possibly also in mitochondria, and its activation by Δ^9-THC results in reduction of intracellular cAMP-levels, activation of inward-rectifying K^+-channels and inhibition of voltage-sensitive Ca^{2+}-channels, thereby inhibiting neurotransmitter release and modulation of synaptic plasticity. A second Δ^9-THC-binding protein, the cannabinoid CB_2 receptor was identified in 1993.[7] It is primarily found in peripheral immune cells,[8,9] such as B-cells, macrophages and monocytes. Activation of the CB_2 receptor exerts immunosuppressive effects.[10]

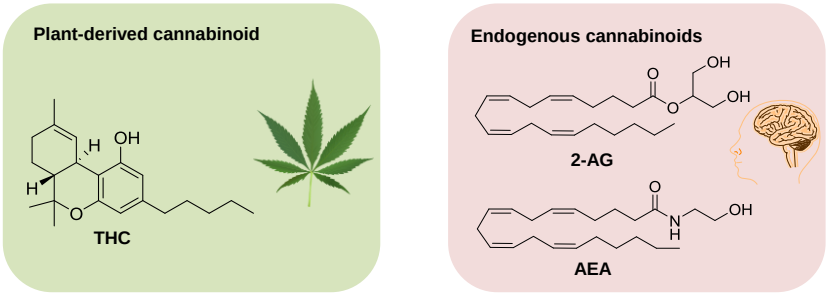

Figure 1. Chemical structures of THC and the two most abundant endocannabinoids: 2-arachidonoylglycerol (2-AG) and anandamide (*N*-arachidonoylethanolamine, AEA).

The discovery of cannabinoid CB_1 receptor initiated the search for endogenous compounds in mammals that could activate this protein. In 1992, the first endogenous ligand was isolated and named anandamide (*N*-arachidonoylethanolamine; AEA, Figure 1), which is derived from the Sanskrit word for bliss.[11] Three years after the discovery of AEA, 2-arachidonoylglycerol (2-AG, Figure 1), a common intermediate in phospholipid and triglyceride metabolism, was reported as the second endogenous lipid that modulated cannabinoid CB_1 receptor function.[12] 2-AG and AEA are the most abundant endogenous ligands of the cannabinoid receptors and are termed "endocannabinoids". Some other lipids, such as 2-arachidonoylglycerylether (noladin ether), *O*-arachidonoylethanolamine (O-AEA, virodhamine) and *N*-arachidonolyl-dopamine (NADA), have also been reported to activate the cannabinoid receptors, but their role as endocannabinoids is under debate.[13,14] (Figure 2).

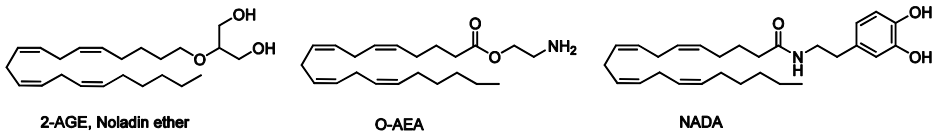

Figure 2. Chemical structures of some other putative endocannabinoids: Noladin ether, virodhamine (O-AEA) and *N*-arachidonoyldopamine (NADA).

AEA and 2-AG are often found together, but their individual levels vary between cell types, brain regions, tissues, species, developmental stages and pathological conditions.[15-17] Endocannabinoids play an essential role in the brain by activating the cannabinoid CB_1 receptor in different brain cells. They modulate neurotransmitter release (Figure 3) and regulate many physiological processes, including pain perception, learning and memory, energy balance, emotional states (anxiety, fear), and

reward-related behaviour.[18] The exact contribution of each individual endocannabinoid in specific brain regions to these (patho)physiological functions remains, however, poorly understood.

Continuous activation of the CB_1 receptor by endocannabinoids is associated with nicotine addiction, obesity and metabolic syndrome.[19,20] Endocannabinoids play also an important role during neurodegeneration and inflammation. All of these are major risk factors for illness and death. The CB_1 receptor antagonist rimonabant was effective in obese patients, but was withdrawn from the market due to unacceptable psychiatric side effects (depression and suicidal ideation in some individuals).[21] This highlights the medical need to understand modulation of the endocannabinoid levels in the brain in a more detailed manner. Inhibitors of the biosynthetic enzymes of the endocannabinoids would provide valuable tools to study the role of each endocannabinoid in the various physiological processes. This thesis will focus on the enzymes that control 2-AG levels. Activity-based protein profiling is applied as a chemoproteomic method to identify inhibitors of these enzymes in order to modulate cannabinoid CB_1 receptor activation by 2-AG.

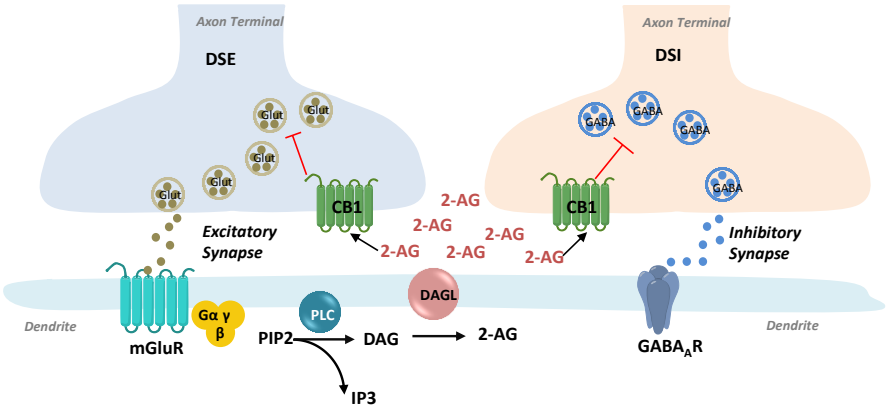

Figure 3. A schematic view of endocannabinoid signaling. Glutamate released from the excitatory axon terminal activates type I metabotropic glutamate receptor (mGluR), which stimulates 2-AG production through the phospholipase C (PLC) and diacylglycerol lipase (DAGL) pathway. 2-AG then crosses the synaptic cleft and activates presynaptic CB_1 receptors, which induces the suppression of glutamate or *γ*-aminobutyric acid (GABA) release.

Diacylglycerol lipases

2-AG is produced from membrane phospholipids via a two-step process starting with *sn*-2 arachidonoyl phosphatidylinositol 4,5-bisphosphate (PIP_2) (Figure 3 and 4).[22] In the first step, PIP_2 is hydrolyzed into arachidonyl-containing diacylglycerol (DAG) species by phospholipase Cβ (PLCβ), which is activated by various G-protein-coupled receptors. The second step is catalyzed by diacylglycerol lipase (DAGL), in which DAG is converted

into 2-AG in a *sn*-1 specific manner.[23,24] In addition, there are some other proposed pathways for 2-AG synthesis.[25,26] For example, hydrolysis of 2-arachidonoyl-LPA by an LPA phosphatase may also provide 2-AG (Figure 4).[25]

The rate-limiting step in 2-AG production is controlled by two homologous isoforms of DAGLs, DAGLα (120 kDa) and DAGLβ (70 kDa).[23] Both proteins are multi-domain membrane-spanning enzymes that belong to the serine hydrolase family and differ from each other by the presence of a long C-terminal tail (~300 amino acids) in DAGLα. This C-terminal tail is involved in the regulation of the catalytic activity of the enzyme.[27-29]

Genetic studies with DAGL knockout mice have demonstrated that DAGLα and DAGLβ regulate 2-AG production in a tissue type dependent manner.[28,30] DAGLα is the principal regulator of 2-AG formation in the nervous system, whereas DAGLβ is the dominant enzyme for 2-AG production in peripheral tissues such as the liver. Interestingly, basal brain anandamide levels are also reduced in DAGLα$^{-/-}$ mice, but not in DAGLβ$^{-/-}$ mice.[31,32] Therefore, a pharmacological agent to modulate DAGLα or DAGLβ activity in an acute and temporal manner would provide an important counterpart for DAGLα$^{-/-}$ or DAGLβ$^{-/-}$ mice to study the physiological functions of DAGLs in complex biological systems.

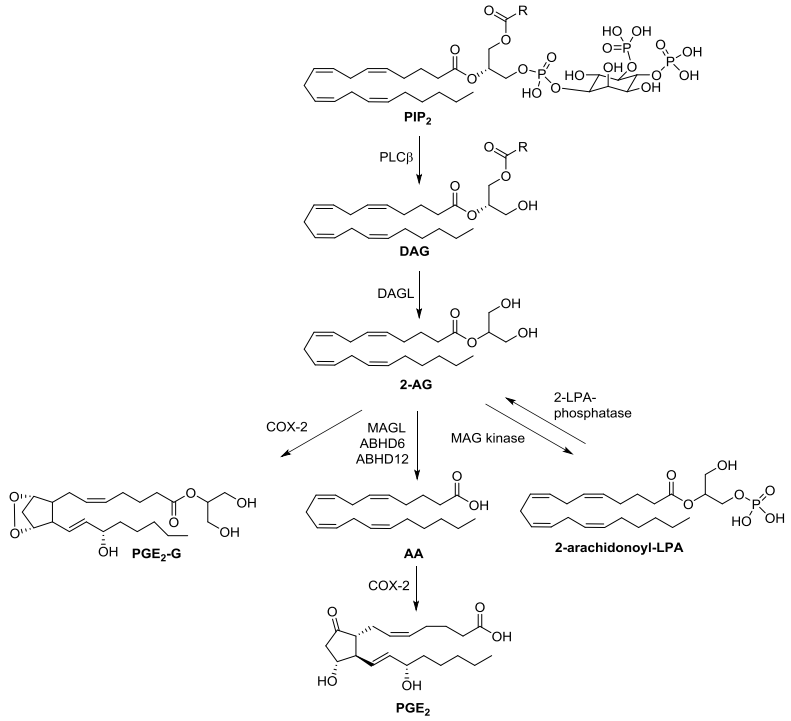

Figure 4. Biosynthetic and metabolic pathways of 2-arachidonoylglycerol (2-AG).

Inhibitors of diacylglycerol lipases

In early studies, the general lipase inhibitors tetrahydrolipostatin (THL, Orlistat) and RHC-80267, a bis-oximino-carbamate have been reported to inhibit DAGL-mediated 2-AG production using a radiometric assay with 1-[^{14}C]oleoyl-2-arachidonoylglycerol as natural substrate. They are, however, poorly active and/or lack the selectivity over other serine hydrolases (Figure 5).[33-35] In 2006, Bisogno *et al.* discovered fluorophosphonate inhibitors against DAGLα (O-3640 and O-3841). These compounds are active *in vitro* systems, but are not suitable for *in vivo* studies due to their poor stability and lack of cell permeability.[68] Further structure-activity relationship studies of fluorophosphonate inhibitors led to the discovery of O-5596, which is a relatively stable and potent DAGLs inhibitor.[36] However, O-5596 cross-reacts with several off-targets, which prohibits its use as a specific DAGLs inhibitor. Recently, the α-ketoheterocycles LEI104 and LEI105 were disclosed as a new chemotype of selective, reversible DAGLs inhibitors, but no *in vivo* activity was reported. In 2012, Hsu *et al.* published the first *in vivo* active DAGLβ inhibitor KT109 (Figure 5), which is based on a triazole urea scaffold.[37] KT109 was ~60-fold selective over DAGLα. However, KT109 does not cross the blood-brain barrier.

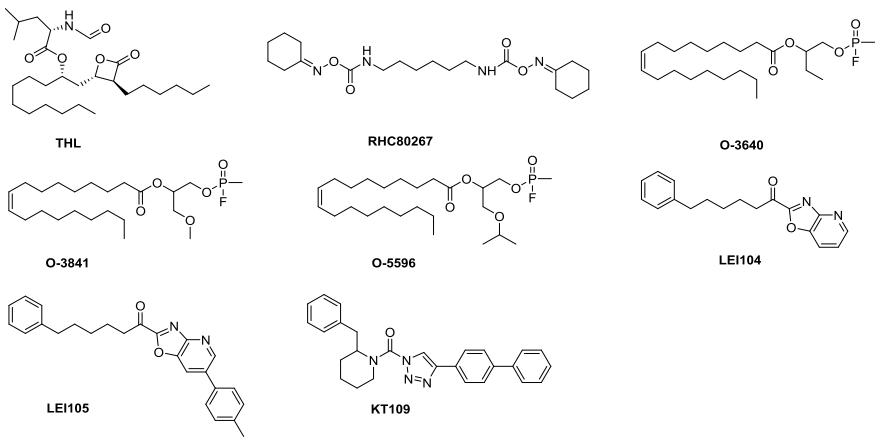

Figure 5. Chemical structures of known DAGL inhibitors. RHC80267, THL, O-3640, O-3841 and O-5596 are first generation DAGL inhibitors, which were non-selective, not potent, or not *in vivo* active. LEI105 is a reversible inhibitor with high selectivity. KT109 is an *in vivo* active DAGLβ inhibitor with good selectivity.

Monoacylglycerol lipase

Monoacylglycerol lipase (MAGL) is the main responsible enzyme for terminating 2-AG signaling by catalyzing the hydrolysis of the ester bond, thereby producing arachidonic acid and glycerol. Other serine hydrolases, including ABHD6, ABHD12 and FAAH, play a

minor and cell-type specific role in the metabolism of 2-AG. MAGL is primarily located at pre-synaptic membranes.[38,39] Studies using MAGL$^{-/-}$ mice and pharmacological tools showed dramatically elevated 2-AG levels in the brain and peripheral tissues.[40] 2-AG can also be transformed into other bioactive lipids, such as prostaglandin-glyceryl esters by cyclooxygenase-2,[41] which are involved in the inflammatory responses. Furthermore, lipid kinases such as monoacylglycerol kinases can phosphorylate 2-AG, thereby producing lysophosphatidic acid.[42] Several MAGL inhibitors disclosed in the literature include URB602, *N*-arachidonoyl maleimide (NAM) and OMDM169 (Figure 6). These compounds have low potency, cross-react with FAAH and other enzymes. Thus, they are not suitable for the functional study of MAGL *in vivo*.[43-45] In 2009, Long *et al.* reported JZL184 as the first, highly selective, *in vivo* active MAGL inhibitor. JZL184 contains a piperidine carbamate as electrophile that reacts to the catalytic serine of MAGL to form a stable and irreversible carbamate adduct. Using competitive activity-based protein profiling, JZL184 was shown to be 100-fold selective over FAAH and other serine hydrolases.[46] JZL184 is less active on rat MAGL than mouse MAGL. The new MAGL inhibitor KML29 does not suffer from this species-dependent activity and shows high potency against rat MAGL resulting increased 2-AG levels in rats.[47] MAGL inhibitors display anti-inflammatory and neuroprotective effects in multiple mice models of neurodegenerative disorders.[48] In addition, Nomura *et al.* demonstrated that inhibition of MAGL activity in aggressive cancer models impaired cell survival, migration and tumor growth.[49] Thus, MAGL inhibitors may have potential therapeutic utility in various diseases.

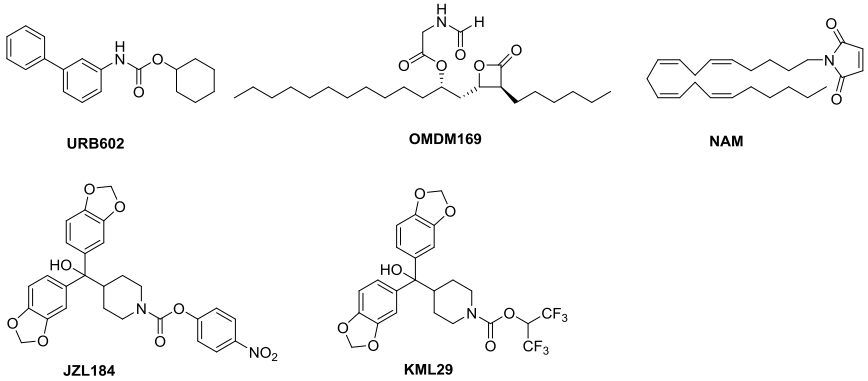

Figure 6. Chemical structures of known MAGL inhibitors. URB602, OMDM169 and NAM are first-generation inhibitors with poor selectivity and potency. JZL184 and KML29 are selective MAGL inhibitors with high *in vivo* potency.

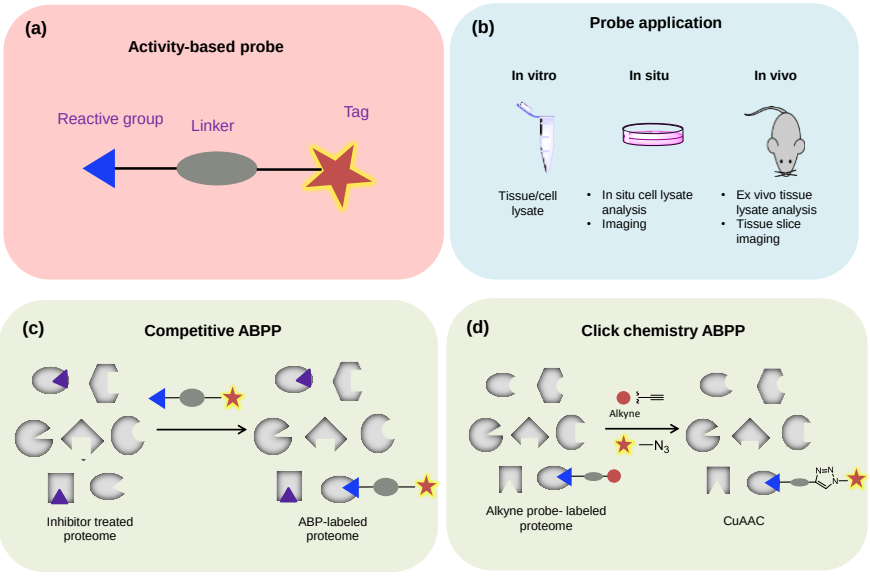

Figure 7. Schematic overview of activity-based protein profiling (ABPP). (a) Representative cartoons of activity-based probes: reactive group (blue), linker (gray) and reporter tag (red) (e.g. fluorophore or biotin affinity tag). (b) ABPs can be used in various biological systems, including cell/tissue lysates *in vitro*, living cellular systems, and *in vivo* animal models. (c) In competitive ABPP, proteomes are pre-incubated with inhibitors, followed by co-incubation with an ABP. (d) Two-steps probes (Click chemistry ABPP) provide a post-detection of protein labeling.

Activity-based protein profiling

Activity-based proteome profiling (ABPP) is a chemical proteomics method that allows the study of proteins and their perturbation by small molecules in their native cellular context.[50,51] ABPP will only visualize active proteins, takes all post-translational modifications (PTMs) into account and by this virtue is complementary to other techniques that detect messenger RNA or polypeptides/proteins (that is, *in situ* hybridization and immunohistology, respectively). ABPP makes use of organic molecules, termed activity-based probes (ABPs) to label the active site of a protein (Figure 7a). ABPs are compounds that covalently and irreversibly inhibit enzymes and that are equipped with a tag (fluorophore, biotin, bioorthogonal tag) through which the target enzyme, or enzyme family, is visualized by fluorescence microscopy, or enriched to enable identification and characterization using chemical proteomics methodology by mass spectrometry. In comparative ABPP two biological samples are interrogated with ABPs. Differences in enzyme activities are monitored and identified with various ABPs. Comparative ABPP allows the discovery of targets and validation of drug-target interaction in live cells, tissue lysates, and sometimes in animals (Figure

7b). In competitive ABPP a small molecule is pre-incubated with a biological sample and residual enzyme activities are subsequently monitored with an ABP (Figure 7c). Activity and selectivity of the small molecules is easily visualized in a complex proteome across the complete protein family. Competitive ABPP can also be used to determine target engagement *in situ* and *in vivo*. In both experimental set ups, two different type of probes can be used. Broad-spectrum ABPs target a whole (or to a large extent) family of proteins, whereas tailor-made ABPs are designed to target a specific protein of interest. The latter type of probe can also be used to validate the target in different therapeutic animal models and serve as a biomarker for target engagement in clinical trials. In case the ABP fall short and do not work due to a lack of bioavailability or enzyme specificity, two-step ABPs can be applied. Two-step ABPs do not constitute a reporter tag, but instead carry a small ligation handle, which can be conjugated to a biotin or fluorescent tag via bio-orthogonal ligation chemistry, only after the ABP has covalently reacted with the target of interest (Figure 7d). These combined ABPP technologies provide a highly attractive platform, both to discern aberrant enzyme functioning in physiological processes, and to identify compounds able to correct for this.

Aim and outline of the thesis

The aim of this thesis is to design, synthesize and apply chemical tools to study the physiological roles of DAGLα/β and MAGL in vitro and in vivo.

Chapter 2 reports on the design, synthesis and *in vitro* characterization of DH376 as a new dual DAGL inhibitor. In **Chapter 3** the discovery of DH379 as a tailor-made activity-based probe for DAGLα/β and the effects of acute pharmacological blockade of DAGLs by DH376 in healthy and lipopolysaccharide-treated mice on brain lipid networks and neuroinflammation is reported. **Chapter 4** describes the efficacy of DH376 in refeeding behavior of fasted mice. In **Chapter 5** the development of the first DAGL PET ligand [^{18}F]DH439 is disclosed. The structure-activity relationship of disubstituted piperidinyl ureas as DAGL inhibitors is reported in **Chapter 6**. The design, synthesis and application of a highly selective tailor-made activity-based imaging probe for MAGL is discussed in **Chapter 7**. Finally, **Chapter 8** provides a summary of the results described in the thesis and proposes some directions for future research.

References

1. Mendizabal, V. E.; Adler-Graschinsky, E. Cannabinoids as therapeutic agents in cardiovascular disease: a tale of passions and illusions. *British Journal of Pharmacology* **2007,** 151, 427-440.
2. Agarwal, N.; Pacher, P.; Tegeder, I.; Amaya, F.; Constantin, C. E.; Brenner, G. J.; Rubino, T.; Michalski, C. W.; Marsicano, G.; Monory, K.; Mackie, K.; Marian, C.; Batkai, S.; Parolaro, D.; Fischer, M. J.; Reeh, P.; Kunos, G.; Kress, M.; Lutz, B.; Woolf, C. J.; Kuner, R. Cannabinoids mediate analgesia largely via peripheral type 1 cannabinoid receptors in nociceptors. *Nature Neuroscience* **2007,** 10, 870-879.
3. Rinder, I. D. The effects of marijuana: a social psychological interpretation. *Psychiatry* **1978,** 41, 202-6.
4. Gaoni, Y.; Mechoulam, R. Isolation, structure, and partial synthesis of an active constituent of hashish. *Journal of the American Chemical Society* **1964,** 86, 1646-1647.
5. Matsuda, L. A.; Lolait, S. J.; Brownstein, M. J.; Young, A. C.; Bonner, T. I. Structure of a cannabinoid receptor and functional expression of the cloned cDNA. *Nature* **1990,** 346, 561-4.
6. Van Waes, V.; Beverley, J. A.; Siman, H.; Tseng, K. Y.; Steiner, H. CB1 Cannabinoid Receptor Expression in the striatum: association with corticostriatal circuits and developmental regulation. *Frontiers in Pharmacology* **2012,** 3, 1-8.
7. Munro, S.; Thomas, K. L.; Abu-Shaar, M. Molecular characterization of a peripheral receptor for cannabinoids. *Nature* **1993,** 365, 61-65.
8. Ashton, J. C., Friberg, D., Darlington, C. L., Smith, P. F. Expression of the cannabinoid CB2 receptor in the rat cerebellum: an immunohistochemical study. *Neuroscience Letters* **2006,** 396, 113-116.
9. Galiegue, S.; Mary, S.; Marchand, J.; Dussossoy, D.; Carriere, D.; Carayon, P.; Bouaboula, M.; Shire, D.; Lefur, G.; Casellas, P. Expression of Central and Peripheral Cannabinoid Receptors in Human Immune Tissues and Leukocyte Subpopulations. *European Journal of Biochemistry* **1995,** 232, 54-61.
10. Cabral, G. A.; Griffin-Thomas, L. Emerging role of the cannabinoid receptor CB2 in immune regulation: therapeutic prospects for neuroinflammation. *Expert Reviews in Molecular Medicine* **2009,** 11, 1-24.
11. Devane, W. A.; Hanus, L.; Breuer, A.; Pertwee, R. G.; Stevenson, L. A.; Griffin, G.; Gibson, D.; Mandelbaum, A.; Etinger, A.; Mechoulam, R. Isolation and structure of a brain constituent that binds to the cannabinoid receptor. *Science* **1992,** 258, 1946-1949.
12. Mechoulam, R.; Benshabat, S.; Hanus, L.; Ligumsky, M.; Kaminski, N. E.; Schatz, A. R.; Gopher, A.; Almog, S.; Martin, B. R.; Compton, D. R.; Pertwee, R. G.; Griffin, G.; Bayewitch, M.; Barg, J.; Vogel, Z. Identification of an endogenous 2-monoglyceride, present in canine gut, that binds to cannabinoid receptors. *Biochemical Pharmacology* **1995,** 50, 83-90.
13. Hanus, L.; Abu-Lafi, S.; Fride, E.; Breuer, A.; Vogel, Z.; Shalev, D. E.; Kustanovich, I.; Mechoulam, R. 2-Arachidonyl glyceryl ether, an endogenous agonist of the cannabinoid CB1 receptor. *Proceedings of the National Academy of Sciences of the United States of America* **2001,** 98, 3662-3665.

14. Iannotti, F. A.; Di Marzo, V.; Petrosino, S. Endocannabinoids and endocannabinoid-related mediators: Targets, metabolism and role in neurological disorders. *Progress in Lipid Research* **2016,** 62, 107-128.
15. Stella, N.; Piomelli, D. Receptor-dependent formation of endogenous cannabinoids in cortical neurons. *European Journal of Pharmacology* **2001,** 425, 189-196.
16. van Beugen, B. J.; Nagaraja, R. Y.; Hansel, C. Climbing fiber-evoked endocannabinoid signaling heterosynaptically suppresses presynaptic cerebellar long-term potentiation. *Journal of Neuroscience* **2006,** 26, 8289-8294.
17. Witting, A.; Walter, L.; Wacker, J.; Moller, T.; Stella, N. P2X7 receptors control 2-arachidonoylglycerol production by microglial cells. *Proceedings of the National Academy of Sciences of the United States of America* **2004,** 101, 3214-3219.
18. Kano, M.; Ohno-Shosaku, T.; Hashimotodani, Y.; Uchigashima, M.; Watanabe, M. Endocannabinoid-mediated control of synaptic transmission. *Physiological Reviews* **2009,** 89, 309-380.
19. Pagotto, U.; Marsicano, G.; Cota, D.; Lutz, B.; Pasquali, R. The emerging role of the endocannabinoid system in endocrine regulation and energy balance. *Endocrine Reviews* **2006,** 27, 73-100.
20. Castane, A.; Valjent, E.; Ledent, C.; Parmentier, M.; Maldonado, R.; Valverde, O. Lack of CB1 cannabinoid receptors modifies nicotine behavioural responses, but not nicotine abstinence. *Neuropharmacology* **2002,** 43, 857-867.
21. Pacher, P.; Kunos, G. Modulating the endocannabinoid system in human health and disease successes and failures. *FEBS Journal* **2013,** 280, 1918-1943.
22. Farooqui, A. A.; Rammohan, K. W.; Horrocks, L. A. Isolation, Characterization, and regulation of diacylglycerol lipases from the bovine brain. *Annals of the New York Academy of Sciences* **1989,** 559, 25-36.
23. Bisogno, T.; Howell, F.; Williams, G.; Minassi, A.; Cascio, M. G.; Ligresti, A.; Matias, I.; Schiano-Moriello, A.; Paul, P.; Williams, E. J.; Gangadharan, U.; Hobbs, C.; Di Marzo, V.; Doherty, P. Cloning of the first sn1-DAG lipases points to the spatial and temporal regulation of endocannabinoid signaling in the brain. *Journal of Cell Biology* **2003,** 163, 463-468.
24. Reisenberg, M.; Singh, P. K.; Williams, G.; Doherty, P. The diacylglycerol lipases: structure, regulation and roles in and beyond endocannabinoid signalling. *Philosophical Transactions of the Royal Society London B Biological Sciences* **2012,** 367, 3264-3275.
25. Nakane, S.; Oka, S.; Arai, S.; Waku, K.; Ishima, Y.; Tokumura, A.; Sugiura, T. 2-arachidonoyl-sn-glycero-3-phosphate, an arachidonic acid-containing lysophosphatidic acid: occurrence and rapid enzymatic conversion to 2-arachidonoyl-sn-glycerol, a cannabinoid receptor ligand, in rat brain. *Archives of Biochemistry and Biophysics* **2002,** 402, 51-58.
26. Higgs, H. N.; Glomset, J. A. Identification of a phosphatidic acid-preferring phospholipase A1 from bovine brain and testis. *Proceedings of the National Academy of Sciences of the United States of America* **1994,** 91, 9574-9578.
27. Tanimura, A.; Yamazaki, M.; Hashimotodani, Y.; Uchigashima, M.; Kawata, S.; Abe, M.; Kita, Y.; Hashimoto, K.; Shimizu, T.; Watanabe, M.; Sakimura, K.; Kano, M. The endocannabinoid 2-arachidonoylglycerol produced by diacylglycerol lipase alpha mediates retrograde suppression of synaptic transmission. *Neuron* **2010,** 65, 320-327.

28. Gao, Y.; Vasilyev, D. V.; Goncalves, M. B.; Howell, F. V.; Hobbs, C.; Reisenberg, M.; Shen, R.; Zhang, M. Y.; Strassle, B. W.; Lu, P.; Mark, L.; Piesla, M. J.; Deng, K.; Kouranova, E. V.; Ring, R. H.; Whiteside, G. T.; Bates, B.; Walsh, F. S.; Williams, G.; Pangalos, M. N.; Samad, T. A.; Doherty, P. Loss of retrograde endocannabinoid signaling and reduced adult neurogenesis in diacylglycerol lipase knock-out mice. *Journal of Neuroscience* **2010,** 30, 2017-2024.
29. Shonesy, B. C.; Wang, X. H.; Rose, K. L.; Ramikie, T. S.; Cavener, V. S.; Rentz, T.; Baucum, A. J.; Jalan-Sakrikar, N.; Mackie, K.; Winder, D. G.; Patel, S.; Colbran, R. J. CaMKII regulates diacylglycerol lipase-alpha and striatal endocannabinoid signaling. *Nature Neuroscience* **2013,** 16, 456-463.
30. Powell, D. R.; Gay, J. P.; Wilganowski, N.; Doree, D.; Savelieva, K. V.; Lanthorn, T. H.; Read, R.; Vogel, P.; Hansen, G. M.; Brommage, R.; Ding, Z. M.; Desai, U.; Zambrowicz, B. Diacylglycerol lipase a knockout mice demonstrate metabolic and behavioral phenotypes similar to those of cannabinoid receptor 1 knockout mice. *Frontiers in Endocrinology* **2015,** 6, 1-13.
31. Marinelli, S.; Pacioni, S.; Bisogno, T.; Di Marzo, V.; Prince, D. A.; Huguenard, J. R.; Bacci, A. The endocannabinoid 2-arachidonoylglycerol is responsible for the slow self-inhibition in neocortical interneurons. *Journal of Neuroscience* **2008,** 28, 13532-13541.
32. Marinelli, S.; Pacioni, S.; Cannich, A.; Marsicano, G.; Bacci, A. Self-modulation of neocortical pyramidal neurons by endocannabinoids. *Nature Neuroscience* **2009,** 12, 1488-1490.
33. Ortar, G.; Bisogno, T.; Ligresti, A.; Morera, E.; Nalli, M.; Di Marzo, V. Tetrahydrolipstatin analogues as modulators of endocannabinoid 2-arachidonoylglycerol metabolism. *Journal of Medicinal Chemistry* **2008,** 51, 6970-6979.
34. Bisogno, T.; Cascio, M. G.; Saha, B.; Mahadevan, A.; Urbani, P.; Minassi, A.; Appendino, G.; Saturnino, C.; Martin, B.; Razdan, R.; Di Marzo, V. Development of the first potent and specific inhibitors of endocannabinoid biosynthesis. *Biochimica Et Biophysica Acta-Molecular and Cell Biology of Lipids* **2006,** 1761, 205-212.
35. Ghisdal, P.; Vandenberg, G.; Hamaide, M. C.; Wibo, M.; Morel, N. The diacylglycerol lipase inhibitor RHC-80267 potentiates the relaxation to acetylcholine in rat mesenteric artery by anti-cholinesterase action. *European Journal of Pharmacology* **2005,** 517, 97-102.
36. Bisogno, T.; Burston, J. J.; Rai, R.; Allara, M.; Saha, B.; Mahadevan, A.; Razdan, R. K.; Wiley, J. L.; Di Marzo, V. Synthesis and pharmacological activity of a potent inhibitor of the biosynthesis of the endocannabinoid 2-arachidonoylglycerol. *ChemMedChem* **2009,** 4, 946-950.
37. Hsu, K. L.; Tsuboi, K.; Adibekian, A.; Pugh, H.; Masuda, K.; Cravatt, B. F. DAGLbeta inhibition perturbs a lipid network involved in macrophage inflammatory responses. *Nature Chemical Biology* **2012,** 8, 999-1007.
38. Gulyas, A. I.; Cravatt, B. F.; Bracey, M. H.; Dinh, T. P.; Piomelli, D.; Boscia, F.; Freund, T. F. Segregation of two endocannabinoid-hydrolyzing enzymes into pre- and postsynaptic compartments in the rat hippocampus, cerebellum and amygdala. *European Journal of Neuroscience* **2004,** 20, 441-458.
39. Blankman, J. L.; Simon, G. M.; Cravatt, B. F. A comprehensive profile of brain enzymes that hydrolyze the endocannabinoid 2-arachidonoylglycerol. *Chemistry & Biology* **2007,** 14, 1347-1356.

40. Taschler, U.; Radner, F. P. W.; Heier, C.; Schreiber, R.; Schweiger, M.; Schoiswohl, G.; Preiss-Landl, K.; Jaeger, D.; Reiter, B.; Koefeler, H. C.; Wojciechowski, J.; Theussl, C.; Penninger, J. M.; Lass, A.; Haemmerle, G.; Zechner, R.; Zimmermann, R. Monoglyceride lipase deficiency in mice impairs lipolysis and attenuates diet-induced insulin resistance. *Journal of Biological Chemistry* **2011,** 286, 17467-17477.
41. Kozak, K. R.; Rowlinson, S. W.; Marnett, L. J. Oxygenation of the endocannabinoid, 2-arachidonylglycerol, to glyceryl prostaglandins by cyclooxygenase-2. *Journal of Biological Chemistry* **2000,** 275, 33744-33749.
42. Maccarrone, M.; Salvati, S.; Bari, M.; Finazzi-Agro, A. Anandamide and 2-arachidonoylglycerol inhibit fatty acid amide hydrolase by activating the lipoxygenase pathway of the arachidonate cascade. *Biochemical and Biophysical Research Communications* **2000,** 278, 576-583.
43. Hohmann, A. G.; Suplita, R. L.; Bolton, N. M.; Neely, M. H.; Fegley, D.; Mangieri, R.; Krey, J. F.; Walker, J. M.; Holmes, P. V.; Crystal, J. D.; Duranti, A.; Tontini, A.; Mor, M.; Tarzia, G.; Piomelli, D. An endocannabinoid mechanism for stress-induced analgesia. *Nature* **2005,** 435, 1108-1112.
44. Muccioli, G. G.; Xu, C.; Odah, E.; Cudaback, E.; Cisneros, J. A.; Lambert, D. M.; Rodriguez, M. L. L.; Bajjalieh, S.; Stella, N. Identification of a novel endocannabinoid-hydrolyzing enzyme expressed by microglial cells. *Journal of Neuroscience* **2007,** 27, 2883-2889.
45. Vandevoorde, S.; Jonsson, K. O.; Labar, G.; Persson, E.; Lambert, D. M.; Fowler, C. J. Lack of selectivity of URB602 for 2-oleoylglycerol compared to anandamide hydrolysis in vitro. *British Journal of Pharmacology* **2007,** 150, 186-191.
46. Long, J. Z.; Li, W. W.; Booker, L.; Burston, J. J.; Kinsey, S. G.; Schlosburg, J. E.; Pavon, F. J.; Serrano, A. M.; Selley, D. E.; Parsons, L. H.; Lichtman, A. H.; Cravatt, B. F. Selective blockade of 2-arachidonoylglycerol hydrolysis produces cannabinoid behavioral effects. *Nature Chemical Biology* **2009,** 5, 37-44.
47. Ignatowska-Jankowska, B. M.; Ghosh, S.; Crowe, M. S.; Kinsey, S. G.; Niphakis, M. J.; Abdullah, R. A.; Tao, Q.; O'Neal, S. T.; Walentiny, D. M.; Wiley, J. L.; Cravatt, B. F.; Lichtman, A. H. In vivo characterization of the highly selective monoacylglycerol lipase inhibitor KML29: antinociceptive activity without cannabimimetic side effects. *British Journal of Pharmacology* **2014,** 171, 1392-1407.
48. Chen, R. Q.; Zhang, J.; Wu, Y.; Wang, D. Q.; Feng, G. P.; Tang, Y. P.; Teng, Z. Q.; Chen, C. Monoacylglycerol lipase is a therapeutic target for Alzheimer's disease. *Cell Reports* **2012,** 2, 1329-1339.
49. Nomura, D. K.; Long, J. Z.; Niessen, S.; Hoover, H. S.; Ng, S. W.; Cravatt, B. F. Monoacylglycerol lipase regulates a fatty acid network that promotes cancer pathogenesis. *Cell* **2010,** 140, 49-61.
50. Cravatt, B. F.; Wright, A. T.; Kozarich, J. W. Activity-based protein profiling: from enzyme chemistry to proteomic chemistry. *Annual Review of Biochemistry* **2008,** 77, 383-414.
51. Niphakis, M. J.; Cravatt, B. F. Enzyme inhibitor discovery by activity-based protein profiling. *Annual Review of Biochemistry* **2014,** 83, 341-377.

2

Discovery of DH376, a 2,4-substituted triazole urea, as a potent and selective inhibitor for diacylglycerol lipases

Based on

H. Deng, S. Kooijman, A. M.C.H. van den Nieuwendijk, D. Ogasawara, T. van der Wel, F. van Dalen, M. P. Baggelaar, F. J. Janssen, R. J.B.H.N. van den Berg, H. den Dulk, V. Kantae, T. Hankemeier, B. F. Cravatt, H. S. Overkleeft, P. C.N. Rensen, M. van der Stelt, *J. Med. Chem., doi 10.1021/acs.jmedchem.6b01482*

Introduction

Compound libraries that contain a 1,2,3-triazole urea scaffold have previously been applied to the discovery of potent inhibitors of diverse serine hydrolases, such as diacylglycerol lipase-β (DAGLβ), α,β-hydrolase domain (ABHD) 6/11, DDHD2, APEH and PAFAH2.[1-5] 1,2,3-Triazole ureas constitute a versatile chemotype for the covalent, irreversible and selective inhibition of serine hydrolases. They contain an electrophilic carbonyl group with tunable reactivity as well as a scaffold to introduce functional groups conferring enzyme potency and/or specificity. 1,2,3-Triazole ureas irreversibly inhibit serine hydrolases via carbamoylation of the active-site serine alcohol. Some reported triazole urea inhibitors were proven to be potent and selective for specific serine hydrolases both in cells and mouse models, and are effective chemical probes to study the biological function of serine hydrolases in diverse

biological systems.[1,2] For example, KT109 (**1**), a selective and *in vivo* active DAGLβ inhibitor, reduces 2-arachidonoylglycerol (2-AG), arachidonic acid and eicosanoid levels in peritoneal macrophages of lipopolysaccharide (LPS)-treated mice and significantly decreases the pro-inflammatory cytokine, tumour necrosis factor α (TNFα) in LPS-treated mice.[4]

Two isoforms of DAGL exist, and that are expressed in a tissue-dependent manner. Both isoforms, termed DAGLα and DAGLβ, employ a Ser-His-Asp catalytic triad characteristic for serine hydrolases to hydrolyse ester bond of diacylglycerol (DAG) in a *sn*-1 specific manner. DAGLα and DAGLβ share extensive homology, but differ in size: DAGLα is about 120 kDa and DAGLβ is around 70 kDa.[6,7] DAGLα is the principal regulator of 2-AG formation in the nervous system, where it controls the activity of this endocannabinoid, which activates the cannabinoid CB_1 receptor, as a retrograde messenger at neuronal synapses. DAGLβ in turn is the dominant enzyme for 2-AG production in the periphery during inflammation.[8,9]

To study the function of DAGLs in a temporal and dynamic manner, *in vivo*-active inhibitors of these enzymes would be of great value. Particularly, a CNS-active chemical probe is required for DAGLα (mainly expressed in the brain) that can be used to acutely perturb 2-AG production in the central nervous system. The known DAGL inhibitors can be classified into six different chemotypes: α-ketoheterocycles, glycine sulfonamides (both reversible, competitive DAGL inhibitor classes), bis-oximino-carbamates, β-lactones, fluorophosphonates and 1,2,3-triazole ureas (the latter four being mechanism-based and irreversible).[4,10-14] These inhibitors have been used to study the function of 2-AG in cellular models and brain slice preparations, but they lack selectivity over serine hydrolases, potency and/or chemical properties required for central activity. Of note, with the exception of the α-ketoheterocycles, all DAGL inhibitors reported to date also inhibit ABHD6, which also involved in the hydrolysis of partial 2-AG.

KT109 was selected as a suitable starting point for the rational design of new, potent and selective inhibitors for DAGLα, because it inhibits DAGLα with an IC_{50} of 2.3 μM in a competitive activity-based protein profiling (ABPP) assay.[4] In a first round of optimization, KT109 was converted into **38** (DH376), a highly potent, *in vivo* active compound that inhibits DAGLα in a time- and dose-dependent manner in mouse brain. Using **38**, as well as the structurally distinct compound DO34, functional studies on DAGLα in nervous system were performed (which will be described in Chapter 3 in detail).[15]

In this chapter, a full account of the discovery and development of DH376 (**38**) as an inhibitor of DAGLα is described. The influence of regioselectivity of the 1,4- and 2,4-triazole moiety, the nature of the substituents on the triazole core, the chirality of the benzylpiperidine and the substituent pattern of the piperidine ring on DAGLα and ABHD6 activity was systematically investigated. To this end, an enantioselective synthesis route to obtain both enantiomers of 2-benzylpiperidine and their derivatives was developed. Additionally, competitive activity-based protein profiling was employed to evaluate the selectivity profiles of the 1,2,3-triazole ureas in mouse brain membrane proteome. Finally, the cellular activity of DH376 in Neuro2A cells was determined.

Table 1. pIC_{50} values of compounds **1-6** against DAGLα and DAGLβ as determined by the colorimetric assay with PNP butyrate as substrate and competitive ABPP assay. Data represent average values ± SEM; n = 4 per group for substrate assays, and n = 3 per group for ABPP assays.

	Substrate assay (PNP butyrate)		**ABPP** (DH379)	
	hDAGLα	mDAGLβ	hDAGLα	hDAGLβ
1	8.9±0.1	7.1±0.2	8.1±0.1	8.2±0.1
2	7.2±0.1	4.9±0.3	6.2±0.1	6.0±0.1
3	7.6±0.1	7.1±0.1	6.8±0.1	6.2±0.1
4	8.6±0.1	7.9±0.1	7.8±0.1	7.6±0.1
5	7.7±0.1	4.7±0.2	6.7±0.1	6.1±0.1
6	5.4±0.1	N.A.	N.A.	N.A.

Results and Discussion

Discovery of 2,4-substituted 1,2,3-triazole urea as new chemotype of DAGLα inhibitor

In the search for CNS-active DAGLα inhibitors, a rational design drug discovery approach was employed in which KT109 (**1**) and a closely related analogue, ML226 (**2**), served as starting points (structures are shown in Figure 1). KT109 is a peripherally restricted DAGLβ inhibitor with 60-fold selectivity over DAGLα. ML226 in turn, is a potent, cellular and *in vivo* active ABHD11 inhibitor with excellent physicochemical properties.[1,4] First, the activity of KT109 and ML226 on HEK293T membranes overexpressing human DAGLα and mouse DAGLβ were tested in a colorimetric assay using *para*-nitrophenylbutyrate (PNP) as a surrogate substrate (Figure 1b, c; Table 1).[10,11] In this assay, KT109 inhibites mouse DAGLβ with a pIC_{50} of 7.1±0.2, which is consistent with previously reported in a gel-based ABPP assay using HT-01 as a chemical probe (pIC_{50} = 7.4)[4]. However, KT109 (pIC_{50} = 8.9±0.1) was much more potent on human DAGLα in the assay, than previously reported in a gel-based ABPP assay using HT-01 as a chemical probe (pIC_{50} = 5.6)[4]. The difference might be due to the weak labeling efficiency of HT-01 for DAGLα. In contrast, ML226 demonstrated weak DAGLα activity with a pIC_{50} of 7.2±0.1 and poor DAGLβ activity in the PNP-assay. At first sight this is in line with the previously reported preference of DAGLβ for 1,4-regioisomers of the triazole ureas over the corresponding 2,4-regioisomers.[16] ML226 lacks, however, the 2-benzyl substituent on the piperidine moiety thus blocking an appropriate comparison between the two inhibitors. Therefore, compounds **3-6** were synthesized as hybrid structures harbouring elements of both KT109 and ML226. To this end, the triazole building

blocks and the final compounds were synthesized as previously reported.[4,15] Interestingly, compound **4**, a 2-benzylpiperidine urea of a 2,4-triazole with a 1,1-diphenylmethanol substituent at the 4-position (as in ML226), showed the highest DAGLα and DAGLβ inhibitory activity with pIC_{50} of 8.6±0.1 and 7.9±0.1, respectively. Its 1,4-regioisomer (compound **3**) is 10-fold less potent. This indicates that 2,4-triazole is the preferred regioisomer for DAGLα and DAGLβ inhibition (Figure 1d, e; Table 1). Hybrid compounds (**5** and **6**) with an ethyl substituent at the 2-position of the piperidine ring appeared less potent than KT109, which suggests that the benzyl substituent is required to address an additional lipophilic pocket near the active site in the enzymes (Figure 1d, e). Competitive ABPP assays were next employed to confirm the inhibitory activities of compounds **1-6** against recombinant human DAGLα/β. DAGL-tailored activity-based probe DH379 (which will be described in Chapter 3) was used for these studies.[15] The results of gel-based ABPP assay were in line with the above PNP-assay that KT109 potently inhibited DAGLα and DAGLβ labeling by DH379, and compound **4** showed the highest potency against human DAGLα and DAGLβ among the hybrid compounds (Figure 1f and g).

The contribution of the phenyl groups of the 1,1-diphenylmethanol substituent in compound **4** to DAGLα inhibition was next investigated (Table 2). To this end, the phenyl substituents were replaced by cyclohexyl (**7**, **8**); removed one (**9**) or both (**10**) phenyl groups; replaced them by a pyridyl (**11**) or introduced fluorine atoms (**12**). The biochemical assay revealed *para*-fluoro substituted inhibitor (**12**) as the most potent agent in this series against hDAGLα with a pIC_{50} of 9.0, which suggested that its increased lipophilicity and/or electron withdrawing effect is beneficial. The ~100-fold drop in potency of the more polar (compared to lead **4**) pyridyl-containing compound (**11**), suggested that lipophilicity is more important than electron withdrawing properties. Indeed, the lipophilic interactions of the phenyl groups are essential features of the DAGLα inhibitor, because their removal led to a 160-2000 fold decrease in potency (**8**-**10**), whereas retaining two bulky cyclohexyl groups (**7**) resulted in only a 40-fold drop in potency. A role for pi-sigma/cation interactions can, however, also not be excluded. A 10-fold decrease in potency was observed when the tertiary alcohol group was methylated, as in compound (**13**), suggesting that a hydrogen bond donor is important (or alternatively, the grafted methyl group has a steric clash with the enzyme). To reduce the lipophilicity, 2-benzyl substituent of the piperidine ring was substituted for a phenoxymethyl- (**14**, **15**) or (4-fluoro)phenoxymethyl group (**16**, **17**) and polar methoxy substituents on the phenyl ring were introduced as well (**18**, **19**). These substitutions were tolerated (Table 2), but led to a five-fold reduced activity.

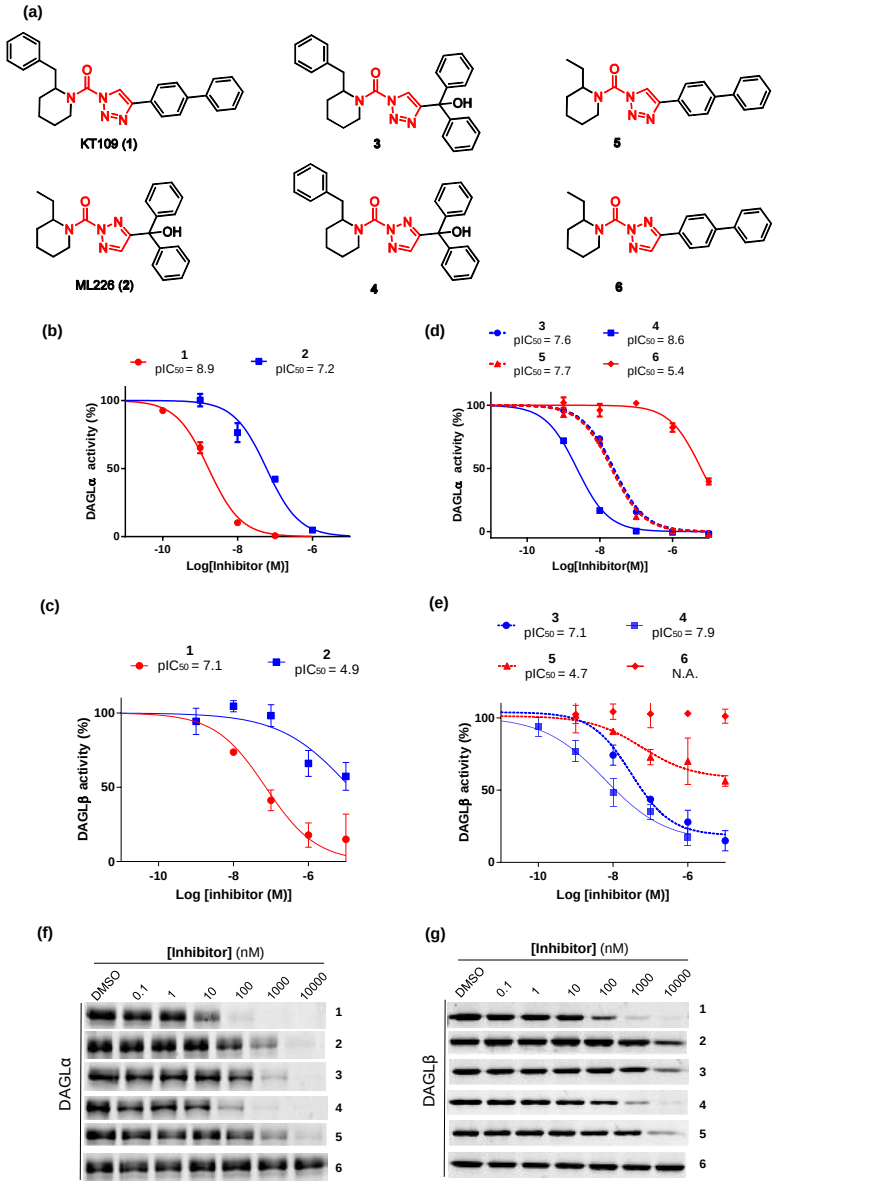

Figure 1. (a) The structures of 1,2,3-triazole ureas **1**-**6**. (b, d) Concentration-dependent inhibition of recombinant human DAGLα by compounds **1**-**6** as measured with a colorimetric assay based on the hydrolysis of PNP butyrate from DAGL-transfected HEK293T cells. (c, e) Concentration-dependent inhibition of recombinant mouse DAGLβ by compounds **1**-**6** as measured with the PNP butyrate substrate assay. Data represent average values ± SEM; n = 4 per group. (f, g) Representative fluorescent gel-based competitive ABPP with compounds **1**-**6** against recombinant human DAGLα and DAGLβ by tailored activity-based probe DH379 (1 µM, 30 min).

Table 2. Structure-activity relationship of triazole ureas with N2-isomers as leaving group. Inhibition of recombinant human DAGLα or ABHD6 was measured by the indicated colorimetric assay based on PNP or 2-AG substrate assay, repectively. Data represent average values ± SEM; n = 4 per group.

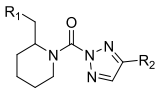

Entry	R_1	R_2	pIC_{50}±SEM (DAGLα)	pIC_{50}±SEM (ABHD6)
7			7.0±0.1	5.1±0.2
8			5.8±0.1	5.5±0.1
9			6.4±0.1	5.5±0.1
10			5.3±0.2	<5
11			6.8±0.1	5.5±0.2
12			9.0±0.1	7.6±0.1
13			7.9±0.2	<5
14			8.1±0.1	6.8±0.1
15			8.3±0.1	6.7±0.1
16			8.2±0.1	6.6±0.1
17	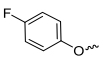		8.3±0.1	6.7±0.1
18			8.5±0.5	6.8±0.2
19			8.3±0.1	6.6±0.1

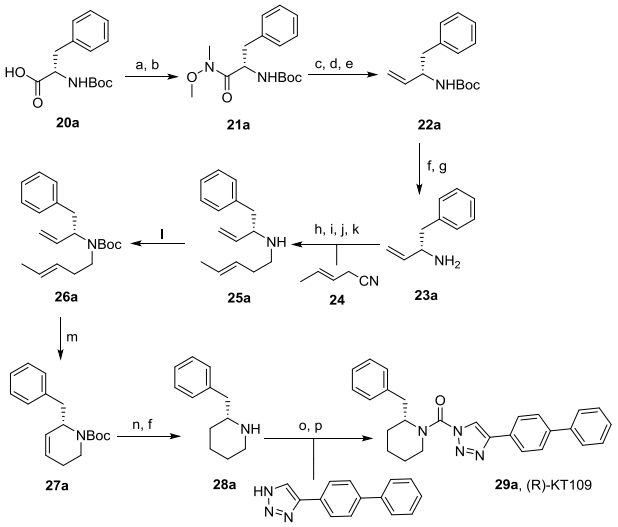

Scheme 1. Enantioselective synthesis of (*R*)-KT109 (**29a**) Reagents and conditions: (a) Me(OMe)NH·HCl; (b) EDCI, NMM; (c) $LiAlH_4$; (d) H_3O^+; (e) $(Ph)_3P{=}CH_2$, 86% (**22a**, based on **20a**); (f) MeOH, HCl; 70% (**28a**) (g) NaOH, 89%; (h) **24**, diethyl ether, DIBAL-H, -80 °C to 0 °C; (i) MeOH, -90 °C; (j) amine **23a** (3 equiv), r.t., 20h; (k) $NaBH_4$, 0 °C to r.t., 5h, 44%; (l) Boc_2O, Et_3N, THF, 50 °C, 20h, 92%; (m) Grubbs I cat. 4 mol%, DCM, reflux, 48h, 68%; (n) H_2, Pd/C, MeOH; (o) DIPEA, triphosgene, THF, 0 °C; (p) DIPEA, DMAP, triazole , THF, 60 °C, 30%.

(*R*)-KT109 is the most active DAGL inhibitor

Previously, the eutomer of KT109 was found to be 100-fold more potent than the distomer against DAGLβ.[16] The absolute configuration of the eutomer (and distomer) was, however, not assigned. To determine whether (*R*)-KT109 (**29a**) or (*S*)-KT109 (**29b**) is the most potent enantiomer, a enantioselective synthesis route (Scheme 1) was develeoped. The synthesis of the separate enantiomers of KT109 began with the preparation of chiral amine **23a** in four steps from commercially available Boc-protected L-phenylalanine **20a**.[17] Amine **23a** was reacted with 3-pentene nitrile **24** to give secondary amine **25a** via a one-pot DIBAL-H reduction-transimination-$NaBH_4$ reduction sequence.[18] Subsequent Boc-protection of the amine, ring-closing metathesis, hydrogenation and Boc-deprotection led to key chiral 2-benzylpiperidine building block **28a**. Direct coupling of the chiral piperidine with 4-([1,1'-biphenyl]-4-yl)-1*H*-1,2,3-triazole using triphosgene provided final compound **29a** in >95% e.e. as determined by chiral HPLC. The synthesis of enantiomer **29b** proceeded in a similar fashion using chiral amine **23b** (see experimental section, Scheme 5).

To correlate the activity of the compounds with their stereochemistry, both enantiomers and a 1:1 mixture were tested in the colorimetric surrogate PNP-substrate assay using HEK293T membranes expressing recombinant human

DAGLα. Compound **29a** proved to be the eutomer with a pIC_{50} of 9.1±0.1, while compound **29b** showed ~100-fold less activity (pIC_{50} of 7.4±0.1) (Figure 2a) in the PNP-assay. The 1:1 racemic mixture demonstrated a pIC_{50} of 8.2±0.1. A real-time, fluorescence-based assay was also employed to test the activity of the inhibitors on DAGLα-mediated hydrolysis of its natural substrate 1-stearoyl-2-arachidonoly-*sn*-glycerol.[19] Again, compound **29a** was the most active DAGLα inhibitor with a pIC_{50} of 7.6±0.1 (Figure 2b). Since ABHD6 was previously reported as an off-target of KT109, the activities of both enantiomers (**29a** and **29b**) against human ABHD6 were also tested.[11,20] Compound **29a** (pIC_{50} 8.6±0.1) was ~100-fold more potent than **29b** (pIC_{50} 6.2±0.1) (Figure 2c), which reveals that the inhibitory activity for both DAGLα and ABHD6 resides in the (*R*)-enantiomer. To assess the activity and selectivity of compounds **29a** and **29b** on endogenously expressed DAGLα in mouse brain membrane proteome, a competitive ABPP method with MB064 was used.[10] Consistent with the biochemical assays, compounds **29a** and **29b** were found to block DAGLα labeling by MB064 with pIC_{50} of 8.1±0.1 and 6.2±0.1, respectively (Figure 2d and e). Additionally, both **29a** and **29b** showed same selectivity profile (with ABHD6 as only identified off-target) in mouse brain membrane proteome determined by a broad-spectrum TAMRA-FP probe.

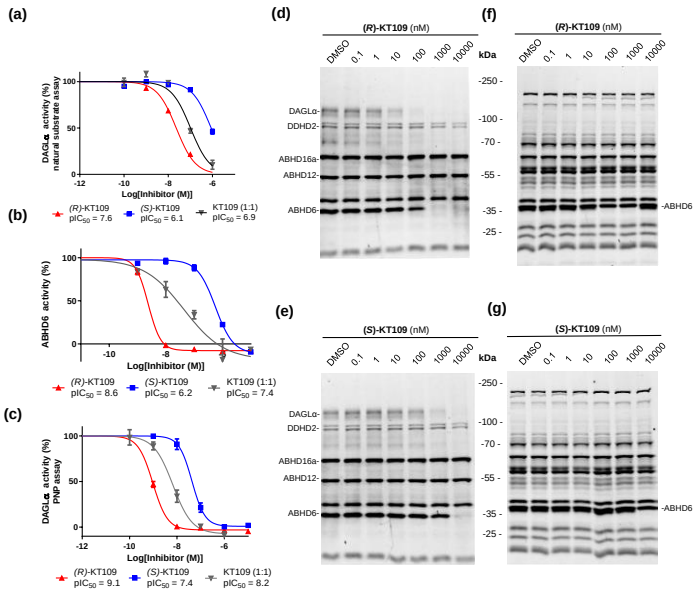

Figure 2. Characterization of both enantiomers of KT109 as DAGLα inhibitors: (a) Concentration-dependent inhibition of recombinant hDAGLα by (*R*)-KT109 (**29a**), (*S*)-KT109 (**29b**) and racemic KT-109 (1:1) as measured with a colorimetric assay based on the hydrolysis of PNP butyrate. (b) Concentration-dependent inhibition of recombinant hDAGLα by (*R*)-KT109 (**29a**), (*S*)-KT109 (**29b**) and racemic KT-109 (1:1) as measured with a SAG substrate assay from DAGLα-transfected HEK293T cells. (c) Concentration-dependent inhibition of hABHD6 by (*R*)-KT109 (**29a**), (*S*)-KT109 (**29b**) and racemic KT-109 (1:1) as measured with a 2-AG

substrate assay. Data represent average values ± SEM; n = 4 per group. (d, e) Representative fluorescent gel-based competitive ABPP with (*R*)-KT109 (**29a**) and (*S*)-KT109 (**29b**) in mouse brain proteome by tailored activity-based probe MB064 (0.25 µM, 30 min). (f-g) Selectivity profiles of *(R)*-KT109 (f) and (*S*)-KT109 (g) across mouse brain serine hydrolases as determined by competitive ABPP using broad-spectrum probe FP-TAMRA (0.5 µM, 20 min). Of note, in these gel profiles for FP-TAMRA labeling, ABHD6 and MAGL signals were not resolved, and DAGLs are not visualized.

Table 3. Structure-activity relationship of N2-triazole urea isomers with functionalized chiral pure (2-benzyl)-piperidine staying groups. Inhibition of recombinant human DAGLα or ABHD6 was measured by the indicated colorimetric assay based on PNP or 2-AG substrate assay, repectively. Data represent average values ± SEM; n = 4 per group.

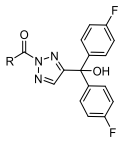

Entry	R	pIC_{50} (DAGLα)	pIC_{50} (ABHD6)	Entry	R	pIC_{50} (DAGLα)	pIC_{50} (ABHD6)
30	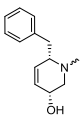	7.9±0.1	7.4±0.1	**35**	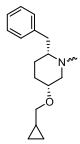	9.2±0.1	7.4±0.1
31	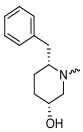	7.7±0.1	6.8±0.1	**36**	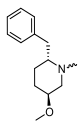	8.1±0.1	6.9±0.2
32	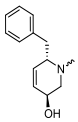	7.7±0.1	6.6±0.1	**37**	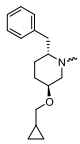	7.7±0.1	5.6±0.1
33	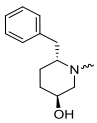	5.2±0.1	6.7±0.2	**38** (DH376)	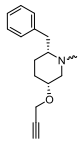	8.9±0.1	8.6±0.2
34	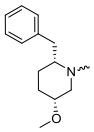	9.1±0.1	7.3±0.1				

Discovery of highly potent DAGL inhibitors

Having discovered that the (*R*)-enantiomer is the most active compound in the 1,4-triazole series, this knowledge was transferred to the 2,4-triazole series. To this end, the chiral amine building block **23a** was coupled to the triazole scaffold to provide compound **(*R*)-12**. **(*R*)-12** was found to have a pIC_{50} of 9.1±0.1, which was slightly higher than the racemic mixture (Figure 3a). To improve solubility and to mimic the natural substrate diacylglycerol, several new analogues were designed with a chiral hydroxyl group at the C-5 position (Scheme 2 and Scheme S.4 in experimental section; **30-33**). The chiral, diastereomers were synthesized according to Scheme 2. In brief, cyanohydrin **40** was enzymatically produced by the almond (*R*)-hydroxynitrile lyase using crotonic aldehyde **39** as a substrate.[21] After silyl protection of the alcohol, key intermediate **44** was generated by the same strategy as described for the synthesis of **29a**. After *N*-Boc deprotection, and optional hydrogenation, compounds **45** and **48** were coupled to the 1,2,3-triazole building block, yielding *O*-silyl protected intermediates **46** and **49**. Deprotection gave compounds **30** and **31**. Further alkylation of intermediate **50**, *N*-Boc deprotection and coupling with 1,2,3-triazole building block afforded compounds **34** and **35**. Compounds **32**, **33**, **36** and **37** were synthesized in the same fashion as described for the corresponding diastereoisomers (See experimental Scheme 6). Compounds **30**-**38** were tested in the PNP-assay and found that the free alcohol derivatives **30**-**33** are less potent than compound **12** (Table 1 and 2). Capping the secondary hydroxyl group with an alkyl moiety yielded (ultra)potent inhibitors. For example, compounds **34** and **35** demonstrated picomolar activity with pIC_{50} values of 9.1±0.1 and 9.2±0.1, respectively (Table 3). Comparison of the diastereoisomers (**34** vs **36**; **35** vs **37**) revealed that the back isomer at C-5 is the active diastereomer (**34**, **35**) (with ~10-fold higher potency). To visualize target engagement, a propargyl at C-5 was introduced, which serves as a ligation handle to introduce reporter groups by copper catalyzed azide-alkyne cycloaddition (or "click"-chemistry). This yielded inhibitor **38** (DH376) with a pIC_{50} = 8.9±0.1.

Activity and selectivity on endogenous DAGLα and ABHD6 in brain membrane proteome

To determine the activity and selectivity of the inhibitors in native proteomes, the most potent chiral inhibitors **34-38** were incubated for 30 min with mouse brain membrane homogenates and a gel-based ABPP-assay using ABPs MB064 and TAMRA-FP was performed. All compounds block DAGLα labeling in a concentration-dependent manner. Complete blockade of DAGLα was already observed at 10 nM for compounds **34**, **35** and **38**, whereas the diastereoisomers **36** and **37** were less active (Figure 3b and Figure S.3). Compound **35** inhibited labeling of DAGLα and ABHD6 with pIC_{50} of 8.7±0.1 and 6.5±0.1, respectively. This indicated that **35** was ~160-fold selective over ABHD6 (Figure 3c). Of note, compound **38** showed ~126 fold selectivity over ABHD6. No additional off-targets were identified using FP-TAMRA as a probe (Figure 4).

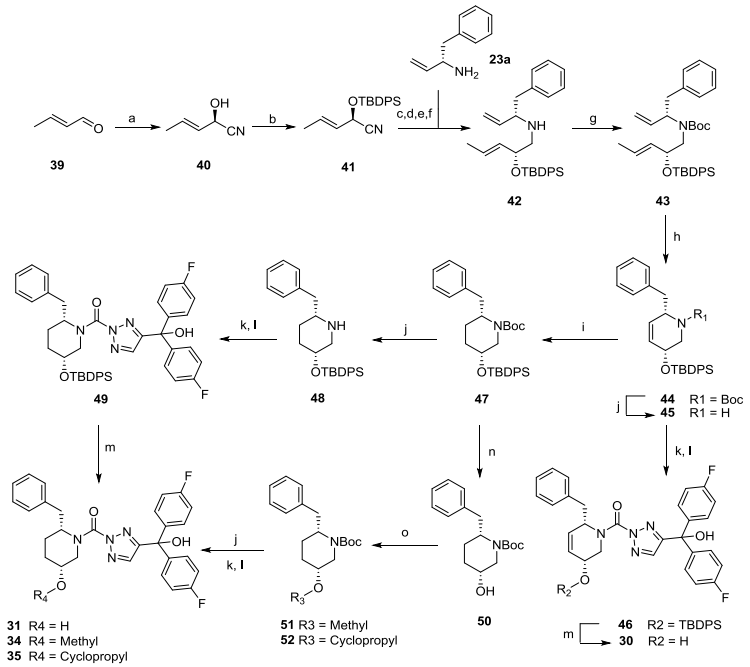

Scheme 2. Enantioselective synthesis of 1,2,3 triazole ureas **30**, **31**, **34** and **35.** Reagents and conditions: (a) HCN, EtOAc, 0.1 M aq. citrate buffer, pH 5.4, hydroxynitrile lyases, 83%; (b) TBDPS-Cl, imidazole, DMF, 0 ^{o}C, 94%; (c) diethyl ether, DIBAL-H, -80 ^{o}C to 0 ^{o}C; (d) MeOH, -90 ^{o}C; (e) (*S*)-amine (**23a**) (3 equiv), r.t., 20h; (f) $NaBH_4$; (g) Boc_2O, Et_3N, THF, 50 ^{o}C, 20h; (h) Grubbs G1 cat. 4 mol%, DCM, reflux, 48h, 72% (**44**, based on **41)**; (i) hydrazine, $CuSO_4$, EtOH, 0 ^{o}C to 70 ^{o}C, 65% (**47**); (j) 25% TFA, DCM, r.t.; (k) DIPEA, triphosgene, THF, 0 ^{o}C; (l) DIPEA, DMAP, triazole, THF, 60 ^{o}C, 28% (**34**, based on **51**), 22% (**35**, based on **52**); (m) HF-pyridine, THF : pyridine = 1:1 (v/v), 24% (**30**, based on **44**), 16% (31, based on **47**); (n) TBAF, THF, r.t., 72%; (o) NaH, corresponding bromide, 83% (**51**), 81% (**52**).

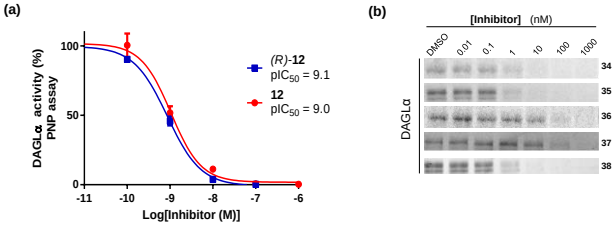

(c)

pIC_{50} ABPP (MB064)	**34**	**35**	**36**	**37**	**38** (DH376)
DAGLα	8.7±0.1	8.7±0.1	7.1±0.1	7.1±0.1	9.2±0.1
ABHD6	7.3±0.1	6.5±0.1	6.4±0.1	<5	7.1±0.1
Selectivity fold	~25	~160	~5	~145	~126

Figure. 3 (a) Concentration-dependent inhibition of hDAGLα by **12** and **(*R*)-12** as measured with a colorimetric assay based on the hydrolysis of PNP butyrate. Data represent average values ± SEM; n = 4 per group. (b) Representative fluorescent gel-based competitive ABPP with **34-38** in mouse brain proteome by activity-based probe MB064 (0.25 µM, 30 min). (c) pIC_{50} ± SEM and selectivity of compounds **34-38** against DAGLα and ABHD6 as determined by competitive ABPP (n = 3 per group).

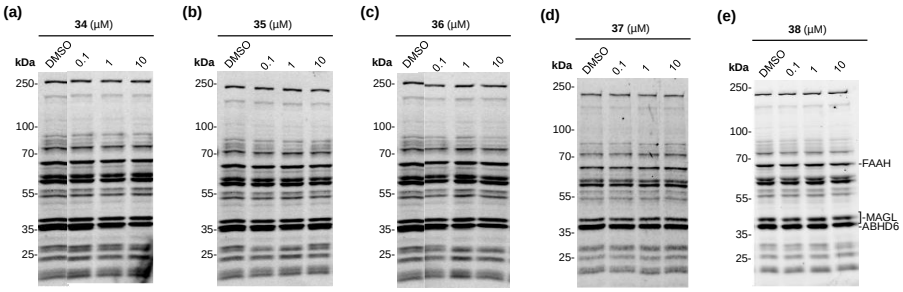

Figure 4. Selectivity profiles of compounds **34-38** across mouse brain serine hydrolases as determined by competitive ABPP using broad-spectrum probe FP-TAMRA (0.5 µM, 20 min).

DH376 reduces 2-AG levels in Neuro2A cells

A mouse neuroblastoma cell line (Neuro2A), known to express both DAGLα and DAGLβ, was used to evaluate the cellular activity of DH376.[22,23] Neuro2A cells were incubated with a range of concentrations of DH376 for 1h, lysed and analyzed by competitive gel-based ABPP using DH379 as an activity-based probe to establish cellular target engagement. DH376 blocked the labeling of DAGLβ in Neuro2A cells with low-nanomolar potency (IC_{50} = 1.3 nM, Figure 5a,b). As expected, DH376 also prevented the labeling of ABHD6 (Figure 5a,b), but did not inhibit the labeling of any of the other serine hydrolase as demonstrated in a competitive gel-based ABPP using the broad-spectrum probe TAMRA-FP (Figure 5c). Next, the effect of DH376 on the cellular levels of 2-AG was determined using targeted lipidomics. Neuro 2A cells treated for 1h with DH376 (1 µM) strongly reduced cellular 2-AG levels (Figure 5d), whereas no effect on anandamide was observed (Figure 5e).

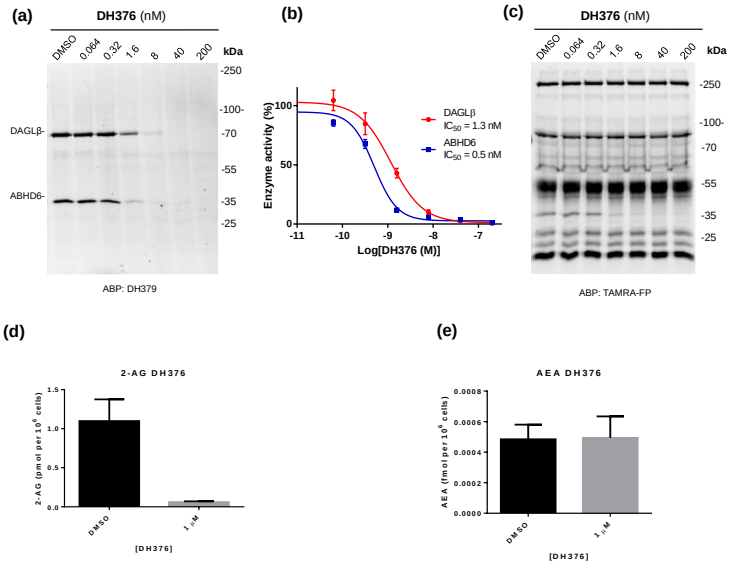

Figure 5. *In situ* activity of DH376. (a) Neuro2A cells were treated with various concentrations of DH376 for 1h at 37 °C, lysed and analyzed by gel-based competitive ABPP using ABP DH379 (1 uM, 30 min). (b) *In situ* concentration-dependent inhibition curves for endogenous DAGLβ and ABHD6 as measured by competitive ABPP using DH379 as probe. DH376 (pIC_{50} = 8.9±0.1 for DAGLβ, 9.3±0.1 for ABHD6). Data represent average values ± SEM, n=3 per group. (c) Selectivity profile of DH376 in Neuro 2A cells was determined by competitive ABPP using a broad-spectrum ABP TAMRA-FP (500 nM, 30 min). (d-e) *In situ* treatment of Neuro2A cells (1h, 37 °C) with DH376 (1 µM) abolished 2-AG levels (d), while keeping anandamide (AEA) levels constant (e) (mean ± SEM; n = 4).

Conclusion

In summary, the enantioselective synthesis and structure-activity relationship (SAR) studies of 2,4-regioisomers of 1,2,3-triazole ureas as a new chemotype of DAGLα inhibitors were described in this chapter. (*R*)-benzylpiperidine substituted triazole ureas were found to constitute the active enantiomer for DAGLα inhibition as measured in biochemical assays and activity-based protein profiling. (*R*)-KT109 (**29a**) was shown to be a potent DAGLα inhibitor. The investigations culminated in the discovery of compound **38** (DH376), a cellular-active DAGL inhibitor.

Experimental section

Experimental Procedures: Biochemistry

Cloning Procedures

For the preparation of the different constructs, full length human cDNA was purchased from Source Bioscience and cloned into mammalian expression vector pcDNA3.1, containing genes for ampicillin and neomycin resistance. DAGLα and ABHD6 constructs were obtained as reported previously.[10,15] Plasmids were isolated from transformed XL-10 Z-competent cells (Maxi Prep, Qiagen) and verified by Sanger sequencing (BaseClear). The sequences were confirmed by sequence analysis at the Leiden Genome Technology Centre.

Cell culture and membrane preparation

Cell culture was performed as previously reported.[15] In brief, HEK293T cells were grown in DMEM with stable glutamine and phenolred (PAA or Sigma) with 10% New Born Calf serum, penicillin and streptomycin. Cells were passaged every 2-3 days by resuspending in medium and seeding them to appropriate confluence. Membranes were prepared from transiently transfected HEK293T cells. One day prior to transfection 10^7 cells were seeded in a 15 cm petri dish. Cells were transfected by the addition of a 3:1 mixture of polyethyleneimine (60 µg) and plasmid DNA (20 µg) in 2 mL serum free medium. The medium was refreshed after 24h, and after 72h the cells were harvested by suspending them in 20 mL medium. The suspension was centrifuged for 10 min at 1000 rpm, and the supernatant was removed. The cell pellet was stored at -80 ^{o}C until use.

Cell pellets were thawed on ice and suspended in lysis buffer A (20 mM HEPES, 2 mM DTT, 0.25 M sucrose, 1 mM $MgCl_2$, 1x Cocktail (Roche complete EDTA free), 25 U/mL benzonase). The suspension was homogenized by polytrone (3 × 7 sec) and incubated for 30 min on ice. The suspension was subjected to ultracentrifugation

(93,000 × g, 30 min, 4 ^{o}C, Beckman Coulter, Type Ti70 rotor) to yield the cytosolic fraction in the supernatant and the membrane fraction as a pellet. The pellet was resuspended in lysis buffer B (20 mM HEPES, 2 mM DTT, 1x Cocktail (Roche cOmplete EDTA free)). The protein concentration was determined with Quick Start Bradford reagent (BioRad) or QubitTM fluorometric quantitation (Life Technologies). The protein fractions were diluted to a total protein concentration of 1 mg/mL and stored in small aliquots at -80 ^{o}C until use.

Biochemical DAGL activity assay

The biochemical hDAGLα assay was performed as reported previously.[10] In brief, the biochemical hDAGLα activity assay is based on the hydrolysis of para-nitrophenylbutyrate (PNP-butyrate) by membrane preparations from HEK293T cells transiently transfected with hDAGLα. Reactions were performed in 50 mM pH 7.2 HEPES buffer with 0.05 µg/µL final protein concentration hDAGLα transfected protein.

Natural substrate based fluorescence assay (DAGLα and ABHD6)

The natural substrate assay was performed as reported previously.[11,19] Standard assay conditions: 0.2 U/mL glycerol kinase (GK), glycerol-3-phosphate oxidase (GPO) and horseradish peroxidase (HRP), 0.125 mM ATP, 10 µM Amplifu™Red, 5% DMSO in a total volume of 200 µL. For ABHD6, the assay additionally contained 25 µM 2-AG and 0.5% acetonitrile, with a final protein concentration of 40 µg/mL. For DAGLα, the assay additionally contained 5 µg/mL MAGL-overexpressing membranes, 100 µM SAG and 0.0075% (w/v) Triton X-100, with a final protein concentration of 50 µg/mL.

Preparation of mouse brain membrane proteome

Mouse brain membrane proteome preparation was performed as previously reported.[15] In brief, mouse brains were isolated according to guidelines approved by the ethical committee of Leiden University (DEC#10095). Mouse brains were Dounce homogenized in pH 7.2 lysis buffer A (20 mM HEPES pH 7.2, 2 mM DTT, 1 mM $MgCl_2$, 25 U/mL Benzonase) and incubated for 5 min on ice, followed by low speed spin (2,500 × g, 3 min, 4 ^{o}C) to remove debris. The supernatant was subjected to ultracentrifugation (100,000 × g, 45 min, 4 ^{o}C, Beckman Coulter, Type Ti70 rotor) to yield the cytosolic fraction in the supernatant and the membrane fraction as a pellet. The pellet was resuspended in storage buffer B (20 mM HEPES pH 7.2, 2 mM DTT). The total protein concentration was determined with Quick Start Bradford reagent (Bio-Rad) or QubitTM fluorometric quantitation (Life Technologies). Membranes and supernatant were flash frozen in liquid nitrogen and stored in aliquots at -80 ^{o}C until use.

Activity based protein profiling in mouse brain

Mouse brain proteome (2 mg/mL, 19.5 µL) was incubated with DMSO or inhibitor in 0.5 µL DMSO for 30 min at r.t. and subsequently incubated with 250 nM (final

concentration) ABP MB064, or 500 nM (final concentration) ABP TAMRA-FP for 20 min at r.t. before the reaction was quenched with standard 3x Laemmli sample buffer. The gels were scanned using a ChemiDoc MP system and analyzed using Image Lab 4.1.

ABPP inhibitor activity measurements

The percentage of activity remaining was determined by measuring the integrated optical intensity of the fluorescent protein bands using Image Lab 4.1. The relative intensity was compared to the vehicle-treated proteins, which were set to 100%. IC_{50} values were determined by plotting a log (inhibitor) vs. normalized response (Variable slope) dose-response curve generated using Prism software (Graphpad Prism 5.0).

Synthesis

General Remarks. Reagents were purchased from Sigma Aldrich, Acros or Merck and used without further purification unless noted otherwise. Some reactions were performed using oven or flame-dried glassware and dry solvents. All moisture sensitive reactions were performed under an argon atmosphere. Traces of water were removed from starting compounds by co-evaporation with toluene.

^{1}H- and ^{13}C-NMR spectra were recorded on a Bruker AV 400 MHz spectrometer at 400 (^{1}H) and 101 (^{13}C) MHz, or on a Bruker DMX-600 spectrometer 600 (^{1}H) and 150 (^{13}C) MHz using $CDCl_3$, CD_3OD or $(CD_3)_2SO$ as solvent, unless stated otherwise. Chemical shift values are reported in ppm with tetramethylsilane or solvent resonance as the internal standard ($CDCl_3$, δ 7.26 for ^{1}H, δ 77.16 for ^{13}C; CD_3OD, δ 3.31 for ^{1}H, δ 49.00 for ^{13}C; $(CD_3)_2SO$, δ 2.50 for ^{1}H, δ 39.52 for ^{13}C). Data are reported as follows: chemical shifts (δ), multiplicity (s = singlet, d = doublet, dd = double doublet, td = triple doublet, t = triplet, q = quartet, m = multiplet, br = broad), coupling constants *J* (Hz), and integration. High-resolution mass spectra (HRMS) were recorded by direct injection (2 µL of a 2 µM solution in water/acetonitrile 50/50 (v/v) and 0.1% formic acid) on a mass spectrometer (Thermo Finnigan LTQ orbitrap) equipped with an electrospray ion source in positive mode (source voltage 3.5 kV, sheath gas flow 10, capillary temperature 250 ^{o}C) with resolution R = 60,000 at m/z 400 (mass range m/z = 150-2,000) and dioctylphthalate (m/z = 391.28428) as a “lock mass”. The high resolution mass spectrometer was calibrated prior to measurements with a calibration mixture (Thermo Finnigan). LC-MS analysis was performed on a Finnigan Surveyor HPLC system with a Gemmi C_{18} 50x4.60 mm column (detection at 200-600 nm), coupled to a Finnigan LCQ Adantage Max mass spectrometer with ESI. The applied buffers were H_2O, MeCN and 1.0% TFA in H_2O (0.1% TFA end concentration). HPLC purification was performed on a preparative LC-MS system (Agilent 1200 series) with an Agilent 6130 Quadruple MS detector. IR spectra were recorded on a Shimadzu FTIR-8300 and are reported in cm^{-1}. Optical rotations were measured on a Propol automatic polarimeter (Sodium D-line, λ = 589 nm). Flash chromatography was performed using SiliCycle silica gel type SilicaFlash P60 (230 – 400 mesh). TLC

analysis was performed on Merck silica gel 60/Kieselguhr F254, 0.25 mm. Compounds were visualized using either Seebach's reagent (a mixture of phosphomolybdic acid (25 g), cerium (IV) sulfate (7.5 g), H_2O (500 mL) and H_2SO_4 (25 mL)) or a $KMnO_4$ stain (K_2CO_3 (40 g), $KMnO_4$ (6 g), H_2O (600 mL) and 10% NaOH (5 mL)).

Analysis of Compound Purity by LC/MS. Compound purity was determined by an LCQ Adventage Max (Thermo Finnigan) ion-trap spectrometer (ESI+) coupled to a Surveyor HPLC system (Thermo Finnigan) equipped with a C_{18} (Gemini, 4.6 mm x 50 mm, 3 µm particle size, Phenomenex) equipped with buffer A: H_2O, B: acetonitrile (MeCN) and C: 1% aqueous TFA. All final compounds were determined to be above 95% pure by this method.

(4-([1,1'-Biphenyl]-4-yl)-1*H*-1,2,3-triazol-1-yl)(2-benzylpiperidin-1-yl)methanone (1, KT109). A solution of 2-benzylpiperidine (90.0 mg, 0.513 mmol) in THF was treated with DIPEA (0.269 mL, 1.54 mmol) and bis(trichloromethyl) carbonate (76.0 mg, 0.257 mmol) and the reaction mixture was stirred for 30 min at 0 ^oC. After that the reaction mixture was poured into water and extracted with ethyl acetate (3 x 10 mL).The organic layer was washed with water, brine and dried over $MgSO_4$, filtered, and concentrated under reduced pressure. The intermediate was dissolved in THF and DIPEA (0.269 mL, 1.54 mmol), DMAP (62.7 mg, 0.513 mmol) and 4-([1,1'-biphenyl]-4-yl) -1*H*-1,2,3-triazole (125 mg, 0.565 mmol) were added to the solution. The mixture was stirred for 2h at 60 ^oC and poured into saturated aqueous NH_4Cl solution (20 mL). The mixture was extracted with ethyl acetate (3 x 20 mL), washed with water, brine, dried over $MgSO_4$ and filtered. The solvents are removed under reduced pressure to yield the crude triazole urea as a mixture of N1- and N2-carbamoylated regioisomers. The N1-carbamoyl triazole was isolated by silica gel chromatography (pentane/EtOAc 100:1 → 5:1) to afford KT109 (**1**) (99.0 mg, 0.234 mmol, 46% yield). LC-MS m/z: calculated for $C_{27}H_{26}N_4O$ $[M+H]^+$ 423.22, found: 423.04. ^1H NMR (400 MHz, $CDCl_3$) δ 7.87 (br s, 2H), 7.74 – 7.60 (m, 4H), 7.47 (t, *J* = 7.5 Hz, 2H), 7.42 – 7.34 (m, 1H), 7.22 (br s, 4H), 7.01 (br s, 1H), 4.86 (br s, 1H), 4.37 (br d, *J* = 13.6 Hz, 1H), 3.43 – 3.18 (m, 2H), 2.70 (br s, 1H), 2.07 – 1.67 (m, 6H).

(2-Ethylpiperidin-1-yl)(4-(hydroxydiphenylmethyl)-2*H*-1,2,3-triazol-2-yl)methanone (2, ML226). The title compound was synthesized from 2-ethylpiperidine (0.057 mL, 0.430 mmol) and diphenyl(1*H*-1,2,3-triazol-4-yl)methanol (90.0 mg, 0.358 mmol) according to the procedures described for compound **1**. The N2-carbamoyl triazole was isolated by silica gel chromatography (pentane/EtOAc 100:1 → 5:1) to afford 2,4-triazole urea ML226 (76.0 mg, 0.195 mmol, 54% yield). LC-MS m/z: calculated for $C_{23}H_{26}N_4O_2$ $[M+H]^+$ 391.49, found: 391.14. ^1H NMR (400 MHz, $CDCl_3$) δ 7.56 (s, 1H), 7.39 – 7.24 (m, 10H), 4.22 (br s, 1H), 3.98 – 3.03 (m, 3H), 1.84 – 1.50 (m, 8H), 1.11 – 0.58 (m, 3H).

(2-Benzylpiperidin-1-yl)(4-(hydroxydiphenylmethyl)-1*H*-1,2,3-triazol-1-yl)methanone (3). A solution of 2-benzylpiperidine (50.0 mg, 0.285 mmol) in THF (4 mL) was

treated with DIPEA (0.249 mL, 1.426 mmol) and bis(trichloromethyl) carbonate (42.3 mg, 0.143 mmol) and the reaction mixture was stirred for 30 min at 0 °C. The mixture was poured into water and extracted with ethyl acetate (3 x 20 mL). The organic layer was washed with water, brine, dried over $MgSO_4$, filtered and concentrated under reduced pressure. The intermediate was dissolved in a mixture of THF (8 mL) and DIPEA (0.249 mL, 1.426 mmol), DMAP (34.9 mg, 0.285 mmol) and diphenyl(1H-1,2,3-triazol-4-yl)methanol (71.7 mg, 0.285 mmol) were added to the solution. The mixture was stirred for two hours at 60 °C and poured into a saturated aqueous NH_4Cl solution. The mixture was extracted with ethyl acetate (3 x 20 mL), washed with water, brine, dried over $MgSO_4$ and filtered. The solvents were removed under reduced pressure to yield the crude triazole urea as a mixture of N1- and N2-carbamoylated regioisomers. The N1-carbamoyl triazole was isolated by silica gel chromatography (pentane/EtOAc 100:1 → 5:1) to afford 1,4-triazole urea **3** (29.7 mg, 0.066 mmol, 23% yield). HRMS [ESI+] m/z: calculated for $C_{28}H_{28}N_4O_2$ $[M+H]^+$ 453.2285, found: 453.2283. ^{1}H NMR (400 MHz, $CDCl_3$) δ 7.39 – 7.27 (m, 10H), 7.04 – 6.82 (m, 5H), 4.76 (s, 1H), 4.28 (br s, 1H), 3.71 (br s, 1H), 3.33 – 3.21 (m, 2H), 2.63 (br s, 1H), 2.00 – 1.66 (m, 6H). ^{13}C NMR (101 MHz, $CDCl_3$) δ 145.28, 137.90, 129.03, 128.78, 128.18, 127.76, 127.29, 127.23, 127.22, 126.80, 123.76, 69.63, 57.47, 40.46, 36.50, 29.18, 25.32, 18.75.

(2-Benzylpiperidin-1-yl)(4-(hydroxydiphenylmethyl)-2*H*-1,2,3-triazol-2-yl)methanone (4). The title compound was isolated from the mixture of compound **3**. The N2-carbamoyl triazole regioisomer was purified by silica gel chromatography (pentane/EtOAc 100:1 → 5:1) to afford 2,4-triazole urea **4** (39.0 mg, 0.086 mmol, 30% yield). HRMS [ESI+] m/z: calculated for $C_{28}H_{28}N_4O_2$ $[M+H]^+$ 453.2285, found: 453.2284. ^{1}H NMR (400 MHz, $CDCl_3$) δ 7.52 (s, 1H), 7.35 – 7.27 (m, 10H), 7.22 – 6.97 (m, 5H), 4.75 – 4.17 (m, 1H), 3.68 (br s, 1H), 3.26 – 3.19 (m, 1H), 3.10 – 3.15 (m, 1H), 2.93 (br s, 1H), 1.79 – 1.60 (m, 6H). ^{13}C NMR (101 MHz, $CDCl_3$) δ 155.48, 149.55, 145.04, 137.91, 135.14, 129.07, 128.64, 128.21, 127.84, 127.22, 126.64, 69.61, 53.28, 42.44, 36.31, 26.05, 25.24, 18.71.

(4-([1,1'-Biphenyl]-4-yl)-1*H*-1,2,3-triazol-1-yl)(2-ethylpiperidin-1-yl)methanone (5). The title compound was synthesized from 2-ethylpiperidine (0.059 mL, 0.442 mmol) and 4-([1,1'-biphenyl]-4-yl)-1H-1,2,3-triazole (98.0 mg, 0.442 mmol) according to the procedures described for compound **3**. The N1-carbamoyl triazole was isolated by silica gel chromatography (pentane/EtOAc 100:1 → 5:1) to afford 1,4-triazole urea **5** (48.0 mg, 0.133 mmol, 30% yield). HRMS [ESI+] m/z: calculated for $C_{22}H_{24}N_4O$ $[M+H]^+$ 361.2023, found: 361.2022. ^{1}H NMR (400 MHz, $CDCl_3$) δ 8.35 (s, 1H), 7.95 (d, *J* = 8.4 Hz, 2H), 7.69 (d, *J* = 8.4 Hz, 2H), 7.66 – 7.61 (m, 2H), 7.47 – 7.44 (m, 2H), 7.38 -7.34 (m, 1H), 4.55 (q, *J* = 6.6 Hz, 1H), 4.29 (br d, *J* = 13.4 Hz, 1H), 3.20 (br s, 1H), 1.87 – 1.66 (m, 8H), 0.94 (s, 3H). ^{13}C NMR (101 MHz, $CDCl_3$) δ 146.54, 141.42, 140.52, 128.93, 128.71, 127.70, 127.63, 127.08, 126.35, 120.95, 55.26, 53.87, 42.83, 28.15, 25.74, 22.60, 18.86, 10.70.

(4-([1,1'-Biphenyl]-4-yl)-2*H*-1,2,3-triazol-2-yl)(2-ethylpiperidin-1-yl)methanone (6).

The title compound was isolated from the mixture of compound **5**. The N2-carbamoyl triazole regioisomer was isolated by silica gel chromatography (pentane/EtOAc 100:1 → 5:1) to afford 2,4-triazole urea **6** (36.0 mg, 0.100 mmol, 23% yield). HRMS [ESI+] m/z: calculated for $C_{22}H_{24}N_4O$ $[M+H]^+$ 361.2023, found: 361.2024. ^{1}H NMR (400 MHz, $CDCl_3$) δ 8.08 (s, 1H), 7.94 (d, *J* = 8.3 Hz, 2H), 7.69 (d, *J* = 8.3 Hz, 2H), 7.63 (d, *J* = 7.7 Hz, 2H), 7.46 (t, *J* = 7.6 Hz, 2H), 7.38 (t, *J* = 7.5 Hz, 1H), 4.26 (br s, 2H), 3.16 (br s, 1H), 1.88 – 1.63 (m, 8H), 0.96 (s, 3H). ^{13}C NMR (101 MHz, $CDCl_3$) δ 148.64, 142.12, 140.36, 132.95, 128.96, 128.25, 127.77, 127.70, 127.10, 126.90, 53.85, 43.21, 42.24, 28.01, 25.94, 22.78, 18.93, 10.76.

(2-Benzylpiperidin-1-yl)(4-(dicyclohexyl(hydroxy)methyl)-2*H*-1,2,3-triazol-2-yl)methanone (7). The title compound was synthesized from 2-benzylpiperidine (73.6 mg, 0.42 mmol) and dicyclohexyl(2*H*-1,2,3-triazol-4-yl) methanol (122 mg, 0.462 mmol). According to the procedures described for compound **3**. The N2-carbamoyl triazole was isolated by silica gel chromatography (pentane/EtOAc 100:1 → 5:1) to afford 2,4-triazole urea **7** (31.0 mg, 0.067 mmol, 16% yield). HRMS [ESI+] m/z: calculated for $C_{28}H_{40}N_4O_2$ $[M+H^+]$ 465.3224, found: 465.3221. ^{1}H NMR (400 MHz, $CDCl_3$) δ 7.59 (s, 1H), 7.37 – 7.04 (m, 5H), 4.59 (br s, 1H), 3.81 – 3.68 (m, 1H), 3.28 (td, *J* = 13.3, 2.9 Hz, 1H), 3.10 (dd, *J* = 13.3, 6.4 Hz, 1H), 2.99 (t, *J* = 11.6 Hz, 1H), 1.93 – 1.59 (m, 16H), 1.45 – 1.34 (m, 2H), 1.27 – 1.15 (m, 4H), 1.10 – 0.98 (m, 4H), 0.84 – 0.72 (m, 2H). ^{13}C NMR (101 MHz, $CDCl_3$) δ 153.64, 149.83, 137.99, 134.24, 129.10, 128.60, 126.64, 78.22, 67.99, 43.88, 42.45, 36.10, 29.71, 27.22, 26.52, 26.42, 26.21, 25.46, 18.78.

(2-Benzylpiperidin-1-yl)(4-(1-hydroxycyclohexyl)-2*H*-1,2,3-triazol-2-yl)methanone (8). The title compound was synthesized from 2-benzylpiperidine (88.0 mg, 0.500 mmol) and 1-(2*H*-1,2,3-triazol-4-yl)cyclohexan-1-ol (92 mg, 0.550 mmol). According to the procedures described for compound **3**. The N2-carbamoyl triazole was isolated by silica gel chromatography (pentane/EtOAc 100:1 → 5:1) to afford 2,4-triazole urea **8** (61.0 mg, 0.17 mmol, 34% yield). HRMS [ESI+] m/z: calculated for $C_{21}H_{28}N_4O_2$ $[M+H^+]$ 369.2285, found: 369.2288. ^{1}H NMR (400 MHz, $CDCl_3$) δ 7.76 (s, 1H), 7.36 – 7.09 (m, 5H), 4.63 (br s, 1H), 4.14 (br s, 1H), 3.29 (td, *J* = 13.2, 2.9 Hz, 1H), 3.16 (dd, *J* = 13.3, 6.1 Hz, 1H), 3.06 – 2.98 (m, 1H), 2.29 (br s, 1H), 2.02 – 1.55 (m, 16H), 1.45 – 1.33 (m, 1H). ^{13}C NMR (101 MHz, $CDCl_3$) δ 157.07, 149.78, 138.07, 132.99, 129.11, 128.59, 126.61, 69.77, 53.47, 42.23, 38.01, 36.04, 26.62, 25.47, 25.25, 21.79, 18.78.

(2-Benzylpiperidin-1-yl)(4-(1-hydroxy-1-phenylethyl)-2*H*-1,2,3-triazol-2-yl)methanone (9). The title compound was synthesized from 2-benzylpiperidine (88.0 mg, 0.500 mmol) and 1-phenyl-1-(1*H*-1,2,3-triazol-4-yl)ethan-1-ol (104 mg, 0.550 mmol) according to the procedures described for compound **3**. The N2-carbamoyl triazole was isolated by silica gel chromatography (pentane/EtOAc 100:1 → 5:1) to afford 2,4-triazole urea **9** (25.0 mg, 0.064 mmol, 13% yield). HRMS [ESI+] m/z: calculated for $C_{23}H_{26}N_4O_2$ $[M+H^+]$ 391.2129, found: 391.2131. ^{1}H NMR (400 MHz, $CDCl_3$) δ 7.66 (d, *J* = 3.5 Hz, 1H), 7.53 – 7.46 (m, 2H), 7.42 – 7.34 (m, 2H), 7.34 – 7.30 (m, 1H), 7.29 – 7.17 (m, 5H), 4.76 – 4.31 (m, 2H), 3.30 (td, *J* = 13.4, 2.8 Hz, 1H), 3.15 (dd, *J* = 13.3,

6.2 Hz, 1H), 3.08 – 2.95 (m, 1H), 2.86 (br s, 1H), 2.02 (d, *J* = 2.5 Hz, 3H), 1.90 – 1.57 (m, 6H). ^{13}C NMR (101 MHz, $CDCl_3$) δ 145.82, 138.03, 133.69, 129.12, 128.66, 128.45, 127.57, 126.67, 125.15, 72.39, 63.05, 35.57, 30.64, 25.48, 18.81.

(2-Benzylpiperidin-1-yl)(4-(2-hydroxypropan-2-yl)-2*H*-1,2,3-triazol-2-yl)methanone (10). The title compound was synthesized from 2-benzylpiperidine (88.0 mg, 0.500 mmol) and 2-(2*H*-1,2,3-triazol-4-yl)propan-2-ol (69.9 mg, 0.550 mmol) according to the procedures described for compound **3**. The N2-carbamoyl triazole was isolated by silica gel chromatography (pentane/EtOAc 100:1 → 5:1) to afford 2,4-triazole urea **10** (17.0 mg, 0.052 mmol, 11% yield). HRMS [ESI+] m/z: calculated for $C_{18}H_{24}N_4O_2$ $[M+H^+]$ 329.1972, found: 329.1971. ^{1}H NMR (400 MHz, $CDCl_3$) δ 7.76 (s, 1H), 7.43 – 6.95 (m, 5H), 4.65 (br s, 1H), 4.37 – 3.94 (m, 1H), 3.49 (br s, 1H), 3.30 (td, *J* = 13.3, 2.8 Hz, 1H), 3.16 (br s, 1H), 3.06 – 2.98 (m, 1H), 1.89 – 1.61 (m, 12H). ^{13}C NMR (101 MHz, $CDCl_3$) δ 157.12, 149.78, 138.03, 132.74, 129.09, 128.62, 126.57, 68.82, 55.06, 42.43, 36.02, 30.31, 25.42, 18.83.

(2-Benzylpiperidin-1-yl)(4-(hydroxydi(pyridin-2-yl)methyl)-2*H*-1,2,3-triazol-2-yl)methanone (11). The title compound was synthesized from 2-benzylpiperidine (59.6 mg, 0.340 mmol) and di(pyridin-2-yl)(1*H*-1,2,3-triazol-4-yl)methanol (95.0 mg, 0.374 mmol) according to the procedures described for compound **3**. The N2-carbamoyl triazole was isolated by silica gel chromatography (pentane/EtOAc 100:1 → 5:1) to afford 2,4-triazole urea **11** (30 mg, 0.066 mmol, 19% yield). HRMS [ESI+] m/z: calculated for $C_{26}H_{26}N_6O_2$ $[M+H]^+$ 455.2190, found: 455.2186. ^{1}H NMR (400 MHz, $CDCl_3$) δ 8.66 (br d, *J* = 4.4 Hz, 2H), 8.43 (br s, 2H), 8.02 – 7.90 (m, 4H), 7.48 – 7.45 (m, 2H), 7.24 – 6.95 (m, 4H), 4.70 – 3.80 (m, 2H), 3.23 (td, *J* = 13.5, 2.6 Hz, 1H), 3.07 (dd, *J* = 13.1, 6.3 Hz, 1H), 2.96 (br s, 1H), 1.79 – 1.61 (m, 6H). ^{13}C NMR (101 MHz, $CDCl_3$) δ 158.82, 152.26, 149.47, 145.84, 140.26, 137.96, 135.16, 129.20, 128.68, 126.69, 124.42, 123.99, 76.10, 56.46, 45.37, 36.00, 25.57, 25.47, 18.79.

(2-Benzylpiperidin-1-yl)(4-(bis(4-fluorophenyl)(hydroxy)methyl)-2*H*-1,2,3-triazol-2-yl)methanone (12). The title compound was synthesized from 2-benzylpiperidine (100 mg, 0.571 mmol) and bis(4-fluorophenyl)(1*H*-1,2,3-triazol-4-yl)methanol (164 mg, 0.571 mmol) according to the procedures described for compound **3**. The N2-carbamoyl triazole was isolated by silica gel chromatography (pentane/EtOAc 100:1 → 5:1) to afford 2,4-triazole urea **12** (71.0 mg, 0.145 mmol, 26% yield). HRMS [ESI+] m/z: calculated for $C_{28}H_{26}F_2N_4O_2$ $[M+H]^+$ 489.2097, found: 489.2097. ^{1}H NMR (400 MHz, $CDCl_3$) δ 7.51 (s, 1H), 7.34 – 7.24 (m, 5H), 7.18 (br, 3H), 7.02 – 6.97 (m, 5H), 4.47 – 4.26 (m, 1H), 3.80 (br s, 1H), 3.28 – 3.21 (m, 1H), 3.08 (dd, *J* = 13.2, 6.5 Hz, 1H), 2.94 (br s, 1H), 1.77 – 1.63 (m, 6H). ^{13}C NMR (101 MHz, $CDCl_3$) δ 162.35 (d, *J* = 248.5 Hz), 155.29, 149.47, 140.84, 137.91, 134.89, 131.03, 129.08 (d, *J* = 8.1 Hz), 128.69, 126.75, 115.15 (d, *J* = 21.2 Hz), 76.50, 56.81, 43.26, 36.12, 25.56, 25.55, 18.88.

(2-Benzylpiperidin-1-yl)(4-(bis(4-fluorophenyl)(methoxy)methyl)-2*H*-1,2,3-triazol-2-yl)methanone (13). The title compound was synthesized from 2-benzylpiperidine

(50.8 mg, 0.290 mmol) and 4-(bis(4-fluorophenyl)(methoxy)methyl)-1H-1,2,3-triazole (96.0 mg, 0.319 mmol) according to the procedures described for compound **3**. The N2-carbamoyl triazole was isolated by silica gel chromatography (pentane/EtOAc 100:1 → 5:1) to afford 2,4-triazole urea **13** (13.0 mg, 0.025 mmol, 10% yield). HRMS [ESI+] m/z: calculated for $C_{29}H_{28}F_2N_4O_2$ $[M+Na]^+$ 525.2073, found: 525.2069. ^{1}H NMR (400 MHz, $CDCl_3$) δ 7.61 (s, 1H), 7.49 – 7.39 (m, 4H), 7.32 – 7.15 (m, 5H), 7.03 (td, *J* = 8.6, 1.5 Hz, 4H), 4.73 (br s, 1H), 4.39 (br s, 1H), 3.28 (td, *J* = 13.3, 2.9 Hz, 1H), 3.18 (s, 3H), 3.10 (dd, *J* = 13.2, 6.4 Hz, 1H), 3.04 – 2.94 (m, 1H), 1.85 – 1.56 (m, 6H). ^{13}C NMR (101 MHz, $CDCl_3$) δ 162.14 (d, *J* = 247.2 Hz), 152.51, 149.48, 138.30, 137.87, 135.89, 129.68 (d, *J* = 13.0 Hz), 129.11, 128.59, 126.63, 115.07 (d, *J* = 21.4 Hz), 81.60, 54.56, 52.45, 43.32, 36.21, 26.40, 25.42, 18.72.

(4-(Hydroxydiphenylmethyl)-2*H*-1,2,3-triazol-2-yl)(2-(phenoxymethyl)piperidin-1-yl)methanone (14). The title compound was synthesized from 2-(phenoxymethyl)piperidine (60.0 mg, 0.314 mmol) and diphenyl(1*H*-1,2,3-triazol-4-yl)methanol (87.0 mg, 0.345 mmol) according to the procedures described for compound **3**. The N2-carbamoyl triazole was isolated by silica gel chromatography (pentane/EtOAc 100:1 → 5:1) to afford 2,4-triazole urea **14** (36.7 mg, 0.078 mmol, 25 % yield). HRMS [ESI+] m/z: calculated for $C_{28}H_{28}N_4O_3$ $[M+H]^+$ 469.2234, found: 469.2233. ^{1}H NMR (400 MHz, $CDCl_3$) δ 7.56 (s, 1H), 7.34 – 7.21 (m, 12H), 6.94 (t, *J* = 7.4 Hz, 1H), 6.84 (br d, *J* = 8.0 Hz, 2H), 4.74 (br s, 1H), 4.26 – 4.22 (m, 1H), 4.06 (br s, 1H), 3.54 (br s, 1H), 3.15 (br s, 1H), 1.91 – 1.85 (m, 2H), 1.79 – 1.63 (m, 4H). ^{13}C NMR (101 MHz, $CDCl_3$) δ 158.33, 155.75, 150.53, 144.98, 135.39, 129.62, 128.27, 127.91, 127.26, 121.27, 114.70, 77.33, 65.77, 53.87, 41.89, 25.45, 25.11, 19.46.

(4-(Bis(4-fluorophenyl)(hydroxy)methyl)-2*H*-1,2,3-triazol-2-yl)(2-(phenoxymethyl) piperidin-1-yl)methanone (15). The title compound was synthesized from 2-(phenoxymethyl)piperidine (60.0 mg, 0.314 mmol) and bis(4-fluorophenyl)(1*H*-1,2,3-triazol-4-yl)methanol (99.0 mg, 0.345 mmol) according to the procedures described for compound **3**. The N2-carbamoyl triazole was isolated by silica gel chromatography (pentane/EtOAc 100:1 → 5:1) to afford 2,4-triazole urea **15** (71.0 mg, 0.141 mmol, 45% yield). HRMS [ESI+] m/z: calculated for $C_{28}H_{26}F_2N_4O_3$ $[M+H]^+$ 505.2046, found: 505.2046. ^{1}H NMR (400 MHz, $CDCl_3$) δ 7.55 (s, 1H), 7.30 – 7.21 (m, 6H), 6.98 – 6.92 (m, 5H), 6.82 (br d, *J* = 8.0 Hz, 2H), 4.70 (br s, 1H), 4.26 – 4.22 (m, 1H), 4.05 (br s, 1H), 3.76 (br s, 1H), 3.14 (br s, 1H), 1.93 – 1.59 (m, 6H). ^{13}C NMR (101 MHz, $CDCl_3$) δ 162.32 (d, *J* = 248.5 Hz), 158.25, 155.52, 150.42, 140.78 (d, *J* = 10.1 Hz), 135.11, 129.57, 129.10 (d, *J* = 9.1 Hz), 121.35, 115.13 (d, *J* = 21.2 Hz), 114.63, 76.51, 65.65, 53.83, 41.99, 25.45, 25.07, 19.42.

(2-((4-Fluorophenoxy)methyl)piperidin-1-yl)(4-(hydroxydiphenylmethyl)-2*H*-1,2,3 -triazol-2-yl)methanone (16). The title compound was synthesized from 2-((4-fluorophenoxy)methyl)piperidine (60.0 mg, 0.287 mmol) and diphenyl(1*H*-1,2,3-triazol-4-yl) methanol (79.0 mg, 0.315 mmol) according to the procedures described for compound **3**. The N2-carbamoyl triazole was isolated by

silica gel chromatography (pentane/EtOAc 100:1 → 5:1) to afford 2,4-triazole urea **16** (27.9 mg, 0.057 mmol, 20% yield). HRMS [ESI+] m/z: calculated for $C_{28}H_{27}FN_4O_3$ $[M+H]^+$ 487.2140, found: 487.2140. ^{1}H NMR (400 MHz, $CDCl_3$) δ 7.58 (s, 1H), 7.32 – 7.27 (m, 11H), 6.90 (t, *J* = 8.4 Hz, 2H), 6.77 (br s, 1H), 4.71 (br s, 1H), 4.28 – 4.13 (m, 1H), 4.01 (br s, 2H), 3.13 (br s, 1H), 1.91 – 1.85 (m, 2H), 1.75 – 1.64 (m, 4H). ^{13}C NMR (101 MHz, $CDCl_3$) δ 157.53 (d, *J* = 239.4 Hz), 155.83, 154.42, 150.56, 145.10, 135.41, 128.23, 127.87, 127.35 (d, *J* = 22.2 Hz), 115.99, 115.73 (d, *J* = 8.1 Hz), 77.28, 66.42, 53.87, 42.94, 25.36, 25.05, 19.42.

(4-(Bis(4-fluorophenyl)(hydroxy)methyl)-2*H*-1,2,3-triazol-2-yl)(2-((4-fluorophenoxy)methyl)piperidin-1-yl)methanone (17). The title compound was synthesized from 2-((4-fluorophenoxy)methyl)piperidine (60.0 mg, 0.287 mmol) and bis(4-fluorophenyl)(1*H*-1,2,3- triazol-4-yl)methanol (82.0 mg, 0.287 mmol) according to the procedures described for compound **3**. The N2-carbamoyl triazole was isolated by silica gel chromatography (pentane/EtOAc 100:1→5:1) to afford 2,4-triazole urea **17** (30.3 mg, 0.058 mmol, 20% yield). HRMS [ESI+] m/z: calculated for $C_{28}H_{25}F_3N_4O_3$ $[M+H]^+$ 523.1952, found: 523.1952. ^{1}H NMR (400 MHz, $CDCl_3$) δ 7.56 (s, 1H), 7.30 – 7.26 (m, 5H), 6.99 – 6.89 (m, 6H), 6.76 (br s, 1H), 4.69 (br s, 1H), 4.23 – 4.18 (m, 1H), 4.01 (br s, 2H), 3.79 (br s, 1H), 3.13 (t, *J* = 11.8 Hz, 1H), 1.88 – 1.65 (m, 6H). ^{13}C NMR (101 MHz, $CDCl_3$) δ 162.36 (d, *J* = 247.5 Hz), 157.59 (d, *J* = 240.4 Hz), 155.58, 154.41, 150.47, 140.8 (d, *J* = 9.0 Hz), 135.13, 129.08 (d, *J* = 8.1 Hz), 115.94 (d, *J* = 23.2 Hz), 115.71 (d, *J* = 8.1 Hz), 115.1 (d, *J* = 22.2 Hz), 76.54, 66.42, 53.07, 43.12, 25.39, 25.05, 19.42.

(4-(Bis(4-fluorophenyl)(hydroxy)methyl)-2*H*-1,2,3-triazol-2-yl)(2-(3-methoxybenzyl)piperidin-1-yl)methanone (18). The title compound was synthesized from 2-(3-methoxybenzyl)piperidine (130 mg, 0.634 mmol) and bis(4-fluorophenyl)(1*H*-1,2,3- triazol-4-yl)methanol (200 mg, 0.697 mmol) according to the procedures described for compound **3**. The N2-carbamoyl triazole was isolated by silica gel chromatography (pentane/EtOAc 100:1 → 5:1) to afford 2,4-triazole urea **18** (118 mg, 0.227 mmol, 36% yield). HRMS [ESI+] m/z: calculated for $C_{29}H_{28}F_2N_4O_3$ $[M+H]^+$ 519.2202, found: 519.2204. ^{1}H NMR (500 MHz, $CDCl_3$) δ 7.47 (s, 1H), 7.31 – 7.25 (m, 5H), 7.13 (br s, 1H), 7.04 – 6.98 (m, 5H), 6.72 (d, *J* = 8.0 Hz, 1H), 3.73 (s, 3H), 3.67 (br s, 1H), 3.49 (br s, 2H), 3.25 (t, *J* = 13.2 Hz, 1H), 3.07 (dd, *J* = 13.2, 6.7 Hz, 1H), 2.91 (br s, 1H), 1.82 – 1.57 (m, 6H). ^{13}C NMR (126 MHz, $CDCl_3$) δ 162.42 (d, *J* = 248.2 Hz), 159.78, 155.32, 149.57, 140.85, 139.46, 134.95, 129.72, 129.11 (d, *J* = 7.6 Hz), 121.49, 115.21 (d, *J* = 21.4 Hz), 112.48, 111.80, 76.51, 57.52, 55.27, 41.10, 36.24, 28.99, 25.51, 18.83.

(4-(Bis(4-fluorophenyl)(hydroxy)methyl)-2*H*-1,2,3-triazol-2-yl)(2-(4-methoxybenzyl)piperidin-1-yl)methanone (19). The title compound was synthesized from 2-(4-methoxybenzyl)piperidine (92 mg, 0.448 mmol) and bis(4-fluorophenyl)(1*H*-1,2,3-triazol-4-yl) methanol (142 mg, 0.493 mmol) according to the procedures described for compound **3**. The N2-carbamoyl triazole was isolated by silica gel chromatography (pentane/EtOAc 100:1 → 5:1) to afford 2,4-triazole urea **19**

(116 mg, 0.224 mmol, 30% yield). HRMS [ESI+] m/z: calculated for $C_{29}H_{28}F_2N_4O_3$ $[M+H]^+$ 519.2202, found: 519.2199. ^{1}H NMR (500 MHz, $CDCl_3$) δ 7.48 (s, 1H), 7.32 – 7.24 (m, 5H), 7.06 – 6.97 (m, 5H), 6.74 (br s, 2H), 4.37 (br s, 2H), 3.75 (s, 3H), 3.24 (td, *J* = 13.4, 2.6 Hz, 1H), 3.03 (dd, *J* = 13.5, 6.6 Hz, 1H), 2.89 (br s, 1H), 2.43 (br s, 1H), 1.86 – 1.57 (m, 6H).^{13}C NMR (126 MHz, $CDCl_3$) δ 162.47 (d, *J* = 248.2 Hz), 158.45, 155.27, 149.53, 140.85, 134.87, 130.11, 129.93, 129.14 (d, *J* = 7.56 Hz), 115.27 (d, *J* = 21.42 Hz), 114.17, 76.58, 55.33, 51.04, 40.78, 35.33, 26.24, 25.55, 18.83.

(*S,E*)-N-(1-Phenylbut-3-en-2-yl)pent-3-en-1-amine (25a). Under an argon atmosphere, a flame dried three necked reaction flask was charged with a solution of 3-pentene nitrile **24** (285 mg, 3.34 mmol) in dry diethyl ether. At -78 °C a 1.0 M solution of DIBAL-H (12 mL, 12 mmol) in toluene was added drop wise. The reaction was warmed slowly on the cooling bath until 0 °C in circa 2h. After re-cooling to -90 °C, dry MeOH (10 mL) was added at once. After 5 min followed by a solution of (*S*)-1-phenylbut-3-en-2-amine[15,17] **23a** (1.80 g, 12.2 mmol, e.e. = 99%) in MeOH (10 mL). The cooling bath was removed and the mixture stirred at room temperature for 6h. Subsequently, an excess of $NaBH_4$ (870 mg, 22.9 mmol) was added at 0 °C in two portions with a five minute interval. The reaction was left stirring on the ice bath and slowly warmed up to room temperature overnight. The reaction mixture was poured into 0.8 M aqueous NaOH solution (80 mL) and extracted with diethyl ether (3 x 30 mL). The organic layers were combined, washed with brine (20 mL), dried ($MgSO_4$), filtered and concentrated *in vacuo* to afford the crude product as an orange oil that was purified by silica gel column chromatography using pentane: EtOAc : TEA = 9 : 1 : 0 → 90 : 10 : 5 → 85 : 15 : 5 as the eluent to give the target compound (315 mg, 1.47 mmol, 44% yield). $[\alpha]_D^{23}$ = -9.2 (c = 1.0, $CHCl_3$). HRMS calculated for $C_{15}H_{21}N$ $[M+H]^+$ 202.1590; found: 202.1593. IR (film) 3063, 3026, 2967, 2918, 2818, 1495, 1554, 1111, 966, 918. ^{1}H NMR (400 MHz, $CDCl_3$) δ 7.35 – 7.25 (m, 2H), 7.20 (m, 3H), 5.65 (ddd, *J* = 16.9, 10.5, 8.1 Hz, 1H), 5.58 – 5.36 (m, 2H), 5.16 – 5.00 (m, 2H), 3.31 (m, 1H), 3.25 – 3.14 (m, 1H), 3.03 – 2.95 (m, 1H), 2.77 (d, *J* = 6.9 Hz, 2H), 1.64 (dd, *J* = 6.0, 1.2 Hz, 3H), 1.42 – 1.34 (m, 1H). ^{13}C NMR (101 MHz, $CDCl_3$) δ 140.65, 138.51, 129.38, 129.29, 128.31, 127.09, 126.25, 116.14, 62.27, 49.09, 42.45, 17.77.

***tert*-Butyl *(S,E)*-pent-3-en-1-yl(1-phenylbut-3-en-2-yl)carbamate (26a)**. The amine from above **25a** (315 mg, 1.47 mmol) was dissolved in a mixture of THF (20 mL) and Et_3N (1 mL). Boc_2O (450 mg, 2.06 mmol) was added and the reaction refluxed overnight. TLC analysis confirmed complete conversion of the amine and after evaporation of the solvents and silica gel column chromatography using pentane: EtOAc = 98 : 2 as the eluent afforded the Boc-protected amine (425 mg, 1.35 mmol, 92% yield). $[\alpha]_D^{22}$ = -58 (c =1.0, $CHCl_3$). HRMS calculated for $C_{20}H_{29}NO_2$ $[M+H]^+$: 316.2271; found: 316.2272. IR (film) 3029, 2980, 2936, 1690, 1456, 1396, 1371, 1308, 1256, 1211, 1169, 1117, 1069. ^{1}H NMR (400 MHz, $CDCl_3$) δ 7.96 – 6.77 (m, 5H), 5.96 (ddd, *J* = 16.6, 10.5, 6.0 Hz, 1H), 5.55 – 5.20 (m, *J* = 33.4 Hz, 2H), 5.17 – 5.07 (m, 2H), 4.48 (m, 1H), 3.41 – 2.69 (m, 4H), 2.38 – 1.92 (m, 2H), 1.62 (d, *J* = 6.1 Hz, 3H), 1.38 (s, 9H). ^{13}C NMR (101 MHz, $CDCl_3$) δ 155.09, 138.59, 137.32, 129.26, 129.20,

128.16, 128.11, 126.62, 126.13, 115.91, 79.16, 61.12, 45.76, 38.24, 33.12, 28.32, 17.93.

***tert*-Butyl *(S)*-6-benzyl-3,6-dihydropyridine-1(2H)-carboxylate (27a)**. The diene from above (425 mg, 1.35 mmol) was dissolved in DCM (10 mL) and purged with argon. After the addition of Grubb's 1st generation catalyst (42.0 mg, 0.050 mmol, 3.6 mol%) and refluxing overnight TLC analysis confirmed complete conversion. The solvent was evaporated and the crude product purified by silica gel column chromatography using pentane : EtOAc = 97 : 3 as the eluent to afford the title compound (252 mg, 0.920 mmol, 68% yield). $[\alpha]_D^{21}$ = +161 (c = 1.0, $CHCl_3$). HRMS calculated for $C_{17}H_{23}NO_2$ $[M+H]^+$: 274.1802; found: 274.1802. ^{1}H NMR (400 MHz, $CDCl_3$, 60 ^oC) δ 7.28 – 7.21 (m, 2H), 7.20 – 7.14 (m, 3H), 5.79 (dd, *J* = 10.3, 6.1 Hz, 1H), 5.54 (dt, *J* = 10.3, 3.3 Hz, 1H), 4.54 (s, 1H), 4.11 (s, 1H), 2.89 (dd, *J* = 13.0, 6.2 Hz, 1H), 2.83 – 2.67 (m, 2H), 2.15 (m, 1H), 1.88 (m, 1H), 1.39 (s, 9H). ^{13}C NMR (101 MHz, $CDCl_3$, 60 ^oC) δ 154.28, 138.23, 129.36, 128.10, 127.94, 126.06, 125.38, 79.17, 53.47, 40.20, 36.30, 28.29, 24.85.

(*R*)-2-Benzylpiperidine (28a). The compound from above **27a** (680 mg, 2.49 mmol) was dissolved in MeOH (10 mL) and an aqueous 6.0 M HCl solution (1 mL) and Pd/C-10% (24 mg) were added subsequently. The reaction was stirred overnight under a balloon of hydrogen. After filtering over a Whatman® filter and evaporation of the solvents, (*R*)-2-benzylpiperidine hydrochloride was obtained. The salt from above was dissolved in water (20 mL) and washed with EtOAc (2 x 10 mL). The water layer was basified with an aqueous 4.0 M NaOH solution (4 mL) and extracted with $CHCl_3$ (4 x 10 mL). The combined $CHCl_3$ layers were dried over Na_2SO_4, filtered and concentrated to give the crude material as a yellow oil that was purified by silica gel column chromatography (pentane : EtOAc : Et_3N = 80 : 15 : 5) to afford *(R)*-2-benzylpiperidine (306 mg, 1.75 mmol, 70%). $[\alpha]_D^{23}$ = -13 (c = 0.5, $CHCl_3$). HRMS calculated for $C_{12}H_{17}N$ $[M+H]^+$ 176.1432; found: 176.1434. ^{1}H NMR (400 MHz, $CDCl_3$) δ 7.32 – 7.23 (m, 2H), 7.23 – 7.16 (m, 3H), 2.98 (d, *J* = 11.5 Hz, 1H), 2.74 – 2.62 (m, 2H), 2.61 – 2.44 (m, 2H), 1.89 – 1.72 (m, 2H), 1.68 (d, *J* = 12.7 Hz, 1H), 1.57 (d, *J* = 12.5 Hz, 1H), 1.43 (m, 1H), 1.36 – 1.13 (m, 2H). ^{13}C NMR (101 MHz, $CDCl_3$) δ 139.11, 129.12, 128.27, 126.06, 58.15, 47.05, 43.83, 32.83, 26.10, 24.77.

(*R*)-(4-([1,1'-Biphenyl]-4-yl)-1*H*-1,2,3-triazol-1-yl)(2-benzylpiperidin-1-yl)methanone (29a, *(R)*-KT109**)**. A solution of *(R)*-2-benzylpiperidine (40.0 mg, 0.229 mmol) in THF was treated with DIPEA (0.120 mL, 0.685 mmol) and bis(trichloromethyl) carbonate (33.9 mg, 0.114 mmol) and the reaction mixture was stirred for 30 min at 0 ^oC. The mixture was poured into water and extracted with ethyl acetate (3 times). The organic layer was washed with water, brine, dried over $MgSO_4$, and concentrated under reduced pressure. The intermediate was dissolved in THF and DIPEA (0.120 mL, 0.685 mmol), DMAP (27.9 mg, 0.228 mmol) and triazole (55.5 mg, 0.251 mmol) were added to the solution. The mixture was stirred for 2h at 60 ^oC and poured into saturated aqueous NH_4Cl solution. The mixture was extracted with ethyl acetate, washed with water, brine, dried over $MgSO_4$, and concentrated under reduced

pressure. The residue was purified by flush column chromatography (pentane/EtOAc = 100 : 1 → 8 : 1) to afford 1,4-triazole urea *(R)*-KT109 (24.0 mg, 0.057 mmol, 30% yield) as top TLC spot. $[\alpha]_D^{22}$ = -14 (*c* = 0.1, $CHCl_3$). The enantiomeric purity was determined on a Daicel Chiralcel OD-H column (4.6 X 250 mm, 20:80 IPA/Hex, flow rate of 1 mL/min): 14.4 min, e.e.>95%. HRMS calculated for $C_{27}H_{26}N_4O$ $[M+H]^+$ 423.2179, found: 423.2179. ^{1}H NMR ($CDCl_3$, 400 MHz) δ 7.90 (br s, 1H), 7.75 – 7.67 (m, 4H), 7.53 – 7.48 (m, 2H), 7.43 – 7.04 (m, 6H), 4.90 (br s, 1H), 4.40 (br d, *J* = 16.0 Hz, 1H), 3.39 – 3.26 (m, 2H), 2.74 (br s, 1H), 2.07 – 1.69 (m, 6H). ^{13}C NMR ($CDCl_3$, 101 MHz) δ 146.14, 141.28, 140.49, 137.99, 129.20, 128.88, 128.74, 128.64, 127.61, 127.57, 127.03, 126.63, 126.18, 120.56, 57.20, 40.80, 36.41, 29.65, 25.44, 18.75.

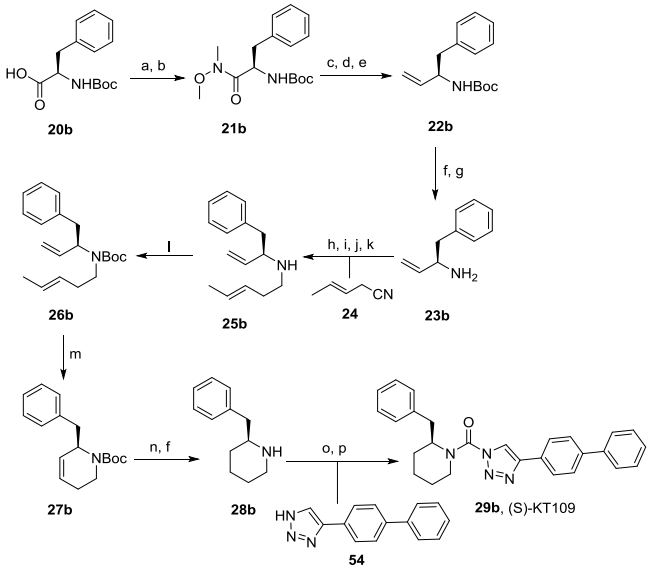

Scheme 3. Enantioselective synthesis of (*S*)-KT109Reagents and conditions: (a) Me(OMe)NH·HCl; (b) EDCI, NMM; (c) $LiAlH_4$; (d) H_3O^+; (e) $(Ph)_3P{=}CH_2$, 79% (**22b**, based on **20b**); (f) MeOH, HCl, 81% (**28b**); (g) NaOH; (h) compound **24**, diethyl ether, DIBAL-H, -80 °C to 0 °C, 64% (**25b**, based on **23b**); (i) MeOH, -90 °C; (j) corresponding amine **23b** (3 equiv), r.t., 20h; (k) $NaBH_4$, 0 °C to r.t., 5h; (l) Boc_2O, Et_3N, THF, 50 °C, 20h; (m) Grubbs I cat. 4 mol %, DCM, reflux, 48h, 25%; (n) H_2, Pd/C, MeOH; (o) DIPEA, Triphosgene, THF, 0 °C; (p) DIPEA, DMAP, triazole , THF, 60 °C, 33%.

(*R*)-1-phenylbut-3-en-2-amine (23b). Compound **22b** was prepared according the procedure reported [17] on 48 mmol scale, affording 9.40 g of compound **22b** (79%, $[\alpha]_D^{23}$ = -34 (*c* = 1.0, $CHCl_3$); Lit [17]: $[\alpha]_D^{25}$ = -37 (*c* = 0.28, $CHCl_3$)). The Boc-protetected amine **22b** (9.40 g, 38.1 mmol) was dissolved in a mixture of MeOH (100 mL) and aqueous 6.0 M HCl (20 mL). After TLC confirmed total conversion of compound **22b**, evaporation of the solvents afforded a white solid that was dissolved in water (50 mL). After addition of aqueous 8.0 M NaOH (10 mL), extraction with chloroform (4 x 30 mL), drying ($MgSO_4$), filtering and evaporation of the solvent, amine **23b** was obtained as a pale brown liquid that was used without further purification. $[\alpha]_D^{20}$ = -14 (*c* = 1.0,

$CHCl_3$); Lit[24] $[\alpha]_D^{25}$ = -15 (*c* = 1.0, $CHCl_3$). ^{1}H NMR (400 MHz, $CDCl_3$) δ 7.25 (m, 5H), 5.88 (ddd, *J* = 17.2, 10.3, 6.3 Hz, 1H), 5.13 (d, *J* = 17.2 Hz, 1H), 5.03 (d, *J* = 10.3 Hz, 1H), 3.59 (q, *J* = 6.3 Hz, 1H), 2.82 (dd, *J* = 13.3, 5.3 Hz, 1H), 2.61 (dd, *J* = 13.3, 8.3 Hz, 1H), 1.28 (br s, 2H). ^{13}C NMR (101 MHz, $CDCl_3$) δ 142.30, 138.65, 129.29, 128.28, 126.22, 113.52, 55.36, 44.23. For chiral HPLC analysis amine **23b** was derivatized as its benzoate, followed by analysis on a Daicel Chiralpak AD column (250 x 4.5 mm, 10µm particle size). Eluent hexane / 2-propanol = 90 /10, 1.0 mL / min., detection UV 254 nm. (*R*)-Enantiomer, R_t = 12.3 min (97.4%); (*S*)-enantiomer, R_t = 14.7 min (1.3%).

***tert*-Butyl *(R,E)*-pent-3-en-1-yl(1-phenylbut-3-en-2-yl)carbamate (26b)**. *(R,E)*-N-(1-Phenylbut -3-en-2-yl)pent-3-en-1-amine **25b** was prepared from 3-pentene nitrile **24** (586 mg, 7.23 mmol) and (*R*)-1-phenylbut-3-en-2-amine **23b** (e.e. = 97%, 3.50 g, 13.8 mmol) in 64% yield (1.24 g, ≈80% purity, 4.61 mmol) following the procedure as described for **25a**. This material was converted into Boc-protected compound **26b** as described for **26a**. The Boc-protected amine **26b** was obtained as colorless oil contaminated with circa 40 mol% Boc_2O (1.22 g). Analytical data from a pure sample: $[\alpha]_D^{22}$ = +66 (c =1.0 $CHCl_3$). HRMS calculated for $[C_{20}H_{29}NO_2+H]^+$: 316.2271; found: 316.2272. IR 2972, 2930, 1690, 1454, 1404, 1366, 1252, 1169, 1136, 966. ^{1}H NMR (400 MHz, $CDCl_3$) δ 7.33 – 7.15 (m, 5H), 5.96 (ddd, *J* = 16.7, 10.7, 6.0 Hz, 1H), 5.48 – 5.25 (m, 2H), 5.19 – 5.01 (m, 2H), 4.67 – 4.28 (m, 1H), 3.16 – 2.80 (m, 4H), 2.32 – 1.85 (m, 2H), 1.62 (d, *J* = 6.1 Hz, 3H), 1.38 (s, 9H). ^{13}C NMR (101 MHz, $CDCl_3$) δ 155.09, 138.61, 137.41, 129.27, 129.21, 128.18, 128.13, 126.63, 126.14, 115.92, 79.31, 77.32, 77.00, 76.68, 60.18, 45.80, 38.25, 28.34, 17.93.

***tert*-Butyl *(R)*-6-benzyl-3,6-dihydropyridine-1(2*H*)-carboxylate (27b)**. Prepared as described for **27a**. The Boc-protected diene from above (1.22 g, 3.87 mmol) afforded the title compound in 25% overall yield (491 mg, 1.80 mmol). $[\alpha]_D^{21}$ = -172 (c =1.0 $CHCl_3$). HRMS calculated for $C_{17}H_{23}NO_2$ $[M+H]^+$: 274.1802; found: 274.1803. IR 2974, 2926, 1690, 1454, 1416, 1391, 1364, 1337, 1279, 1250, 1171, 1107. ^{1}H NMR (400 MHz, $CDCl_3$) δ 7.38 – 7.08 (m, 5H), 5.81 (s, 1H), 5.63 – 5.48 (m, 1H), 4.68 – 4.42 (m, 1H), 4.33 – 3.94 (m, 1H), 2.99 – 2.82 (m, 1H), 2.84 – 2.67 (m, 2H), 2.19 (m, 1H), 2.02 – 1.83 (m, 1H), 1.36 (s, 9H). ^{13}C NMR (101 MHz, $CDCl_3$) δ 154.34, 138.25, 129.40, 128.22, 127.70, 126.15, 125.63, 79.33, 53.84, 40.27, 35.87, 28.29, 24.85.

(*S*)-2-Benzylpiperidine(28b). A solution of *tert*- butyl *(R)*-6-benzyl-3,6-dihydropyridine-1(2*H*) -carboxylate **27b** (277 mg, 1.01 mmol) in methanol (10 mL) and 6.0 M HCl (1 mL) was purged with argon and Pd/C 10% (100 mg) was added subsequently. The flask was sealed with a septum, placed under a balloon of hydrogen, and stirred vigorously overnight. The mixture was filtered over a Whatman® filter and the solvents evaporated to afford the hydrochloride as a white foam that was dissolved in methanol (1 mL) and loaded onto a flash silica gel column that was eluted subsequently with pentane/EtOAc/Et_3N = 97:3:0 → 9:1:0 → 85:10:5 → 75:20:5 to yield the target compound as a pale yellow oil (142 mg, 81%). $[\alpha]_D^{27}$ = +14 (c = 1.0, $CHCl_3$). HRMS calculated for $[C_{12}H_{17}N+H]^+$: 176.1434; found: 176.1433. IR

3026, 2928, 2851, 2799, 1495, 1452, 1441, 1331, 1319, 1119, 1053. ^{1}H NMR (400 MHz, $CDCl_3$) δ 7.32 – 7.25 (m, 2H), 7.20 (dt, *J* = 7.1, 2.9 Hz, 3H), 2.99 (ddt, *J* = 11.5, 3.9, 2.1 Hz, 1H), 2.76 – 2.63 (m, 2H), 2.63 – 2.46 (m, 1H), 2.04 (s, 1H), 1.83 – 1.74 (m, 1H), 1.68 (d, *J* = 12.7 Hz, 1H), 1.62 – 1.52 (m, 1H), 1.44 (qt, *J* = 12.2, 3.7 Hz, 1H), 1.37 – 1.13 (m, 2H). ^{13}C NMR (101 MHz, $CDCl_3$) δ 139.10, 129.14, 128.30, 126.08, 58.17, 47.03, 43.80, 32.79, 26.08, 24.76.

***(S)*-(4-([1,1'-Biphenyl]-4-yl)-1*H*-1,2,3-triazol-1-yl)(2-benzylpiperidin-1-yl)methano ne (29b**, (*S*)-KT109). The title compound was synthesized from (*S*)-2-benzylpiperidine **28b** (40.0 mg, 0.229 mmol) according to the procedures described for *(R)*-KT109. This yielded (*S*)-(4-([1,1'-biphenyl]-4-yl)-1H-1,2,3-triazol-1-yl)(2-benzylpiperidin-1-yl) methanone (*S*)-KT109 (66.0 mg, 0.156 mmol, 33 % yield). $[\alpha]_D^{22}$ = 13 (*c* = 1.0, $CHCl_3$). The enantiomeric purity was determined on a Daicel Chiralcel OD-H column (4.6 X 250 mm, 20:80 IPA/Hex, flow rate of 1 mL/min): 18.4 min, e.e.>95%. HRMS calculated for $C_{27}H_{27}N_4O$ $[M+H]^+$ 423.2179, found: 423.2179. ^{1}H NMR ($CDCl_3$, 400 MHz): δ 7.86 (s, 2H), 7.68 (d, *J* = 8.0 Hz, 2H), 7.63 (d, *J* = 4.0 Hz, 2H), 7.49 – 7.41 (m, 3H), 7.39 – 7.33 (m, 1H), 7.21 – 7.01 (m, 5H), 4.85 (s, 1H), 4.35 (d, *J* = 12.0 Hz, 1H), 3.35 (br d, *J* = 12.0 Hz, 1H), 3.21 (s, 1H), 2.69 (s, 1H), 1.93 – 1.69 (m, 6H). ^{13}C NMR ($CDCl_3$, 101 MHz) δ 146.13, 142.13, 141.37, 140.55, 138.05, 129.25, 128.94, 128.79, 128.74, 127.67, 127.62, 127.08, 126.68, 126.24, 120.61, 50.75, 40.28, 36.47, 28.67, 25.50, 19.08.

((*3R,6S*)-6-Benzyl-3-hydroxy-3,6-dihydropyridin-1(2H)-yl)(4-(bis(4-fluorophenyl)(hydroxy)methyl)-2*H*-1,2,3-triazol-2-yl)methanone (30). The title compound was synthesized from (*3R,6S*)-6-benzyl-3-((tert-butyldiphenylsilyl)oxy)-1,2,3,6-tetrahydropyridine (120 mg, 0.281 mmol) and bis(4-fluorophenyl)(1*H*-1,2,3-triazol-4-yl) methanol (89.0 mg, 0.309 mmol) according to the procedures described for compound **3**. The N2-carbamoyl triazole urea was isolated by silica gel chromatography (pentane/EtOAc 100:1 → 8:1). HF-pyridine (1.55 mL, 1.70 mmol) was subsequently added to a solution of N2-carbamoyl triazole urea in THF and pyridine (1:1) with ice cooling, and the reaction mixture was stirred overnight at room temperature. The mixture was diluted with ethyl acetate (40 eq.), and then washed with $NaHCO_3$, brine, dried with $MgSO_4$, and concentrated under reduced pressure. Purified by flash chromatography to furnish the title compound **30** (34.2 mg, 0.068 mmol, 24% yield for four steps). HRMS [ESI+] m/z: calculated for $C_{28}H_{24}F_2N_4O_3$ $[M+H]^+$ 503.1889, found: 503.1889. $[\alpha]_D^{20}$ = 245 (*c* = 0.1, $CHCl_3$). ^{1}H NMR (400 MHz, $CDCl_3$) δ 7.59 (s, 1H), 7.32 – 7.24 (m, 9H), 7.05 – 6.98 (m, 4H), 5.84 (br d, *J* = 10.4 Hz, 1H), 5.64 (br s, 1H), 4.79 (br s, 1H), 4.49 (br s, 1H), 3.25 (s, 4H), 2.95 (t, *J* = 8.0 Hz, 1H), 2.88 (br s, 1H). ^{13}C NMR (101 MHz, $CDCl_3$) δ 162.51 (d, *J* = 248.5 Hz), 156.03, 149.01, 140.63, 136.67, 135.68, 130.76, 129.54, 129.12 (d, *J* = 8.1 Hz), 128.77, 128.20, 127.10, 115.38 (d, *J* = 22.2 Hz), 76.65, 63.99, 55.62, 47.98, 38.94.

((*2R,5R*)-2-Benzyl-5-hydroxypiperidin-1-yl)(4-(bis(4-fluorophenyl)(hydroxy)meth yl)-2*H*-1,2,3-triazol-2-yl)methanone (31). The title compound was synthesized *(2R,5R)*-2-benzyl-5-((tert-butyldiphenylsilyl)oxy)piperidine (80.0 mg, 0.186 mmol),

bis(4-fluorophenyl)(1*H*-1,2,3-triazol-4-yl)methanol (58.8 mg, 0.205 mmol) and HF-pyridine (0.612 mL, 0.673 mmol) according to the procedures described for compound **30**. This furnished N2-carbamoyl triazole urea ((*2R,5R)*-2-benzyl-5-hydroxypiperidin-1-yl)(4-(bis(4-fluorophenyl) (hydroxy)methyl)-2*H*-1,2,3-triazol-2-yl)methanone **31** (13.6 mg, 0.027 mmol, 16% yield). $[\alpha]_D^{20}$ = 191 (*c* = 0.1, $CHCl_3$). HRMS [ESI+] m/z: calculated for $C_{28}H_{26}F_2N_4O_3$ $[M+H]^+$ 505.2046, found: 505.2046. ^{1}H NMR (400 MHz, $CDCl_3$) δ 7.52 (s, 1H), 7.34 – 7.16 (m, 9H), 7.07 – 6.98 (m, 4H), 4.57 (br s, 1H), 4.21 (br s, 1H), 3.88 – 3.80 (m, 1H), 3.16 – 3.02 (m, 2H), 2.98 – 2.89 (m, 1H), 2.35 (br s, 2H), 2.03 – 2.00 (m, 1H), 1.79 – 1.72 (m, 3H). ^{13}C NMR (214 MHz, $CDCl_3$) δ 162.50 (d, *J* = 248.2 Hz), 155.67, 149.43, 140.68, 137.62, 135.21, 131.07, 129.16 (d, *J* = 8.6 Hz), 128.86, 126.78, 115.34 (d, *J* = 21.4 Hz), 76.62, 67.08, 53.68, 45.66, 35.89, 28.59, 27.80.

((*3S,6S*)-6-Benzyl-3-hydroxy-3,6-dihydropyridin-1(2*H*)-yl)(4-(bis(4-fluorophenyl)(hydroxy)methyl)-2*H*-1,2,3-triazol-2-yl)methanone (32). The title compound was synthesized from *(3S,6S)*-6-benzyl-3-((tert-butyldiphenylsilyl)oxy)-1,2,3,6-tetrahydropyridine (80.0 mg, 0.187 mmol), bis(4-fluorophenyl)(2*H*-1,2,3-triazol-4-yl) methanol (59.1 mg, 0.206 mmol) and HF-pyridine (0.613 mL, 0.675 mmol) according to the procedures described for compound **30**. This furnished N2-carbamoyl triazole urea ((*3S,6S*)-6-benzyl-3-hydroxy-3,6-dihydropyridin-1(2*H*)-yl)(4- (bis(4-fluorophenyl) (hydroxy)methyl)-2*H*-1,2,3-triazol-2-yl)methanone **32** (13.9 mg, 0.028 mmol, 15% yield). $[\alpha]_D^{20}$ = 142 (*c* = 0.5, $CHCl_3$). HRMS [ESI+] m/z: calculated for $C_{28}H_{24}F_2N_4O_3$ $[M+H]^+$ 503.1889, found: 503.1888. ^{1}H NMR (400 MHz, $CDCl_3$) δ 7.58 (s, 1H), 7.45 – 7.19 (m, 9H), 7.04 – 7.00 (m, 4H), 6.03 – 5.99 (m, 1H), 5.82 (br s, 1H), 4.96 – 4.88 (m, 1H), 4.14 – 4.03 (m, 2H), 3.25 – 3.17 (m, 2H), 3.03 – 2.90 (m, 1H). ^{13}C NMR (101 MHz, $CDCl_3$) δ 162.50 (d, *J* = 248.5 Hz), 156.00, 149.43, 140.64, 136.46, 135.48, 130.05, 129.67, 129.13 (d, *J* = 8.1 Hz), 128.77, 127.12, 124.90, 115.38 (d, *J* = 22.2 Hz), 76.58, 62.51, 55.90, 48.00, 38.19.

((*2R,5S*)-2-Benzyl-5-hydroxypiperidin-1-yl)(4-(bis(4-fluorophenyl)(hydroxy)meth yl)-2*H*-1,2,3-triazol-2-yl)methanone (33). The title compound was synthesized (*2R,5S*)-2-benzyl-5- ((*tert*-butyldiphenylsilyl)oxy)piperidine (100 mg, 0.233 mmol), bis(4-fluorophenyl)(1*H*-1,2,3- triazol-4-yl)methanol (73.5 mg, 0.256 mmol) and HF-pyridine (2.45 mL, 2.69 mmol) according to the procedures described for compound **30**. This furnished N2-carbamoyl triazole urea **33** (18.3 mg, 0.036 mmol, 16% yield). $[\alpha]_D^{20}$ = 48 (*c* = 0.5, $CHCl_3$). HRMS [ESI+] m/z: calculated for $C_{28}H_{26}F_2N_4O_3$ $[M+H]^+$ 505.2046, found: 505.2045. ^{1}H NMR (600 MHz, $CDCl_3$) δ 7.72 (s, 1H), 7.33 – 7.31 (m, 6H), 7.03 – 6.99 (m, 7H), 4.65 (br s, 1H), 4.30 (br s, 1H), 3.54 (br s, 3H), 3.02 (br s, 2H), 1.57 – 1.32 (m, 5H). ^{13}C NMR (151 MHz, $CDCl_3$) δ 162.41 (d, *J* = 247.6 Hz), 152.82, 148.40, 140.91, 137.26, 133.37, 130.98, 129.13, 126.88, 124.21, 115. 22 (d, *J* = 21.1 Hz), 76.02, 51.09, 45.71, 41.81, 38.56, 37.57, 30.18, 27.42.

((*2R,5R*)-2-Benzyl-5-methoxypiperidin-1-yl)(4-(bis(4-fluorophenyl)(hydroxy)meth yl)-2*H*-1,2,3-triazol-2-yl)methanone (34). The title compound was synthesized

(2R,5R)-2-benzyl- 5-methoxypiperidine (100 mg, 0.487 mmol), bis(4-fluorophenyl)(1*H*-1,2,3- triazol-4-yl)methanol (154 mg, 0.536 mmol) according to the procedures described for compound **3**. The N2-carbamoyl triazole urea was isolated by silica gel chromatography (pentane/EtOAc 100:1 → 5:1) to afford 2,4-triazole urea **34** (70.7 mg, 0.136 mmol, 28% yield). $[\alpha]_D^{22}$ = -3.1 (*c* = 0.5, $CHCl_3$). HRMS [ESI+] m/z: calculated for $C_{29}H_{28}F_2N_4O_3$ $[M+H]^+$ 519.2202, found: 519.2203. ^{1}H NMR (400 MHz, $CDCl_3$) δ 7.53 (s, 1H), 7.32 – 7.19 (m, 9H), 7.04 – 6.92 (m, 4H), 4.84 – 3.93(m, 2H), 3.57 (br s, 1H), 3.50 – 3.33 (m, 3H), 3.25 (br s, 1H), 3.07 (br s, 1H), 3.03 – 2.92 (m, 2H), 2.05 (br s, 1H), 1.67 (br s, 3H). ^{13}C NMR (101 MHz, $CDCl_3$) δ 162.45 (d, *J* = 246.4 Hz), 155.75, 149.25, 140.68, 137.63, 135.27, 130.84, 129.05 (d, *J* = 8.1 Hz), 128.82, 126.93, 115.31 (d, *J* = 21.2 Hz), 76.58, 75.46, 56.35, 56.07, 46.52, 35.82, 25.59, 25.42.

((*2R,5R*)-2-Benzyl-5-(cyclopropylmethoxy)piperidin-1-yl)(4-(bis(4-fluorophenyl)(hydroxy)methyl)-2*H*-1,2,3-triazol-2-yl)methanone (35). The title compound was synthesized from *(2R,5R)*-2-benzyl-5-(cyclopropylmethoxy)piperidine (50.0 mg, 0.204 mmol) according to the procedures described for compound **3**. The N2-carbamoyl triazole urea was isolated by silica gel chromatography (pentane/EtOAc 100:1→5:1) to afford 2,4-triazole urea (*(2R,5R)*-2-benzyl-5-(cyclopropylmethoxy)piperidin-1-yl)(4-(bis(4-fluorophenyl)(hydroxy)methyl)-2*H*-1,2,3-triazol-2-yl)methanone **35** (25.0 mg, 0.045 mmol, 22% yield). $[\alpha]_D^{20}$ = 21.4 (*c* = 0.5, $CHCl_3$). HRMS calculated for $C_{32}H_{33}F_2N_4O_3$ $[M+H]^+$ 559.2515, found: 559.2516. ^{1}H NMR (400 MHz, $CDCl_3$) δ 7.52 (br s, 1H), 7.32 – 7.27 (m, 6H), 7.17 (br s, 2H), 7.05 – 6.99 (m, 4H), 6.90 (br s, 1H), 4.65 (br s, 1H), 4.38 – 4.02 (m, 1H), 3.50 – 3.42 (m, 3H), 3.19 – 2.90 (m, 3H), 2.02 (br s, 1H), 1.80 – 1.62 (m, 3H), 1.12 – 0.90 (m, 1H), 0.57 (br s, 2H), 0.28 – 0.08 (m, 2H). ^{13}C NMR (101 MHz, $CDCl_3$) δ 162.48 (d, *J* = 251.5 Hz), 155.54, 149.15, 140.73, 137.68, 135.15, 130.92, 129.43, 129.09 (d, *J* = 8.1 Hz), 128.82, 126.91, 115.30 (d, *J* = 21.2 Hz), 76.60, 73.80, 56.49, 46.94, 44.55, 35.63, 26.10, 24.65, 11.05, 3.24.

((*2R,5S*)-2-Benzyl-5-methoxypiperidin-1-yl)(4-(bis(4-fluorophenyl)(hydroxy)methyl)-2*H*-1,2,3-triazol-2-yl)methanone (36). The title compound was synthesized from *(2R,5S)*-2-benzyl-5-methoxypiperidine (20.0 mg, 0.097 mmol) according to the procedures described for compound **3**. The N2-carbamoyl triazole urea was isolated by silica gel chromatography (pentane/EtOAc 100:1→5:1) to afford 2,4-triazole urea (*(2R,5S)*-2-benzyl-5-methoxypiperidin-1-yl)(4-(bis(4-fluorophenyl)(hydroxy)methyl)-2*H*-1,2,3-triazol-2-yl)methanone **36** (13.1 mg, 0.025 mmol, 26% yield). $[\alpha]_D^{22}$ = -8.1 (*c* = 0.4, $CHCl_3$). HRMS [ESI+] m/z: calculated for $C_{29}H_{28}F_2N_4O_3$ $[M+H]^+$ 519.2202, found: 519.2202. ^{1}H NMR (400 MHz, $CDCl_3$) δ 7.48 (s, 1H), 7.33 – 7.19 (m, 8H), 7.05 – 6.94 (m, 5H), 4.87 – 4.28 (m, 2H), 3.65 – 2.87 (m, 6H), 2.72 (br s, 4H), 2.09 – 1.83 (m, 2H), 1.54 – 1.39 (m, 1H). ^{13}C NMR (101 MHz, $CDCl_3$) δ 162.44 (d, *J* = 251.5 Hz), 155.37, 149.24, 140.83, 137.80, 134.91, 130.01, 129.18 (d, *J* = 9.1 Hz), 128.79, 126.89, 115.18 (d, *J* = 21.2 Hz), 76.57, 73.10, 56.63, 56.46, 45.70, 35.95, 23.09, 21.09.

((*2R,5S*)-2-Benzyl-5-(cyclopropylmethoxy)piperidin-1-yl)(4-(bis(4-fluorophenyl)(hydroxy)methyl)-2*H*-1,2,3-triazol-2-yl)methanone (37). The title compound was

synthesized from *(2R,5S)*-2-benzyl-5-(cyclopropylmethoxy)piperidine (50.0 mg, 0.204 mmol) according to the procedures described for compound **3**. The N2-carbamoyl triazole urea was isolated by silica gel chromatography (pentane/EtOAc 100:1→5:1) to afford 2,4-triazole urea **37** (23.9 mg, 0.043 mmol, 21% yield). $[\alpha]_D^{22}$ = -16 (*c* = 0.3, $CHCl_3$). HRMS calculated for $C_{32}H_{33}F_2N_4O_3$ $[M+H]^+$ 559.2515, found: 559.2516. ^{1}H NMR (400 MHz, $CDCl_3$) δ 7.47 (s, 1H), 7.34 – 7.24 (m, 5H), 7.19 (s, 3H), 7.04 – 6.99 (m, 5H), 4.56 (br s, 2H), 3.65 (br s, 1H), 3.31 (br d, *J* = 18.0 Hz, 1H), 3.11 (dd, *J* = 13.4, 6.9 Hz, 2H), 2.99 – 2.88 (m, 1H), 2.80 (br s, 2H), 2.24 – 2.03 (m, 1H), 1.96 – 1.77 (m, 2H), 1.47 –137 (m, 1H), 0.88 – 0.83 (m, 1H), 0.44 (br s, 2H), 0.12 (br s, 2H). ^{13}C NMR (101 MHz, $CDCl_3$) δ 162.46 (d, *J* = 248.5 Hz), 155.27, 150.05, 140.72, 137.85, 134.83, 129.22, 129.18 (d, *J* = 8.1 Hz), 129.04, 128.77, 126.85, 115.29 (d, *J* = 21.2 Hz), 76.57, 72.97, 55.84, 45.20, 42.84, 36.01, 24.09, 21.31, 10.73, 3.23.

((2*R*,5*R*)-2-benzyl-5-(prop-2-yn-1-yloxy)piperidin-1-yl)(4-(bis(4-fluorophenyl)(hydroxy)methyl)-2*H*-1,2,3-triazol-2-yl)methanone (38, DH376). The title compound was synthesized from (2*R*,5*R*)-2-benzyl-5-(prop-2-yn-1-yloxy)piperidine (80 mg, 0.349 mmol) according to the procedures described for compound **3**. The N2-carbamoyl triazole urea was isolated by silica gel chromatography (pentane/EtOAc 100:1→5:1) to afford 2,4-triazole urea **38** (47.3 mg, 0.087 mmol, 25% yield) as lower TLC spot. $[\alpha]_D^{22}$ = -5.16 (*c* = 1.00, $CHCl_3$); HRMS(m/z):$[M+H]^+$ calcd. for $C_{31}H_{28}F_2N_4O_3$, 543.21575; found 543.21552. ^{1}H NMR (400 MHz, $(CD_3)_2SO$, 110 ^oC) δ 7.90 (s, 1H), 7.39 – 7.35 (m, 4H), 7.23 – 7.16 (m, 3H), 7.13 – 7.07 (m, 5H), 6.64 (br d, *J* = 4.0 Hz, 1H), 4.38 (br s, 1H), 4.16 (d, *J* = 2.4 Hz, 2H), 4.05 (br d, *J* = 12.0 Hz, 1H), 3.62 – 3.55 (m, 1H), 3.15 (br d, *J* = 4.0 Hz, 1H), 3.08 – 2.97 (m, 3H), 2.01 – 1.96 (m, 1H), 1.76 – 1.63 (m, 3H); ^{13}C NMR (101 MHz, $CDCl_3$, 60 ^oC) δ 162.57 (d, *J* = 247 Hz), 155.76, 149.37, 140.95 (d, *J* = 3.0 Hz), 137.67, 135.22, 129.96, 129.20 (d, *J* = 8.1 Hz), 128.83, 126.94, 115.28 (d, *J* = 22 Hz), 79.88, 76.69, 74.77, 73.61, 56.26, 55.17, 45.94, 36.10, 25.99, 25.88; IR (film)：3425, 2925, 1709, 1602, 1506, 1429, 1225, 1159, 1093 cm^{-1}.

(*3R,6S*)-6-Benzyl-3-((*tert*-butyldiphenylsilyl)oxy)-1,2,3,6-tetrahydropyridine (45). To a solution of *tert*-butyl (*3R,6S*)-6-benzyl-3-((*tert*-butyldiphenylsilyl)oxy)-3,6-dihydropyridine-1(2*H*)-carboxylate **44** [15] (120 mg, 0.227 mmol) in DCM was added 20% TFA, the reaction mixture was stirred at r.t. for 2.5h until TLC showed the reaction was completed. When the reaction is finished, the mixture was co-evaporated with toluene (3 times), the residue was diluted with ethyl acetate and washed with 10% Na_2CO_3, water, brine and dried over $MgSO_4$, and concentrated under reduced pressure. Filtering and concentration under reduced pressure afforded the crude product that was used without further purification. ^{1}H NMR (400 MHz, $CDCl_3$) δ 7.62 – 7.59 (m, 4H), 7.45 – 7.29 (m, 8H), 7.28 – 7.18 (m, 3H), 5.72 – 5.61 (m, 2H), 4.18 (br s, 1H), 4.09 (br s, 1H), 3.29 (br d, *J* = 31.9 Hz, 2H), 3.09 (br d, *J* = 48.0 Hz, 2H), 1.02 (s, 9H). ^{13}C NMR (101 MHz, $CDCl_3$) δ 135.86, 135.72, 134.10, 132.91, 132.42, 130.36, 130.24, 129.69, 129.12, 128.39, 128.11, 127.91, 127.74, 126.24, 61.00, 54.53, 48.13, 38.18, 26.75, 19.01.

***tert*-Butyl *(2R,5R)*-2-benzyl-5-methoxypiperidine-1-carboxylate (51)**. To a solution of *tert*-butyl *(2R,5R)*-2-benzyl-5-hydroxypiperidine-1-carboxylate **50**[15]. (100 mg, 0.343 mmol) and NaH (60%, 34.3 mg, 0.858 mmol) in DMF (3 mL) at 0 °C, MeI (0.064 mL, 1.03 mmol) was added dropwise with continuous stirring, and the mixture was allowed to stand at room temperature for 24h. The mixture was diluted with water (10 mL), and extracted with ethyl acetate (3 x 20 mL). The organic layer was washed with water, brine, dried over $MgSO_4$, filtered, and concentrated *in vacuo*. The residue was purified by flash chromatography (pentane/ethyl acetate = 20:1 → 5:1) to furnish *tert*-butyl (*2R,5R*)-2-benzyl-5-methoxypiperidine-1- carboxylate (87.0 mg, 0.285 mmol, 83% yield). $[\alpha]_D^{22}$ = -31 (*c* = 0.8, $CHCl_3$). LC-MS m/z: calculated for $C_{18}H_{27}NO_3$ $[M+H]^+$ 306.20, found: 306.27. ^{1}H NMR (400 MHz, $CDCl_3$) δ 7.30 – 7.24 (m, 2H), 7.18 – 7.12 (m, 3H), 4.39 (br s, 2H), 3.41 (s, 3H), 3.18 (t, *J* = 4.0 Hz, 1H), 2.97 – 2.87 (m, 1H), 2.74 – 2.58 (m, 2H), 1.96 (br s, 1H), 1.66 – 1.49 (m, 3H), 1.29 (s, 9H). ^{13}C NMR (101 MHz, $CDCl_3$) δ 154.82, 139.12, 129.22, 128.47, 126.29, 79.61, 75.89, 56.33, 52.24, 42.06, 35.94, 26.25, 26.21, 25.84.

***(2R,5R)*-2-Benzyl-5-methoxypiperidine.** To a solution of compound *tert*-butyl *(2R,5R)*-2-benzyl- 5-methoxypiperidine-1-carboxylate **51** (44.0 mg, 0.144 mmol) in DCM was added 20% TFA, the reaction mixture was stirred at r.t. for 2.5h until TLC showed the reaction was completed. When the reaction is finished, the mixture was co-evaporated with toluene (3 times), the residue was diluted with ethyl acetate and washed with 10% Na_2CO_3, water, brine and dried over $MgSO_4$, and concentrated under reduced pressure. Filtering and concentration under reduced pressure afforded the crude product *(2R,5R)*-2-benzyl-5-methoxypiperidine that was used without further purification. ^{1}H NMR (400 MHz, $CDCl_3$) δ 7.30 – 7.22 (m, 3H), 7.18 (d, *J* = 6.5 Hz, 2H), 3.57 (s, 1H), 3.46 (br s, 1H), 3.33 (s, 4H), 3.17 (br d, *J* = 11.6 Hz, 1H), 3.03 (br s, 1H), 2.84 (br s, 1H), 2.07 (d, *J* = 15.0 Hz, 1H), 1.92 – 1.73 (m, 1H), 1.61 (d, *J* = 13.4 Hz, 1H), 1.53 – 1.41 (m, 1H). ^{13}C NMR (101 MHz, $CDCl_3$) δ 135.33, 129.47, 128.91, 127.35, 70.16, 58.07, 56.12, 47.01, 39.64, 25.73, 22.63.

***tert*-Butyl *(2R,5R)*-2-benzyl-5-(cyclopropylmethoxy)piperidine-1-carboxylate (52)**. To a solution of *tert*-butyl *(2R,5R)*-2-benzyl-5-hydroxypiperidine-1-carboxylate (100 mg, 0.343 mmol) and NaH (60%, 24.7 mg, 1.03 mmol) in DMF (3 mL) at 0 °C, (bromomethyl)cyclopropane (139 mg, 1.03 mmol) was added dropwise with continuous stirring, and the mixture was allowed to stand at room temperature for 24h. The mixture was diluted with water (10 mL), and extracted with ethyl acetate (3 x 20 mL). The organic layer was washed with water, brine, dried over $MgSO_4$, filtered, and concentrated *in vacuo*. The residue was purified by flash chromatography (pentane/ethyl acetate = 20:1 → 5:1) to furnish *tert*-butyl *(2R,5R)*-2-benzyl-5-(cyclopropylmethoxy)piperidine- 1-carboxylate (96.0 mg, 0.277 mmol, 81% yield). $[\alpha]_D^{22}$ = -32 (*c* = 0.9, $CHCl_3$). LC-MS m/z: calculated for $C_{21}H_{31}NO_3$ $[M+H]^+$ 346.23, found: 346.40. ^{1}H NMR (400 MHz, $CDCl_3$) δ 7.28 – 7.25 (m, 2H), 7.20 – 7.15 (m, 3H), 4.58 – 4.11 (m, 2H), 3.37 (d, *J* = 4.0 Hz, 2H), 3.30 – 3.20 (m, 1H), 2.96 – 2.85 (m, 1H), 2.71 (t, *J* = 8.0 Hz, 2H), 1.93 (br s, 1H), 1.62 (br s, 2H), 1.39 (br s, 1H), 1.28 (s, 9H), 1.12 – 1.03 (m, 1H), 0.54 (br d, *J* = 8.0 Hz, 2H), 0.21 (br d, *J* = 4.0 Hz, 2H). ^{13}C NMR

(101 MHz, $CDCl_3$) δ 154.79, 138.71, 129.23, 128.46, 126.27, 79.56, 74.18, 73.72, 52.25, 42.57, 36.01, 28.26, 26.44, 26.11, 11.02, 3.21.

***(2R,5R)*-2-Benzyl-5-(cyclopropylmethoxy)piperidine** To a solution of compound *tert*-butyl *(2R,5R)*-2-benzyl-5-(cyclopropylmethoxy)piperidine-1-carboxylate (30.0 mg, 0.087 mmol) in DCM was added 20% TFA, the reaction mixture was stirred at r.t. for 2.5h until TLC showed the reaction was completed. When the reaction is finished, the mixture was co-evaporated with toluene (3 times), the residue was diluted with ethyl acetate and washed with 10% Na_2CO_3, water, brine and dried over $MgSO_4$. Filtering and concentration under reduced pressure afforded the crude product that was used without further purification. ^{1}H NMR (400 MHz, $CDCl_3$) δ 7.35 – 7.18 (m, 5H), 3.75 (s, 1H), 3.47 (s, 1H), 3.41 – 3.17 (m, 2H), 3.17 (d, *J* = 10.1 Hz, 2H), 3.06 (d, *J* = 12.1 Hz, 1H), 2.88 (d, *J* = 7.7 Hz, 1H), 2.03 (d, *J* = 11.7 Hz, 1H), 1.85 (d, *J* = 11.5 Hz, 1H), 1.62 (d, *J* = 14.2 Hz, 1H), 1.26 (br s, 1H), 1.02 (br s, 1H), 0.52 (d, *J* = 8.0 Hz, 2H), 0.16 (d, *J* = 4.0 Hz, 2H). ^{13}C NMR (101 MHz, $CDCl_3$) δ 135.43, 129.50, 128.89, 127.30, 73.27, 68.20, 57.92, 47.49, 39.39, 26.29, 22.70, 10.49, 3.08, 3.04.

***tert*-Butyl (2*R*,5*R*)-2-benzyl-5-(prop-2-yn-1-yloxy)piperidine-1-carboxylate**: To a solution of *tert*-butyl *(2R,5R)*-2-benzyl-5-hydroxypiperidine-1-carboxylate (130 mg, 0.446 mmol) in DMF (3 mL) at 0 ^{o}C, was added NaH (44.6 mg, 1.12 mmol). After 5 minutes followed by drop wise addition of 3-bromoprop-1-yne (0.144 mL, 1.34 mmol). The reaction was allowed to warm to room temperature and stirred for 24 h. The mixture was diluted with water (10 mL), and extracted with ethyl acetate (3 x 20 mL). The organic layer was washed with water, brine, dried over $MgSO_4$, filtered, and concentrated under reduced pressure. The residue was purified by flash chromatography (5-20% ethyl acetate/pentane) to furnish title compound (128 mg, 0.389 mmol, 87 %) as a yellow oil. $[\alpha]_D^{22}$ = -24.9 (*c* = 1.00, $CHCl_3$); HRMS(m/z):$[M+H]^+$ calcd. for $C_{20}H_{27}NO_3$, 330.20637; found 330.20643. ^{1}H NMR (400 MHz, $CDCl_3$) δ 7.29 – 7.25 (m, 2H), 7.20 – 7.16 (m, 3H), 4.42 (br s, 1H), 4.32 (br s, 1H), 4.22 (s, 2H), 3.50 – 3.45 (m, 1H), 2.88 (dd, *J* = 13.5, 7.9 Hz, 1H), 2.76 – 2.70 (m, 2H), 2.46 (t, *J* = 4.0 Hz, 1H), 2.00 – 1.93 (m, 1H), 1.66 – 1.57 (m, 3H), 1.28 (s, 9H). ^{13}C NMR (101 MHz, $CDCl_3$) δ 154.71, 138.96, 129.24, 128.51, 126.34, 80.03, 79.71, 74.43, 74.07, 56.02, 52.14, 42.15, 35.90, 28.31, 25.85;

(2*R*,5*R*)-2-benzyl-5-(prop-2-yn-1-yloxy)piperidine: To a solution of *tert*-Butyl (2*R*,5*R*)-2-benzyl-5-(prop-2-yn-1-yloxy)piperidine-1-carboxylate (140 mg, 0.425 mmol) in DCM (2 mL) was added 20% TFA/DCM (5 mL), the reaction mixture was stirred at room temperature for 2.5 hours, after which TLC showed complete conversion of the starting material. Toluene (20 mL) was added and the mixture concentrated. The mixture was dissolved in toluene (2 x 20 mL) two times more and concentrated *in vacuo*. The residue was diluted with ethyl acetate and washed subsequently with aqueous 10% Na_2CO_3 solution, water, brine and dried over $MgSO_4$. Filtering and concentration under reduced pressure afforded the crude product **21** that was used without further purification. LC-MS (m/z) :$[M+H]^+$ calcd. for $C_{15}H_{19}NO$, 230.32; found 230.10. ^{1}H NMR (400 MHz, $CDCl_3$) δ 7.31 – 7.26 (m, 2H), 7.23 (d, *J* =

6.9 Hz, 1H), 7.18 (d, *J* = 6.9 Hz, 2H), 4.21 (s, 2H), 4.03 (s, 1H), 3.45 (d, *J* = 12.7 Hz, 1H), 3.29 (br s, 1H), 3.17 (dd, *J* = 12.9, 4.1 Hz, 2H), 3.06 (d, *J* = 11.5 Hz, 1H), 2.85 (dd, *J* = 12.9, 9.7 Hz, 1H), 2.41 (t, *J* = 2.1 Hz, 1H), 2.05 (d, *J* = 13.3 Hz, 1H), 1.92 – 1.77 (m, 1H), 1.62 (d, *J* = 11.9 Hz, 1H), 1.51 (t, *J* = 13.3 Hz, 1H), 1.26 (br s, 1H). ^{13}C NMR (101 MHz, $CDCl_3$) δ135.40, 129.45, 128.87, 127.28, 78.87, 75.31, 66.94, 57.89, 55.32, 47.04, 39.54, 25.91, 22.66.

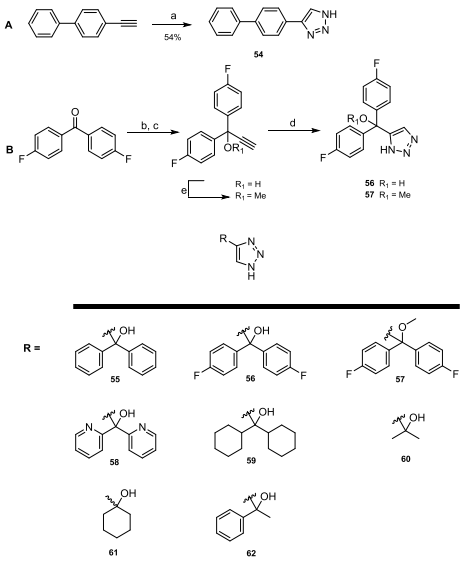

Scheme 4. Synthesis of triazole building blocks (A and B). Reagents and conditions: (a) CuI, azidotrimethylsilane, DMF:MeOH = 5:1, 100 °C; (b) butyllithium, ethynyltrimethylsilane, THF, -10 °C; (c) NaOH, MeOH; (d) MeI, K_2CO_3, DMF, 60 °C, 48% (**55**), 48% (**56**), 35% (**57**), 44% (**58**), 49% (**59**), 84% (**60**), 90% (**61**), 80% (**62**).

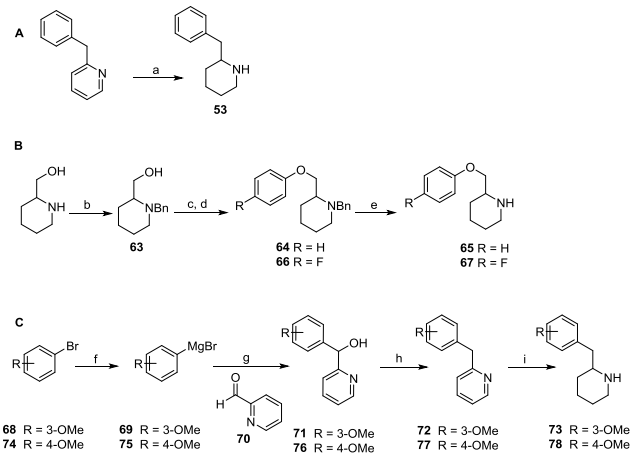

Scheme 5 Synthesis of 2-substituent piperidine building blocks. Reagents and conditions: (a) PtO_2, H_2 (1.6 bar), HCl/EtOH (1:25), r.t., 1.5h, 57%; (b) $NaBH_4$, AcOH, benzylaldehyde, THF, r.t., 90%; (c) tosylchloride, Et_3N, DMAP, DCM, 0 °C; (d) NaH, corresponding phenol, THF, 0 °C (30 min), reflux (16h), 77%; (e) Pd/C (10 mol%), H_2, DCM/MeOH=1:2, r.t., 58% (**65**), 35% (**67**); (f) Mg, I_2, dry THF, 60 °C, 15 min; (g) pyridine-2-aldehyde, dry THF, r.t., overnight, 97% (**71**), 94% (**76**); (h) H_2 (1 bar), Pd/C, H_2SO_4 (98%)/MeOH (1:5), r.t., 3.5 – 5.5h, 57% (**72**), 55% (**77**); (i) H_2 (1.6 bar), PtO_2, HCl/EtOH (1:25), r.t., 1.5h.

2-Benzylpiperidine (**53**)**.** To a solution of 2-benzylpyridine (3.00 mL, 18.7 mmol) in EtOH (25 mL) was added HCl ((37% in H_2O), 1 mL) and PtO_2 (170 mg, 0.750 mmol, 0.04%). The suspension was purged with hydrogen three times and was put under 1.2 bar of H_2. The reaction was shaken vigorously for 1 hour after which the hydrogen had been absorbed. Repeating this step twice led to the desired hydrogenated adduct. The mixture was filtered and washed with EtOH (2 x 5 mL) and solvents were removed under reduced pressure. The residue was further washed with 10% Na_2CO_3, water, brine and dried over $MgSO_4$, and concentrated under reduced pressure to yield the crude product **53** (1.93 g, 11.0 mmol, 57%), which was used for the next step without further purification. ^{1}H NMR (400 MHz, $CDCl_3$) δ 7.26 – 7.19 (m, 5H), 3.20 – 3.09 (m, 1H), 2.71 – 2.59 (m, 2H), 2.59 – 2.47 (m, 2H), 1.98 (br s, 1H), 1.81 – 1.22 (m, 6H). ^{13}C NMR (101 MHz, $CDCl_3$) δ 138.60, 128.51, 128.12, 127.48, 58.12, 46.44, 42.23, 32.97, 25.82, 24.93.

4-([1,1'-Biphenyl]-4-yl)-2*H*-1,2,3-triazole (**54**)**.** In a 50 mL 2-neck round-bottom flask, a solution of 4-ethynyl-1,1'-biphenyl (415 mg, 2.30 mmol) in DMF (20 mL) and MeOH (6 mL) was purged with argon three times. To this solution was added N_3-TMS (0.772 mL, 5.82 mmol) and CuI (100 mg, 0.538 mmol). The reaction mixture was stirred for 2 days at 120 °C. The reaction was allowed to cool to room temperature and H_2O (30 mL) was added after removal of the solvents. Products were extracted with DCM (3 x 75 mL). Organic fractions were combined, washed with brine (30 mL), and dried over $MgSO_4$. After filtering and removal of the solvents, the crude material was purified over silica gel using pentane/ethyl acetate (1:1, 1% Et_3N) and yielded **54** (277 mg,

1.25 mmol, 54%). ^{1}H NMR (400 MHz, DMSO) δ: 8.42 (s, 1H), 7.98 (d, *J* = 8.4 Hz, 2H), 7.77 (d, *J* = 8.4 Hz, 2H), 7.75 – 7.68 (m, 2H), 7.48 (t, *J* = 7.6 Hz, 2H), 7.38 (t, *J* = 7.3 Hz, 1H). ^{13}C NMR (101 MHz, DMSO) δ 139.73, 139.46, 129.38, 129.02, 127.58, 127.12, 126.48, 126.14.

1,1-Diphenylprop-2-yn-1-ol. To a solution of ethynyltrimethylsilane (0.430 mL, 3.10 mmol) in anhydrous THF (10 mL) under nitrogen atmosphere was added slowly butyllithium (1.92 mL, 3.02 mmol) (1.6 M in hexane) at -10 °C and the solution was stirred 1h at – 10 °C. A solution of benzophenone (500 mg, 2.74 mmol) in dry THF 5 mL was then added at -10 °C. After 3h stirring at -10 °C, the temperature was raised to 0°C and a solution of NaOH (143 mg, 3.57 mmol) in MeOH (2.80 mL) was added. After warming the solution to room temperature, the solution was neutralized to pH 7 with acetic acid and the resulting solution poured into water (38 mL). The organic layer was extracted with EtOAc (3 x 10 mL). The combined organic layers were dried over $MgSO_4$. The combined organic layers were dried over $MgSO_4$, filtered and concentrated. The crude product was purified by flash chromatography over silica gel using pentane/ethyl acetate and finished the title compound (1.08 g, 4.42 mmol, 96% yield). ^{1}H NMR (400 MHz, $CDCl_3$) δ 7.53 (d, *J* = 8.0 Hz, 4H), 7.25 – 7.11 (m, 6H), 3.16 (s, 1H), 2.70 (s, 1H). ^{13}C NMR (101 MHz, $CDCl_3$) δ 144.38, 128.22, 127.74, 126.00, 86.36, 75.70, 74.22.

Diphenyl(1*H*-1,2,3-triazol-4-yl)methanol (55). 1,1-Diphenylprop-2-yn-1-ol (260 mg, 1.25 mmol) and CuI (12.0 mg, 0.062 mmol) were dissolved in DMF/MeOH (5:1, 36 mL), azidotrimethylsilane (0.250 mL, 1.87 mmol) was added and the reaction mixture was stirred at 100 °C over the weekend. The reaction mixture was quenched with H_2O, and the organic layer was extracted with DCM. The combined organic layers were washed with H_2O and brine, dried on $MgSO_4$, filtered and concentrated under reduced pressure. The residue was purified by flash chromatography over silica gel using pentane/ethyl acetate (1:1) with 1% Et_3N, yielding **55** (151 mg, 0.599 mmol, 48% yield). ^{1}H NMR (400 MHz, MeOD) δ 7.54 (s, 1H), 7.36 – 7.26 (m, 10H).

Bis(4-fluorophenyl)(1*H*-1,2,3-triazol-4-yl)methanol (56). To a solution of ethynyltrimethylsilane (0.712 mL, 5.04 mmol) in anhydrous THF (20 mL) under a nitrogen atmosphere was slowly added n-butyllithium (3.15 mL, 5.04 mmol) (1.6 M in hexane) at -10°C. After stirring for one hour at -10 °C a solution of bis(4-fluorophenyl)methanone (1.00 g, 4.58 mmol) in dry THF (10 mL) was added. After stirring for three hours at -10 °C, the temperature was raised to 0 °C and a solution of NaOH (238 mg, 5.95 mmol) in MeOH (4.60 mL) was added. The solution was warmed to room temperature, neutralized to pH 7 with acetic acid and poured into water. Subsequent extraction with ethyl acetate (3x10 mL), drying over $MgSO_4$, filtering and concentration *in vacuo* afforded a crude product that was purified by flash chromatography over silica gel using pentane/ethyl acetate, yielding 1,1-bis(4-fluorophenyl)prop-2-yn-1-ol (1.08 g, 4.42 mmol, 96 %) as a yellow oil. ^{1}H NMR (400 MHz, $CDCl_3$) δ 7.57 – 7.51 (m, 4H), 7.03 – 6.98 (m, 4H), 2.89 (s, 2H); ^{13}C NMR (101 MHz, $CDCl_3$) δ 162.50 (d, *J* = 248 Hz), 140.24 (d, *J* = 3.1 Hz), 127.98 (d, *J*

= 9.1 Hz), 115.32 (d, *J* = 21 Hz), 86.08, 76.09, 73.52; HRMS(m/z):$[M+H]^+$ calcd. for $C_{15}H_{10}F_2O$, 245.07782; found: 245.07735. 1,1-bis(4-fluorophenyl)prop-2-yn-1-ol (1.00 g, 4.09 mmol) and CuI (0.153 g, 0.819 mmol) were dissolved in DMF/MeOH (5:1, 36 mL). Azidotri- methylsilane (0.815 mL, 6.14 mmol) was added and the mixture was stirred at 100 °C over the weekend. The reaction mixture was quenched with H_2O (90 mL), the organic layer extracted with DCM (3 x 100 mL). The combined organic layers were washed with H_2O and brine and dried on $MgSO_4$. Filtering and concentration under reduced pressure gave a residue that was purified by flash chromatography over silica gel using pentane/ethyl acetate with 1% Et_3N (30–100% pentane/ethyl acetate) yielding **56** (0.694 g, 2.42 mmol, 59 %) as a white solid. ^{1}H NMR (400 MHz, MeOD) δ 7.58 (s, 1H), 7.38 – 7.31 (m, 4H), 7.06 – 7.01 (m, 4H); ^{13}C NMR (101 MHz, MeOD) δ 163.45 (d, *J* = 246 Hz), 143.57 (d, *J* = 2.0 Hz), 130.62, 128.59, 130.31 (d, *J* = 9.1 Hz), 115.52 (d, *J* = 22 Hz), 76.99; HRMS(m/z):$[M+H]^+$ calcd. for $C_{15}H_{11}F_2N_3O$, 288.09429; found 288.09473.

4-(Bis(4-fluorophenyl)(methoxy)methyl)-1H-1,2,3-triazole (57). (1,1'-Bis(4-fluorophenyl)prop- 2-yn-1-ol) (50.0 mg, 0.205 mmol) was dissolved in anhydrous THF (5 mL) and purged with argon 3 times. NaH (60%, 10 mg, 0.25 mmol;) was added and the reaction mixture was stirred for 30 min at 0°C. Subsequently, MeI (16.0 µL, 0.250 mmol) was added and the mixture was stirred for 3h at 0 °C. The mixture was washed with NH_4Cl solution (10 mL), H_2O (5 mL) and extracted with DCM (3 x 20 mL). Organic fractions were combined, washed with brine, dried over $MgSO_4$, filtered and concentrated under reduced pressure. The residue was purified with pentane/ethyl acetate (1:1, 1% Et_3N) and obtained the methylated compound (45.0 mg, 87%). ^{1}H NMR (400 MHz, $CDCl_3$) δ 7.58 – 7.48 (m, 4H), 7.11 – 6.98 (m, 4H), 3.37 (s, 3H), 2.94 (s, 1H). ^{13}C NMR (101 MHz, $CDCl_3$) δ 162.32 (d, *J* = 246.9 Hz), 138.63 (d, *J* = 3.2), 128.38 (d, *J* = 7.7 Hz), 115.12 (d, *J* = 21.6 Hz), 82.03, 79.75, 78.01, 52.42. The obtained intermediate (46.0 mg, 0.178 mmol) was converted into 1,2,3-triazole according to the same procedures described for compound **55** (20.0 mg, 35%). LC-MS m/z: calculated for $C_{16}H_{13}N_3O$ $[M+H]^+$ 302.10, found 302.52. ^{1}H NMR (400 MHz, MeOD) δ 7.56 (s, 1H), 7.53 – 7.42 (m, 4H), 7.14 – 7.01 (m, 4H), 3.17 (s, 3H). ^{13}C NMR (101 MHz, MeOD) δ 163.42 (d, *J* = 245.4 Hz), 144.20, 140.83, 130.91 (d, *J* = 8.2 Hz), 123.55, 115.62 (d, *J* = 21.7 Hz), 93.33, 52.63.

1,1-Di(pyridin-2-yl)prop-2-yn-1-ol. To a solution of ethynyltrimethylsilane (0.850 mL, 6.00 mmol) in anhydrous THF (20 mL) under nitrogen atmosphere was added slowly butyllithium (3.69 mL, 5.90 mmol) (1.6 M in hexane) at -10 °C and the solution was stirred 1h at -10 °C. A solution of di(pyridin-2-yl)methanone (1.00 g, 5.43 mmol) in dry THF (10 mL) was then added at -10 °C. After 3h stirring at -10 °C, the temperature was raised to 0 °C and a solution of NaOH (238 mg, 5.95 mmol) in MeOH (4.60 mL) was added. After the solution was warmed to room temperature, the solution was neutralized to pH 7 with acetic acid and the resulting solution poured into water (38 mL). The organic layer was extracted with EtOAc (3 x 10 mL). The combined organic layers were dried over $MgSO_4$, filtered and concentrated. The residue was purified by flash chromatography over silica gel using pentane/ethyl acetate (1:1) with 1% Et_3N.

Yielding 1,1-di(pyridin-2-yl)prop-2-yn-1-ol (690 mg, 3.27 mmol, 60% yield). LC-MS m/z: calculated for $C_{13}H_{10}N_2O$ $[M+H]^+$ 211.08, found: 211.11. ^{1}H NMR (400 MHz, $CDCl_3$) δ 8.56 (d, *J* = 4.8 Hz, 2H), 7.86 (d, *J* = 8.0 Hz, 2H), 7.72 (td, *J* = 7.8, 4.0 Hz, 2H), 7.25 – 7.21 (m, 2H), 6.79 (br s, 1H), 2.75 (s, 1H).^{13}C NMR (101 MHz, $CDCl_3$) δ 160.44, 148.06, 137.49, 123.22, 121.37, 85.85, 75.73, 73.66.

Di(pyridin-2-yl)(1*H*-1,2,3-triazol-4-yl)methanol (58). The title compound was synthesized from 1,1-di(pyridin-2-yl)prop-2-yn-1-ol (1.10 g, 5.23 mmol) according to the same procedures described for compound **55**. This furnished di(pyridin-2-yl)(1*H*-1,2,3-triazol-4-yl)methanol **58** (580 mg, 2.30 mmol, 44% yield). LC-MS m/z: calculated for $C_{13}H_{11}N_5O$ $[M+H]^+$ 254.10, found: 254.32. ^{1}H NMR (400 MHz, $CDCl_3$) δ 8.53 – 8.51 (m, 2H), 7.82 (d, *J* = 8.0 Hz, 2H), 7.72 (s, 1H), 7.67 (td, *J* = 7.8, 1.8 Hz, 2H), 7.20 – 7.17 (m, 2H), 4.99 (s, 1H). ^{13}C NMR (101 MHz, $CDCl_3$) δ 161.30, 159.55, 147.58, 136.98, 130.82, 122.75, 121.98, 75.87.

Dicyclohexyl(2*H*-1,2,3-triazol-4-yl)methanol (59). Following the procedure that was described for 1,1-diphenylprop-2-yn-1-ol, dicyclohexylmethanone (0.990 mL, 5.20 mmol) was reacted with ethynyltrimethylsilane (0.710 mL, 5.66 mmol), n-BuLi (3.33 mL, 5.66 mmol) and NaOH (206 mg, 5.15 mmol, in 5 mL MeOH) to obtain 1,1-dicyclohexylprop-2-yn-1-ol (1.06 g, 94%) as yellow oil. ^{1}H NMR (400 MHz, $CDCl_3$) δ 2.43 (s, 1H), 1.93 – 1.25 (m, 22H). ^{13}C NMR (101 MHz, $CDCl_3$) δ 85.8, 73.43, 43.4, 27.7, 26.5, 26.5, 26.3, 26.0. The obtained 1,1-dicyclohexylprop-2-yn-1-ol (804 mg, 3.65 mmol) was converted into its 1,2,3-triazole according to the same procedures described for compound **55**. This furnished **59** (469 mg, 49%). LC-MS m/z: calculated for $C_{15}H_{25}N_3O$ $[M+H]^+$ 264.20, found: 264.24. ^{1}H NMR (400 MHz, $CDCl_3$) δ 7.75 – 7.37 (m, 1H), 1.98 – 0.68 (m, 22H). ^{13}C NMR (101 MHz, $CDCl_3$) δ 152.53, 139.29, 44.11, 29.72, 27.13, 26.54, 26.38, 26.22

2-(2*H*-1,2,3-Triazol-4-yl)propan-2-ol (60). The title compound was synthesized from 2-methyl-3-butyn-2-ol (581 µL, 5.94 mmol) according to the same procedures described for compound **55**. This furnished **60** (635 mg, 84%). LC-MS m/z: calculated for $C_5H_9N_3O$ $[M+Na]^+$ 150.06, found: 150.21. ^{1}H NMR (400 MHz, $CDCl_3$) δ 7.58 (s, 1H), 1.59 (s, 6H). ^{13}C NMR (101 MHz, $CDCl_3$) δ 156.52, 131.53, 68.48, 30.12.

1-(2*H*-1,2,3-Triazol-4-yl)cyclohexan-1-ol (61). The title compound was synthesized from 1-ethynyl-1-cyclohexanol (642 µL, 5.00 mmol) according to the same procedures described for compound **55**. This furnished **61** (843 mg, 90%). LC-MS m/z: calculated for $C_8H_{13}N_3O$ $[M+Na]^+$ 190.10, found: 190.41. ^{1}H NMR (400 MHz, $CDCl_3$) δ 7.61 (s, 1H), 1.91 (dt, *J* = 9.2, 4.7 Hz, 4H), 1.81 – 1.71 (m, 2H), 1.68 – 1.52 (m, 3H), 1.42 – 1.23 (m, 1H). ^{13}C NMR (101 MHz, $CDCl_3$) δ 131.42, 123.03, 76.33, 69.82, 38.24, 38.15, 25.28, 21.90.

1-Phenyl-1-(1*H*-1,2,3-triazol-4-yl)ethan-1-ol (62). The title compound was synthesized from 2-phenylbut-3-yn-2-ol (500 mg, 3.42 mmol) according to the same procedures described for compound **55**. This furnished 1-phenyl-1-(1*H*-1,2,3

-triazol-4-yl)ethan-1-ol **62** (453 mg, 2.40 mmol, 80% yield). LC-MS m/z: calculated for $C_{10}H_{11}N_3O$ $[M+H]^+$ 212.08, found 212.10. ^{1}H NMR (400 MHz, MeOD) δ 7.67 (d, *J* = 16.0 Hz, 1H), 7.53 (m, 2H), 7.39 – 7.15 (m, 3H), 2.00 (s, 3H). ^{13}C NMR (101 MHz, MeOD) δ 156.22, 146.91, 132.63, 127.89, 126.92, 125.10, 75.92, 29.69.

(1-Benzylpiperidin-2-yl)methanol (63). $NaBH_4$ (1.97 g, 52.1 mmol) was treated with AcOH (10.4 mL, 174 mmol) in anhydrous THF (50 mL) for 30 min at 0 °C. To this solution was added 2-hydroxymethyl piperidine (2.00 g, 17.4 mmol) in anhydrous THF (10 mL), and benzaldehyde (5.30 mL, 51.9 mmol). The reaction mixture was stirred overnight at room temperature. The mixture was filtered and concentrated *in vacuo*. Purification by column chromatography over silica gel (pentane/EtOAc = 10:1 → 1:1) yielded **63** (1-benzyl)2-hydroxymethyl piperidine as yellow oil (3.19 g, 15.5 mmol, 90%). LC-MS *m/z*: calculated for $C_{13}H_{19}NO$ $[M+H]^+$ 206.15, found: 206.16. ^{1}H NMR (400 MHz, $CDCl_3$) δ 7.42 – 7.21 (m, 5H), 4.11 (d, *J* = 13.4 Hz, 1H), 3.86 (dd, *J* = 10.8, 4.2 Hz, 1H), 3.61 (dd, *J* = 10.8, 3.6 Hz, 1H), 3.35 (d, *J* = 13.4 Hz, 1H), 3.21 (s, 1H), 2.89 (d, *J* = 11.5 Hz, 1H), 2.47 (s, 1H), 2.14 (t, *J* = 10.5 Hz, 1H), 1.83 – 1.24 (m, 6H). ^{13}C NMR (101 MHz, $CDCl_3$) δ: 139.02, 129.01, 128.45, 127.12, 62.48, 61.32, 57.91, 51.13, 27.6, 24.29, 23.52.

1-Benzyl-2-(phenoxymethyl)piperidine (64). ((1-Benzyl)2-hydroxymethyl piperidine) (200 mg, 0.975 mmol) was dissolved in DCM (2 mL) and cooled to 0 °C. To this were added Et_3N (215 µL, 2.93 mmol), DMAP (24.0 mg, 0.195 mmol) and *p*-toluenesulfonyl chloride (558 mg, 2.93 mmol). The reaction mixture was stirred at 0°C for 16h, warming up to room temperature 20 °C overnight. The mixture was concentrated *in vacuo* and dissolved in DCM (50 mL). The organic layer was washed with H_2O (25 mL), brine (25 mL), dried over $MgSO_4$, filtered and concentrated. The crude product was obtained. Phenol (175 mg, 1.86 mmol) was reacted with NaH (60% dispersion, 74.3 mg, 1.86 mmol) in anhydrous THF (2 mL) at 0 °C for 30 min. After which the crude product from above (139 mg, 0.62 mmol) was added and the mixture heated to reflux for 16h. The reaction mixture was concentrated *in vacuo* and dissolved in DCM (25 mL). Organic layer was washed with 1M NaOH (2 x 10 mL), brine (10 mL), and dried over $MgSO_4$, filtered,. concentrated and purified over silica gel (pentane/EtOAc 10:1 → 1:1), yielding **64** (134 mg, 0.477 mmol, 77%). LC-MS m/z: calculated for $C_{19}H_{23}NO$ $[M+H]^+$ 282.18, found: 282.34. ^{1}H NMR (400 MHz, $CDCl_3$) δ 7.43 – 7.22 (m, 7H), 7.03 – 6.86 (m, 3H), 4.23 (dd, *J* = 9.8, 4.9 Hz, 1H), 4.14 (d, *J* = 13.7 Hz, 1H), 4.04 (dd, *J* = 9.8, 4.7 Hz, 1H), 3.44 (d, *J* = 13.7 Hz, 1H), 2.90 – 2.74 (m, 2H), 2.20 – 2.09 (m, 1H), 1.92 – 1.83 (m, 1H), 1.79 – 1.37 (m, 5H). ^{13}C NMR (101 MHz, $CDCl_3$) δ 158.89, 129.43, 128.92, 128.13, 126.75, 120.67, 118.90, 114.64, 70.32, 60.45, 59.03, 52.04, 29.45, 25.42, 23.46.

2-(Phenoxymethyl)piperidine (65). 1-Benzyl-2-(phenoxymethyl)piperidine (118 mg, 0.420 mmol) was treated with 10% palladium on carbon (44.0 mg, 0.042 mmol) in MeOH/DCM (2:1, 1.5 mL) under hydrogen atmosphere for 16h at room temperature. After reaction was completed, solvents were removed under reduced pressure and mixture was dissolved in EtOAc (30 mL). Organic layer was washed with H_2O (10 mL),

sat. $NaHCO_3$ (10 mL), and brine (10 mL) before dried over $MgSO_4$, concentrated and purified over silica gel (pentane/EtOAc 10:1 → 1:1) yielding **65** (47.0 mg, 0.246 mmol, 58%). LC-MS *m/z*: calculated for $C_{12}H_{17}NO$ $[M+H]^+$ 192.13, found: 192.15. ^{1}H NMR (400 MHz, $CDCl_3$) δ 7.31 – 7.22 (m, 2H), 6.97 – 6.85 (m, 3H), 3.89 (dd, *J* = 9.0, 3.6 Hz, 1H), 3.80 (t, *J* = 9.0 Hz, 1H), 3.15 – 3.06 (m, 1H), 3.00 – 2.90 (m, 1H), 2.69 (td, *J* = 11.6, 2.7 Hz, 1H), 1.88 – 1.80 (m, 1H), 1.71 – 1.59 (m, 2H), 1.55 – 1.19 (m, 4H). ^{13}C NMR (101 MHz, $CDCl_3$) δ 158.9, 129.4, 120.8, 114.9, 72.54, 53.1, 46.6, 28.7, 26.3, 24.4.

2-((4-Fluorophenoxy)methyl)piperidine (67). ((1-Benzyl)2-hydroxymethyl piperidine) (200 mg, 0.974 mmol) was dissolved in DCM (2 mL) and cooled to 0 °C. To this were added Et_3N (407 µL, 2.92 mmol), DMAP (24.0 mg, 0.196 mmol) and *p*-toluenesulfonyl chloride (558 mg, 2.90 mmol). The reaction mixture was stirred at 0 °C for 16h, slowly warming up to room temperature. The mixture was concentrated *in vacuo* and dissolved in DCM (50 mL). The organic layer was washed with H_2O, brine, dried over $MgSO_4$, filtrated and the crude tosylate product was obtained. 4-Fluorophenol (752 mg, 6.71 mmol) was reacted with NaH (60% dispersion, 179 mg, 4.47 mmol) over 30 min at 0 °C in anhydrous DMF (5 mL). The crude tosylate product from above in anhydrous DMF (2 mL) was added to the reaction mixture and stirred at 70 °C for 18h. The mixture was cooled to room temperature, diluted with H_2O (50 mL) and extracted with DCM (3 x 75 mL). Organic fractions were combined, dried over $MgSO_4$, filtered and concentrated *in vacuo*. The crude **66** was then dissolved in MeOH/DCM (6 mL, 2:1), 10% Pd/C (200 mg) was added and the mixture was flushed with hydrogen gas three times. The reaction mixture was stirred under hydrogen atmosphere for 16h. Purification over silica gel using pentane : EtOAc = 1:1 as the eluent with 1% Et_3N to yield product **67** (71.0 mg, 0.340 mmol, 35%). LC-MS m/z: calculated for $C_{12}H_{16}FNO$ $[M+H]^+$ 210.12, found: 210.41. ^{1}H NMR (400 MHz, $CDCl_3$) δ 6.94 (t, *J* = 8.7 Hz, 2H), 6.85 – 6.79 (m, 2H), 3.84 (dd, *J* = 8.9, 3.6 Hz, 1H), 3.74 (t, *J* = 8.6 Hz, 1H), 3.09 (d, *J* = 11.8 Hz, 1H), 2.98 – 2.88 (m, 1H), 2.68 (td, *J* = 11.7, 2.7 Hz, 1H), 1.88 – 1.78 (m, 1H), 1.68 – 1.59 (m, 2H), 1.55 – 1.31 (m, 2H), 1.30 – 1.17 (m, 1H). ^{13}C NMR (101 MHz, $CDCl_3$) δ 157.32 (d, *J* = 238.2 Hz), 155.01 (d, *J* = 2.1 Hz), 115.68 (d, *J* = 23.0 Hz), 115.52 (d, *J* = 7.9 Hz), 73.31, 55.82, 46.53, 28.62, 26.28, 24.32.

(3-Methoxyphenyl)(pyridin-2-yl)methanol (71). After flame-drying and flushing with argon, the flask containing magnesium turnings (156 mg, 6.50 mmol) was charged, dry THF (2.5 mL) and a catalytic amount of iodine were added under argon atmosphere. Then, 1/10 of a argon flushed solution of 1-bromo-3-methoxybenzene **68** (0.675 mL, 5.33 mmol) in dry THF (2.5 mL) was added at room temperature. The mixture was heated with a heating gun until initiation of the reaction was observed. The rest of the 1-bromo-3-methoxybenzene solution was then added dropwise, and the reaction mixture was stirred under reflux for 15 min, after which it was allowed to cool to room temperature. The solution containing Grignard reagent **69** was cooled to 0 °C and pyridine-2-aldehyde **70** (0.430 mL, 4.52 mmol) was added dropwise under argon atmosphere. Extra dry THF was added (2.5 mL) and the reaction mixture was allowed to warm to room temperature while stirring overnight. After quenching with

aqueous saturated NH_4Cl (35 mL), the aqueous layer was extracted with EtOAc (3 x 60 mL). The combined organic layers were washed with brine, dried over $MgSO_4$, filtered and concentrated *in vacuo*. Purification by column chromatography (pentane/EtOAc = 10:1→2:1) afforded compound **71** (940 mg, 4.37 mmol, 97%). ^{1}H NMR (500 MHz, $CDCl_3$) δ 8.43 (d, *J* = 4.8 Hz, 1H), 7.52 (td, *J* = 7.7, 1.7 Hz, 1H), 7.21 – 7.17 (m, 2H), 7.10 – 7.05 (m, 1H), 6.95 – 6.93 (m, 2H), 6.78 – 6.74 (m, 1H), 5.72 (s, 1H), 5.56 (br s, 1H), 3.69 (s, 3H). ^{13}C NMR (126 MHz, $CDCl_3$) δ 161.16, 159.64, 147.75, 144.76, 136.81, 129.40, 122.31, 121.11, 119.20, 113.19, 112.20, 75.03, 55.02. LC-MS m/z: calculated for $C_{13}H_{13}NO_2$ $[M+H]^+$ 216.10, found 215.73.

2-(3-Methoxybenzyl)pyridine (72). A hydrogenation flask containing compound **71** (100 mg, 0.465 mmol) in a mixture of H_2SO_4 (98%)/MeOH (1:5, 5.6 mL) was flushed with argon. Pd/C (10%, 250 mg) was added and the mixture was hydrogenated at 1 bar at room temperature for 4h. The reaction mixture was then filtered, concentrated *in vacuo* and neutralize with aqueous NaOH solution (1.0 M). The aqueous layer was extracted with DCM (3 x 20 mL) and the combined organic layers were washed with brine, dried over $MgSO_4$, filtered and concentrated *in vacuo*. Purification by column chromatography (pentane/EtOAc = 10:1→4:1) afforded compound **72** (51.0 mg, 0.256 mmol, 57%). LC-MS m/z: calculated for $C_{13}H_{13}NO$ $[M+H]^+$ 200.10, found 200.41. ^{1}H NMR (400 MHz, $CDCl_3$) δ 8.54 (d, *J* = 7.3 Hz, 1H), 7.56 (td, *J* = 7.7, 1.8 Hz, 1H), 7.27 – 7.18 (m, 1H), 7.14 – 7.06 (m, 2H), 6.87 – 6.80 (m, 2H), 6.76 (dd, *J* = 8.2, 2.4 Hz, 1H), 4.13 (s, 2H), 3.76 (s, 3H). ^{13}C NMR (101 MHz, $CDCl_3$) δ 160.88, 159.83, 149.36, 141.08, 136.66, 129.62, 123.22, 121.57, 121.36, 114.87, 111.87, 55.22, 44.79.

2-(3-Methoxybenzyl)piperidine (**73**). A hydrogenation flask containing compound **72** (51.0 mg, 0.256 mmol) in a mixture of HCl/EtOH (1:25, 6.7 mL) was flushed with argon. PtO_2 (4.60 mg, 20.3 µmol) was added and the mixture was hydrogenated at 1 bar at room temperature for 2h. The reaction mixture was filtered, concentrated *in vacuo* and coevaporated with EtOH (3 x 10 mL) and with toluene (3 x 10 mL) to give crude compound **73**, which was used in the following step without any further purification. LC-MS m/z: calculated for $C_{13}H_{19}NO$ $[M+H]^+$ 206.10, found 206.21. ^{1}H NMR (400 MHz, $CDCl_3$) δ 7.26 – 7.08 (m, 1H), 6.96 – 6.58 (m, 3H), 3.79 (s, 3H), 3.57 (d, *J* = 7.0 Hz, 2H), 3.28 (br s, 1H), 2.97 (d, *J* = 5.3 Hz, 2H), 2.08 – 1.59 (m, 6H). ^{13}C NMR (101 MHz, $CDCl_3$) δ 159.46, 137.00, 129.48, 121.67, 114.95, 112.34, 58.50, 55.38, 49.03, 39.91, 29.32, 27.39, 22.25.

(4-Methoxyphenyl)(pyridin-2-yl)methanol (**76**). After flame-drying and flushing with argon, the flask containing magnesium turnings (156 mg, 6.50 mmol) was charged dry THF (2.5 mL) and a catalytic amount of iodine were added. Then, 1/10 of a argon flushed solution of 1-bromo-4-methoxybenzene **74** (0.675 mL, 5.33 mmol) in dry THF (2.5 mL) was added at room temperature. The mixture was heated with a heating gun until initiation of the reaction was observed. The rest of the 1-bromo-4-methoxybenzene solution was added dropwise, and the reaction mixture was stirred under reflux for 15 min, after which it was allowed to cool to room temperature. The solution containing Grignard reagent **75** was then further cooled to 0

°C and pyridine-2-aldehyde **70** (0.430 mL, 4.52 mmol) was added dropwise under argon atmosphere. Extra dry THF(2.5 mL) was added and the reaction mixture was allowed to warm to room temperature while stirring overnight. After quenching with aqueous saturated NH_4Cl (35 mL), the aqueous layer was extracted with EtOAc (3 x 60 mL). The combined organic layers were washed with brine, dried over $MgSO_4$, filtered and concentrated *in vacuo*. Purification by column chromatography (pentane/EtOAc = 10:1→2:1) afforded compound **76** (910 mg, 4.23 mmol, 94%). LC-MS m/z: calculated for $C_{13}H_{13}NO_2$ $[M+H]^+$ 216.10, found: 215.73. ^{1}H NMR (400 MHz, MeOD) δ 8.45 – 8.37 (m, 1H), 7.82 (td, *J* = 7.7, 1.7 Hz, 1H), 7.62 (d, *J* = 7.9 Hz, 1H), 7.30 – 7.25 (m, 3H), 6.89 – 6.81 (m, 2H), 5.76 (s, 1H), 4.91 (s, 1H), 3.75 (s, 3H). ^{13}C NMR (101 MHz, MeOD) δ 164.75, 160.65, 149.06, 138.84, 136.64, 129.19, 123.73, 122.06, 114.76, 77.06, 55.66.

2-(4-Methoxybenzyl)pyridine (77). The title compound was prepared from compound **76** (100 mg, 0.465 mmol) and Pd/C (10%, 250 mg) in H_2SO_4/MeOH (1:5, 8.4 mL) according to the same procedures described for compound **72**. Purification by column chromatography (pentane/EtOAc = 10:1 → 4:1) afforded compound **77** (80.0 mg, 0.404 mmol, 55%) as a yellow oil. LC-MS m/z: calculated for $C_{13}H_{13}NO$ $[M+H]^+$ 200.11, found: 199.87. ^{1}H NMR (400 MHz, $CDCl_3$) δ 8.53 (d, *J* = 3.8 Hz, 1H), 7.54 (t, *J* = 7.7 Hz, 1H), 7.17 (d, *J* = 8.5 Hz, 2H), 7.08 (d, *J* = 7.7 Hz, 2H), 6.84 (d, *J* = 8.5 Hz, 2H), 4.09 (s, 2H), 3.75 (s, 3H). ^{13}C NMR (101 MHz, $CDCl_3$) δ 161.39, 158.19, 149.27, 136.55, 131.60, 130.07, 122.99, 121.17, 114.01, 55.22, 43.81.

2-(4-Methoxybenzyl)piperidine (78). The title compound was prepared from compound **77** (68.0 mg, 0.342 mmol) and PtO_2 (6.20 mg, 27.3 µmol) in HCl/EtOH (1:25, 10 mL) according to the same procedures described for compound **72**. This furnished crude compound **78**, which was used in the following steps without any further purification. LC-MS m/z: calculated for $C_{13}H_{19}NO$ $[M+H]^+$ 206.16, found 205.93. ^{1}H NMR (400 MHz, $CDCl_3$) δ 7.16 (s, 2H), 6.82 (s, 2H), 3.77 (s, 3H), 3.50 (br s, 2H), 3.17 (br s, 1H), 2.93 (br s, 2H), 2.03 – 1.66 (m, 6H). ^{13}C NMR (101 MHz, $CDCl_3$) δ 158.59, 130.67, 127.72, 114.14, 58.91, 55.37, 45.58, 39.03, 29.64, 27.53, 22.45.

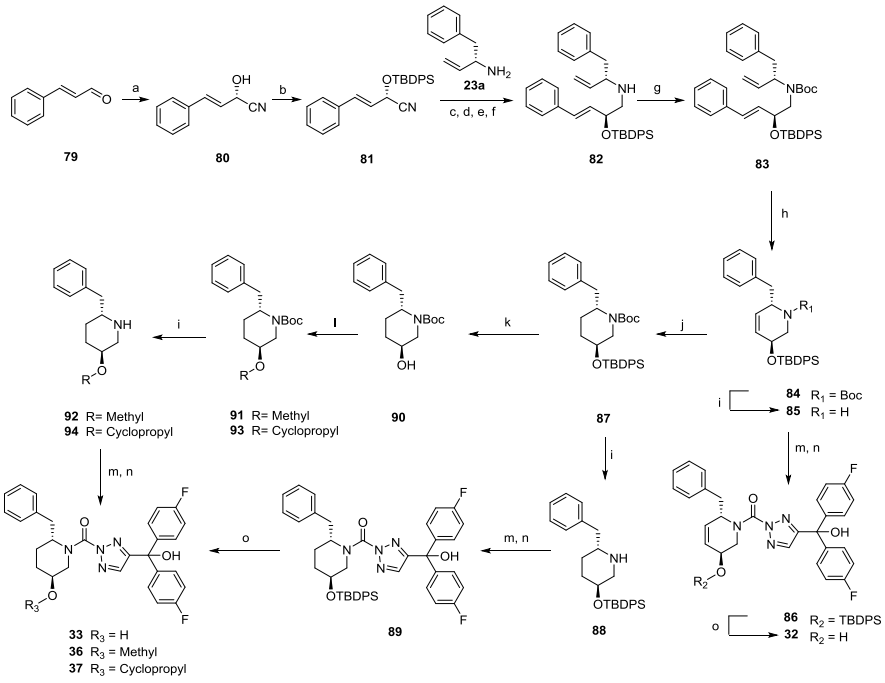

Scheme 6 Enantioselective synthesis of chiral compounds. Reagents and conditions: (a) HCN, EtOAc, 0.1M aq. citrate buffer, pH 5.4, Hydroxynitrile lyase, 55%; (b) TBDPS-Cl, imidazole, DMF, 0 °C, 98%; (c) diethyl ether, DIBAL-H, -80 °C to 0 °C; (d) MeOH, -90 °C; (e) *(S)*-amine (**23a**) (3 equiv), r.t., 20h; (f) $NaBH_4$, 93%; (g) Boc_2O, TEA, THF, 50 °C, 20h; (h) Grubbs I cat. 4 mol %, DCM, reflux, 48h, 87% (**84**, based on **82**); (i) 25% TFA, DCM, r.t.; (j) Hydrazine, $CuSO_4$, EtOH, 0 °C to 70 °C, 80%; (k) TBAF, THF, r.t., 80%; (l) NaH, corresponding bromide, 83% (**91**), 89% (**93**); (m) DIPEA, Triphosgene, THF, 0 °C; (n) DIPEA, DMAP, triazole, THF, 60 °C, 26% (**36**, based on **91**), 21% (**37**, based on **93**); (o) HF-pyridine, THF : pyridine = 1:1 (v/v), 15% (**32**, based on **84**), 16% (**33**, based on **87**).

(*S,E*)-2-((*tert*-Butyldiphenylsilyl)oxy)-4-phenyl-*N*-((*S*)-1-phenylbut-3-en-2-yl)but-3-en-1-amine (82). Under an argon atmosphere cyanohydrin **81**[25,26] (2.80 g, 7.05 mmol) was dissolved in dry diethyl ether (40 mL) and at -78 °C a 1.0 M solution of DIBAL-H in toluene (11.0 mL, 11.0 mmol) was added dropwise in 15 min. The mixture was slowly warmed on the cooling bath to 5 °C. After re-cooling to -90 °C methanol (10 mL) was added at once, followed by a solution of *(S)*-1-phenylbut-3-en-2-amine **23a** (3.00 g, 20.4 mmol) in methanol (10 mL). The cooling bath was removed and the remaining mixture stirred at room temperature, under a light flow of argon, for 28h. The remaining mixture was cooled on an ice-bath and $NaBH_4$ (880 mg, 23.0 mmol) was added in three portions with five minute intervals. The mixture was stirred overnight while slowly warming to room temperature. The reaction was quenched with a 0.8 M NaOH solution (150 mL) and the resulting mixture extracted with diethyl ether (3 x 60 mL). The combined organic layers were washed subsequently with 1.0 M HCl solution (2 x 30 mL) and 0.8 M NaOH solution, dried ($MgSO_4$), filtered and concentrated *in*

vacuo to afford the crude product that was purified by silica gel column chromatography (pentane/EtOAc = 97 : 3 → 9 : 1) to give the target amine **82** as a colorless oil (3.50 g, 93%). $[\alpha]^{23}_{D}$ = +116 (*c* = 1.0, $CHCl_3$). HRMS calculated for $C_{36}H_{41}NOSi$ $[M+H]^+$: 532.3030 found: 532.3021. IR: 3071, 3026, 2930, 2893, 2857, 1495, 1454, 1427, 1362, 1109, 1059, 962, 918. ^{1}H NMR (400 MHz, $CDCl_3$) δ 7.66 (dd, *J* = 8.0, 1.4 Hz, 2H), 7.61 (dd, *J* = 8.0, 1.4 Hz, 2H), 7.42 – 7.05 (m, 16H), 6.09 – 5.91 (m, 2H), 5.59 (ddd, *J* = 17.0, 10.3, 8.0 Hz, 1H), 5.07 – 4.92 (m, 2H), 4.37 (app. q, *J* = 6.1 Hz, 1H), 3.23 (app q, *J* = 7.7 Hz, 1H), 2.76 – 2.61 (m, 4H), 1.59 (br s, 1H), 1.00 (s, 9H). ^{13}C NMR (101 MHz, $CDCl_3$) δ 140.67, 138.36, 136.66, 135.89, 135.88, 134.05, 133.95, 131.00, 130.58, 129.54, 129.41, 129.28, 128.30, 128.22, 127.47, 127.34, 127.30, 126.38, 126.21, 116.00, 74.22, 62.69, 53.55, 42.40, 26.99, 19.25.

The acidic water layer was basified with 8.0 M NaOH (12 mL) and extracted with $CHCl_3$ (4 x 30 mL). After drying ($MgSO_4$), filtering and evaporation of the solvent, excess (*S*)-1-phenylbut-3-en-2-amine (2.02 g, 13.7 mmol) was recovered.

***tert*-Butyl ((*S,E*)-2-((*tert*-butyldiphenylsilyl)oxy)-4-phenylbut-3-en-1-yl)((*S*)-1-phenylbut-3-en- 2-yl)carbamate (83)**. The amine from above (3.30 g, 6.21 mmol) was dissolved in THF (50 mL), Boc_2O (2.80 g, 12.8 mmol) and Et_3N (2 mL) were added subsequently. The mixture was refluxed overnight upon which TLC confirmed complete conversion. Concentration *in vacuo* and purification by silica gel column chromatography (pentane/EtOAc = 99 : 1 → 97 : 3) afforded the title compound (5.10 g) as a mixture with unseparated Boc_2O. Analytical data are from a pure fraction. $[\alpha]_D^{21}$ = -4.6 (c =1.0, $CHCl_3$). HRMS calculated for $C_{41}H_{49}NO_3Si$ $[M+H]^+$: 632.3555; found: 632.3555. IR 3069, 3028, 2963, 2930, 2859, 1694, 1454, 1427, 1410, 1366, 1250, 1167, 1113, 964. ^{1}H NMR (400 MHz, $CDCl_3$) mixture of rotamers (2:1 ratio): δ 7.75 (d, *J* = 6.8 Hz, 2H),7.68 (d, *J* = 6.8 Hz, 2H), 7.47 – 7.29 (m, 6H), 7.29 – 7.11 (m, 8H), 7.08 – 6.95 (m, 2H), 6.10 (s, 0.35H), 6.06 (s, 0.65H), 5.92 – 5.63 (m, 2H), 4.93 (d, *J* = 10.5 Hz, 1H), 4.88 (d, *J* = 17.4 Hz, 1H), 4.33 (br s, 0.4H), 4.12 (br s, 1H), 3.91 (br s, 0.6H), 3.53 – 3.15 (m, 1H), 3.13 – 2.64 (m, 3H), 1.23 (s, 3H), 1.19 (s, 6H), 1.07 (s, 9H). ^{13}C NMR (101 MHz, $CDCl_3$) mixture of rotamers (2:1 ratio): δ 154.77, 138.63, 137.93, 137.23, 137.01, 135.98, 135.88, 134.16, 133.59, 130.73, 130.41, 129.66, 129.30, 128.22, 128.16, 127.59, 127.47, 127.11, 126.35, 126.17, 115.87, 79.34, 73.59 (minor CHO), 72.58 (major CHO), 62.70 (major CHN), 61.71 (minor CHN), 53.02 (major CH_2N), 50.99 (minor CH_2N), 38.64 (minor CH_2Ph), 38.12 (major CH_2Ph), 28.13, 27.03, 19.27.

***tert*-Butyl *(3S,6S)*-6-benzyl-3-((*tert*-butyldiphenylsilyl)oxy)-3,6-dihydropyridine-1(2H)-carboxylate (84)**. The Boc-protected diene **83** (max 6.21 mmol) from above was dissolved in DCM under argon. Grubbs I catalyst (309 mg, 0.375 mmol) was added and the mixture refluxed overnight after which TLC confirmed complete conversion. The solvent was evaporated and the crude product purified by silica gel column chromatography (pentane/EtOAc = 99 : 1 → 96 : 4) to afford the target cyclic alkene as a colorless oil (2.84 g, 5.39 mmol, 76% over two steps). $[\alpha]_D^{21}$ = +159 (c =1.0,

$CHCl_3$). HRMS calculated for $C_{33}H_{41}NO_3Si$ $[M+H]^+$: 528.2929; found: 528.2922. IR 3028, 2971, 2931, 2858, 1810, 1756, 1692, 1454, 1448, 1417, 1364, 1112, 1072. ^1H NMR (400 MHz, $CDCl_3$, 60 ^oC) δ 7.70 (d, *J* = 7.4 Hz, 2H), 7.64 (d, *J* = 7.7 Hz, 2H), 7.41 – 7.27 (m, 6H), 7.24 – 7.09 (m, 5H), 5.62 (dd, *J* = 10.1, 3.7 Hz, 1H), 5.59 – 5.52 (m, 1H), 4.69 (br s, 1H), 4.23 (br s, 1H), 4.07 – 3.98 (m, 1H), 2.82 (dd, *J* = 12.9, 5.9 Hz, 1H), 2.77 – 2.67 (m, 2H), 1.44 (s, 9H), 1.04 (s, 9H). ^{13}C NMR (101 MHz, $CDCl_3$, 60 ^oC) δ 154.73, 138.04, 135.80, 134.65, 134.22, 131.16, 129.60, 129.46, 128.22, 127.61, 127.42, 126.53, 126.25, 79.35, 64.08, 38.95, 28.44, 26.95, 19.20.

***tert*-Butyl *(2R,5S)*-2-benzyl-5-((*tert*-butyldiphenylsilyl)oxy)piperidine-1-carboxylate (87)**. A suspension of substrate *tert*-butyl *(3S,6S)*-6-benzyl-3-((tert-butyldiphenylsilyl)oxy)-3,6-dihydropyridine-1(2H)-carboxylate (500 mg, 0.947 mmol) and copper (II) sulfate (1.50 g, 9.47 mmol) in ethanol (2 mL) was cooled on an ice bath. Hydrazine (3.01 mL, 96.0 mmol) was added drop wise and the reaction was subsequently stirred for 15 min. After that, the reaction mixture was stirred at 70 °C for 24h until TLC showed the reaction was completed. The mixture was filtered over celite and concentrated *in vacuo*. The residue was diluted with ethyl acetate and washed with water, brine and dried over $MgSO_4$, and concentrated *in vacuo*. The residue was purified by flash chromatography (pentane/EtOAc = 99 : 1 → 90 : 10) to furnish *tert*-butyl *(2R,5S)*-2-benzyl-5-((*tert*-butyldiphenylsilyl)oxy)piperidine-1-carboxylate **87** (400 mg, 0.756 mmol, 80 % yield) as a colorless oil. LC-MS m/z: calculated for $C_{33}H_{43}NO_3Si$ $[M+H]^+$ 530.30, found 530.81. ^1H NMR (400 MHz, $CDCl_3$) δ 7.72 – 7.65 (m, 4H), 7.42 – 7.33 (m, 6H), 7.27 – 7.20 (m, 2H), 7.18 – 7.14 (m, 3H), 4.56 (br s, 1H), 4.09 (br d, *J* = 7.0 Hz, 1H), 3.91 (br s, 1H), 2.94 – 2.78 (m, 2H), 2.72 – 2.61 (m, 1H), 2.19 (br, 1H), 1.72 – 1.47 (m, 3H), 1.35 (s, 9H), 1.06 (s, 9H). ^{13}C NMR (101 MHz, $CDCl_3$) δ 155.20, 139.35, 135.97, 135.79, 134.52, 133.99, 129.72, 129.66, 129.27, 128.36, 127.69, 127.64, 126.16, 79.04, 65.79, 50.37, 44.02, 35.99, 28.41, 27.04, 26.24, 20.28, 19.38.

(*2R,5S*)-2-Benzyl-5-((*tert*-butyldiphenylsilyl)oxy)piperidine (88). To a solution of *tert*-butyl *(2R,5S)*-2-benzyl-5-((*tert*-butyldiphenylsilyl)oxy)piperidine-1-carboxylate **87** (120 mg, 0.226 mmol) in DCM was added 20% TFA, the reaction mixture was stirred at r.t. for 2.5h until TLC showed the reaction was completed. When the reaction is finished, the mixture was co-evaporated with toluene (3 times), the residue was diluted with ethyl acetate and washed with 10% Na_2CO_3, water, brine and dried over $MgSO_4$, and concentrated under reduced pressure. Filtering and concentration under reduced pressure afforded the crude product that was used without further purification. $[\alpha]_D^{20}$ = -13 (c =1.0, $CHCl_3$). HRMS calculated for $C_{28}H_{35}NOSi$ $[M+H]^+$: 430.2554; found: 430.2555. IR 3069, 3026, 2930, 2855, 2805, 1495, 1454, 1427, 1288, 1103, 1082, 1030, 993. ^1H NMR (400 MHz, $CDCl_3$) δ 7.59 (d, *J* = 7.9 Hz, 4H), 7.42 – 7.29 (m, 6H), 7.26 – 7.18 (m, 3H), 7.08 – 7.03 (m, 2H), 4.00 (br s, 1H), 3.19 (br d, *J* = 10.0 Hz, 1H), 3.14 – 2.90 (m, 2H), 2.73 (br d, *J* = 10.2 Hz, 1H), 2.63 – 2.49 (m, 1H), 1.86 (br s, 1H), 1.69 (br s, 1H), 1.38 (br t, *J* = 11.3 Hz, 2H), 1.02 (s, 9H). ^{13}C NMR (101 MHz, $CDCl_3$) δ 135.63, 135.57, 135.46, 133.41, 133.00, 130.17, 130.07, 129.29, 128.89, 127.96, 127.84, 127.36, 66.03, 57.45, 49.28, 39.12, 32.21, 26.91, 26.04, 19.20.

***tert*-Butyl *(2R,5S)*-2-benzyl-5-hydroxypiperidine-1-carboxylate (90)**. A solution of TBAF (2.83 mL, 2.83 mmol) was added to a solution of *tert*-butyl *(2R,5S)*-2-benzyl-5-((*tert*-butyldiphenylsilyl)oxy)piperidine-1-carboxylate **87** (1.00 g, 1.89 mmol) in THF (15 mL) with ice cooling and the mixture was stirred at r.t. for 2.5h, After being diluted with water, the mixture was extracted with ethyl acetate (3 times), the organic layer was washed with water and brine, dried over $MgSO_4$ and concentrated under *in vacuo*. The residue was purified by flash chromatography (pentane/EtOAc = 99 : 1→80 : 20) to furnish *tert*-butyl *(2R,5S)*-2-benzyl-5- hydroxypiperidine-1-carboxylate (440 mg, 1.51 mmol, 80% yield) as a colorless oil. $[\alpha]_D^{22}$ = -33 (*c* = 1.0, $CHCl_3$). LC-MS m/z: calculated for $C_{17}H_{25}NO_3$ $[M+H]^+$ 292.18, found: 292.71. ^{1}H NMR (400 MHz, $CDCl_3$) δ 7.30 – 7.25 (m, 2H), 7.21 – 7.15 (m, 3H), 4.35 (br s, 1H), 4.25 (br s, 1H), 3.64 – 3.57 (m, 1H), 2.91 (dd, *J* = 13.1, 8.1 Hz, 1H), 2.75 (dd, *J* = 12.8, 10.8 Hz, 2H), 1.90 (br s, 1H), 1.66 -1.59 (m, 3H), 1.30 (s, 9H). ^{13}C NMR (101 MHz, $CDCl_3$) δ 154.78, 138.98, 129.20, 128.44, 126.26, 79.72, 67.03, 53.90, 45.69, 35.81, 28.26, 28.12, 26.28.

***tert*-Butyl (*2R,5S*)-2-benzyl-5-methoxypiperidine-1-carboxylate (91)**. To a solution of *tert*-butyl *(2R,5S)*-2-benzyl-5-hydroxypiperidine-1-carboxylate (70.0 mg, 0.240 mmol) and NaH (60%, 17.3 mg, 0.721 mmol) in DMF (3 mL) at 0 °C, MeI (0.045 mL, 0.721 mmol) was added dropwise with continuous stirring, and the mixture was allowed to stand at room temperature for 24h. The mixture was diluted with water (10 mL), and extracted with ethyl acetate (3 x 20 mL). The organic layer was washed with water, brine, dried over $MgSO_4$, filtered, and concentrated *in vacuo*. The residue was purified by flash chromatography (pentane/EtOAc = 99 : 1→90 : 10) to furnish *tert*-butyl *(2R,5S)*-2-benzyl-5-methoxypiperidine-1-carboxylate (61.0 mg, 0.200 mmol, 83% yield). $[\alpha]_D^{22}$ = -36 (*c* = 0.6, $CHCl_3$). LC-MS m/z: calculated for $C_{18}H_{27}NO_3$ $[M+H]^+$ 306.20, found: 306.82. ^{1}H NMR (400 MHz, $CDCl_3$) δ 7.31 – 7.24 (m, 2H), 7.19 – 7.14 (m, 3H), 4.43 (br s, 1H), 4.33 (br d, *J* = 13.5 Hz, 1H), 3.41 (br s, 1H), 3.34 (s, 3H), 2.97 – 2.82 (m, 2H), 2.74 (dd, *J* = 13.1, 8.3 Hz, 1H), 1.94 – 1.85 (m, 1H), 1.88 – 1.72 (m, 2H), 1.34 (s, 9H), 1.31 – 1.28 (m, 1H). ^{13}C NMR (101 MHz, $CDCl_3$) δ 155.27, 139.22, 129.28, 128.48, 126.28, 79.35, 73.19, 56.08, 52.47, 40.38, 36.00, 28.42, 23.84, 21.47.

***(2R,5S)*-2-Benzyl-5-methoxypiperidine (92).** To a solution of compound *tert*-butyl *(2R,5S)*-2-benzyl-5-methoxypiperidine-1-carboxylate (30.0 mg, 0.098 mmol) in DCM was added 20% TFA, the reaction mixture was stirred at r.t. for 2.5h until TLC showed the reaction was completed. When the reaction is finished, the mixture was co-evaporated with toluene (3 times), the residue was diluted with ethyl acetate and washed with 10% Na_2CO_3, water, brine and dried over $MgSO_4$, and concentrated under reduced pressure. Filtering and concentration under reduced pressure afforded the crude product *(2R,5S)*-2-benzyl-5-methoxypiperidine **92** that was used without further purification. ^{1}H NMR (400 MHz, $CDCl_3$) δ 7.34 – 7.23 (m, 3H), 7.19 – 7.13 (m, 2H), 3.69 – 3.46 (m, 2H), 3.36 (s, 3H), 3.25 – 2.95 (m, 2H), 2.77 – 2.71 (m, 1H), 2.66 – 2.62 (m, 1H), 2.21 (br s, 1H), 1.98 – 1.83 (m, 1H), 1.71 – 1.52 (m, 1H), 1.34 – 1.16 (m, 1H). ^{13}C NMR (101 MHz, $CDCl_3$) δ 135.46, 129.34, 128.99, 127.47, 72.84, 57.81, 56.77, 47.10, 39.13, 28.58, 25.86.

***tert*-Butyl *(2R,5S)*-2-benzyl-5-(cyclopropylmethoxy)piperidine-1-carboxylate (93).** To a solution of *tert*-butyl *(2R,5S)*-2-benzyl-5-hydroxypiperidine-1-carboxylate **90** (100 mg, 0.344 mmol) and NaH (60%, 24.7 mg, 1.03 mmol) in DMF (3 mL) at 0 °C, (bromomethyl)cyclopropane (139 mg, 1.03 mmol) was added dropwise with continuous stirring, and the mixture was allowed to stand at room temperature for 24h. The mixture was diluted with water (10 mL), and extracted with ethyl acetate (3 x 20 mL). The organic layer was washed with water, brine, dried over $MgSO_4$, filtered, and concentrated. The residue was purified by flash chromatography (pentane/EtOAc = 99 : 1→90 : 10) to furnish *tert*-butyl *(2R,5S)*-2-benzyl-5-(cyclopropylmethoxy) piperidine-1- carboxylate **93** (110 mg, 0.318 mmol, 89% yield). $[\alpha]_D^{22}$ = -38 (*c* = 1.0, $CHCl_3$). LC-MS m/z: calculated for $C_{21}H_{31}NO_3$ $[M+H]^+$ 346.18, found 346.40. ^{1}H NMR (400 MHz, $CDCl_3$) δ 7.29 – 7.25 (m, 2H), 7.22 – 7.15 (m, 3H), 4.44 (br s, 1H), 4.28 (d, *J* = 13.9 Hz, 1H), 3.54 (s, 1H), 3.40 – 3.20 (m, 2H), 2.96 – 2.84 (m, 2H), 2.74 (dd, *J* = 13.2, 8.1 Hz, 1H), 2.02 – 1.93 (m, 1H), 1.89 – 1.67 (m, 2H), 1.34 (s, 9H), 1.29 – 1.24 (m, 1H), 1.08 – 0.98 (m, 1H), 0.50 – 0.47 (m, 2H), 0.30 – 0.10 (m, 2H). ^{13}C NMR (101 MHz, $CDCl_3$) δ 155.17, 139.27, 129.27, 128.33, 126.23, 79.20, 72.66, 71.08, 51.90, 40.42, 36.08, 28.40, 24.50, 21.74, 10.83, 3.18, 2.92.

***(2R,5S)*-2-Benzyl-5-(cyclopropylmethoxy)piperidine (94)**. To a solution of solution of *tert*-butyl *(2R,5R)*-2-benzyl-5-(cyclopropylmethoxy)piperidine-1-carboxylate **93** (50.0 mg, 0.145 mmol) in DCM was added 20% TFA, the reaction mixture was stirred at r.t. for 2.5h until TLC showed the reaction was completed. When the reaction is finished, the mixture was co-evaporated with toluene (3 times), the residue was diluted with ethyl acetate and washed with 10% Na_2CO_3, water, brine, dried over $MgSO_4$, filtered and concentrated under reduced pressure afforded the crude product that was used without further purification. ^{1}H NMR (400 MHz, $CDCl_3$) δ 7.31 – 7.23 (m, 3H), 7.20 – 7.10 (m, 2H), 3.70 (s, 1H), 3.51 (s, 1H), 3.31 (p, *J* = 9.9 Hz, 2H), 3.16 (s, 2H), 2.74 (br s, 2H), 2.17 (br d, *J* = 11.6 Hz, 1H), 1.87 (br d, *J* = 13.4 Hz, 1H), 1.62 (br d, *J* = 11.5 Hz, 1H), 1.32 (br d, *J* = 11.7 Hz, 1H), 0.99 (br s, 1H), 0.51 (d, *J* = 7.7 Hz, 2H), 0.16 (d, *J* = 4.5 Hz, 2H). ^{13}C NMR (101 MHz, $CDCl_3$) δ 135.38, 129.33, 128.98, 127.46, 74.17, 71.12, 57.86, 47.58, 39.23, 29.26, 26.09, 10.82, 3.12, 3.07.

Supporting Figures

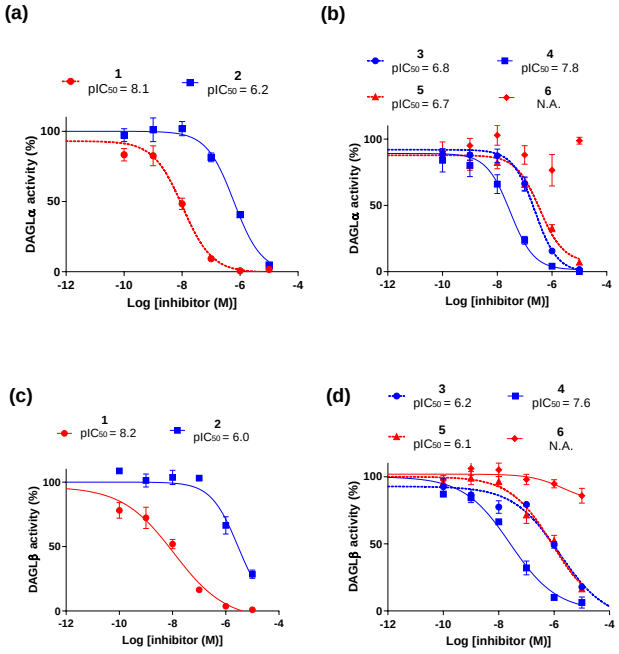

Figure S.1. Concentration-dependent inhibition curves of recombinant human DAGLα (a, b) and human DAGLβ (c, d) as determined with competitive ABPP labeled by DH379 (representative gels in Figure 1f and g). Data represent average values ± SEM; n = 3 per group .

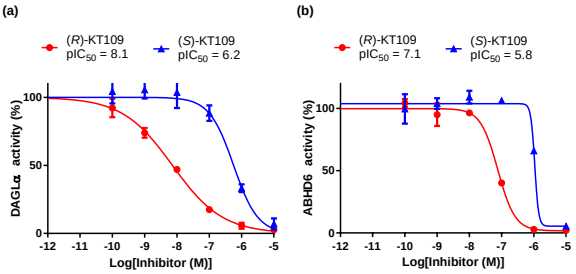

Figure S.2. *In vitro* characterization of *(R)*-KT109 and *(S)*-KT109 in mouse brain membrane proteome. (a-b) Dose response curves of DAGLα (a) and ABHD6 (b) inhibition as determined with competitive ABPP labeled by MB064 (Figure 2d and e). Data represent average values ± SEM; n = 3 per group.

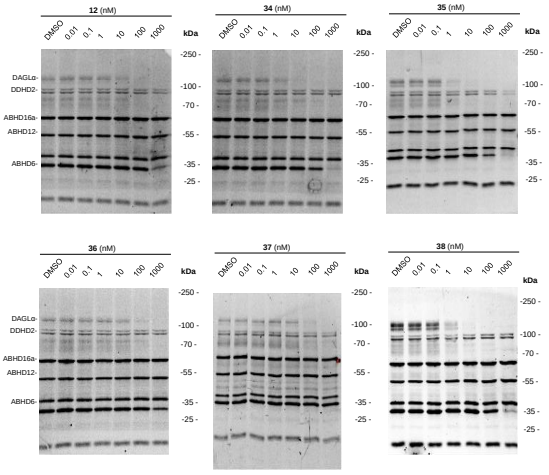

Figure S.3., related to Figure 3b. Full gels of *in vitro* competitive ABPP for compounds **34-38**, and **12** in mouse brain membrane proteome using probe MB064 (0.25 µM, 20 min).

References

1. Adibekian, A.; Hsu, K. L.; Speers, A. E.; Brown, S. J.; Spicer, T.; Fernandez-Vega, V.; Ferguson, J.; Cravatt, B. F.; Hodder, P.; Rosen, H. Optimization and characterization of a triazole urea inhibitor for alpha/beta hydrolase domain-containing protein 11 (ABHD11): anti-probe for LYPLA1/LYPLA2 dual inhibitor ML211. In *Probe Reports from the NIH Molecular Libraries Program*, Bethesda (MD), 2010.
2. Adibekian, A.; Martin, B. R.; Wang, C.; Hsu, K. L.; Bachovchin, D. A.; Niessen, S.; Hoover, H.; Cravatt, B. F. Click-generated triazole ureas as ultrapotent in vivo-active serine hydrolase inhibitors. *Nature Chemical Biology* **2011,** 7, 469-478.
3. Hsu, K. L.; Tsuboi, K.; Chang, J. W.; Whitby, L. R.; Speers, A. E.; Pugh, H.; Cravatt, B. F. Discovery and optimization of piperidyl-1,2,3-triazole ureas as potent, selective, and in vivo-active inhibitors of alpha/beta-hydrolase domain containing 6 (ABHD6). *Journal of Medicinal Chemistry* **2013,** 56, 8270-8279.
4. Hsu, K. L.; Tsuboi, K.; Adibekian, A.; Pugh, H.; Masuda, K.; Cravatt, B. F. DAGLbeta inhibition perturbs a lipid network involved in macrophage inflammatory responses. *Nature Chemical Biology* **2012,** 8, 999-1007.
5. Inloes, J. M.; Hsu, K. L.; Dix, M. M.; Viader, A.; Masuda, K.; Takei, T.; Wood, M. R.; Cravatt, B. F. The hereditary spastic paraplegia-related enzyme DDHD2 is a principal brain triglyceride lipase. *Proceedings of the National Academy of Sciences of the United States of America* **2014,** 111, 14924-14929.
6. Bisogno, T.; Howell, F.; Williams, G.; Minassi, A.; Cascio, M. G.; Ligresti, A.; Matias, I.; Schiano-Moriello, A.; Paul, P.; Williams, E. J.; Gangadharan, U.; Hobbs, C.; Di Marzo, V.; Doherty, P. Cloning of the first sn1-DAG lipases points to the spatial and temporal regulation of endocannabinoid signaling in the brain. *Journal of Cell Biology* **2003,** 163, 463-468.
7. Reisenberg, M.; Singh, P. K.; Williams, G.; Doherty, P. The diacylglycerol lipases: structure, regulation and roles in and beyond endocannabinoid signalling. *Philosophical Transactions of the Royal Society London B Biological Sciences* **2012,** 367, 3264-3275.
8. Tanimura, A.; Yamazaki, M.; Hashimotodani, Y.; Uchigashima, M.; Kawata, S.; Abe, M.; Kita, Y.; Hashimoto, K.; Shimizu, T.; Watanabe, M.; Sakimura, K.; Kano, M. The endocannabinoid 2-arachidonoylglycerol produced by diacylglycerol lipase alpha mediates retrograde suppression of synaptic transmission. *Neuron* **2010,** 65, 320-327.
9. Gao, Y.; Vasilyev, D. V.; Goncalves, M. B.; Howell, F. V.; Hobbs, C.; Reisenberg, M.; Shen, R.; Zhang, M. Y.; Strassle, B. W.; Lu, P.; Mark, L.; Piesla, M. J.; Deng, K.; Kouranova, E. V.; Ring, R. H.; Whiteside, G. T.; Bates, B.; Walsh, F. S.; Williams, G.; Pangalos, M. N.; Samad, T. A.; Doherty, P. Loss of retrograde endocannabinoid signaling and reduced adult neurogenesis in diacylglycerol lipase knock-out mice. *Journal of Neuroscience* **2010,** 30, 2017-2024.
10. Baggelaar, M. P.; Janssen, F. J.; van Esbroeck, A. C.; den Dulk, H.; Allara, M.; Hoogendoorn, S.; McGuire, R.; Florea, B. I.; Meeuwenoord, N.; van den Elst, H.; van der Marel, G. A.; Brouwer, J.; Di Marzo, V.; Overkleeft, H. S.; van der Stelt, M. Development of an activity-based probe and in silico design reveal highly selective inhibitors for

diacylglycerol lipase-alpha in brain. *Angewandte Chemie International Edition* **2013,** 52, 12081-12085.

11. Janssen, F. J.; Deng, H.; Baggelaar, M. P.; Allara, M.; van der Wel, T.; den Dulk, H.; Ligresti, A.; van Esbroeck, A. C.; McGuire, R.; Di Marzo, V.; Overkleeft, H. S.; van der Stelt, M. Discovery of glycine sulfonamides as dual inhibitors of sn-1-diacylglycerol lipase alpha and alpha/beta-hydrolase domain 6. *Journal of Medicinal Chemistry* **2014,** 57, 6610-6622.
12. Bisogno, T.; Cascio, M. G.; Saha, B.; Mahadevan, A.; Urbani, P.; Minassi, A.; Appendino, G.; Saturnino, C.; Martin, B.; Razdan, R.; Di Marzo, V. Development of the first potent and specific inhibitors of endocannabinoid biosynthesis. *Biochimica Biophysica Acta-Molecular and Cell Biology of Lipids* **2006,** 1761, 205-212.
13. Bisogno, T.; Burston, J. J.; Rai, R.; Allara, M.; Saha, B.; Mahadevan, A.; Razdan, R. K.; Wiley, J. L.; Di Marzo, V. Synthesis and pharmacological activity of a potent inhibitor of the biosynthesis of the endocannabinoid 2-arachidonoylglycerol. *ChemMedChem* **2009,** 4, 946-950.
14. Bisogno, T.; Mahadevan, A.; Coccurello, R.; Chang, J. W.; Allara, M.; Chen, Y. G.; Giacovazzo, G.; Lichtman, A.; Cravatt, B.; Moles, A.; Di Marzo, V. A novel fluorophosphonate inhibitor of the biosynthesis of the endocannabinoid 2-arachidonoylglycerol with potential anti-obesity effects. *British Journal of Pharmacology* **2013,** 169, 784-793.
15. Ogasawara, D.; Deng, H.; Viader, A.; Baggelaar, M. P.; Breman, A.; den Dulk, H.; van den Nieuwendijk, A. M.; Soethoudt, M.; van der Wel, T.; Zhou, J.; Overkleeft, H. S.; Sanchez-Alavez, M.; Mo, S.; Nguyen, W.; Conti, B.; Liu, X.; Chen, Y.; Liu, Q. S.; Cravatt, B. F.; van der Stelt, M. Rapid and profound rewiring of brain lipid signaling networks by acute diacylglycerol lipase inhibition. *Proceedings of the National Academy of Sciences of the United States of America* **2016,** 113, 26-33.
16. Hsu, K. L.; Tsuboi, K.; Whitby, L. R.; Speers, A. E.; Pugh, H.; Inloes, J.; Cravatt, B. F. Development and optimization of piperidyl-1,2,3-triazole ureas as selective chemical probes of endocannabinoid biosynthesis. *Journal of Medicinal Chemistry* **2013,** 56, 8257-8269.
17. Velmourougane, G.; Harbut, M. B.; Dalal, S.; McGowan, S.; Oellig, C. A.; Meinhardt, N.; Whisstock, J. C.; Klemba, M.; Greenbaum, D. C. Synthesis of new (-)-bestatin-based inhibitor libraries reveals a novel binding mode in the S1 pocket of the essential malaria M1 metalloaminopeptidase. *Journal of Medicinal Chemistry* **2011,** 54, 1655-1666.
18. van den Nieuwendijk, A. M.; Ruben, M.; Engelsma, S. E.; Risseeuw, M. D.; van den Berg, R. J.; Boot, R. G.; Aerts, J. M.; Brussee, J.; van der Marel, G. A.; Overkleeft, H. S. Synthesis of L-altro-1-deoxynojirimycin, D-allo-1-deoxynojirimycin, and D-galacto-1-deoxynojirimycin from a single chiral cyanohydrin. *Organic Letters* **2010,** 12, 3957-3959.
19. van der Wel, T.; Janssen, F. J.; Baggelaar, M. P.; Deng, H.; den Dulk, H.; Overkleeft, H. S.; van der Stelt, M. A natural substrate-based fluorescence assay for inhibitor screening on diacylglycerol lipase alpha. *Journal of Lipid Research* **2015,** 56, 927-935.
20. Navia-Paldanius, D.; Savinainen, J. R.; Laitinen, J. T. Biochemical and pharmacological characterization of human alpha/beta-hydrolase domain containing 6 (ABHD6) and 12 (ABHD12). *Journal of Lipid Research* **2012,** 53, 2413-2424.
21. Manabe, K. Synthesis of novel chiral quaternary phosphonium salts with a multiple hydrogen-bonding site, and their application to asymmetric phase-transfer alkylation. *Tetrahedron* **1998,** 54, 14465-14476.

22. Jung, K. M.; Astarita, G.; Thongkham, D.; Piomelli, D. Diacylglycerol Lipase-alpha and -beta Control Neurite Outgrowth in Neuro-2a Cells through Distinct Molecular Mechanisms. *Molecular Pharmacology* **2011,** 80, 60-67.
23. Baggelaar, M. P.; Chameau, P. J. P.; Kantae, V.; Hummel, J.; Hsu, K. L.; Janssen, F.; van der Wel, T.; Soethoudt, M.; Deng, H.; den Dulk, H.; Allara, M.; Florea, B. I.; Di Marzo, V.; Wadman, W. J.; Kruse, C. G.; Overkleeft, H. S.; Hankemeier, T.; Werkman, T. R.; Cravatt, B. F.; van der Stelt, M. Highly Selective, Reversible Inhibitor Identified by Comparative Chemoproteomics Modulates Diacylglycerol Lipase Activity in Neurons. *Journal of the American Chemical Society* **2015,** 137, 8851-8857.
24. Blacker, A. J.; Roy, M.; Hariharan, S.; Headley, C.; Upare, A.; Jagtap, A.; Wankhede, K.; Mishra, S. K.; Dube, D.; Bhise, S.; Vishwasrao, S.; Kadam, N. Convenient Method for Synthesis of N-Protected alpha-Amino Epoxides: Key Intermediates for HIV Protease Inhibitors. *Organic Process Research & Development* **2011,** 15, 331-338.
25. Jiang, J. B.; Kallemeijn, W. W.; Wright, D. W.; van den Nieuwendijk, A. M. C. H.; Rohde, V. C.; Folch, E. C.; van den Elst, H.; Florea, B. I.; Scheij, S.; Donker-Koopman, W. E.; Verhoek, M.; Li, N.; Schurmann, M.; Mink, D.; Boot, R. G.; Codee, J. D. C.; van der Marel, G. A.; Davies, G. J.; Aerts, J. M. F. G.; Overkleeft, H. S. In vitro and in vivo comparative and competitive activity-based protein profiling of GH29 alpha-L-fucosidases. *Chemical Science* **2015,** 6, 2782-2789.
26. Griengl, H.; Klempier, N.; Pochlauer, P.; Schmidt, M.; Shi, N. Y.; Zabelinskaja-Mackova, A. A. Enzyme catalysed formation of (S)-cyanohydrins derived from aldehydes and ketones in a biphasic solvent system. *Tetrahedron* **1998,** 54, 14477-14486.

3

Rapid and profound rewiring of brain lipid signaling networks by acute diacylglycerol lipase inhibition

Based on
H. Deng, D. Ogasawara, A. Viader, M. P. Baggelaar, A. Breman, H. den Dulk, A. M. C. H. van den Nieuwendijk, M. Soethoudt, T. van der Wel, J. Zhou, H. S. Overkleeft, M. Sanchez-Alavez, S. Mori, W. Nguyen, B. Conti, X.J. Liu, Y. Chen, Q.S. Liu, B. F. Cravatt, M. van der Stelt, *Proc. Natl. Acad. Sci. USA*, **2016**, 113, 26-33.

Introduction

Classically understood forms of neurotransmission involve polar small molecules that are stored in synaptic vesicles and released in response to depolarizing signals that promote vesicle fusion with the presynaptic plasma membrane of neurons.[1] More recently, lipids have emerged as a distinct type of chemical messenger in the nervous system that appear to be generated at the time of their intended action rather than amassed in vesicles.[2-5] This “on-demand” model for production implicates lipid biosynthetic enzymes as major regulators of chemical signaling in the central nervous system (CNS). In support of this premise, the enzymes that produce several classes of lipid transmitters, including lysophospholipids,[6] eicosanoids,[7] and endocannabinoids[8,9] are highly expressed in the nervous system and play important roles in brain development, synaptic plasticity, and the modulation of complex

behaviors. The diacylglycerol (DAG) lipase enzymes DAGLα and DAGLβ,[10] for instance, produce the endocannabinoid 2-arachidonoylglycerol (2-AG),[11,12] and the constitutive genetic disruption of DAGLα lowers brain 2-AG and arachidonic acid content,[13,14] resulting in impaired synaptic plasticity,[13,14] hypophagia,[15] enhanced anxiety and fear responses,[16,17] and propensity for spontaneous seizures.[15]

Many bioactive lipids share structural features and can be, in principle, connected to one another through multi-step metabolic routes,[2,18,19] suggesting the potential for crosstalk among lipid signaling pathways *in vivo*. Such crosstalk could produce more sophisticated forms of integrated or counter-balanced signal transduction to affect complex physiological or disease processes in a dynamic manner. The extent to which individual enzymes within larger metabolic pathways exert control over a multitude of bioactive lipids, however, remains poorly understood. This question can be studied in genetically modified mice lacking specific lipid metabolic enzymes, but the long-term, constitutive inactivation of enzymes renders these models poorly suited for distinguishing rapid and dynamic processes from slower, adaptive changes that may occur in lipid pathways. Pharmacological approaches, on the other hand, provide a powerful means to assess the temporal consequences of acute enzyme blockade on the dynamic composition of lipid networks in the brain under both physiological and pathological conditions. Unfortunately, selective and *in vivo*-active inhibitors are not yet available for many lipid biosynthetic enzymes. Known inhibitors for DAGLs, for instance, have been used to study the function of 2-AG as a retrograde messenger in neuronal cell and/or brain slice preparations,[20-25] but these inhibitors lack the selectivity,[26] potency, and/or chemical properties[21] required for central activity *in vivo*.

In Chapter 2, DH376 was described as a potent and selective, covalent 1,2,3-triazole urea inhibitor for DAGLα and DAGLβ, which provides an excellent chemical tool for investigating DAGL function *in vivo*. This Chapter presents data revealing that acute pharmacological blockade of DAGL by using DH376 and its analogue DO34 leads to a rapid and dramatic reorganization of lipid signaling pathways in the brain that includes elevations in bioactive DAGs and reductions in the two major endocannabinoids, 2-arachidonoylglycerol (2-AG) and *N*-arachidonoylethanolamine (anandamide or AEA), arachidonic acid, and the prostaglandins PGD_2 and PGE_2. The DAGL inhibitors also impaired endocannabinoid-dependent forms of synaptic plasticity and attenuated lipopolysaccharide-induced neuroinflammatory responses, including reductions in core body temperature (anapyrexia). These findings highlight the special role that DAGL enzymes play as integrative nodes for coordinating crosstalk among several classes of lipid transmitters to modulate neuro(immuno)logical functions in the CNS.

Results and Discussion

Potent and selective 1,2,3-triazole ureas inhibitors of DAGLα

The development of DAGL inhibitors has been historically hindered by a dearth of assays for monitoring the activity of these enzymes in native biological systems. Recently tailored activity-based probes were introduced that enable the independent and concurrent monitoring of DAGLα and DAGLβ activities in brain and other tissue/cell types.[27,28] Guided by competitive activity-based protein profiling (ABPP) methods,[29] one of these tailored probes was converted into a series of potent 1,4-substituted, 1,2,3-triazole urea (1,2,3-TU) inhibitors of DAGLβ that displayed peripheral, but not central activity *in vivo*[27] (e.g., KT172 (**1**), Figure 1a). Further modification and optimization of the 1,2,3-TU scaffold was performed to generate selective and CNS-active inhibitors of DAGLα and β. In brief, modifications to the distal phenyl ring appended to the triazole leaving group of KT172 yielded inhibitors with good potency for DAGLα and moderate inhibition of DAGLβ, but the resulting compounds showed little or no CNS activity *in vivo*. Therefore, attention was turned to modifying the staying group of the 1,2,3-TU scaffold (Figure 1a, blue). This, in combination with truncated variations of the triazole leaving group (Figure 1a, black), furnished DO34, a structural analog distinct from DH376 (See Chapter 2), which was identified as a highly potent DAGL inhibitor (Figure 1a). Both DH376 and DO34 blocked the DAGLα conversion of 1-stearoyl-2-arachidonoyl-*sn*-glycerol (SAG) to 2-AG with IC_{50} values of 7 nM (2–26 nM; 95% CI, n=4) and 27 nM (7-98 nM; 95% CI, n=4), respectively (Figure 1b and Table 1), as determined using a real-time, fluorescence-based natural substrate assay with membrane lysates from HEK293T cells expressing recombinant human DAGLα.[30] Using this substrate assay, DH376 and DO34 were also confirmed as potent inhibitors of DAGLβ with IC_{50} values of 1.5-5.6 nM (Figure 1b and Table 1).

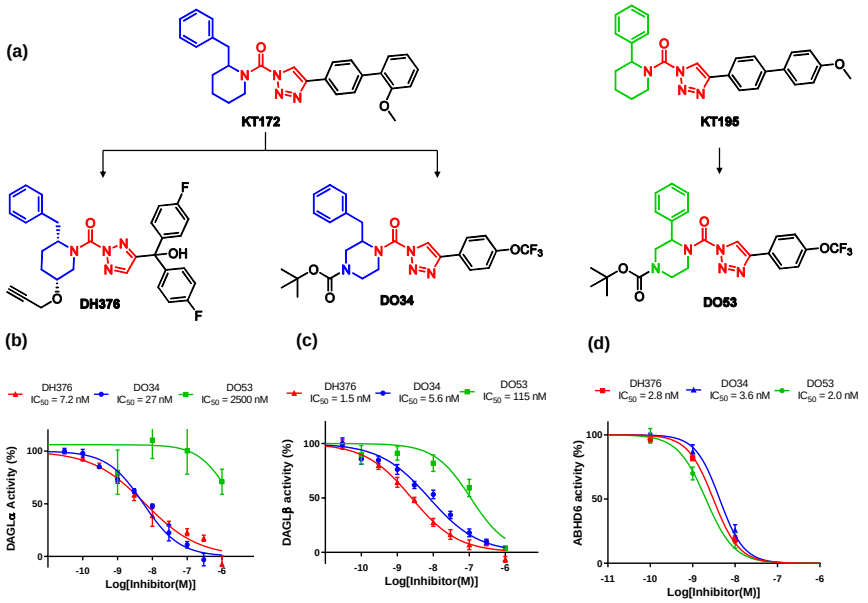

Figure 1. Discovery of triazole urea inhibitors (DH376, DO34) and a control probe DO53 for DAGLs. (a) Chemical structures of original DAGL inhibitor KT172 and structurally related control probe KT195 highlighting conserved features (blue [staying groups, KT172, DH376, DO34], red (triazole urea reactive groups), green (staying groups, KT195 and DO53]) and modifications (black) that furnished potent DAGL inhibitors DH376 and DO34 and the control probe DO53. (b-c) Concentration-dependent inhibition of recombinant human DAGLα (b) and mouse DAGLβ (b) activity by DH376, DO34, and DO53 as measured with a 1-stearoyl-2-arachidonoyl-sn-glycerol (SAG) substrate assay in DAGL-transfected HEK293T cells. Data represent average values ± SD; n = 4 per group. (d) Concentration-dependent inhibition of recombinant human ABHD6 activity by DH376, DO34 and DO53 as measured with 2-AG substrate assay in ABHD6-transfected HEK293T cells. Data represent average values ± SD; n = 4 per group.

Table 1. Inhibitory values for DH376, DO34, and DO53 versus recombinant and native DAGL enzymes using the indicated assays. Data represent average values ± SD; n = 3 per group.

		pIC_{50}	
Enzyme	Compound	DAGLα	DAGLβ
Recombinant enzymes	DH376	8.2 ± 0.3	8.6 ± 0.3
(SAG hydrolysis assay)	DO34	8.2 ± 0.3	8.1 ± 0.3
	DO53	5.6 ± 0.4	7.0 ± 0.2
Brain enzymes			
ABPP (DH379)	DH376	9.2 ± 0.1	8.6 ± 0.1
	DO34	9.1 ± 0.1	8.6 ± 0.1
	DO53	7.4 ± 0.1	7.6 ± 0.1
Brain enzymes			
ABPP (HT-01)	DH376	8.9 ± 0.1	8.3 ± 0.1
	DO34	9.3 ± 0.1	8.6 ± 0.1
	DO53	7.6 ± 0.1	7.1 ± 0.1

DH376 possesses a chiral propargyl ether at the C5 position of the staying group, which may serve as a handle to introduce reporter groups by copper-catalyzed azide-alkyne cycloaddition (CuAAC, or "click") chemistry[31] to generate an additional class of DAGL-tailored activity-based probes for target engagement studies. With this goal in mind a BODIPY-derivatized analog of DH376 was synthesized and termed DH379 (Scheme 1).

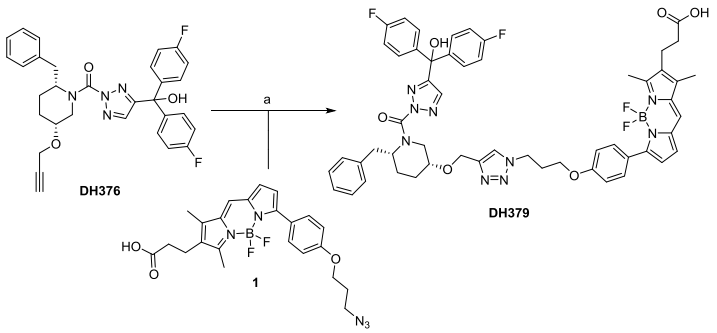

Scheme 1. Synthesis of activity-based probe DH379. Reagents and conditions: (a) $CuSO_4$, sodium ascorbate, DCM/H_2O, r.t., 24h, 32%.

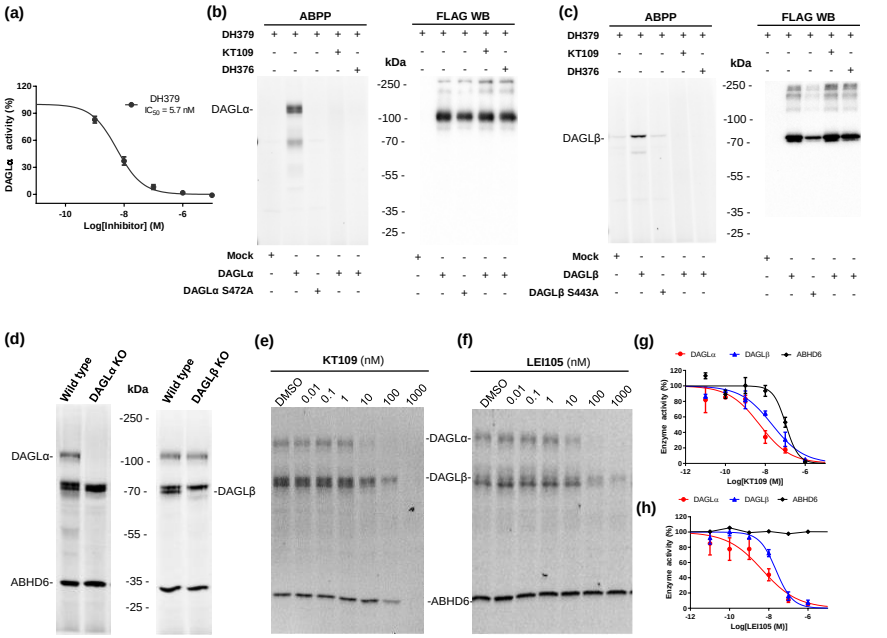

Figure 2. Characterization of DAGLs-tailored activity-based probe DH379. (a) Concentration-dependent inhibition curves against hDAGLα in HEK-293T cell membrane as determined by the PNP colorimetric assay (±SD, n=4). (b-c) Left panels, DH379 labels recombinant, FLAG epitope-tagged wild type DAGLα (b) and DAGLβ (b), but not their catalytically inactive serine mutants (S472A and S443A, respectively) or DAGL enzymes that have been pre-treated with inhibitors KT109 or DH376 (1 µM, 30 min). Right panel, western blots showing DAGL enzyme expression levels in transfected HEK293T cells as determined with an anti-FLAG antibody. (d) Labelling and detection of endogenous DAGLα and DAGLβ in mouse brain membrane proteome by DH379 (1 µM, 20 min). The assignment of DH379-labeled proteins as DAGLα and DAGLβ was confirmed by analyzing brain membrane proteomes from wild type and DAGLα and DAGLβ knockout mice. (e-f) Competitive ABPP with the indicated concentrations of DAGLs inhibitors KT109 (irreversible) (e) and LEI105 (reversible) (f) using ABP DH379 (1 µM, 30 min) in mouse brain membrane proteome. (g-h) Quantification of data shown in (e-f). Data represent average values ± SEM; n = 3 per group.

To validate DH379 as a DAGLα and DAGLβ probe, different hDAGLα and –β constructs were transiently transfected into HEK293T cells (Figure 2). First, it was confirmed that DH379 labeled membrane fractions of hDAGLα-FLAG transfected cells. A strong fluorescence signal was observed at around 120 kDa, which corresponds to the molecular mass of hDAGLα. This band overlapped with a protein visualized by the FLAG-tag antibody and was absent in mock-transfected cells. Pre-incubation of KT109 or DH376 (1 µM, 30 min) inhibited the enzymatic activity and prevented the labeling of the protein at 120 kDa. Site-directed mutagenesis of the catalytic DAGLα nucleophile Ser472 into an alanine abolished labeling of the protein by DH379. Of note, hDAGLα protein expression was not altered by the mutagenesis as determined with the FLAG-tag antibody (Figure 2b). In a similar vein, DH379-mediated labeling of recombinant hDAGLβ was confirmed, (Figure 2c). Mouse

membrane brain proteomes were used to detect labeling of endogenous DAGLα and –β by DH379 (Figure 2d). The fluorescent bands corresponding to DAGLα and – β were absent in proteomes derived from DAGLα, or DAGLβ knockout mice, respectively. In addition to DAGLα and -β, DH379 also labeled two more bands, ~35 kDa (ABHD6) and ~70 kDa (almost overlapped with DAGLβ). Collectively, these data confirm and validate DH379 as a DAGL-tailored activity-based probe.

Competitive activity-based proteome profiling (ABPP) assays were next employed to evaluate the activity and selectivity of DH376 and DO34 against endogenous DAGLs and other serine hydrolases in the mouse brain membrane proteome. These studies were performed with three different activity-based probes: two DAGL-tailored activity based probes – DH379 and HT-01[27] – and a broad-spectrum serine hydrolase-directed probe fluorophosphonate-rhodamine (FP-rhodamine).[32] HT-01 and DH379 provided target engagement assays for DAGLs, while FP-rhodamine assessed cross-reactivity across a broad array of brain serine hydrolases. DH376 and DO34 inhibited DAGLα and β labeling by HT-01 (Figure 3a, b and Table 1) and DH379 (Figure 3C, D and Table 1) with IC_{50} values in the range of 0.4–2.8 (DAGLα) and 0.6-5.8 (DAGLβ) nM, respectively. DO34 and DH376 showed excellent selectivity for DAGLs, with the only detectable serine hydrolase off-targets being ABHD6 and PLA2G7 (Figure 4a). Finally, DH376 and DO34 showed minimal and negligible binding, respectively, to cannabinoid CB_1 (CB_1R) and CB_2 (CB_2R) receptors as measured with radioligand binding assays (IC_{50} values > 1 µM, Figure 4).

Previously, 2-phenyl piperidine analogs, such as KT195[27] (Figure **1a**), were reported to serve as useful inactive control probes that display greatly attenuated inhibition of DAGLs, while maintaining activity against common off-targets like ABHD6.[27] Based on this precedent, DO53 (a 2-phenyl piperazine analog of DO34) was synthesized, and found to exhibit ~100-fold lower activity against DAGLα compared to DO34 or DH376 as measured by DAG substrate hydrolysis (Figure 1b and Table 1) or competitive ABPP assays in mouse brain (Figure 3 and Table 1). On the other hand, DO53 cross-reacted with the shared off-targets of DO34 and DH376 (Figures 1 and 3), designating DO53 as a potentially suitable control compound for biological studies of DAGL enzymes.

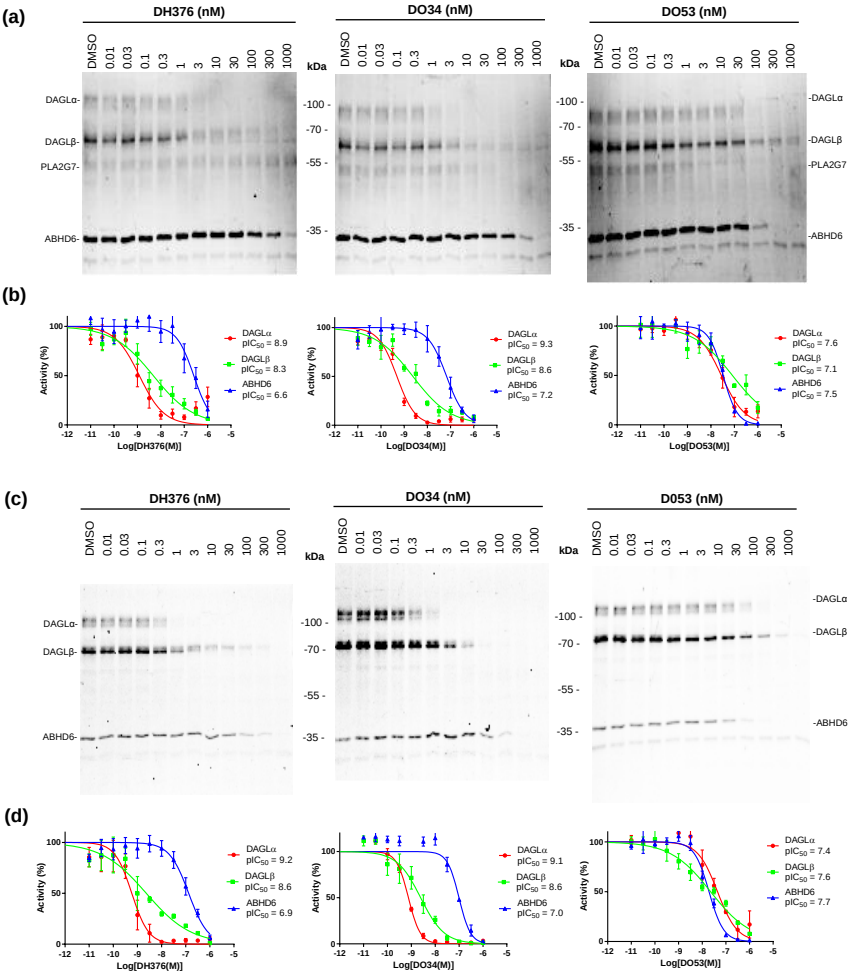

Figure 3. *In vitro* activity characterization of DAGL inhibitors and control probe DO53. (a) Concentration-dependent inhibition of DAGLα and DAGLβ activity by DH376, DO34 and DO53 as measured by gel-based competitive ABPP of mouse brain proteome using the tailored activity-based probe HT-01 (1 μM, 30 min). (b) Quantification of data shown in (a). Data represent average values ± SEM; n = 3 per group. (c) Concentration-dependent inhibition of DAGLα, DAGLβ, and ABHD6 by DH376, DO34 and DO53 as measured by gel-based competitive ABPP of mouse brain proteome using the DH379 probe (1 μM, 30 min). (d) Quantification of data shown in (c). Data represent average values ± SEM; n = 3 per group.

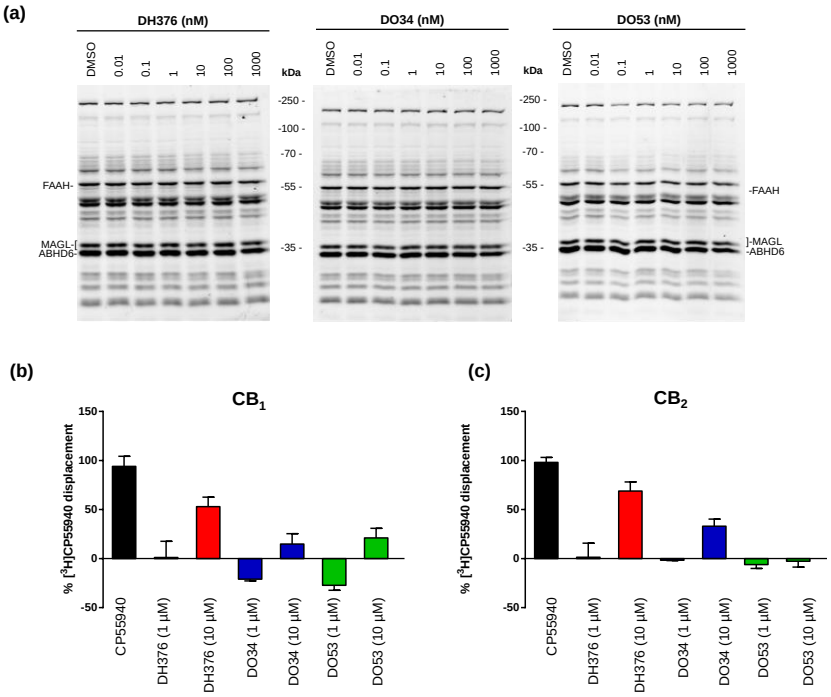

Figure 4. *In vitro* selectivity profiles of DAGL inhibitors and control probe DO53. (a) Selectivity profiles of DH376, DO34, and DO53 across mouse brain serine hydrolases as determined by competitive ABPP using the broad-spectrum probe TAMRA-FP (0.5 µM, 20 min). Representative mouse brain serine hydrolases detected by TAMRA-FP are labeled. Note that, in these gel profiles for TAMRA-FP labeling, the ABHD6 and MAGL signals were not resolved from one another (and DAGLα and DAGLβ are not visualized due to overlapping migration patterns with more abundant serine hydrolases). (b-c) Interactions of DAGL inhibitors and control probe DO53 with cannabinoid receptors (CB_1R and CB_2R). DH376 and DO34 were tested for binding affinity to the CB_1R (b) and CB_2R (c) using competition studies with the radiolabeled CBR ligand [3H]-CP55940 using membranes from recombinant human CB_1R- and CB_2R-overexpressing CHO cells. DO34 was inactive at 10 µM and DH376 was inactive at 1 µM and showed only partial (~50% for CB_1, ~70% for CB_2) inhibition of ligand binding at 10 µM.

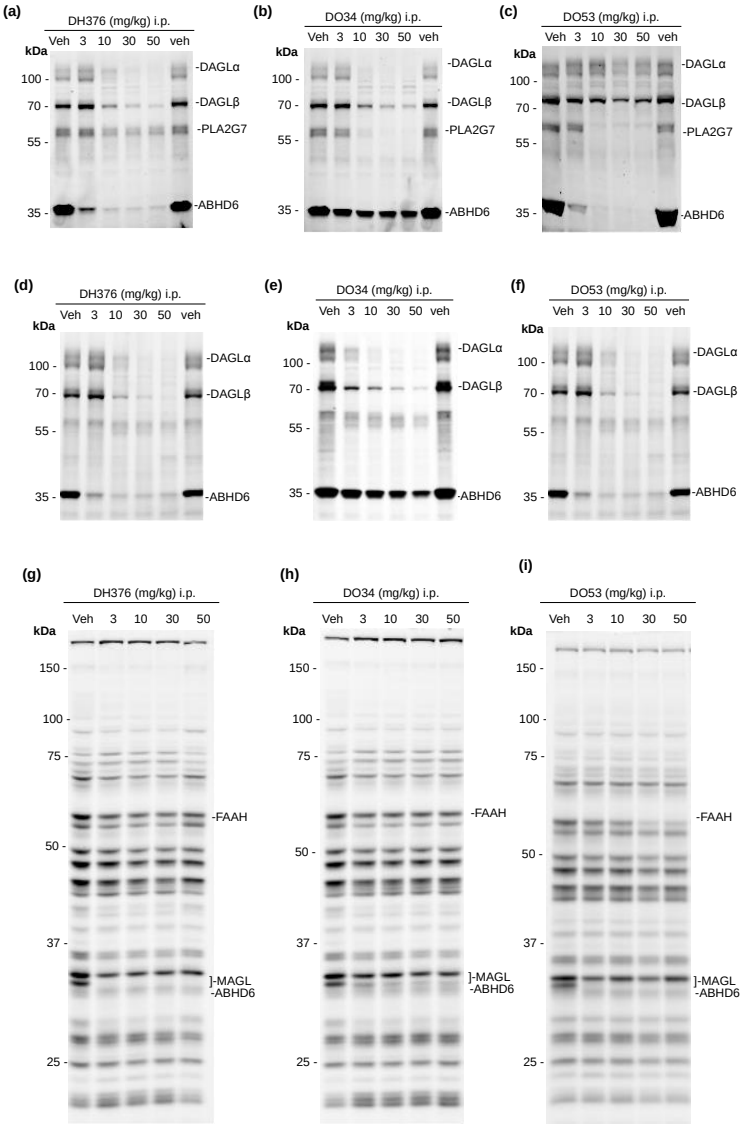

Figure 5. *In vivo* activity and selectivity of DH376, DO34, and DO53 in mice. (a−f) Dose-dependent inhibition of DAGLα and DAGLβ in brain tissue from mice treated with DH376 (a, d), DO34 (b, e), and DO53 (c, f) (indicated doses, i.p., 4 h treatment) as determined by competitive ABPP using DH379 (a-c) and HT-01 (d-f) as probes (1 μM, 30 min). (g-i) Selectivity assessment of cross-reactivity with other serine hydrolases in brain tissue from mice treated with vehicle (Veh) or DH376 (g), DO34 (h), or DO53 (i) (i.p., 4 h) as determined by competitive ABPP using the TAMRA-FP probe (1 μM, 30 min).

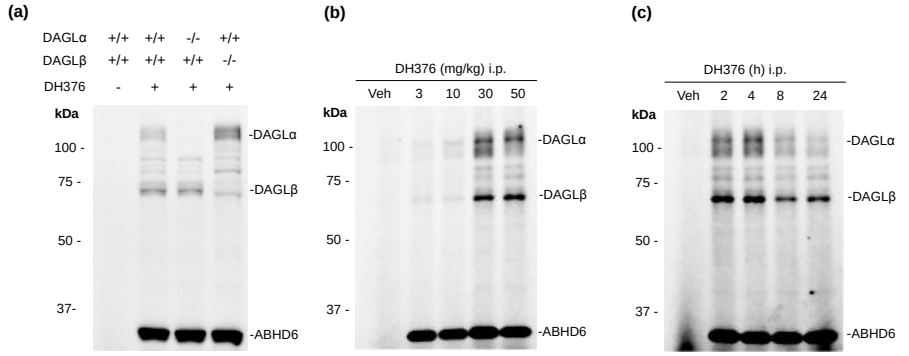

Figure 6. *Ex vivo* Click Chemistry ABPP (CuAAC) analysis of DH376-treated mice. (a) Confirmation of direct, *in vivo*-labeling of DAGLα and DAGLβ by DH376 (50 mg/kg, i.p., 4 h) visualized by CuAAC to a Cy5 reporter group. The assignment of DH376-labeled proteins as DAGLα and DAGLβ was confirmed by analyzing brain membrane proteomes from wild type and DAGLα$^{-/-}$ and DAGLβ$^{-/-}$ mice. (b, c) Dose dependency (b) and time course (c) of direct, *in vivo*-labeling of DAGLα and DAGLβ ABPP in brain tissue from mice treated with DH376 (i.p., 4 h for dose-dependency; 50 mg/kg, i.p. for time-course) visualized by CuAAC to a Cy5 reporter group.

DAGL inhibitors are centrally active *in vivo*

DH376, DO34, DO53 or vehicle was administered intraperitoneally (i.p.) to male C57Bl/6 mice across a dose range of 3 to 50 mg/kg. After 4h, the animals were sacrificed and brain tissue analyzed by competitive ABPP with DH379, HT-01, and TAMRA-FP, which revealed clear dose-dependent blockade of DAGLα activity for both DH376 and DO34 with ED_{50} values of 5-10 mg/kg (Figure 5) and full inhibition of the enzyme being observed at 30-50 mg/kg of inhibitor. DAGLβ (and ABHD6) were also inhibited by DH376, and to a lesser extent by DO34, which instead exhibited cross-reactivity with PLA2G7 (Figure 4a). DO53, on the other hand, did not substantially inhibit DAGLα or DAGLβ at any dose tested, but inhibited both ABHD6 and PLA2G7 (Figure 5). Brain proteomes from DH376-treated mice were conjugated to a Cy5 fluorophore by CuAAC, which confirmed direct, dose-dependent labeling of DAGL enzymes (Figure 6).

These target engagement profiles were confirmed and extended by performing ABPP coupled to high-resolution, quantitative mass spectrometry (MS). In brief, brain proteomes from inhibitor- and vehicle-treated mice were incubated with the serine hydrolase-directed activity-based probe fluorophosphonate (FP)-biotin,[33] and probe-labeled enzymes were enriched by streptavidin chromatography, digested on bead with trypsin, and the resulting tryptic peptides modified by reductive dimethylation (ReDiMe) of lysine residues using isotopically heavy and light formaldehyde, respectively.[34] In these experiments, inhibited serine hydrolases are

identified as enzymes showing low heavy/light ReDiMe ratios. Quantitative MS confirmed complete inhibition of DAGLα by DH376 and DO34, with DAGLβ also being strongly and partially inhibited by these compounds, respectively, and revealed the following off-targets (defined as serine hydrolases with heavy/light ratios < 0.5): ABHD6 (DH376, DO34), CES1C (DH376, DO34), ABHD2 (DO34), BCHE (DH376), LIPE (DH376), PAFAH2 (DO34), and PLA2G7 (DO34) (Figure 7a and 7b). DO53 showed negligible activity against DAGLα or DAGLβ (heavy/light ratios of ~0.8), but cross-reacted with many of the off-targets of DH376 and DO34 (ABHD2, ABHD6, CES1C, PLA2G7, PAFAH2) (Figure 7c and 7d). Taken together (Figure 7d), these competitive ABPP studies designated DH376 and DO34 as *in vivo*-active inhibitor with complementary selectivity profiles that, when used in combination with the control probe DO53, can report on the function of DAGLs in the CNS.

Next, the time course of DAGL inhibition in mice was investigated. At a high dose (50 mg/kg), DH376 and DO34, but not DO53, demonstrated sustained inhibition of DAGLs for up to 8 h, with partial recovery at 24 h post-dosing (Figure 8a-c). Interestingly, a lower dose of DH376 (3 mg/kg) produced substantial inhibition of DAGLα within 30 min after administration, but enzyme activity quickly recovered by 4h (Figure 8g and h). In contrast, DAGLβ was only partly inhibited at 3 mg/kg (Figure 8g), while the off-target ABHD6 remained inhibited up to 8h (Figure 8g and h). These differences in the duration of target engagement were confirmed by *ex vivo* CuAAC-mediated conjugation of a Cy5-azide tag to brain proteomes of DH376-treated mice, which showed strong, but transient DH376 labeling of DAGLα and sustained reactivity with ABHD6 (Figure 8i and j). The recovery of DAGLα activity in this time course study at low drug dose could indicate that DAGLα is a short half-life protein that is rapidly degraded and replaced by newly synthesized enzyme or that the DH376-DAGLα interaction is reversible. Arguing against the latter hypothesis, however, was the observations that the inhibition and direct labeling of DAGLα by DH376 were maintained after size exclusion chromatography, which contrasted with the substantial rescue of DAGLα activity observed in this experiment with the reversible inhibitor LEI-105[35] (Figure 9). DH376, but not LEI-105 also showed a time-dependent increase in potency against DAGLα (Figure 9), another hallmark of an irreversible mechanism of action. The results thus support that DAGLα is a short half-life protein in the CNS and further demonstrate that sustained inhibition of DAGLα for many hours can be achieved at higher doses of DH376 and DO34 (50 mg/kg), where presumably sufficient drug remains in the CNS to block newly synthesized DAGLα protein.

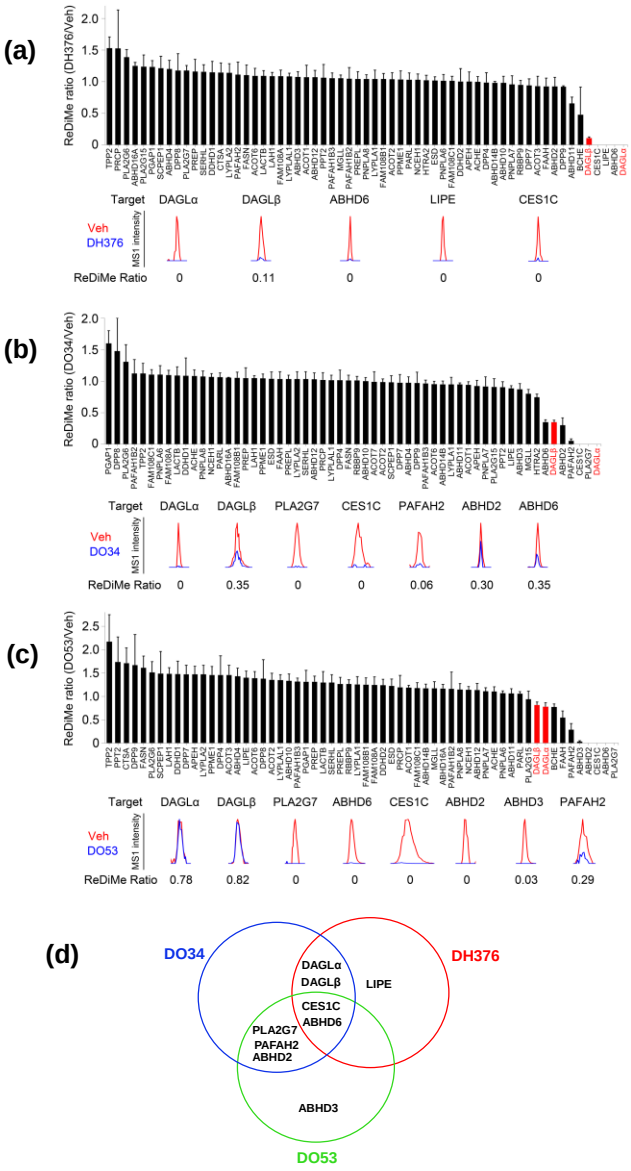

Figure 7. Assessment of *in vivo* activity and selectivity of DH376, DO34 and DO53 by ABPP-ReDiMe analysis. ABPP-ReDiMe analysis of brain serine hydrolase activities from mice treated with DH376 (a), DO34 (b) and DO53 (c) (50 mg/kg, i.p., 4 h treatment), where serine hydrolases were labeled and enriched using an FP-biotin probe. Representative MS1 chromatograms for DAGLα and DAGLβ, as well as additional serine hydrolase targets are shown for each inhibitor. Data represent average values ± SEM; n = 4 mice per group. (d) Summary of the serine hydrolase targets of DH376, DO34, and DO53 in mouse brain. Serine hydrolases with ReDiMe ratio values < 0.5 were defined as targets for each inhibitor. Note that the DAGLα and DAGLβ are the only two serine hydrolases found to be inhibited by both DH376 and DO34, but not DO53, in mouse brain.

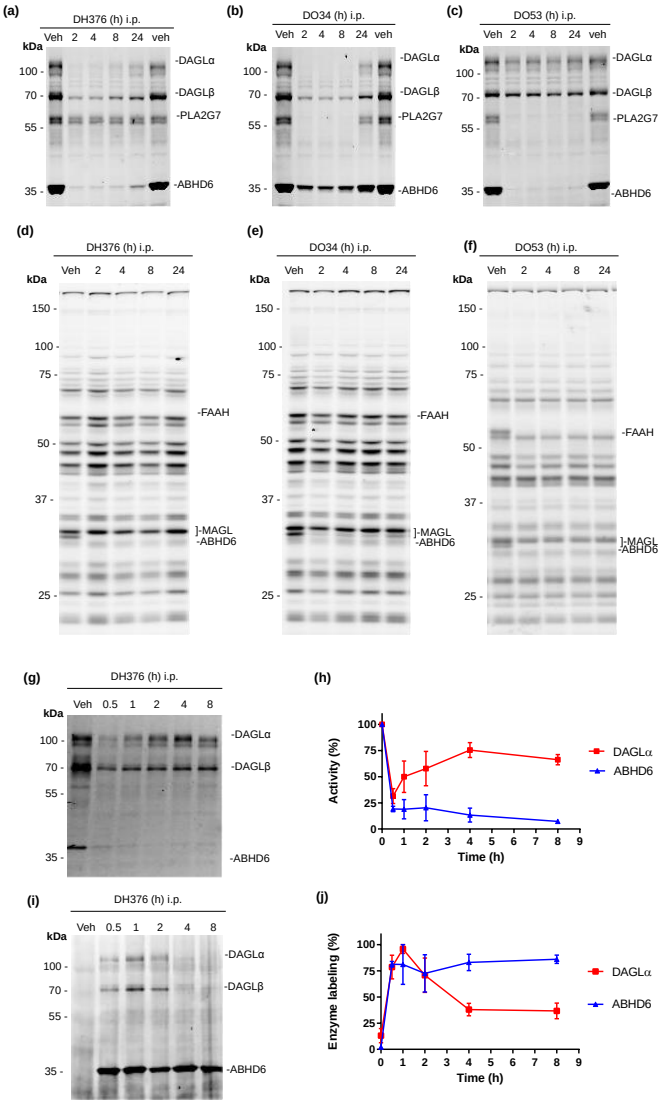

Figure 8. *In vivo* time course analysis of DAGLα inhibition and recovery. (a-f) Assessment of time-course of inhibition of DAGLα and DAGLβ (a-c) and cross-reactivity with other serine hydrolases (d-f) in brain tissue from mice treated with vehicle or DH376 (a, d), DO34 (b, e) or DO53 (c, f) (50 mg/kg, i.p.) as determined by competitive ABPP using the HT-01 (a-c) or TAMRA-FP (d-f) probe (1 μM, 30 min). (g, h) Time course of inhibition of DAGLα in brain tissue from mice treated with a low dose of DH376 (3 mg/kg, i.p.) as determined by competitive ABPP using the DH379 probe (1 μM, 30 min). Gel data (g) and quantification of these data (h) relative to a vehicle-treated control group are shown for both DAGLα and ABHD6, an off-target of DH376. Data represent average values ± SEM; n = 3 mice per group. (i, j) Time course of direct labeling of DAGLα in brain tissue from mice treated with DH376 (3 mg/kg, i.p.) visualized by CuAAC to a Cy5 reporter group. Gel data (i) and quantification of these data (j) relative to a vehicle-treated control group are shown for both DAGLα and ABHD6. Data represent average values ± SEM; n = 3 mice per group.

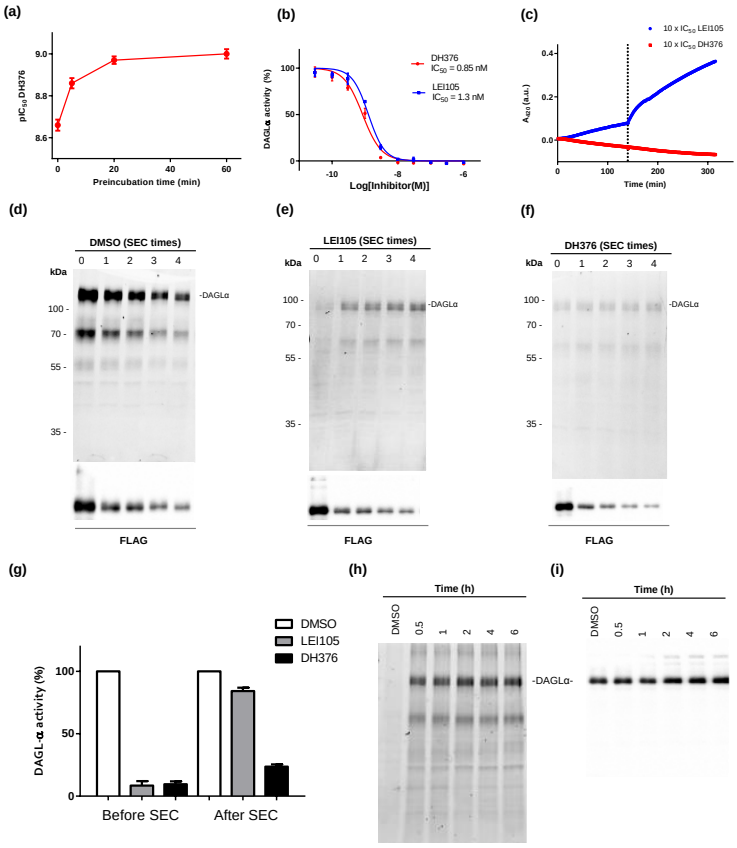

Figure 9. (a) Plot of IC_{50} values for DH376 inhibition of DAGLα measured after the indicated pre-incubation times prior to analysis with a para-nitrophenylbutyrate (PNP) substrate (300 μM). Data represent average values ± SEM; n = 4 per group. (b) Concentration-dependent inhibition of recombinant human DAGLα activity by DH376 and LEI105 (reversible DAGLα inhibitor). Data represent average values ± SEM; n=4 per group. (c) DAGLα product progression curves as a function of time in the presence of PNP substrate (300 μM) and 10 x IC_{50} value concentrations of LEI105 or DH376. After 135 min, a second batch of PNP (300 μM) was added to the reaction vessel. Note that the enzymatic rate of PNP conversion is increased in the LEI105-treated sample (blue line), whereas no effect is observed in enzyme inhibited by DH376 (red line). Shown is a representative experiment of four replicate experiments. (d-f) Recovery of DAGLα activity after exposing the indicated inhibitor (or control)-treated samples to serial size exclusion chromatography (SEC) steps, where activity was measured by gel-based ABPP using probe DH379. Note that little or no DH379 labeling was observed post-SEC in DH376-treated DAGLα samples (f), while substantial MB064 labeling was observed post-SEC for DAGLα samples treated with the reversible inhibitor LEI105 (e). Western blots using anti-FLAG antibodies are shown to assess protein loading. (g) Quantification of the data shown in (d-f) after four SEC steps. Data represent average values±SD; n=3 per group. (h) Assessment of stability of the DH376-DAGLα adduct. Recombinant human DAGLα expressed in transfected HEK293T cell proteomes was treated with DH376 (10 nM) for 30 min and the reaction was exposed to five serial SEC steps and then incubated for the indicated times (0.5-6h) before visualization by CuAAC to a Cy5 reporter group. No appreciable loss of signal intensity for the DH376-DAGLα adduct was observed across the time course analysis. (i) Western blot using anti-FLAG antibodies is shown to assess protein loading.

DAGL inhibitors rapidly and radically alter brain lipid profiles in mice

Three independently generated lines of DAGLα$^{-/-}$ mice have shown that genetic disruption of this enzyme substantially reduces brain 2-AG (~80-90%).[13,14,17,36] These brain 2-AG changes are accompanied by concomitant accumulation of the main 2-AG lipid precursor and protein kinase C (PKC) agonist[37] 1-stearoyl-2-arachidonoylglycerol (SAG)[17] and depletion of the principal 2-AG hydrolytic metabolite and eicosanoid precursor, arachidonic acid (AA)[13,14,17] as well as of the second major endocannabinoid anandamide (AEA)[13,14]. It remains unclear, however, what portion of these widespread alterations reflects the active and dynamic regulation of brain lipid signaling networks by DAGLα versus adaptive changes caused by the constitutive, long-term ablation of this enzyme. This question was therefore addressed by examining the brain lipid profiles of mice treated with the CNS-active DAGL inhibitors DH376 and DO34 and the control probe DO53.

First, the brain lipid profiles of mice were analyzed by LC-MS at a single 4h time point post-dosing with inhibitors (50 mg/kg, i.p.). This revealed dramatic reductions in 2-AG in DH376- and DO34- but not DO53-treated mice (Figure 10a). This reduction in 2-AG was comparable in magnitude to that observed in DAGLα$^{-/-}$ mice (Figure 10a), demonstrating the rapid flux of DAGL-mediated 2-AG production *in vivo*. The robust depletion of brain 2-AG in DH376- and DO34-treated mice was dose-dependent (Figure 10h and i) and was observed within 2 h after injection. The time-dependent changes in 2-AG caused by DH376 appeared to be shorter-lived than those of DO34 (Figure 10g and j). Notably, DH376 and DO34 also caused rapid, dose-dependent changes in other DAGL-regulated lipids, including reductions in AEA (Figure 10b and h-j), AA (Figure 10c and h-j), and the prostaglandins PGD_2 and PGE_2 (Figure 10d, e and h-j), as well as elevations in SAG (Figure 10f and h-j) and C18:1/C20:4 DAG (Figure S1.; Table 2). The changes in each lipid species were again similar in magnitude to those observed in DAGLα$^{-/-}$ mice (Figure 8b-f), were dose-dependent (Figure 8h and f), displayed similar time courses to alterations observed in 2-AG in DH376- and DO34-treated mice (Figure 8g and j), and were absent in DO53-treated mice (Figure 8a-f). While most lipid changes were consistent between DAGL inhibitor-treated and DAGLα$^{-/-}$ mice, it was found that DAGLα$^{-/-}$ mice showed reductions in triglycerides (TAGs), that were not observed in animals treated with DAGL inhibitors (Figure S2). These alterations in TAGs may thus require chronic, long-term inactivation of DAGLα, which is also known to cause significant reductions in total body weight and fat.[15]

These studies, taken together, demonstrate that acute pharmacological blockade of DAGLs produces a rapid and dramatic reorganization of lipid signaling networks in the mammalian brain that largely mirrors the myriad lipid changes observed in the brains of DAGLα$^{-/-}$ mice. Accordingly, it was then asked whether DH376 and DO34 would affect physiological processes that involve one or more components of the DAGL-regulated lipid signaling network.

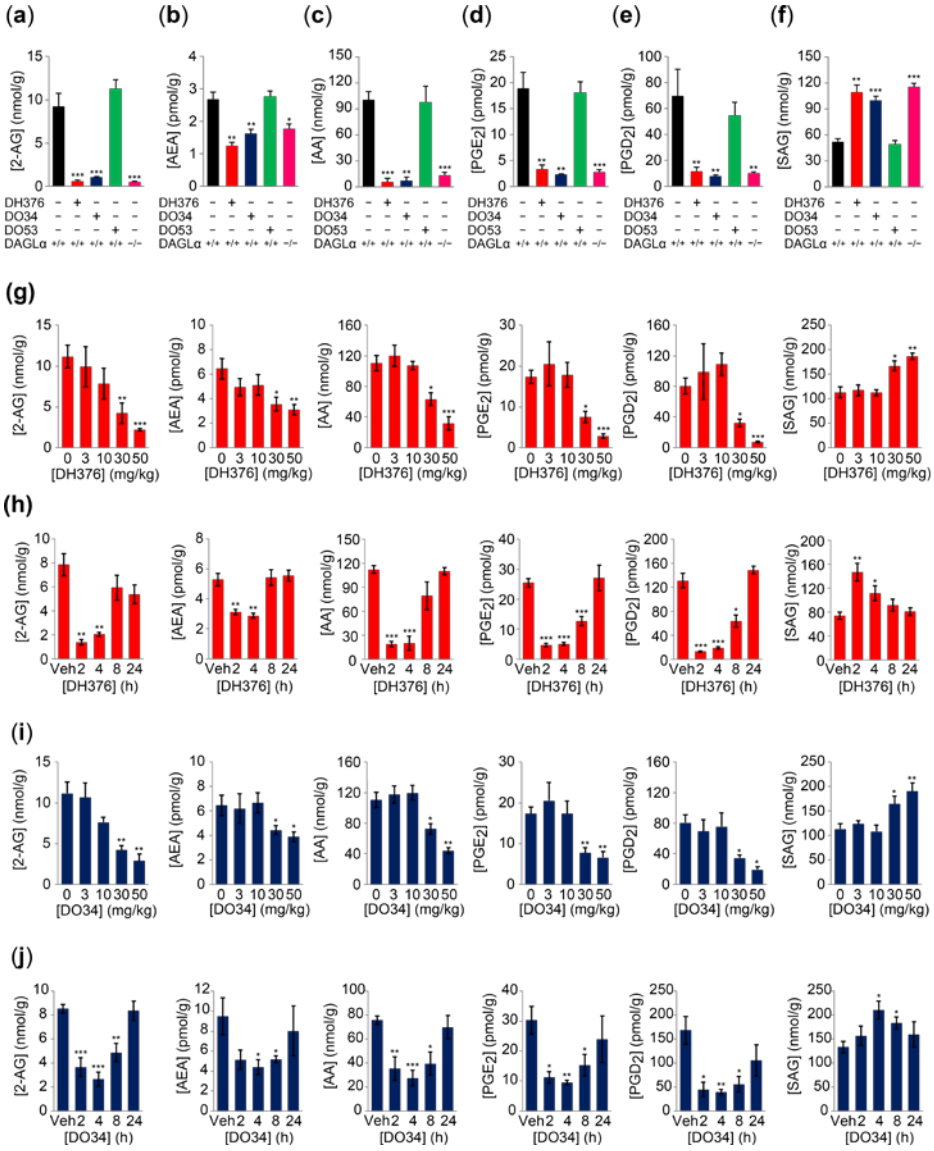

Figure 10. Acute inhibition of DAGLs causes rapid and profound remodeling of bioactive lipid pathways in the brain. (a-f) Quantification of 2-AG (a) and related bioactive lipids (b-f) in brain tissue from mice treated with vehicle or DH376, DO34, and DO53 (50 mg/kg, i.p., 4 h). Lipid profiles from DAGLα$^{-/-}$ mice are shown for comparison. Data represent average values ± SEM; n = 5–6 mice per group. *P < 0.05; **P < 0.01; ***P < 0.001 for inhibitor treated DAGLα$^{+/+}$ mice or DAGLα$^{-/-}$ mice vs. vehicle treated DAGLα$^{+/+}$ mice. (g, i) Dose-dependent changes in 2-AG and other bioactive lipids in brain tissue from mice treated with DH376 (g) and DO34 (i) (i.p., 4 h). Data represent average values ± SEM; n = 4−5 mice per group. *p < 0.05; **p < 0.01; ***p < 0.001 for inhibitor-treated vs vehicle-treated (0 mg/kg) mice. (h, j) Time-dependent changes in 2-AG and other bioactive lipids in brain tissue

from mice treated with DH376 (h) and DO34 (j) (50 mg/kg, i.p.). Data represent average values ± SEM; n = 4−5 mice per group. *p < 0.05; **p < 0.01; ***p < 0.001 for inhibitor treated vs. vehicle-treated mice.

DAGL inhibitors block endocannabinoid-dependent synaptic plasticity

2-AG functions as a major retrograde messenger at synapses throughout the brain that acts on presynaptically localized CB_1Rs to suppress neurotransmitter release.[20] Various forms of synaptic plasticity are regulated by 2-AG signaling, including depolarization-induced suppression of excitation (DSE) and inhibition (DSI),[20] both of which are abolished in DAGLα$^{-/-}$ mice.[13,14] Interestingly, however, conflicting findings have emerged about whether the retrograde signaling 2-AG is biosynthesized by DAGLα on-demand or alternatively pre-synthesized and stored within neurons prior to stimulus-induced release.[21-23,25] As noted by others,[21] these differences may reflect the poor physicochemical properties of the DAGL inhibitors used in past studies, as the high lipophilicity of these molecules could limit their penetration into brain tissue preparations used to measure DSI and DSE, resulting in incomplete inhibition of DAGLs. Therefore, the effects of DH376, DO34 and DO53 in models of endocannabinoid-dependent synaptic plasticity were tested.

DSE at parallel fiber (PF) to Purkinje cell (PC) synapses in acute cerebellar slices were first examined. A brief depolarization of PCs induced robust transient DSE at PF-PC synapses in vehicle-treated cerebellar slices (Figure 9a and b). Bath application of DH376 (1-10 µM) or DO34 (0.1-1 µM) to cerebellar slices 30 min prior to starting electrophysiological recordings blocked DSE in a concentration-dependent manner with a half-maximal inhibition of 1.1 µM and 0.18 µM, respectively (Figure 11a and b). The control probe DO53 did not alter cerebellar DSE (10 µM, Figure 11a and b). Then, DSI at CA1 pyramidal neuron synapses in hippocampal slices were evaluated. DSI was induced in vehicle-treated hippocampal slices by applying a brief depolarization while evoking IPSCs through stimulation of synaptic inhibitory inputs (Figure 11c and d). Bath application of DH376 (10 µM) and DO34 (1 µM), but not DO53 (10 µM), for 30 min prior to starting electrophysiological recordings fully blocked hippocampal DSI (Figure 11c and d).

These results support a model where the 2-AG that regulates both DSE and DSI forms of synaptic plasticity in the brain is produced on-demand by DAGLα.

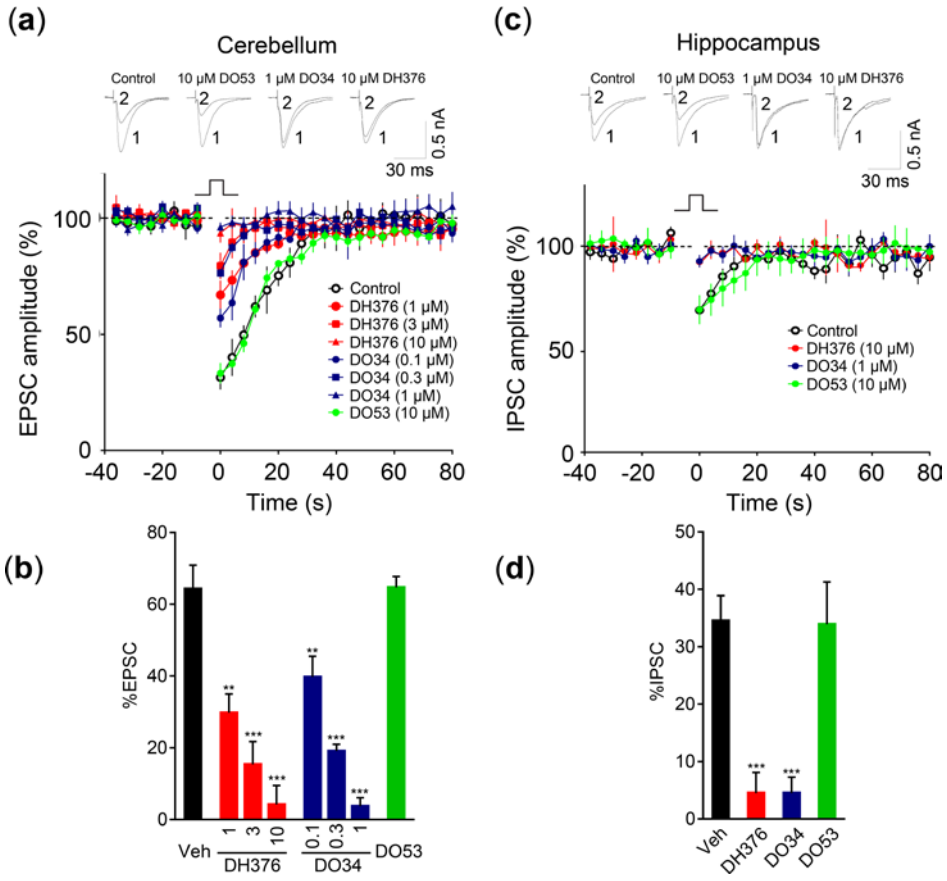

Figure 11. Acute inhibition of DAGLs fully blocks endocannabinoid-mediated forms of synaptic plasticity. (a, b) Sample traces and average time course (a) and magnitude (b) of parallel fiber-excitatory postsynaptic currents (PF-EPSCs) in response to a brief depolarization in cerebellar slices following treatment (30 min) with vehicle, DH376 (1-10 μM), DO34 (0.1−1 μM), or DO53 (10 μM). Data represent average values ± SEM; n = 5-10 samples per group. (c, d) Sample traces and average time course (c) and magnitude (d) of inhibitory postsynaptic currents (IPSCs) in CA1 pyramidal neurons in response to a brief depolarization in hippocampal slices following treatment (30 min) with vehicle, DH376 (10 μM), DO34 (1 μM), and DO53 (10 μM). Data represent average values ± SEM; n = 7−8 samples per group. *p < 0.05; **p < 0.01; ***p < 0.001 vs. vehicle-treated samples.

DAGL inhibitors attenuate neuroinflammatory responses *in vivo*

MAGL-mediated hydrolysis of 2-AG provides a major source of AA substrate for prostaglandin synthesis in the nervous system under basal and neuroinflammatory states.[38-41] Having discovered that acute, pharmacological inhibition of DAGLs coordinately lowers 2-AG and prostaglandin content of the brain (Figure 8), next it was asked whether blocking these enzymes affects neuroinflammatory processes

regulated by these bioactive lipids. High-dose lipopolysaccharide (LPS) treatment induces brain prostaglandin and cytokine production[38,41] and leads to profound anapyrexia in rodents,[42,43] an effect that is thought to be mediated, at least in part, by centrally produced prostaglandins and endocannabinoids.[42] MAGL blockade has been shown to suppress LPS-induced prostaglandin and cytokine production in the CNS,[38,41] but also exacerbates the anapyrexia observed in this paradigm through a CB_1R-dependent mechanism.[43] Building on these observations, the effects of pharmacological and genetic inactivation of DAGL activity were examined on neuroinflammatory responses induced by LPS.

Mice were treated with DH376, DO34, DO53 (50 mg/kg, i.p) or vehicle (60-90 min), followed by LPS (20 mg/kg, i.p., 6 h) or vehicle, and then sacrificed and their brain lipid and cytokine profiles analyzed. As expected, DH376- and DO34-treated mice, as well as DAGLα$^{-/-}$ mice, but not DO53-treated mice, exhibited severely depleted brain 2-AG (Figure 12a), AA (Figure 12c), and PGE_2 (Figure 12d) under basal control conditions. LPS treatment caused a modest, but significant increase in 2-AG (Figure 12a), a reduction in AA (Figure 12c), and a substantial increase in PGE_2 (Figure 12e). The LPS-induced elevations in both 2-AG and PGE_2 were strongly suppressed in DH376- and DO34-treated mice and DAGLα$^{-/-}$ mice, but not DO53-treated mice. LPS treatment also increased brain cytokines, and this effect was significantly attenuated in DAGLα$^{-/-}$ mice (Figure 12f-h). DH376- and DO34-treated mice also showed reductions in LPS-stimulated brain cytokines, but interpreting these effects proved complicated because the control probe DO53 also blocked brain cytokine production to a similar degree (Figure 12f-h). These data could indicate that one or more of the off-targets shared by the DAGL inhibitors and DO53 also participates, along with DAGLα (as supported by studies in DAGLα$^{-/-}$ mice), in LPS-induced cytokine production, or that active metabolites of the inhibitors may suppress cytokines. Finally, it was found that LPS-induced anapyrexia was substantially blunted in DH376- and DO34-treated mice (Figure 13a) and DAGLα$^{-/-}$ mice (Figure 13b), but not DO53-treated mice (Figure 13a).

These results, when combined with previous findings,[38,41,43] indicate that blockade of the principal 2-AG biosynthetic and degradation enzymes in the brain, DAGLα and MAGL, respectively, produces overlapping (reductions in brain prostaglandins and cytokines), but distinct (suppression versus enhancement of anapyrexia) effects on LPS-induced neuroinflammation.

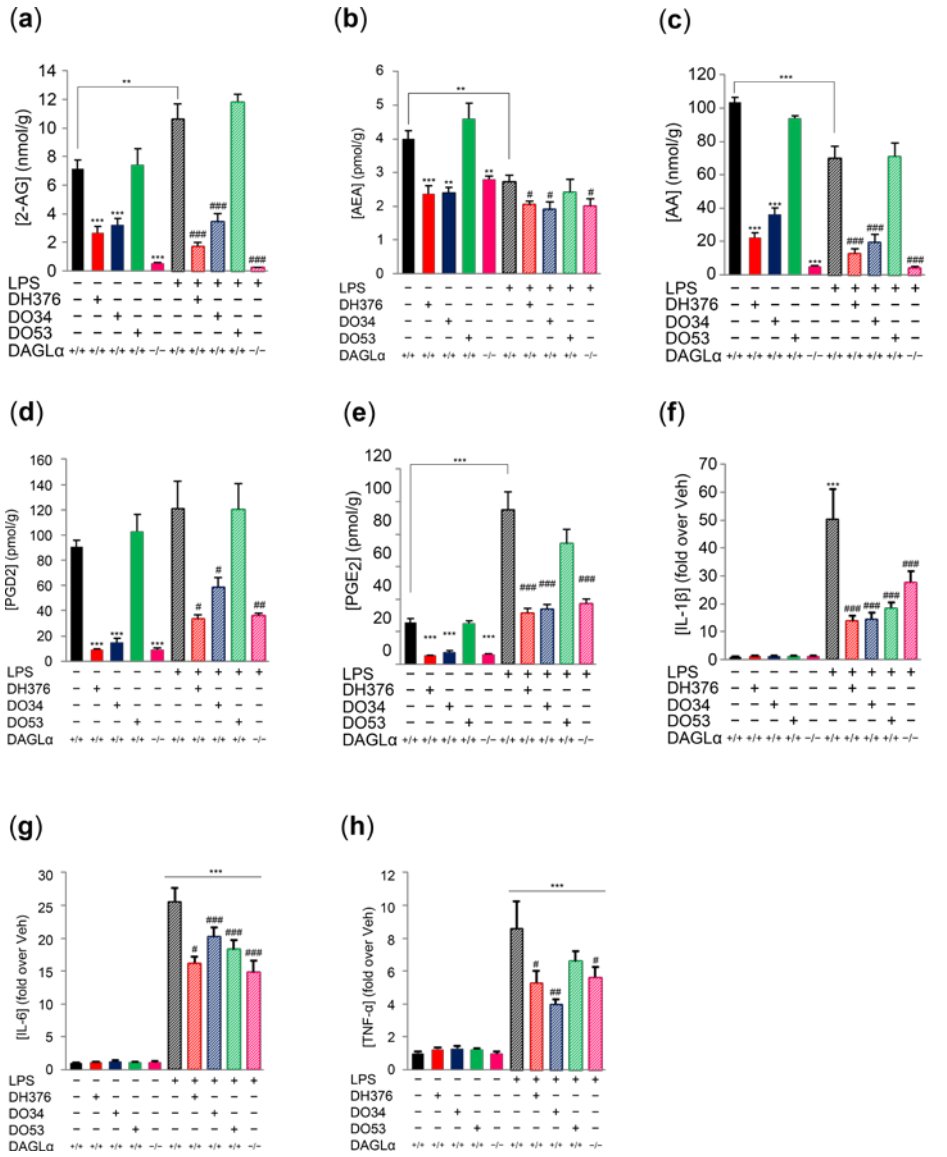

Figure 12. Disruption of DAGLs reduces brain inflammatory cytokine production in LPS-treated mice. (a−e) Quantification of 2-AG and related bioactive lipids in brain tissue from vehicle- or DH376-, DO34-, and DO53-treated (50mg/kg, i.p., 1−1.5 h) or DAGLα$^{-/-}$ mice with or without subsequent treatment with LPS (20 mg/kg, i.p., 6 h). (f-h) Quantification of the IL-1β (f), IL-6 (g) and TNF-α (h) cytokines from DH376-, DO34-, and DO53-treated (50 mg/kg, i.p., 1−1.5 h) or DAGLα$^{-/-}$ mice with or without subsequent treatment with LPS (20 mg/kg, i.p., 6 h). Data represent average values ± SEM; n = 5−8 mice per group. **P < 0.01; ***P <0.001 for all groups vs. vehicle-treated DAGLα$^{+/+}$ mice and $^{###}$P < 0.001 for all groups compared with LPS-treated DAGLα+/+ mice.

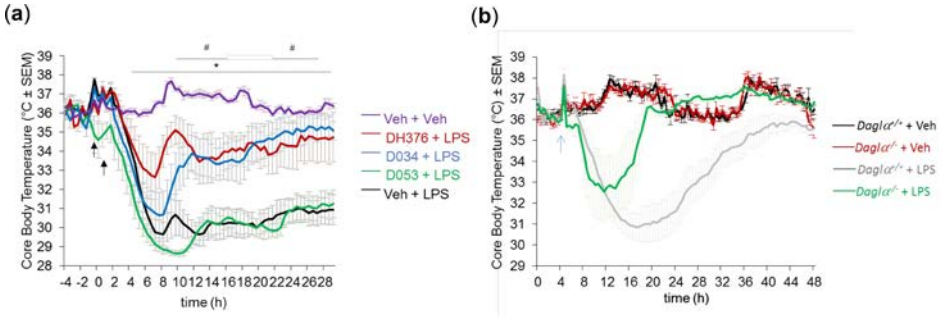

Figure 13. Acute inhibition of DAGLs suppresses LPS-induced neuroinflammatory responses in mouse brain. (a, b) Time course of body temperature changes for mice pretreated with vehicle or DH376, DO34, and DO53 (a) or for DAGLα$^{+/+}$ and DAGLα$^{-/-}$ mice (b) following LPS treatment (10 mg/kg, i.p.). Data represent average values ± SEM; n = 5−6. For E, *P < 0.05 Veh + Veh vs. Veh + LPS group; #P < 0.05 for DH376 + LPS and DO34 + LPS vs. Veh + LPS group. For F, *P < 0.05 for DAGLα$^{+/+}$ + Veh vs. DAGLα$^{+/+}$ + LPS groups; $^{\#}$P < 0.05 for DAGLα$^{-/-}$ + Veh vs. DAGLα$^{-/-}$ + LPS groups; $^{\&}$P < 0.05 for DAGLα$^{-/-}$ + LPS vs. DAGLα$^{+/+}$ + LPS groups.

Discussion

Endocannabinoids regulate synaptic activity throughout the CNS and impact diverse physiological and behavioral processes.[44,45] Inhibitors of enzymes that degrade endocannabinoids have proven useful for elucidating the neurobiological and behavioral effects caused by heightened endocannabinoid activity.[46] It has been more challenging, however, to determine the biological impact of reducing endocannabinoid function due in large part to a lack of selective and CNS-active inhibitors that can block endocannabinoid production *in vivo*. While DAGLα$^{-/-}$ and DAGLβ$^{-/-}$ mice have provided valuable models for investigating the *in vivo* effects of disrupting endocannabinoid biosynthesis, DAGLα plays an important role in brain development[13] and chronic alterations in endocannabinoid tone can lead to substantial CB_1R adaptations in the CNS[47,48] and peripheral tissues.[49] The endocannabinoid system also crosstalks with several other bioactive lipid pathways.[8,50,51] The extent to which this larger lipid network is dynamically regulated in the CNS by acute disruption of endocannabinoid synthesis remains unknown. Here these important questions have been addressed by developing CNS-active irreversible DAGL inhibitors - DH376 and DO34 – along with a structurally related control probe DO53. Key to the development of these chemical probes was the use of both broad-spectrum and tailored ABPP probes for assessing selectivity and DAGL inhibition *in vivo*.

Administration of DH376 and DO34 to mice revealed that brain 2-AG content is rapidly and dramatically reduced following acute inactivation of DAGLα. Both inhibitors also produced near-complete blockade of cerebellar DSE and hippocampal DSI, two forms of CB_1R-mediated synaptic plasticity,[20] following only a 30 minute incubation in

brain slices. These results provide strong experimental support for an on-demand model of endocannabinoid biosynthesis[21] versus alternative hypotheses invoking 2-AG storage and release. DAGL inhibitors and tailored activity probes were also used to discover that DAGLα is a short half-life (< 4 h) protein in the CNS. The factors that regulate DAGLα turnover in brain cells remain unknown, but previous studies have shown that DAGLα localization and activity are regulated by interacts with scaffolding proteins[52] and phosphorylation by CamKII.[53] It is possible that such protein-protein interactions and post-translational modifications (> 30 phosphorylation sites have been identified in DAGLα) regulate DAGLα half-life in brain cells. Endocannabinoid-mediated synaptic plasticity has also been shown to depend on transcription and translation in the post-synaptic neuron,[54] which is consistent with the observation of rapid, ongoing production of new DAGLα protein (Figure 9) that generates a strong, tonic flux of 2-AG in the brain (Figure 10). Modulating the half-life of DAGLα may thus provide neurons with a mechanism to influence the magnitude and duration of 2-AG signaling and associated physiological processes, such as learning and memory, which have been shown to require protein synthesis and degradation.[55]

That the profound reduction in 2-AG caused by DAGL inhibitors was accompanied by alterations in DAGs, arachidonic acid, prostaglandins, and other endocannabinoids (AEA) underscores the remarkable integration of lipid signaling networks in the brain and the key role that DAGLs play in orchestrating this crosstalk. Although it can be interpreted that many of the lipid changes caused by DAGL inhibitors reflect the direct flux of substrate and products through interconnected metabolic pathways,[19] others (e.g., AEA reductions) may be the indirect consequence of alterations in lipid signaling. Such signaling-related crosstalk between endocannabinoids has also been reported for AEA action on TRPV1 channels, which can influence 2-AG production in the brain.[56] Regardless of the precise mechanisms by which DAGLs exert their profound influence over brain lipid networks, the data present in this chapter emphasize that the interpretation of phenotypes caused by DAGL disruption should take into consideration more than just impairments in endocannabinoid signaling. In this regard, the data here, combined with previous studies,[43,57] suggest that the attenuated neuroinflammatory responses in DAGLα-disrupted mice likely reflect the integrated outcome of lowering both endocannabinoids and eicosanoids in the brain, although the additional impact of altering DAG-mediated PKC signaling and/or other lipid processes cannot be excluded. Additionally, the discovery here that the control probe DO53 attenuates LPS-induced cytokine production without altering brain prostaglandins or anapyrexia indicates that the various neuroinflammatory effects of LPS can be mechanistically uncoupled.

Taken together, the studies in this chapter demonstrate that DH376 and DO34, along with the control probe DO53 and tailored DAGL activity probes, such as DH379, constitute a valuable chemical tool kit for studying diverse aspects of DAGL function and regulation both in animals and *ex vivo* brain preparations. Projecting forward, this

toolkit would be further enhanced by the development of inhibitors that can selectively target DAGLα or DAGLβ. Accordingly, even though studies with genetically disrupted mice[13,14,17] would indicate that the most of the lipid changes caused by DAGL inhibitors in the brain are due to blockade of DAGLα, in the pharmacological experiments a contribution from DAGLβ cannot excluded at this stage, especially when evaluating the neuroinflammatory effects of DAGL inhibitors. Indeed, it has been found in other studies that DAGLβ$^{-/-}$ mice also show attenuated LPS-induced anapyrexia, possibly due to functions performed by DAGLβ specifically in microglia.[58]

The short half-life of DAGLα also presents some challenges for the current inhibitor described in this chapter, since it need to be administered to mice at relatively high doses (50 mg/kg) to maintain complete target engagement over a prolonged (> 8 h) period of time. Improving the pharmacokinetic properties of DAGLα inhibitors would thus benefit pharmacological studies aimed at studying prolonged inactivation of DAGLα *in vivo*. From a translational perspective, it will be interesting to determine which of the many phenotypes observed in DAGLα$^{-/-}$ mice are recapitulated in animals treated with DAGL inhibitors. The DAGLα$^{-/-}$ mice show reduced body weight due to hypophagia and, in this regard, resemble animals with genetic or pharmacological disruption of the CB_1R.[15] Humans treated with CB_1R antagonists/inverse agonists likewise exhibit weight loss, but these drugs were ultimately removed from the clinic due to neuropsychiatric side effects.[59] DAGLα$^{-/-}$ mice also display heightened anxiety-related behaviors that can be normalized, along with partial restoration of brain 2-AG content, by treatment with an MAGL inhibitor.[17] Thus, the potential clinical utility of DAGL inhibitors for obesity or other disorders[60-62] may depend on whether a therapeutic window can be established within which partial reductions in endocannabinoid signaling are found to produce beneficial effects while minimizing untoward neurological outcomes. The DAGL inhibitors reported herein, which produce a graded, dose-dependent blockade of 2-AG production in the CNS, provide a first opportunity to experimentally investigate these important questions.

Experimental section

Chemistry

General materials: All of reactions were performed using oven or flame-dried glassware and dry solvents. Reagents were purchased from Sigma Aldrich, Acros and Merck and used without further purification unless noted otherwise. All moisture sensitive reactions were performed under an argon atmosphere. Traces of water were removed from starting compounds by co-evaporation with toluene. ^{1}H-and ^{13}C-NMR spectra were recorded on a Bruker AV 400 MHz spectrometer at 400 (^{1}H) and 101 (^{13}C) MHz, or on a Bruker DMX-600 spectrometer 600 (^{1}H) and 150 (^{13}C) MHz using $CDCl_3$, or CD_3OD solvent, unless stated otherwise. Chemical shift values are reported in ppm with tetramethylsilane or solvent resonance as the internal standard ($CHCl_3$, δ

7.26 for ^{1}H, δ 77.16 for ^{13}C). Data are reported as follows: chemical shifts (δ), multiplicity (s = singlet, d = doublet, dd = double doublet, td = triple doublet, t = triplet, m = multiplet, br = broad), coupling constants *J* (Hz), and integration. High-resolution mass spectra (HRMS) were recorded by direct injection (2 µL of a 2 µM solution in water/acetonitrile 50/50 (v/v) and 0.1% formic acid) on a mass spectrometer (Thermo Finnigan LTQ orbitrap) equipped with an electrospray ion source in positive mode (source voltage 3.5 kV, sheath gas flow 10, capillary temperature 250 ^{o}C) with resolution R = 60,000 at m/z 400 (mass range m/z = 150-2,000) and dioctylphthalate (m/z = 391.28428) as a "lock mass". The high resolution mass spectrometer was calibrated prior to measurements with a calibration mixture (Thermo Finnigan). LC-MS analysis was performed on a Finnigan Surveyor HPLC system with a Gemmi C_{18} 50x4.60 mm column (detection at 200-600 nm), coupled to a Finnigan LCQ Adantage Max mass spectrometer with ESI. The applied buffers were H_2O, MeCN and 1.0% TFA in H_2O (0.1% TFA end concentration). Flash chromatography was performed using SiliCycle silica gel type SilicaFlash P60 (230 – 400 mesh). TLC analysis was performed on Merck silica gel 60/Kieselguhr F254, 0.25 mm. Compounds were visualized using either Seebach's reagent (a mixture of phosphomolybdic acid (25 g), cerium (IV) sulfate (7.5 g), H_2O (500 mL) and H_2SO_4 (25 mL)) or a $KMnO_4$ stain (K_2CO_3 (40 g), $KMnO_4$ (6 g), H_2O (600 mL) and 10% NaOH (5 mL)).

Synthesis of ABP-DH379: Bodipy-Azide **1**[63] (14.2 mg, 0.030 mmol) and DH376 (15.0 mg, 0.028 mmol), were dissolved in degassed DCM/H_2O (1:1, 2 mL) and sodium ascorbate (6.57 mg, 0.033 mmol) and $CuSO_4$ (3.45 mg, 0.014 mmol) were added. The resulting mixture was stirred vigorously for two hours, after which TLC indicated completed conversion of the reaction. The solvents were evaporated *in vacuo* and the residue was taken up in DCM and purified by silica gel column chromatography (ethyl acetate with 1% AcOH) yielding probe DH379 (9.0 mg, 0.009 mmol, 32%) as a purple solid. ^{1}H NMR (600 MHz, $CDCl_3$) δ 7.85 (br s, 2H), 7.43 (br s, 11H), 7.09 – 6.91 (m, 8H), 6.51 (br s, 1H), 4.73 (br s, 2H), 3.94 (br s, 2H), 3.67 (br s, 1H), 3.53 (br s, 1H), 3.04 (br s, 2H), 2.74 (br s, 3H), 2.51 (br s, 5H), 2.21 (br s, 3H), 1.72 (br s, 3H), 1.25 (br s, 5H), 0.92 – 0.84 (m, 2H); ^{13}C NMR (151 MHz, $CDCl_3$) δ 176.20, 162.81 (d, *J* = 242 Hz), 159.61, 159.12, 155.38, 148.95, 141.55, 141.14, 140.72, 140.16, 137.78, 135.10, 134.51, 130.94, 130.05, 129.56, 129.24, 128.76, 128.14, 126.84, 126.22, 123.23, 118.45, 115.19 (d, *J* = 18 Hz), 114.25, 76.24, 73.67, 64.09, 54.22, 51.04, 48.95, 46.61, 35.69, 29.84, 26.55, 24.64, 22.83, 14.27, 13.34, 9.83; HRMS(m/z):$[M+H]^+$ calcd. for $C_{54}H_{52}BF_4N_9O_6$, 1010.41515; found 1010.41550.

Materials of chemical biological assays

Fluorophosphonate (FP)-rhodamine, FP-biotin and HT-01 were synthesized according to a previously described protocol.[64-68] FP-rhodamine is also commercially available at Thermo Fischer Scientific. All deuterated lipid standards and substrates were purchased from Cayman Chemicals.

Molecular cloning and recombinant expression

DAGLα/β plasmids: For the preparation of the different constructs, full length human cDNA was purchased from Source Bioscience and mouse cDNA was purchased from Open Biosystems, and were cloned into mammalian expression vector pcDNA3.1, containing genes for ampicillin and neomycin resistance. DAGLα/β constructs were obtained as reported previously.[68,69] For proteins containing a FLAG-tag, a FLAG-linker was made from primers and cloned into the vector at the C-terminus of hDAGLα or hDAGLβ. Two step PCR mutagenesis was performed to substitute the active site serine for an alanine in the hDAGLβ-FLAG, to obtain hDAGLβ-S443A-FLAG. Plasmids were isolated from transformed XL-10 Z-competent cells (Maxi Prep, Qiagen) and verified by Sanger sequencing (BaseClear).

Cell culture and membrane preparation: Cell culture and membrane preparation were performed as previously described.[68] In brief, HEK293T cells were grown in DMEM with stable glutamine and phenol red (PAA), 10% New Born Calf serum, penicillin and streptomycin. Cells were passaged every 2-3 days by resuspending in medium and seeding them to appropriate confluence. Membranes were prepared from transiently transfected HEK293T cells. One day prior to transfection 10^7 cells were seeded in a 15 cm petri dish. Cells were transfected by the addition of a 3:1 mixture of polyethyleneimine (60 µg) and plasmid DNA (20 µg) in 2 mL serum free medium. The medium was refreshed after 24 h, and after 72h the cells were harvested by suspending them in 20 mL medium. The suspension was centrifuged for 10 min at 1000 rpm, and the supernatant was removed. The cell pellet was stored at -80 ^{o}C until use.

Cell pellets were thawed on ice and suspended in lysis buffer A (20 mM HEPES, 2 mM DTT, 0.25 M sucrose, 1 mM $MgCl_2$, 1x protease inhibitor cocktail (Roche cOmplete EDTA free), 25U/µL Benzonase). The suspension was homogenized by polytrone (3 × 7 sec) and incubated for 30 min on ice. The suspension was subjected to ultracentrifugation (100.000 × g, 30 min, 4 ^{o}C, Beckman Coulter, Type Ti70 rotor) to yield the cytosolic fraction in the supernatant and the membrane fraction as a pellet. The pellet was resuspended in lysis buffer B (20 mM HEPES, 2 mM DTT, 1x protease inhibitor cocktail (Roche cOmplete EDTA free)). The protein concentration was determined with Quick Start Bradford assay (Biorad). The protein fractions were diluted to a total protein concentration of 1 mg/mL and stored in small aliquots at -80 ^{o}C until use.

Enzyme activity assays and IC_{50} measurements

PNP-butyrate DAGL activity assay: The para-nitrophenylbutyrate (PNP-butyrate) substrate assay was performed with hDAGLα as reported previously.[68] In brief, this assay is based on the hydrolysis of PNP-butyrate by membrane preparations from HEK293T cells transiently transfected with hDAGLα. Reactions were performed in 50 mM pH 7.2 HEPES buffer with 0.05 µg/µL final protein concentration to which PNP-butyrate substrate was added (5.0 µL in DMSO) to a final substrate

concentration of 300 µM. For the progression curve, after 135 minutes, another equal amount of substrate (5.0 µL, 12 mM) was added.

Natural substrate-based fluorescence assay (DAGLα/β): The natural DAG substrate assay was performed as reported previously.[70] Standard assay conditions: 0.2 U/mL glycerol kinase (GK), glycerol-3-phosphate oxidase (GPO) and horseradish peroxidase (HRP), 0.125 mM ATP, 10 µM Amplifu™Red, 5% DMSO in a total volume of 200 µL. The assay additionally contained 5 µg/mL MAGL-overexpressing membranes, 100 µM SAG and 0.0075% (w/v) Triton X-100, with a final protein concentration of 50 µg/mL. The mDAGLβ assay was performed as the hDAGLα assay, but assay buffer was supplemented with 5 mM $CaCl_2$ and the SAG concentration was 75 µM.

Activity based protein profiling on transiently transfected HEK293T cells

HEK293T cells were transfected with hDAGLα-FLAG or hDAGLα-S472A-FLAG, hDAGLβ-FLAG or hDAGLβ-S443A-FLAG and the membranes were isolated following a protocol reported previously.[68] For DAGLα ABPP assays the membrane proteome (1 mg/mL, 20 µL) was incubated at rt with vehicle (DMSO) or inhibitor in 0.5 µL DMSO for 30 min. The sample was subsequently treated for 15 min with 1µM (final concentration) ABP DH379 or 500 nM (final concentration) TAMRA-FP. The reactions were quenched with 10 µL 3 × Laemmli sample buffer (final concentrations: 60 mM Tris-Cl pH 6.8, 2% (w/v) SDS, 10% (v/v) glycerol, 5% (v/v) β-mercaptoethanol, 0.01% (v/v) bromophenol blue). The samples were directly loaded and resolved on SDS page gel (10 % acrylamide). The gels were scanned using a ChemiDoc MP system (Cy3 settings, 605/50 filter).

Western blot

Western blot procedure was performed as reported previously.[68] In brief, proteins were transferred from gel to a polyvinyldifluoride membrane using a Trans-Blot® Turbo (BioRad). FLAG-tagged enzymes were stained using rabbit anti-FLAG as primary antibody, and goat-anti-rabbit HRP as secondary antibody. The blot was developed in the dark using a 10 mL luminal solution, 100 µL ECL enhancer and 3 µL H_2O_2. Chemiluminescence was visualized using a ChemiDoc XRS (BioRad).

Size exclusion experiment

Membrane proteome (1 mg/mL, 343 µL) from transfected HEK293T cells was incubated with DMSO or inhibitor in 7.0 µL DMSO for 30 min at r.t. and subsequently the protein-inhibitor complex was loaded on the size exclusion column (Zeba spin desalting columns, 2 mL). After centrifugation (1000g, 2 min) the sample was collected, and the column flushed 3 times by centrifugation (1000g, 2 min) with 1 mL of storage buffer B (20 mM HEPES, pH 7.2; 2 mM DTT). After size exclusion, 19.5 µL of protein-inhibitor complex were used to perform ABPP. The rest of the sample was

reloaded onto the column, and centrifugation of sample, flushing of sample and collection of 19.5 µL of sample for ABPP, were repeated several times.

ABPP inhibitor activity measurements

The percentage of activity remaining was determined by measuring the integrated optical intensity of the fluorescent protein bands using image lab 4.1. The relative intensity was compared to the vehicle treated proteins, which were set to 100%. IC_{50} and IC_{80} values were determined by plotting a log(inhibitor) vs. normalized response (Variable slope) dose-response curve generated using Prism software (GraphPad).

Matings and genotyping of transgenic animals

All animal experiments were carried out in compliance with institutional animal protocols, and mice were housed on a normal 6AM/6PM light/dark phase with ad libitum access to water and food. C56Bl/6 mice were use in all inhibitor treatment studies. DAGLα$^{-/-}$ and DAGLβ$^{-/-}$[67] mice were generated by heterozygous matings and were in a homogeneous C57Bl/6 background. For these DAGL transgenic mice PCR genotyping of genomic tail DNA was performed using the following primers: DAGLα5'-tgagattggtatcaagacctttg-3', 5'-ccttgctcctgccgagaaagtatcc-3', and 5'- gaagaacaggtaaccaggaccat-3' (300-bp product in wild-type mice, 600-bp product in mice with the DAGLα null allele); DAGLβ 5'-aaggaggcaaagacagcaaagtgc-3', 5'-tatcctaggtgcagacagattgtgc-3', and 5'-aaatggcgttacttaagctagcttgc-3' (390-bp product in wild-type mice, 195-bp product in mice with the DAGLβ null allele).

Preparation of tissue proteomes

Mouse tissues were dounce homogenized in lysis buffer (20 mM HEPES, 250 mM sucrose, 2 mM DTT, 1 mM $MgCl_2$ with or without 25 U/mL benzonase) and incubated in ice for 5 min, followed by a low-speed spin (1,400−2.500 x g, 3 min, 4 °C) to remove debris. The membrane and cytosolic fractions were separated by ultracentrifugation (100,000 x *g*, 45 min, 4 °C) of the resulting homogenate lysate. After removal of the soluble supernatant, the membrane pellet was washed 1X with cold HEPES buffer (20 mM, with or without 2 mM DTT) followed by resuspension in cold HEPES buffer (20 mM, with or without 2 mM DTT) by pipetting. Total protein concentrations in membrane and soluble fractions were determined using the Bio-Rad DC protein assay kit. Samples were stored at -80 °C until further use.

Tissue profiling by gel-based competitive ABPP

Gel-based ABPP assays were performed as previously reported.[71] Cell or tissue proteomes were treated with either FP-rhodamine (1 µM or 500 nM final concentration), HT-01 (1 µM final concentration), or DH379 (1 µM final concentration). For HT-01and DH379 labeled samples, 2 mg/mL of proteome was used to enhance endogenous DAGL signals; 1 mg/mL proteome was used for labeling with FP-Rh. Probe labeling was carried out for 30 min at r.t. or 37 °C followed by addition of 4X

SDS-PAGE loading buffer to quench the reaction. After separation by SDS-PAGE (10% acrylamide), samples were visualized by in-gel fluorescence scanning using a ChemiDoc MP system.

Copper-catalyzed azide-alkyne cycloaddition (CuAAC or click) chemistry-ABPP

Mouse brain membrane proteomes from either naïve (in vitro) or inhibitor-treated (in vivo) mice were prepared for analysis as described in preparation of tissue proteome. Using previously developed methods,[72] Cyanine 5-Azide (Cy5−N_3) was conjugated to each alkyne probe for in-gel analysis. Briefly, $CuSO_4$ (1.0 µL/reaction, 100 mM in H_2O), THPTA (0.2 µL/reaction, 100 mM in H_2O), sodium ascorbate (0.6 µL/reaction, 1 M in H_2O [freshly prepared]), and Cy5−N_3 (0.2 µL/reaction, 0.4 mM in DMSO) were premixed. This click reagent mixture (2.0 µL total volume) was immediately added to each proteome (18 µL), and the reaction was stirred by briefly vortexing. After 30 min at room temperature, reactions were diluted with 4×SDS loading buffer (10 µL) and resolved by SDS-PAGE.

***In vivo* studies with DH376, DO34 and DO53**

The animal experiments were conducted in accordance with the guidelines of the Institutional Animal Care and Use Committee of The Scripps Research Institute and the ethical committee of Leiden University (DEC#14137). In vivo studies with DH376, DO34 and DO53 were conducted in C57BL/6 mice. Mice were injected with DH376 i.p. in 18:1:1 (v/v/v) solution of saline/ethanol/PEG40 (ethoxylated castor oil, 10 µL/g body weight of mouse). For dose-response studies, mice were treated with varying doses of compounds for 4 h, anesthetized with isoflurane, and euthanized by cervical dislocation. For time-course studies, mice were treated with 50 mg/kg body weight of compound and euthanized after the indicated times. LPS-induced neuroinflammation studies were performed as previously described[73]. Mice were pretreated with compounds i.p. in vehicle of 18:1:1 (v/v/v) solution of saline/ethanol/PEG40 (ethoxylated castor oil, 10 µL/g body weight of mouse) and incubated for 1-1.5 h. After the pretreatment, mice were treated with 20 mg/kg body weight of LPS i.p. in saline (10 µl/g body weight of mouse) and euthanized after 6 h.

Sample preparation and targeted LC/MS metabolite profiling

Mice were anesthetized by isoflurane and euthanized by decapitation. Brain tissues were harvested, and immediately frozen in liquid nitrogen. Tissues were then dounce-homogenized in 8 ml of 2:1:1 $CHCl_3$/MeOH/PBS containing the internal standard mix (1 nmol of 2-arachidonoylglycerol-d5 (2-AG-d_5), arachidonic acid-d8 (AA-d_8), anandamide-d5 (AEA-d_4), 1-stearoyl-2-arachidonoyl-sn-glycerol-d8 (SAG-d_8), prostaglandin E2-d9 (PGE2-d_9) (Cayman Chemical), 1-heptadecanoyl-2-hydroxy-sn-glycero-3-phosphocholine (LysoPC), 1,2-diheptadecanoyl-sn-glycero-3-phosphocholine (PC), 1,2-diheptadecanoyl-sn-glycero-3-phosphoethanolamine (PE), 1-(10Z-heptadecenoyl)-2-hydroxy-sn-glycero-3-[phosphor-L-serine] (LysoPS),

1,2-diheptadecanoyl-sn-glycero-3-phospho-L-serine (PS), 1,2-diheptadecanoyl-sn-glycero-3-[phosphor-rac-(1-glycerol)] (PG), 1-heptadecanoyl-2-arachidonoyl-sn-glycero-3-phospho(1'-myo-inositol) (PI) (Avanti Polar Lipids) and 1,2-dioleoyl-sn-glycero-3-phospho (N-nonadecenoyl) ethanolamine[74] (NAPE)). Homogenates were centrifuged at 1,400 x *g* for 3 min to separate the two phases. The organic phase (bottom) was removed, 20 µL of formic acid was added to acidify the aqueous homogenate and $CHCl_3$ was added to make up 8 mL volume. The mixture was vortexed and separated using centrifugation as described above. Both the organic extracts were pooled and dried under a stream of N_2. The metabolomes were resolubilized in 480 µL of 2:1 $CHCl_3$/MeOH, and 10 µL were used for the targeted LC/MS analysis.

Metabolites analyzed in this study were quantified using LC/MS–based multiple reaction monitoring (MRM) methods (Agilent Technologies 6460 Triple Quad). Liquid chromatography (LC) separation was achieved using a Gemini reverse-phase C18 column (50 x 4.6 mm with 5 µm diameter particles, Phenomonex) along with a pre-column (C18, 3.5 µm, 2 mm x 20 mm). For analysis of diacylglycerols (DAGs) a Luna C5 column (50 x 4.60 mm with 5 µm diameter particles) was used. Mobile phase A was made of 95:5 (v/v) H_2O:MeOH, and mobile phase B was composed of 60:35:5 (v/v/v) *i*-PrOH:MeOH:H_2O. Ammonium hydroxide (0.1%) and formic acid (0.1%) was included to assist in ion formation in negative and positive ionization modes, respectively. For analysis of DAGs, 5 mM ammonium formate was also used in addition to 0.1% formic acid to assist in positive ionization and NH_4^+ adduct formation. MS analysis was performed with an ESI source in scanning mode from m/z = 50 – 1,200, capillary voltage set to 3.5 kV, and the fragmentor voltage set to 100 V. The drying gas temperature was set to 300 °C, drying gas flow rate was 11 L/min, and nebulizer pressure was 35 psi. The parameters (MS) used for MRM to measure the indicated metabolites are summarized in Table 2. Endogenous lipids were quantified by measuring the area under the peak in comparison with the appropriate unnatural internal standard and normalizing for tissue weight.

ABPP-reductive dimethylation (ReDiMe) sample preparation and analysis

For the ABPP-ReDiMe samples, proteomes (2 mg/mL in 20 mM HEPES buffer) were labeled with FP-biotin (10 µM) for 1h at rt. After labeling, the proteomes were denatured and precipitated using 4:1 MeOH/$CHCl_3$, resuspended in 0.5 mL of 6 M urea in PBS with 0.4% SDS, reduced using Tris(2-carboxyethyl)phosphine (TCEP, 20 mM)/K_2CO_3 (60 mM) for 30 min at 37 °C and then alkylated using iodoacetamide (40 mM) for 30 min at 25 °C in the dark. The biotinylated proteins were enriched with PBS-washed streptavidn-agarose beads (100 µL; Thermo) by shaking at rt for 1.5 h in PBS with 2% SDS to final volume of 5.5 mL. The beads were washed sequentially with 15 mL PBS with 1% SDS (3×), 15 mLPBS (3×) and 15 mL DI H_2O (3×). On-bead digestion was performed using sequence-grade trypsin (1.5 µg; Promega) in 2 M urea in triethylammonium bicarbonate buffer (100 mM, 200 µL) with 1 mM $CaCl_2$ for 12–16 h at 37 °C with constant shaking. Reductive dimethylation was performed as

previously described.[75,76] Briefly, either ^{13}C-labeled deuterated formaldehyde (heavy) or formaldehyde (light) was added to each sample (0.2%) followed by addition of sodium cyanoborohydride (27 mM). Following a 2h incubation period at room temperature, the reaction was quenched by addition of NH_4OH (0.2 %) and formic acid (8 %). The samples were then combined and analyzed by LC/MS analysis.

MS and data analysis

MS was performed using an Orbitrap Velos mass spectrometer following previously described protocols.[77, 78] Peptides were eluted using a five-step multidimensional LC/MS [MudPIT[79]] protocol (using 0%, 25%, 50%, 80% and 100% salt bumps of 500 mM aqueous ammonium acetate, followed by an increasing gradient of aqueous acetonitrile and 0.1% formic acid in each step). For all samples, data were collected in data-dependent acquisition mode over a range from 400–1,800 *m*/*z*. Each full scan was followed by up to 30 fragmentation events for experiments using Orbitrap Velos instruments. Dynamic exclusion was enabled (repeat count of 1, exclusion duration of 20 s) for all experiments. The data were searched using the ProLuCID algorithm against a mouse reverse-concatenated nonredundant (gene-centric) FASTA database that was assembled from the Uniprot database. ProLuCID searches specified static modification of cysteine residues (+57.0215 *m*/*z*; iodoacetamide alkylation) and required peptides to contain at least one tryptic terminus. Each data set was independently searched with light and heavy parameter files; for the light search, static modifications on lysine (+ 28.0313 *m*/*z*) and N termini (+ 28.0313 *m*/*z*) were specified; for the heavy search, static modifications on lysine (+ 34.06312 *m*/*z*) and N termini (+ 34.06312 *m*/*z*) were specified. The resulting matched MS2 spectra were assembled into protein identifications, then filtered using DTASelect (version 2.0.47). Peptides were restricted to a specified false positive rate of <1%. ReDiMe ratios were quantified using in-house CIMAGE[80] software. Briefly, extracted MS1 ion chromatograms (± 10 ppm) from both 'light' and 'heavy' target peptide masses (*m/z*) were generated using a retention time window (± 10 min) centered on the time when the peptide ion was selected for MS/MS fragmentation, and subsequently identified. Next, the ratios of the peak areas under the light and heavy signals (signal-to-noise ratio > 2.5) are calculated. Computational filters used to ensure that the correct peak-pair is used for quantification include a co-elution correlation score filter ($R2 \geq 0.8$), removing target peptides with bad co-elution profile, and an 'envelope correlation score' filter ($R2 > 0.8$) that eliminates target peptides whose predicted pattern of the isotopic envelope distribution does not match the experimentally observed high-resolution MS1 spectrum. Also, peptides detected as singletons, where only the heavy or light isotopically labeled peptide was detected and sequenced, but which passed all other filtering parameters, were given a standard ratio of 20, which is the maximum ReDiMe ratio reported here.

Cytokine measurements

Cytokines were measured using mouse DuoSet® ELISA development kit (R&D Systems). Brains were homogenized in phosphate-buffered saline with 1 x protease

inhibitor cocktail (Roche). The supernatant from a 1400 x g centrifugation of the homogenate was then centrifuged at 100,000 x g for 45 min. The supernatant from this centrifugation (the mouse brain soluble proteome) was used in the assay.

Slice preparation

C57BL/6J mice of either sex were anaesthetized by isoflurane inhalation and decapitated. Parasagittal slices (250 µm thick) were cut from the cerebellar vermis of 10- to 14-day-old mice, and transverse slices (250 µm thick) were cut from the hippocampus of 20- to 30-day-old mice, as it has been described.[81,82] Slices were prepared at 4-6°C in a sucrose-based solution containing (in mM): 78 NaCl, 68 sucrose, 26 $NaHCO_3$, 2.5 KCl, 1.25 NaH_2PO_4, 2 $CaCl_2$, 2 $MgCl_2$ and 25 glucose. Slices were incubated for 30-40 min in sucrose solution and then transferred and stored in the artificial cerebrospinal fluid (ACSF) containing (in mM): 119 NaCl, 2.5 KCl, 2.5 $CaCl_2$, 1 $MgCl_2$, 1.25 NaH_2PO_4, 26 $NaHCO_3$, and 10 glucose. All solutions were saturated with 95% O_2 and 5% CO_2.

Electrophysiology

Whole-cell recordings were made using patch clamp amplifier Multiclamp 700B under infrared-DIC microscopy. Data acquisition and analysis were performed using DigiData 1440A digitizer and analysis software pClamp 10 (Molecular Devices). Signals were filtered at 2 kHz and sampled at 10 kHz. Whole-cell voltage-clamp recordings were made from cerebellar Purkinje cells (PCs) and hippocampal CA1 pyramidal neurons as described previously.[81,82] Excitatory postsynaptic currents (EPSCs) were recorded from cerebellar Purkinje cells (PCs), parallel fibers (PFs) were stimulated with a bipolar tungsten stimulation electrode (WPI) that was placed in the molecular layer. PF-EPSCs showed graded responses and exhibited paired-pulse facilitation (30-50 ms intervals).[83] $GABA_A$ receptor blocker picrotoxin (50 µM) and a low concentration (1 µM) of AMPA receptor antagonist 6-cyano-7-nitroquinoxaline-2,3-dione (CNQX) was present in the ACSF. Glass pipettes (3-5 MΩ) were filled with an internal solution containing (in mM): 140 cesium methanesulfonate, 10 CsCl, 2 QX-314, 10 HEPES, 0.2 EGTA, 2 $MgCl_2$, 4 Mg-ATP, and 0.3 Na_2GTP (pH 7.2 with CsOH). EPSCs were evoked by electrical stimulation at 4 s intervals. DSE was induced by a brief depolarization (1 s from -70 mV to 0 mV).

Inhibitory postsynaptic currents (IPSCs) were recorded from CA1 pyramidal neurons in hippocampal slices. A bipolar tungsten stimulation electrode was placed in the stratum radiatum of the CA1 region to evoke IPSCs. AMPA receptor antagonist CNQX (20 µM) and NMDA receptor antagonist D-2-amino-5-phosphonovaleric acid (D-AP-5, 20 µM) were present in the ACSF. The pipettes were filled with an internal solution containing (in mM): 100 K-gluconate, 50 KCl, 0.1 $CaCl_2$, 1 EGTA-Na_4, 2 $MgCl_2$, 2 Mg-ATP, 0.3 Na_2GTP, and 10 HEPES at pH 7.2 (with KOH). To induce DSI, the CA1 pyramidal neurons were depolarized from -70 mV to 0 mV for 5 s, and IPSCs were evoked at 4 s intervals. All recordings were performed at 32 ± 1°C by using an

automatic temperature controller. DAGL inhibitors and control compounds were dissolved in DMSO and the final concentration of DMSO in the ACSF is ≤0.1%.

Anapyrexia study

Core body temperature was measured by radiotelemetry as previously described.[84-87] Briefly, mice were anesthetized with isofluorane (induction 3-5%, maintenance 1-1.5%) and surgically implanted with radiotelemetry devices (TA-F20, Data Sciences, St. Paul, MN) into the peritoneal cavity for core body temperature (CBT) and locomotor activity (LA) evaluation. Following surgical implantation and appropriate wound closure, the animals were allowed to recover for 2 weeks and then subjected to telemetry recordings. Mice were individually housed in a Plexiglas cage in a room maintained at 25 ± 0.5°C. The cages were positioned onto the receiver plates (RPC-1; Data Sciences) and radio signal reporting CBT and LA information from the implanted transmitter was recorded continuously with a fully automated data acquisition system (Dataquest ART, Data Sciences, St. Paul, MN). Access to food and water was ad libitum and the light:dark cycle was of 12h:12h. Anapyrexia was induced by intraperitoneal injection of *Bacterial lipopolysaccharides (LPS)* (0127:B8, Sigma, St. Louis, MO) at a dose of 10 mg/kg in saline. DH376, DO34 and DO53 were injected intraperitoneally at a dose of 50 mg/kg in emulfor:ethanol:saline 1:1:18 2h before injection of LPS. Saline and emulfor:ethanol:saline were used as vehicle.

Data analysis and statistics

Data are shown as the mean ± SEM. A Student's t test (unpaired, two-tailed) was used to determine differences between two groups. Data that included more than two groups or two factors were analyzed by one-way or two-way ANOVA, respectively, with post hoc Sidak's multiple comparisons test. All statistical analyses were conducted using Excel or GraphPad Prism version 6, and a P value less than 0.05 was considered significant throughout unless indicated otherwise. For brain lipid profiling study for DH376 -, DO34- and DO53-treated mice and DAGLα$^{-/-}$ mice (Table 2), Benjamini Hochberg correction (10 % false discovery rate) was applied. Post-correction p values < 0.007 were designated as significant and are marked in red. P values between 0.007 and 0.05 were also listed in blue, with remaining p values designated as NS (not significant). For electrophysiology data, DSE and DSI were analyzed as described in the previous studies.[81, 82]

Radioligand binding assay

Materials: [^{3}H]CP55940 (specific activity 141.2 Ci/mmol) and GF-C filters were purchased from Perkin Elmer (Waltham, MA). Bicinchoninic acid (BCA) and BCA protein assay reagent were obtained from Pierce Chemical Company (Rochford, IL). The PathHunter® CHO-K1 CNR1 β-Arrestin Cell Line (catalog number 93-0959C2) and the PathHunter® CHO-K1 CNR2 β-Arrestin Cell Line (catalog number 93-0706C2), stably expressing the hCB_1 receptor (CHOK1hCB_1_bgal) or hCB_2 receptor (CHOK1hCB_2_bgal) respectively, was obtained from DiscoveRx.

Cell culture and membrane preparation: CHOK1hCB_1_bgal and CHOK1hCB_2_bgal cells were cultured in Ham's F12 Nutrient Mixture supplemented with 10% fetal calf serum, 1 mM glutamine, 50 µg/mL penicillin, 50 µg/mL streptomycin, 300 mg/mL hygromycin and 800 µg/mL geneticin in a humidified atmosphere at 37 °C and 5% CO_2. Cells were subcultured twice a week at a ratio of 1:20 on 10 cm plates by trypsinization. For membrane preparation the cells were subcultured 1:10 and transferred to large 15-cm diameter plates. Membrane fractions were prepared exactly as described before.[88]

[^{3}H]CP55940 radioligand binding assay: [^{3}H]CP55940 binding assays to determine the cannabinoid CB_1 and CB_2 receptor binding affinity were performed as follows: Ligands of interest were incubated at 30 °C for 1 hr with membrane aliquots containing 5 µg CHOK1hCB_1_bgal membrane protein or 1 µg (CHOK1hCB_2_bgal) in 100 µL assay buffer (50 mM Tris–HCl, 5 mM $MgCl_2$, 0.1% BSA, pH 7.4) with [^{3}H]CP55940 in a concentration of ~1.5 nM (CB_2 receptor) or ~3.5 nM (CB_1 receptor) per assay point. Non-specific binding was determined in the presence of 10 µM Rimonabant (CB_1 receptor) or 10 µM AM630 (CB_2 receptor). Filtration was performed on GF/C filters, presoaked for 30 min with 0.25% polyethylenimine, using a Brandel harvester. Filter-bound radioactivity was determined in a β-counter. The mean % of specific binding for CB_1 and CB_2 receptors were 36 ± 4% and 38 ± 42% for 6-12 experiments.

Supporting Figures

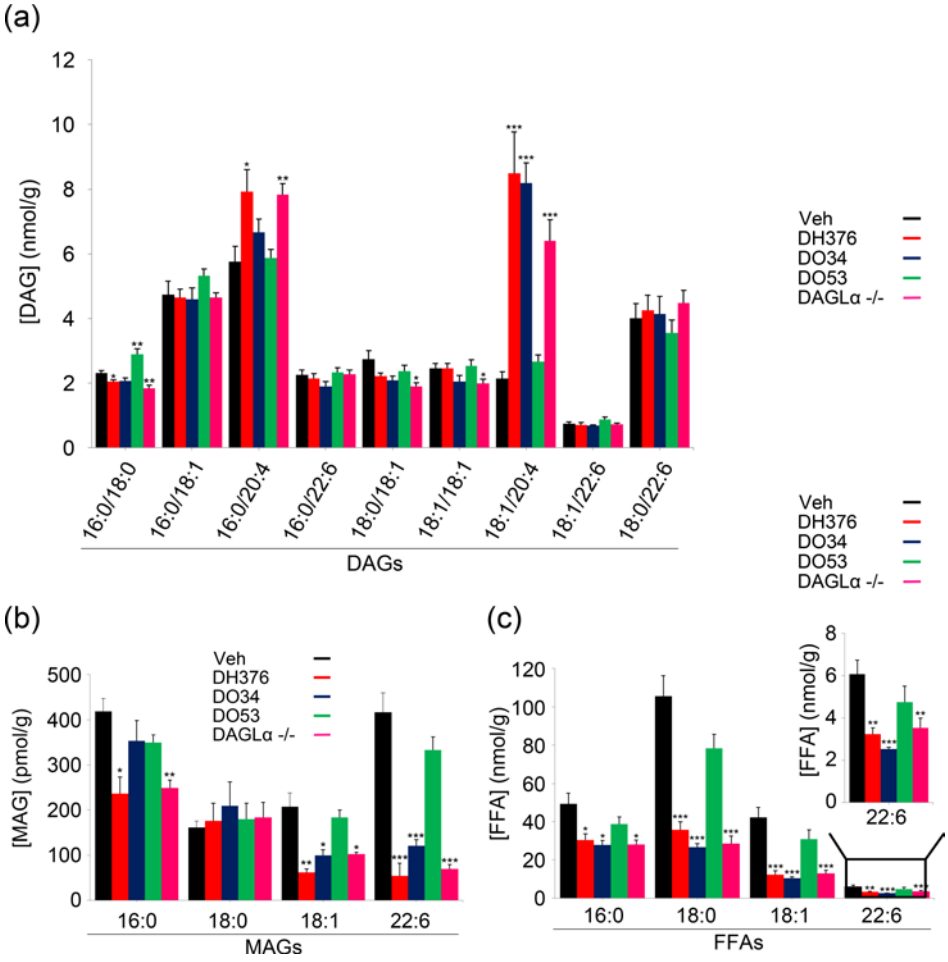

Figure S1. Additional brain lipid profiles in mice treated with DAGL inhibitors. Quantification of DAG (a), MAG (b), FFA (c) in brain tissue from mice treated with vehicle or DH376, DO34, and DO53 (50 mg/kg, i.p., 4 h). Lipid profiles from DAGLα$^{-/-}$ mice are shown for comparison. Data represent average values ± SEM; n = 4-6 mice per group. *p < 0.05; **p < 0.01; ***p < 0.001 for inhibitor-treated DAGLα$^{+/+}$ mice or DAGLα$^{-/-}$ mice vs. vehicle-treated DAGLα$^{+/+}$ mice.

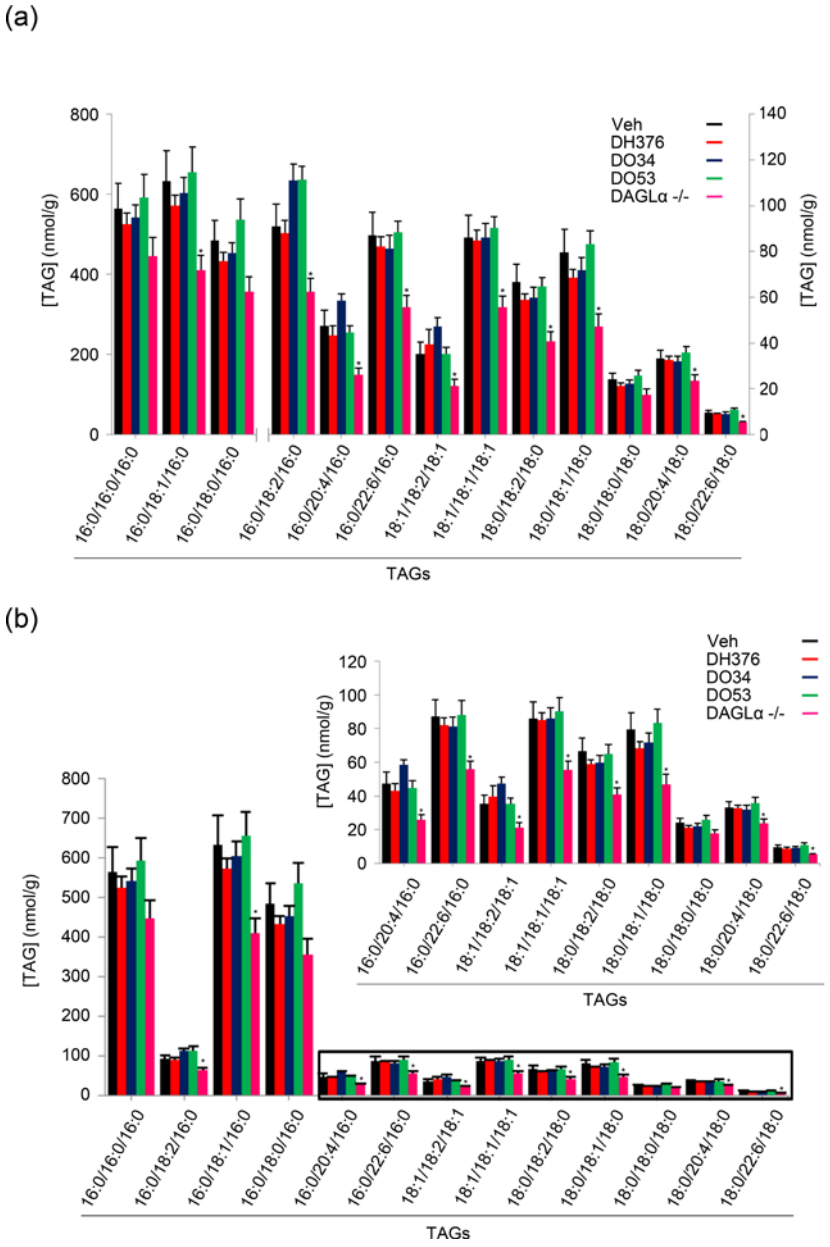

Figure S2. Additional brain lipid profiles in mice treated with DAGL inhibitors. Quantification of TAG in brain tissue from mice treated with vehicle or DH376, DO34, and DO53 (50 mg/kg, i.p., 4 h). Lipid profiles from DAGLα$^{-/-}$ mice are shown for comparison. Data represent average values ± SEM; n = 4-6 mice per group. *p < 0.05; **p < 0.01; ***p < 0.001 for inhibitor-treated DAGLα$^{+/+}$ mice or DAGLα$^{-/-}$ mice vs. vehicle-treated DAGLα$^{+/+}$ mice.

References

1. Brady, S.; Siegel, G.; Albers, R. W.; Price, D. *Basic Neurochemistry*. 8 ed.; Academic Press: Waltham, MA, 2012; p 235-389.
2. Yung, Y. C.; Stoddard, N. C.; Mirendil, H.; Chun, J. Lysophosphatidic acid signaling in the nervous system. *Neuron* **2015,** 85, 669-682.
3. Choi, J. W.; Chun, J. Lysophospholipids and their receptors in the central nervous system. *Biochimica et Biophysica acta* **2013,** 1831, 20-32.
4. Katona, I.; Freund, T. F. Endocannabinoid signaling as a synaptic circuit breaker in neurological disease. *Nature Medicine* **2008,** 14, 923-930.
5. Cimino, P. J.; Keene, C. D.; Breyer, R. M.; Montine, K. S.; Montine, T. J. Therapeutic targets in prostaglandin E2 signaling for neurologic disease. *Current MedicinalCchemistry* **2008,** 15, 1863-1869.
6. Bryan, L.; Kordula, T.; Spiegel, S.; Milstien, S. Regulation and functions of sphingosine kinases in the brain. *Biochimica et Biophysica acta* **2008,** 1781, 459-466.
7. Choi, S. H.; Aid, S.; Bosetti, F. The distinct roles of cyclooxygenase-1 and -2 in neuroinflammation: implications for translational research. *Trends in Pharmacological Sciences* **2009,** 30, 174-181.
8. Reisenberg, M.; Singh, P. K.; Williams, G.; Doherty, P. The diacylglycerol lipases: structure, regulation and roles in and beyond endocannabinoid signalling. *Philosophical Transactions of the Royal Society of London. Series B, Biological Sciences* **2012,** 367, 3264-3275.
9. Murataeva, N.; Straiker, A.; Mackie, K. Parsing the players: 2-arachidonoylglycerol synthesis and degradation in the CNS. *British Journal of Pharmacology* **2014,** 171, 1379-1391.
10. Bisogno, T.; Howell, F.; WIlliams, G.; Minassi, A.; Cascio, M. G.; Ligresti, A.; Matias, I.; Schiano-Moriello, A.; Paul, P.; Williams, E. J.; Gangadharan, U.; Hobbs, C.; Di Marzo, V.; Doherty, P. Cloning of the first sn1-DAG lipases points to the spatial and temporal regulation of endocannabinoid signaling in the brain. *Journal of Cell Biology.* **2003,** 163, 463-468.
11. Mechoulam, R.; Ben-Shabat, S.; Hanus, L.; Ligumsky, M.; Kaminski, N. E.; Schatz, A. R.; Gopher, A.; Almog, S.; Martin, B. R.; Compton, D. R. Identification of an endogenous 2-monoglyceride, present in canine gut, that binds cannabinoid receptors. *Biochemical Pharmacology* **1995,** 50, 83-90.
12. Sugiura, T.; Kondo, S.; Sukagawa, A.; Nakane, S.; Shinoda, A.; Itoh, K.; Yamashita, A.; Waku, K. 2-Arachidonylglycerol: a possible endogenous cannabinoid receptor ligand in brain. *Biochemical Biophysical Research Communications* **1995,** 215, 89-97.
13. Gao, Y.; Vasilyev, D. V.; Goncalves, M. B.; Howell, F. V.; Hobbs, C.; Reisenberg, M.; Shen, R.; Zhang, M. Y.; Strassle, B. W.; Lu, P.; Mark, L.; Piesla, M. J.; Deng, K.; Kouranova, E. V.; Ring, R. H.; Whiteside, G. T.; Bates, B.; Walsh, F. S.; Williams, G.; Pangalos, M. N.; Samad, T. A.; Doherty, P. Loss of retrograde endocannabinoid signaling and reduced adult neurogenesis in diacylglycerol lipase knock-out mice. *The Journal of Neuroscience : the official Journal of the Society for Neuroscience* **2010,** 30, 2017-2024.

14. Tanimura, A.; Yamazaki, M.; Hashimotodani, Y.; Uchigashima, M.; Kawata, S.; Abe, M.; Kita, Y.; Hashimoto, K.; Shimizu, T.; Watanabe, M.; Sakimura, K.; Kano, M. The endocannabinoid 2-arachidonoylglycerol produced by diacylglycerol lipase alpha mediates retrograde suppression of synaptic transmission. *Neuron* **2010,** 65, 320-327.
15. Powell, D. R.; Gay, J. P.; Wilganowski, N.; Doree, D.; Savelieva, K. V.; Lanthorn, T. H.; Read, R.; Vogel, P.; Hansen, G. M.; Brommage, R.; Ding, Z. M.; Desai, U.; Zambrowicz, B. Diacylglycerol lipase alpha knockout mice demonstrate metabolic and behavioral phenotypes similar to those of cannabinoid receptor 1 knockout mice. *Frontiers in Endocrinology* **2015,** 6, 86.
16. Jenniches, I.; Ternes, S.; Albayram, O.; Otte, D. M.; Bach, K.; Bindila, L.; Michel, K.; Lutz, B.; Bilkei-Gorzo, A.; Zimmer, A. Anxiety, stress, and fear response in mice with reduced endocannabinoid levels. *Biological Psychiatry* **2015**.
17. Shonesy, B. C.; Bluett, R. J.; Ramikie, T. S.; Baldi, R.; Hermanson, D. J.; Kingsley, P. J.; Marnett, L. J.; Winder, D. G.; Colbran, R. J.; Patel, S. Genetic disruption of 2-arachidonoylglycerol synthesis reveals a key role for endocannabinoid signaling in anxiety modulation. *Cell Reports* **2014,** 9, 1644-1653.
18. Whatley, R. E.; Zimmerman, G. A.; McIntyre, T. M.; Prescott, S. M. Lipid metabolism and signal transduction in endothelial cells. *Progress in Lipid Research* **1990,** 29, 45-63.
19. Kohnz, R. A.; Nomura, D. K. Chemical approaches to therapeutically target the metabolism and signaling of the endocannabinoid 2-AG and eicosanoids. *Chemical Society Reviews* **2014,** 43, 6859-6869.
20. Kano, M.; Ohno-Shosaku, T.; Hashimotodani, Y.; Uchigashima, M.; Watanabe, M. Endocannabinoid-mediated control of synaptic transmission. *Physiological Reviews* **2009,** 89, 309-380.
21. Hashimotodani, Y.; Ohno-Shosaku, T.; Tanimura, A.; Kita, Y.; Sano, Y.; Shimizu, T.; Di Marzo, V.; Kano, M. Acute inhibition of diacylglycerol lipase blocks endocannabinoid-mediated retrograde signalling: evidence for on-demand biosynthesis of 2-arachidonoylglycerol. *The Journal of Physiology* **2013,** 591, 4765-4776.
22. Min, R.; Testa-Silva, G.; Heistek, T. S.; Canto, C. B.; Lodder, J. C.; Bisogno, T.; Di Marzo, V.; Brussaard, A. B.; Burnashev, N.; Mansvelder, H. D. Diacylglycerol lipase is not involved in depolarization-induced suppression of inhibition at unitary inhibitory connections in mouse hippocampus. *The Journal of Neuroscience : the official Journal of the Society for Neuroscience* **2010,** 30, 2710-2715.
23. Zhang, L.; Wang, M.; Bisogno, T.; Di Marzo, V.; Alger, B. E. Endocannabinoids generated by Ca2+ or by metabotropic glutamate receptors appear to arise from different pools of diacylglycerol lipase. *PloS one* **2011,** 6, e16305.
24. Bisogno, T.; Mahadevan, A.; Coccurello, R.; Chang, J. W.; Allara, M.; Chen, Y.; Giacovazzo, G.; Lichtman, A.; Cravatt, B.; Moles, A.; Di Marzo, V. A novel fluorophosphonate inhibitor of the biosynthesis of the endocannabinoid 2-arachidonoylglycerol with potential anti-obesity effects. *British Journal of Pharmacology* **2013,** 169, 784-793.
25. Baggelaar, M. P.; Chameau, P. J.; Kantae, V.; Hummel, J.; Hsu, K. L.; Janssen, F.; van der Wel, T.; Soethoudt, M.; Deng, H.; den Dulk, H.; Allara, M.; Florea, B. I.; Di Marzo, V.; Wadman, W. J.; Kruse, C. G.; Overkleeft, H. S.; Hankemeier, T.; Werkman, T. R.; Cravatt, B. F.; van der Stelt, M. Highly selective, reversible inhibitor identified by comparative

chemoproteomics modulates diacylglycerol lipase activity in neurons. *Journal of the American Chemical Society* **2015,** 137, 8851-8857.

26. Hoover, H. S.; Blankman, J. L.; Niessen, S.; Cravatt, B. F. Selectivity of inhibitors of endocannabinoid biosynthesis evaluated by activity-based protein profiling. *Bioorganic Medicinal Chemistry Letters* **2008**.
27. Hsu, K. L.; Tsuboi, K.; Adibekian, A.; Pugh, H.; Masuda, K.; Cravatt, B. F. DAGLbeta inhibition perturbs a lipid network involved in macrophage inflammatory responses. *Nature Chemical Biology* **2012,** 8, 999-1007.
28. Baggelaar, M. P.; Janssen, F. J.; van Esbroeck, A. C.; den Dulk, H.; Allara, M.; Hoogendoorn, S.; McGuire, R.; Florea, B. I.; Meeuwenoord, N.; van den Elst, H.; van der Marel, G. A.; Brouwer, J.; Di Marzo, V.; Overkleeft, H. S.; van der Stelt, M. Development of an activity-based probe and in silico design reveal highly selective inhibitors for diacylglycerol lipase-alpha in brain. *Angewandte Chemie International Edition* **2013,** 52, 12081-12085.
29. Niphakis, M. J.; Cravatt, B. F. Enzyme inhibitor discovery by activity-based protein profiling. *Annual Review Biochemistry* **2014,** 83, 341-377.
30. van der Wel, T.; Janssen, F. J.; Baggelaar, M. P.; Deng, H.; den Dulk, H.; Overkleeft, H. S.; van der Stelt, M. A natural substrate-based fluorescence assay for inhibitor screening on diacylglycerol lipase alpha. *Journal of Lipid Research* **2015,** 56, 927-935.
31. Rostovtsev, V. V.; Green, J. G.; Fokin, V. V.; Sharpless, K. B. A stepwise Huisgen cycloaddition process: copper(I)-catalyzed regioselective "ligation" of azides and terminal alkynes. *Angewandte Chemie International Edition* **2002,** 41, 2596-2599.
32. Patricelli, M. P.; Giang, D. K.; Stamp, L. M.; Burbaum, J. J. Direct visualization of serine hydrolase activities in complex proteome using fluorescent active site-directed probes. *Proteomics* **2001,** 1, 1067-1071.
33. Liu, Y. S.; Patricelli, M. P.; Cravatt, B. F. Activity-based protein profiling: The serine hydrolases. *Proceedings of the National Academy of Sciences of the United States of America* **1999,** 96, 14694-14699.
34. Wilson-Grady, J. T.; Haas, W.; Gygi, S. P. Quantitative comparison of the fasted and re-fed mouse liver phosphoproteomes using lower pH reductive dimethylation. *Methods* **2013,** 61, 277-286.
35. Baggelaar, M. P.; Chameau, P. J. P.; Kantae, V.; Hummel, J.; Hsu, K. L.; Janssen, F.; van der Wel, T.; Soethoudt, M.; Deng, H.; den Dulk, H.; Allara, M.; Florea, B. I.; Di Marzo, V.; Wadman, W. J.; Kruse, C. G.; Overkleeft, H. S.; Hankemeier, T.; Werkman, T. R.; Cravatt, B. F.; van der Stelt, M. Highly selective, inhibitor identified by comparative chemoproteomics modulates diacylglycerol lipase activity in neurons. *Journal of the American Chemical Society* **2015,** 137, 8851-8857.
36. Sugiura, T.; Kondo, S.; Sukagawa, A.; Nakane, S.; Shinoda, A.; Itoh, K.; Yamashita, A.; Waku, K. 2-Arachidonoylglycerol: a possible endogenous cannabinoid receptor ligand in brain. *Biochemical Biophysical Research Communications* **1995,** 215, 89-97.
37. Marignani, P. A.; Epand, R. M.; Sebaldt, R. J. Acyl chain dependence of diacylglycerol activation of protein kinase C activity in vitro. *Biochemical Biophysical Research Communications* **1996,** 225, 469-473.
38. Nomura, D. K.; Morrison, B. E.; Blankman, J. L.; Long, J. Z.; Kinsey, S. G.; Marcondes, M. C.; Ward, A. M.; Hahn, Y. K.; Lichtman, A. H.; Conti, B.; Cravatt, B. F. Endocannabinoid

hydrolysis generates brain prostaglandins that promote neuroinflammation. *Science* **2011,** 334, 809-813.

39. Kita, Y.; Yoshida, K.; Tokuoka, S. M.; Hamano, F.; Yamazaki, M.; Sakimura, K.; Kano, M.; Shimizu, T. Fever Is Mediated by Conversion of Endocannabinoid 2-arachidonoylglycerol to prostaglandin E2. *PloS one* **2015,** 10, e0133663.
40. Pasquarelli, N.; Porazik, C.; Hanselmann, J.; Weydt, P.; Ferger, B.; Witting, A. Comparative biochemical characterization of the monoacylglycerol lipase inhibitor KML29 in brain, spinal cord, liver, spleen, fat and muscle tissue. *Neuropharmacology* **2015,** 91, 148-156.
41. Viader, A.; Blankman, J. L.; Zhong, P.; Liu, X.; Schlosburg, J. E.; Joslyn, C. M.; Liu, Q. S.; Tomarchio, A. J.; Lichtman, A. H.; Selley, D. E.; Sim-Selley, L. J.; Cravatt, B. F. Metabolic interplay between astrocytes and neurons regulates endocannabinoid action. *Cell Reports* **2015,** 12, 798-808.
42. Steiner, A. A.; Molchanova, A. Y.; Dogan, M. D.; Patel, S.; Petervari, E.; Balasko, M.; Wanner, S. P.; Eales, J.; Oliveira, D. L.; Gavva, N. R.; Almeida, M. C.; Szekely, M.; Romanovsky, A. A. The hypothermic response to bacterial lipopolysaccharide critically depends on brain CB1, but not CB2 or TRPV1, receptors. *The Journal of Physiology* **2011,** 589, 2415-2431.
43. Nass, S. R.; Long, J. Z.; Schlosburg, J. E.; Cravatt, B. F.; Lichtman, A. H.; Kinsey, S. G. Endocannabinoid catabolic enzymes play differential roles in thermal homeostasis in response to environmental or immune challenge. *Journal of neuroimmune pharmacology : the official journal of the Society on NeuroImmune Pharmacology* **2015,** 10, 364-370.
44. Mechoulam, R.; Parker, L. A. The endocannabinoid system and the brain. *Annual Review of Psychology* **2013,** 64, 21-47.
45. Fowler, C. J. The potential of inhibitors of endocannabinoid metabolism as anxiolytic and antidepressive drugs--A practical view. *European Neuropsychopharmacology : the Journal of the European College of Neuropsychopharmacology* **2015,** 25, 749-762.
46. Blankman, J. L.; Cravatt, B. F. Chemical probes of endocannabinoid metabolism. *Pharmacological Reviews* **2013,** 65, 849-871.
47. Schlosburg, J. E.; Blankman, J. L.; Long, J. Z.; Nomura, D. K.; Pan, B.; Kinsey, S. G.; Nguyen, P. T.; Ramesh, D.; Booker, L.; Burston, J. J.; Thomas, E. A.; Selley, D. E.; Sim-Selley, L. J.; Liu, Q. S.; Lichtman, A. H.; Cravatt, B. F. Chronic monoacylglycerol lipase blockade causes functional antagonism of the endocannabinoid system. *Nature Neuroscience* **2010,** 13, 1113-1119.
48. Chanda, P. K.; Gao, Y.; Mark, L.; Btesh, J.; Strassle, B. W.; Lu, P.; Piesla, M. J.; Zhang, M. Y.; Bingham, B.; Uveges, A.; Kowal, D.; Garbe, D.; Kouranova, E. V.; Ring, R. H.; Bates, B.; Pangalos, M. N.; Kennedy, J. D.; Whiteside, G. T.; Samad, T. A. Monoacylglycerol lipase activity is a critical modulator of the tone and integrity of the endocannabinoid system. *Molecular Pharmacology* **2010,** 78, 996-1003.
49. Taschler, U.; Eichmann, T. O.; Radner, F. P.; Grabner, G. F.; Wolinski, H.; Storr, M.; Lass, A.; Schicho, R.; Zimmermann, R. Monoglyceride lipase deficiency causes desensitization of intestinal cannabinoid receptor type 1 and increased colonic mu-opioid receptor sensitivity. *British Journal of Pharmacology* **2015,** 172, 4419-4429.
50. Piomelli, D. More surprises lying ahead. The endocannabinoids keep us guessing. *Neuropharmacology* **2014,** 76 Pt B, 228-234.

51. Fowler, C. J.; Naidu, P. S.; Lichtman, A.; Onnis, V. The case for the development of novel analgesic agents targeting both fatty acid amide hydrolase and either cyclooxygenase or TRPV1. *British Journal of Pharmacology* **2009,** 156, 412-419.
52. Jung, K. M.; Astarita, G.; Zhu, C.; Wallace, M.; Mackie, K.; Piomelli, D. A key role for diacylglycerol lipase-alpha in metabotropic glutamate receptor-dependent endocannabinoid mobilization. *Molecular Pharmacology* **2007,** 72, 612-621.
53. Shonesy, B. C.; Wang, X.; Rose, K. L.; Ramikie, T. S.; Cavener, V. S.; Rentz, T.; Baucum, A. J., 2nd; Jalan-Sakrikar, N.; Mackie, K.; Winder, D. G.; Patel, S.; Colbran, R. J. CaMKII regulates diacylglycerol lipase-alpha and striatal endocannabinoid signaling. *Nature Neuroscience* **2013,** 16, 456-463.
54. Yuan, S.; Burrell, B. D. Endocannabinoid-dependent long-term depression in a nociceptive synapse requires coordinated presynaptic and postsynaptic transcription and translation. *The Journal of Neuroscience : the official Journal of the Society for Neuroscience* **2013,** 33, 4349-4358.
55. Bingol, B.; Sheng, M. Deconstruction for reconstruction: the role of proteolysis in neural plasticity and disease. *Neuron* **2011,** 69, 22-32.
56. Maccarrone, M.; Rossi, S.; Bari, M.; De Chiara, V.; Fezza, F.; Musella, A.; Gasperi, V.; Prosperetti, C.; Bernardi, G.; Finazzi-Agro, A.; Cravatt, B. F.; Centonze, D. Anandamide inhibits metabolism and physiological actions of 2-arachidonoylglycerol in the striatum. *Nature Neuroscience* **2008,** 11, 152-159.
57. Choi, S. H.; Langenbach, R.; Bosetti, F. Genetic deletion or pharmacological inhibition of cyclooxygenase-1 attenuate lipopolysaccharide-induced inflammatory response and brain injury. *FASEB Journal : official publication of the Federation of American Societies for Experimental Biology* **2008,** 22, 1491-1501.
58. Viader, A.; Ogasawara, D.; Joslyn, C. M.; Sanchez-Alavez, M.; Mori, S.; Nguyen, W.; Conti, B.; Cravatt, B. F. A chemoproteomic atlas of brain serine hydrolases identifies cell type-specific pathways regualting neuroinflammation.eLife **2016,** 5, e12345.
59. Kirilly, E.; Gonda, X.; Bagdy, G. CB1 receptor antagonists: new discoveries leading to new perspectives. *Acta Physiologica* **2012,** 205, 41-60.
60. Busquets-Garcia, A.; Gomis-Gonzalez, M.; Guegan, T.; Agustin-Pavon, C.; Pastor, A.; Mato, S.; Perez-Samartin, A.; Matute, C.; de la Torre, R.; Dierssen, M.; Maldonado, R.; Ozaita, A. Targeting the endocannabinoid system in the treatment of fragile X syndrome. *Nature Medicine* **2013,** 19, 603-607.
61. Bashashati, M.; Nasser, Y.; Keenan, C. M.; Ho, W.; Piscitelli, F.; Nalli, M.; Mackie, K.; Storr, M. A.; Di Marzo, V.; Sharkey, K. A. Inhibiting endocannabinoid biosynthesis: a novel approach to the treatment of constipation. *British Journal of Pharmacology* **2015,** 172, 3099-3111.
62. Oleson, E. B.; Beckert, M. V.; Morra, J. T.; Lansink, C. S.; Cachope, R.; Abdullah, R. A.; Loriaux, A. L.; Schetters, D.; Pattij, T.; Roitman, M. F.; Lichtman, A. H.; Cheer, J. F. Endocannabinoids shape accumbal encoding of cue-motivated behavior via CB1 receptor activation in the ventral tegmentum. *Neuron* **2012,** 73, 360-373.
63. Verdoes, M.; Florea, B. I.; Hillaert, U.; Willems, L. I.; van der Linden, W. A.; Sae-Heng, M.; Filippov, D. V.; Kisseley, A. F.; van der Marel, G. A.; Overkleeft, H. S. Azido-BODIPY acid reveals quantitative Staudinger-Bertozzi ligation in two-step activity-based proteasome profiling. *ChemBioChem* **2008,** 9, 1735-1738.

64. Liu, Y.; Patricelli, M. P.; Cravatt, B. F. Activity-based protein profiling: the serine hydrolases. *Proceedings of the National Academy of Sciences of the United States of America* **1999,** 96, 14694-14699.
65. Kidd, D.; Liu, Y.; Cravatt, B. F. Profiling serine hydrolase activities in complex proteomes. *Biochemistry* **2001,** 40, 4005-4015.
66. Patricelli, M. P.; Giang, D. K.; Stamp, L. M.; Burbaum, J. J. Direct visualization of serine hydrolase activities in complex proteomes using fluorescent active site-directed probes. *Proteomics* **2001,** 1, 1067-1071.
67. Hsu, K.-L. L.; Tsuboi, K.; Adibekian, A.; Pugh, H.; Masuda, K.; Cravatt, B. F. DAGLβ inhibition perturbs a lipid network involved in macrophage inflammatory responses. *Nature Chemical Biology* **2012,** 8, 999-1007.
68. Baggelaar, M. P.; Janssen, F. J.; van Esbroeck, A. C.; den Dulk, H.; Allarà, M.; Hoogendoorn, S.; McGuire, R.; Florea, B. I.; Meeuwenoord, N.; van den Elst, H.; van der Marel, G. A.; Brouwer, J.; Di Marzo, V.; Overkleeft, H. S.; van der Stelt, M. Development of an activity-based probe and in silico design reveal highly selective inhibitors for diacylglycerol lipase-α in brain. *Angewandte Chemie International Edition,* **2013,** 52, 12081-12085.
69. Janssen, F. J.; Deng, H.; Baggelaar, M. P.; Allarà, M.; van der Wel, T.; den Dulk, H.; Ligresti, A.; van Esbroeck, A. C.; McGuire, R.; Di Marzo, V.; Overkleeft, H. S.; van der Stelt, M. Discovery of glycine sulfonamides as dual inhibitors of sn-1-diacylglycerol lipase α and α/β-hydrolase domain 6. *Journal of Medicinal Chemistry* **2014,** 57, 6610-6622.
70. van der Wel, T.; Janssen, F. J.; Baggelaar, M. P.; Deng, H.; den Dulk, H.; Overkleeft, H. S.; van der Stelt, M. A natural substrate-based fluorescence assay for inhibitor screening on diacylglycerol lipase α. *Journal of Lipid Research* **2015,** 56, 927-935.
71. Bachovchin, D. A.; Ji, T.; Li, W.; Simon, G. M.; Blankman, J. L.; Adibekian, A.; Hoover, H.; Niessen, S.; Cravatt, B. F. Superfamily-wide portrait of serine hydrolase inhibition achieved by library-versus-library screening. *Proceedings of the National Academy of Sciences of the United States of America* **2010,** 107, 20941-20946.
72. Alexander, J. P.; Cravatt, B. F. Mechanism of carbamate inactivation of FAAH: implications for the design of covalent inhibitors and in vivo functional probes for enzymes. *Chemistry & Biology* **2005,** 12, 1179-1187.
73. Nomura, D. K.; Morrison, B. E.; Blankman, J. L.; Long, J. Z.; Kinsey, S. G.; Marcondes, M. C.; Ward, A. M.; Hahn, Y. K.; Lichtman, A. H.; Conti, B.; Cravatt, B. F. Endocannabinoid hydrolysis generates brain prostaglandins that promote neuroinflammation. *Science* **2011,** 334, 809-813.
74. Hyeon-Cheol, L.; Gabriel, M. S.; Benjamin, F. C. ABHD4 Regulates multiple classes of N-acyl phospholipids in the mammalian central nervous system. *Biochemistry* **2015**.
75. Inloes, J. M.; Hsu, K.-L. L.; Dix, M. M.; Viader, A.; Masuda, K.; Takei, T.; Wood, M. R.; Cravatt, B. F. The hereditary spastic paraplegia-related enzyme DDHD2 is a principal brain triglyceride lipase. *Proceedings of the National Academy of Sciences of the United States of America* **2014,** 111, 14924-14929.
76. Kamat, S. S.; Camara, K.; Parsons, W. H.; Chen, D.-H. H.; Dix, M. M.; Bird, T. D.; Howell, A. R.; Cravatt, B. F. Immunomodulatory lysophosphatidylserines are regulated by ABHD16A and ABHD12 interplay. *Nature Chemical Biology* **2015,** 11, 164-171.

77. Martin, B. R.; Wang, C.; Adibekian, A.; Tully, S. E.; Cravatt, B. F. Global profiling of dynamic protein palmitoylation. *Nature Methods* **2012,** 9, 84-89.
78. Hulce, J. J.; Cognetta, A. B.; Niphakis, M. J.; Tully, S. E.; Cravatt, B. F. Proteome-wide mapping of cholesterol-interacting proteins in mammalian cells. *Nature Methods* **2013,** 10, 259-264.
79. Washburn, M. P.; Wolters, D.; Yates, J. R. Large-scale analysis of the yeast proteome by multidimensional protein identification technology. *Nature Biotechnology* **2001,** 19, 242-247.
80. Weerapana, E.; Wang, C.; Simon, G. M.; Richter, F.; Khare, S.; Dillon, M. B.; Bachovchin, D. A.; Mowen, K.; Baker, D.; Cravatt, B. F. Quantitative reactivity profiling predicts functional cysteines in proteomes. *Nature* **2010,** 468, 790-795.
81. Pan, B.; Wang, W.; Long, J. Z.; Sun, D.; Hillard, C. J.; Cravatt, B. F.; Liu, Q.-s. S. Blockade of 2-arachidonoylglycerol hydrolysis by selective monoacylglycerol lipase inhibitor 4-nitrophenyl 4-(dibenzo[d][1,3]dioxol-5-yl(hydroxy)methyl)piperidine-1-carboxylate (JZL184) Enhances retrograde endocannabinoid signaling. *The Journal of Pharmacology and Experimental Therapeutics* **2009,** 331, 591-597.
82. Zhong, P.; Pan, B.; Gao, X.-p. P.; Blankman, J. L.; Cravatt, B. F.; Liu, Q.-s. S. Genetic deletion of monoacylglycerol lipase alters endocannabinoid-mediated retrograde synaptic depression in the cerebellum. *The Journal of Physiology* **2011,** 589, 4847-4855.
83. Kreitzer, A. C.; Regehr, W. G. Retrograde inhibition of presynaptic calcium influx by endogenous cannabinoids at excitatory synapses onto Purkinje cells. *Neuron* **2001,** 29, 717-727.
84. Bruno, C.; Manuel, S.-A.; Raphaelle, W.-S.; Maria Concetta, M.; Jacinta, L.; Sara, B.; Veronique, F.; Salvador, H.-R.; Steven, H.; Eric, P. Z.; Luis de, L.; Tamas, B. Transgenic mice with a reduced core body temperature have an increased life span. *Science* **2006**.
85. Eric, P. Z.; Manuel, S.-A.; Shuei, S.; Molly, B.; Rosette, F.; Tamas, B.; Bruno, C. Interleukin-18 controls energy homeostasis by suppressing appetite and feed efficiency. *Proceedings of the National Academy of Sciences* **2007**.
86. Manuel, S.-A.; Izabella, K.; Sara, E. B.; Iustin, V. T.; Christopher, N. D.; Bruno, C.; Tamas, B. Night eating and obesity in the EP3R-deficient mouse. *Proceedings of the National Academy of Sciences* **2007**.
87. Manuel, S.-A.; Iustin, V. T.; Olivia, O.; Kayo, M.; Jean, S.; Jeffrey, D.; Kristina, H. H.; Izabella, K.; Joe, K.; Luis, F. G.; Hartmuth, K.; James, S.; Jeanine, J.; Kevin, M.; Peter, B.; John, R. H.; James, E.; Bruno, C.; Tamas, B. Insulin Causes Hyperthermia by Direct Inhibition of Warm-Sensitive Neurons. *Diabetes* **2010**.
88. Zweemer, A. J.; Nederpelt, I.; Vrieling, H.; Hafith, S.; Doornbos, M. L.; de Vries, H.; Abt, J.; Gross, R.; Stamos, D.; Saunders, J.; Smit, M. J.; Ijzerman, A. P.; Heitman, L. H. Multiple binding sites for small-molecule antagonists at the CC chemokine receptor 2. *Molecular pharmacology* **2013,** 84, 551-561.

4

Diacylglycerol lipase inhibitors prevent fasting-induced refeeding in mice

Based on
H. Deng, S. Kooijman, A. M.C.H. van den Nieuwendijk, D. Ogasawara, T. van der Wel, F. van Dalen, M. P. Baggelaar, F. J. Janssen, R. J.B.H.N. van den Berg, H. den Dulk, K. Vasu, H. Thomas, B. F. Cravatt, H. S. Overkleeft, P. C.N. Rensen, M. van der Stelt, *J. Med. Chem.*

Introduction

Activation of the cannabinoid CB_1 receptor is a clinically proven signalling pathway controlling the energy balance in humans.[1] Rimonabant, a cannabinoid CB_1 receptor inverse agonist, reduced body weight and waist circumference in obese patients and improved cardiovascular risk factors, possibly via reducing food intake and increasing energy expenditure through activation of thermogenic brown adipose tissue.[2] First, several lines of evidence suggest that the endocannabinoid 2-arachidonoylglycerol (2-AG) regulates cannabinoid CB_1 receptor-dependent food intake. Second, 2-AG levels are increased in the hypothalamus of fasting mice and pharmacological intervention using the non-selective fluorophosphonate-based diacylglycerol lipase (DAGL) inhibitors O-5596 and O-7460 lead to reduced food intake in mice.[3,4] Third, DAGLα$^{-/-}$ mice showed hypophagia and leanness similar to that of $CB_1^{-/-}$ mice, while knockout mice of DAGLβ and *N*-acyl phosphatidylethanolamine phospholipase D (NAPE-PLD, the main enzyme responsible for anandamide biosynthesis) did not share this phenotype.[5,6] Interestingly, DAGLα knockout mice also had low fasting insulin, triglyceride, and total cholesterol

levels, and after glucose challenge had normal glucose, but very low insulin levels.[6] Fourth, mice overexpressing monoacylglycerol lipase, the enzyme that inactivates 2-AG, were lean, hyperphagic, resistant to diet induced obesity, hyperthermic and hypersensitive to β_3-adrenergic-stimulated thermogenesis.[7] Taken together, these data suggest that selective interference with DAGLα signaling may represent a novel therapeutic avenue to treat obesity and the metabolic syndrome.

In Chapters 2 and 3, the development and characterization of brain active DAGL inhibitors DH376 and DO34 was described. Competitive ABPP studies revealed a complementary selectivity profile for DH376 and DO34. Administration of DH376 and DO34 to mice significantly decreased 2-AG levels in the brain in a time- and dose dependent manner[8]. In this Chapter, the therapeutic efficacy of DH376 and DO34 as a potential anti-obesity agents is explored by studying their effect on fasting-induced food intake in mice, which is a typical cannabinoid CB_1 receptor mediated behavior.

Results and discussion

In vivo efficacy of DH376 and DO34

Mice were fasted for 18h and received a single intraperitoneal injection of vehicle or DH376 (50 mg/kg) 30 min before refeeding, and cumulative food intake was measured up to 16h. Within 2h, DH376-treated mice only consumed a third of the food compared to the vehicle-treated mice, and the effect of reduction in food-take maintained up to 4h (Figure 1a-d). After 16h, however, food intake in DH376-treated mice was back to the same levels as in vehicle-treated mice (Figure 1d), which paralleled the recovery of brain 2-AG levels. Consistent with the delay in refeeding of DH376-treated mice, indirect calorimetric measurements indicated that carbohydrate and fat oxidation remained respectively low and high for a prolonged period (Figure 1e,f). Importantly, DH376-treated mice showed no effect on locomotor activity (Figure 1g, over 4h; Figure 1h, over 24h) as measured by infrared beam breaks in Y and Z planes. Altogether, these results support the notion that DAGLα regulates food intake.

In Chapter 3, another CNS-active DAGL inhibitor (DO34) and a structurally related control probe DO53 were reported. DO34 reduced brain 2-AG levels in dose- and time-dependent manner, whereas the control probe DO53 did not affect brain 2-AG levels. Therefore, the effects of DO34 and DO53 were examined on fasting-induced refeeding, indirect calorimetry and locomotor activity. It was observed that food intake was completely blocked in DO34-treated mice, which was again also reflected by the calorimetric measurements. Surprisingly, control probe DO53-treated mice also showed significant reductions in fasting-induced refeeding, and both DO34- and DO53-treated mice were hypolocomotive (Figure 1g, h). These data suggest that there are one or more off-targets shared by the DAGL inhibitors and control probe DO53, that may also be involved in controlling food intake in fasting-induced mice. For

example, carboxylesterase was identified by *ex vivo* competitive ABPP in mouse liver as a major off-target shared by all three compounds (Figure 2).

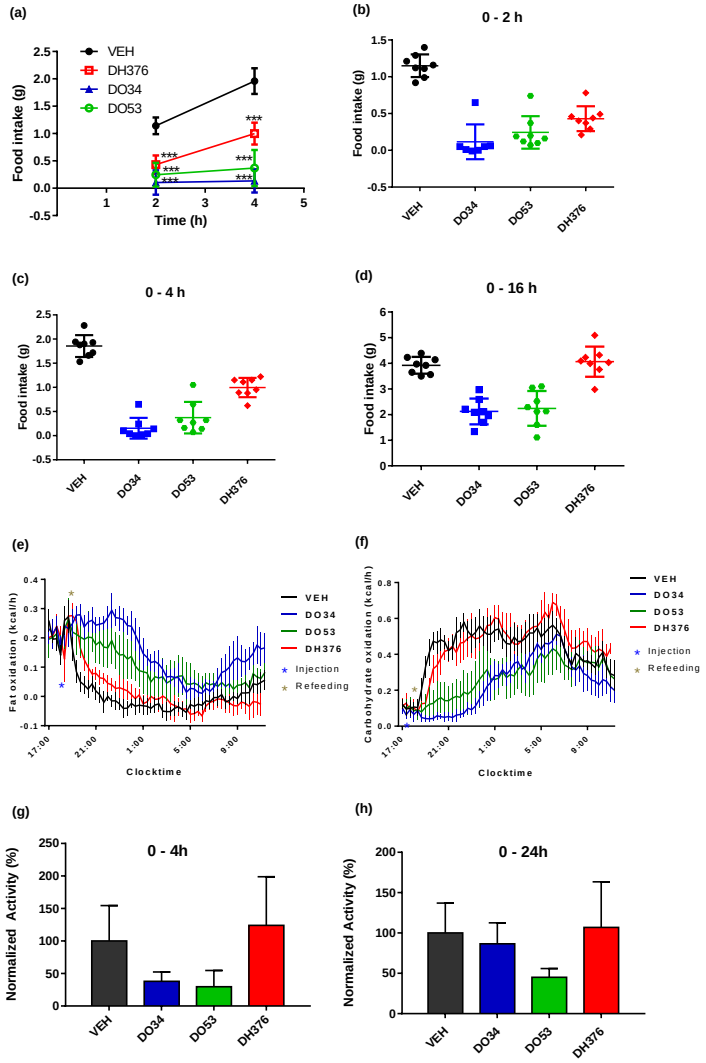

Figure 1. (a-h) *In vivo* effects of DAGL inhibitors DH376, DO34 and control compound DO53 on food intake (a-d), fat/carbohydrate oxidation (e, f) and locomotor activity (g, 0-4h; h, 0-24h) in mice. Cumulative food intake was measured in 18h fasted mice. The animals received a single intraperitoneal injection of vehicle (black), or DH376 (red), DO34 (blue), and DO53 (green) (50 mg/kg) 30 min before the start of refeeding and the testing period. The fat and carbohydrate oxidation of the animals were calculated from the $V{\cdot}O_2$ and $V{\cdot}CO_2$ in metabolic cages (in 20 min bins), and the locomotor activity over 4h of the animals was measured by infrared beam breaks in Y and Z axis. Data represent average values ± SEM; n = 8 mice per group.

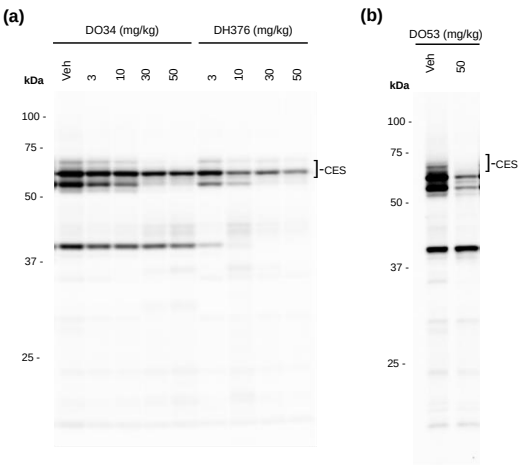

Figure 2. *Ex vivo* selectivity profile of DAGLs inhibitors (DH376 and DO34) and control compound (DO53) in mouse liver. (a) Competitive ABPP analysis in mouse liver from mice treated with various dose (3-20-30-50 mg/kg, i.p., 4h) of DAGLs inhibitors DH376 and DO34 using FP-TAMRA (1 µM, 20 min) as a broad-spectrum probe. (b) Competitive ABPP analysis in mouse liver from DO53-treated mice (50 mg/kg, i.p., 4h) using FP-TAMRA (1 µM, 20 min) as a probe.

A comprehensive profile of endogenous DAGLs activity in mouse tissues

DAGLs are not only expressed in the brain: their mRNA has also been found in peripheral tissues.[9] Genetic studies with constitutive knockout mice have revealed that DAGLα and DAGLβ regulate 2-AG production in a tissue-type dependent manner,[10-12] which may suggest that peripheral DAGLs also contribute to the control of energy balance.[13,14] Competitive activity-based protein profiling (ABPP) using the ABPs DH379 and MB064 was applied to investigate the role of endogenous DAGLα and DAGLβ activity in peripheral tissues, such as liver, kidney, spleen, heart, testis, lung, pancreas and muscle (Chapter 3).[8,15] DAGL inhibitors LEI105[16] and KT109[17] were applied to confirm the identity of the fluorescent bands. A fluorescent band at the molecular weight of DAGLα activity, which was out-competed with LEI105 and KT109, was detected in the brain proteomes treated with both probes, but not in other tissues (Figure 3). This is in line with previous ABPP results.[16] It is currently unknown why DAGLα activity can not be detected by ABPP in peripheral tissues, while mRNA and lipidomics studies indicate otherwise.[18] DH379 labeled a protein at the expected molecular weight of DAGLβ (using mouse brain as a reference) in spleen, kidney, testis, muscle, heart and lung. This labelling was prevented by pre-incubation with LEI105 and KT109 (1 µM, 30min) (Figure 3). Multiple fluorescent signals around ~70kDa were found in the liver, which make it difficult to unequivocally establish the

identity of DAGLβ in this tissue (Figure 3f). DH379 and MB064 can also label α,β-hydrolase domain containing protein 6 (ABHD6),[8, 19] an enzyme involved in lipid metabolism.[20,21] Strong ABHD6 labeling by both probes was observed in testis, liver and brain, whereas only a weak fluorescent band was detected in MB064-treated proteomes of the spleen, kidney, muscle and heart (Figure 3). (Of note, DH379 is less sensitive towards ABHD6.) Taken together, these data suggest that DAGLβ and ABHD6, rather than DAGLα, could be considered to play a peripheral role in controlling the energy balance.

A tissue-wide selectivity profile of DH376

Next, the *in vivo* target engagement and selectivity profile of DH376 was studied in various tissues from mice treated with a low or high dose of DH376 (3 and 30 mg/kg, respectively). Mice were sacrificed 2h after intraperitoneal administration and eight tissues (liver, kidney, spleen, heart, testis, lung, muscle and pancreas) were collected and analyzed by competitive ABPP using TAMRA-FP, a broad-spectrum serine hydrolase probe. Competitive ABPP revealed that DH376 maintained good selectivity for the DAGLβ in most tissues, particularly at the low dose (Figure 4a), whereas at the high dose various off-targets with a MW around 50-70 kDa were identified (Figure 4a). The identity of these off-targets is currently unknown, but carboxylesterases are potential candidates as was previously observed in mouse brain (Chapter 3).

Direct target engagement of DH376 in the mouse tissue proteomes was visualized by conjugation of probe-labeled proteins to a Cy5 fluorophore by copper-catalyzed azide-alkyne cycloaddition (CuAAC).[23] Consistent with the competitive ABPP results, direct conjugation revealed several off-targets at around ~65 kDa and 55 kDa (Figure 4b). In addition, a protein was labeled around 35 kDa, matching the molecular weight of ABHD6. Of note, the identified target band at ~70 kDa by CuAAC could be DAGLβ, but needs further confirmation with MS-based ABPP. Taken together, these results indicate that DH376 maintains relatively good selectivity in most of tissues; only in the liver DH376 cross-reacts with multiple off-targets.

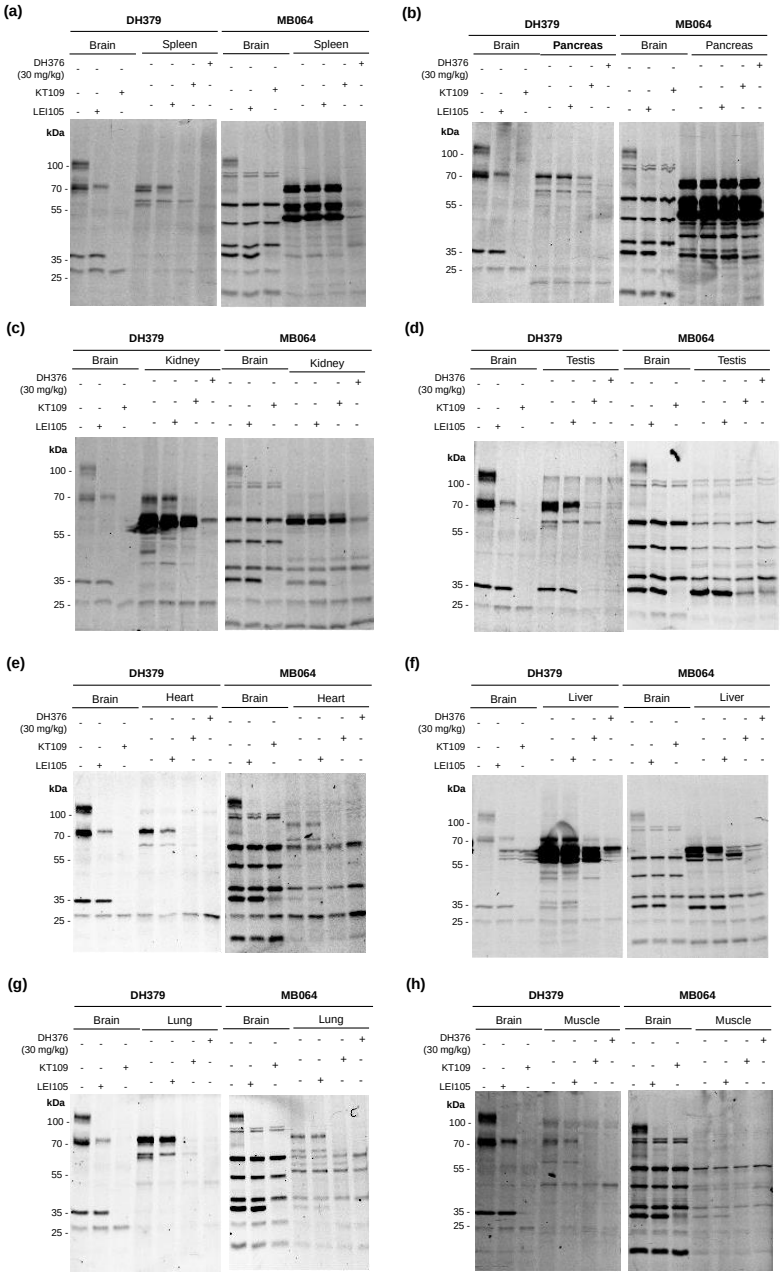

Figure 3. (a-h) Competitive ABPP was employed to screen a set of mouse tissues, including spleen (a), pancreas (b), kidney (c), testis (d), heart (e), liver (f), lung (g) and muscle (h) using DH379 and MB064 as ABPs and obtained a tissue-wide overview of endogenous activities of DAGLα, DAGLβ and ABHD6. Mouse membrane proteome was incubated at r.t. with vehicle (DMSO), LEI105 (1 μM)or KT109 (1μM) for 30 mins.

The sample was subsequently treated with MB064 (0.25 µM), or DH379 (1 µM) for 20 mins at r.t. DH376 (30 mg/kg)-treated mouse membranes as an *ex vivo* control were directly treated with MB064 (0.25 µM), or DH379 (1 µM) for 20 mins at r.t. The fluorescent bands at the molecular weight of ~120 kDa, 70 kDa or 35 kDa, which were prevented by pre-incubation of KT109 or LEI105, are DAGLα, DAGLβ and ABHD6, respectively. Of note, mouse brain was used as a reference for the detection of DAGLs and ABHD6 activity in other mouse tissues.

Table 1. Summary of detection endogenous DAGLα, DAGLβ and ABHD6 activity in mouse tissues using gel-based activity-based protein profiling (related to data from Figure 3).

	Brain	Spleen	Kidney	Testis	Heart	Lung	Liver	Muscle
DAGLα	+	-	-	-	-	-	-	-
DAGLβ	+	+	+	+	+	+	+	+
ABHD6	+	+	+	+	-	-	+	+

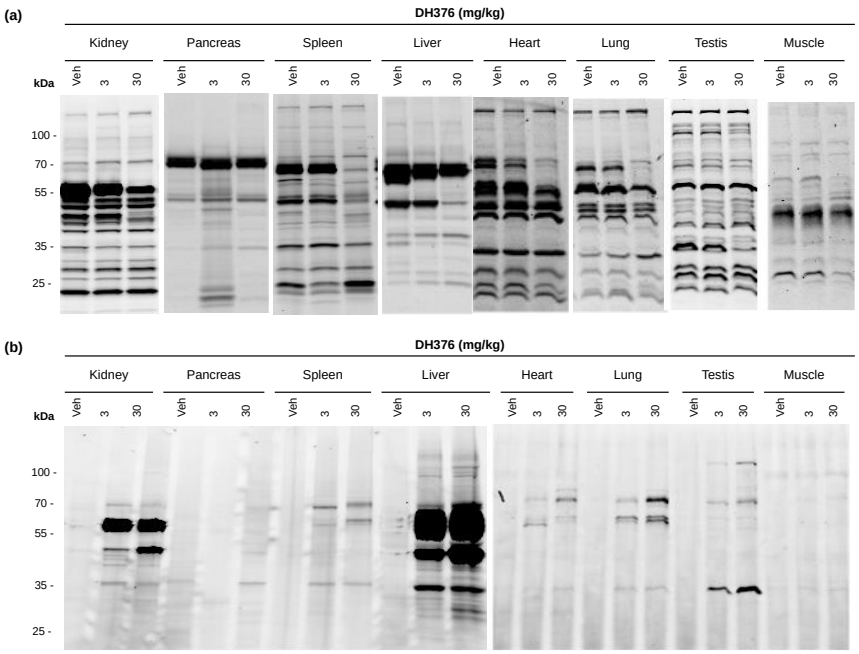

Figure 4. Gel-based ABPP analysis of various mouse tissue proteomes from mice treated with DH376 (3 or 30 mg/kg, i.p., 2h). (a) Competitive ABPP using a broad-spectrum probe TAMRA-FP to measure selectivity profile of DH376 over serine hydrolases. Tissue membrane proteomes from DH376-treated mice were incubated with TAMRA-FP (0.5 µM, 20 min) at r.t. (b) Click chemistry (CuAAC) ABPP of tissues membranes from DH376-treated mice. Tissue membrane proteomes were conjugated with Cy5-azide for 1h followed by SDS-PAGE and in-gel fluorescence scanning. The protein bands (off-targets) were directly visualized.

Conclusions

In summary, *in vivo* efficacy of CNS-active DAGLs inhibitors (DH376 and DO34) was demonstrated in a mouse model of fasting-induced refeeding, which is a typical cannabinoid CB_1-receptor-mediated response. These effects are in line with the phenotypes observed with DAGLα and CB_1 receptor knockout mice. The results also stress the importance of using a negative control compound, because DO53 also reduced food intake and affected locomotion, which indicates that triazole urea inhibitors affect the energy balance and locomotion in mice through multiple, yet to be discovered, molecular targets. While DH376 was found to maintain good selectivity in most of tissues, some other off-targets were also observed. This comprehensive tissue-wide detection of DAGL activity may provide important information for the design of future studies to investigate the peripheral role of DAGLs.

Experimental section

Materials of chemical biological assays

MB064 and DH379 were synthesized according to a previously described protocol.[24-28] FP-TAMRA is commercially available at Thermo Fischer Scientific.

ABPP enzyme activity measurements

The percentage of activity was determined by measuring the integrated optical intensity of the fluorescent protein bands using image lab 4.1. The relative intensity was compared to the vehicle treated proteins, the strongest signal set to 100% after protein loading correction using Coomassie Blue gel. Enzyme activity figures were generated using GraphPad Prism software 7.0.

Preparation of tissue proteomes

Mouse tissues were dounce homogenized in lysis buffer (20 mM HEPES, 250 mM sucrose, 2 mM DTT, 1 mM $MgCl_2$ with or without 25 U/mL benzonase) and incubated in ice for 5 min, followed by a low-speed spin (1,400−2,500 x g, 3 min, 4 °C) to remove debris. The membrane and cytosolic fractions were separated by ultracentrifugation (100,000 x g, 45 min, 4 °C) of the resulting homogenate lysate. After removal of the soluble supernatant, the membrane pellet was washed 1X with cold HEPES buffer (20 mM, with or without 2 mM DTT) followed by resuspension in cold HEPES buffer (20 mM, with or without 2 mM DTT) by pipetting. Total protein concentrations in membrane and soluble fractions were determined using the Bio-Rad DC protein assay kit. Samples were stored at -80 °C until further use.

Tissue profiling by gel-based competitive ABPP

Gel-based ABPP assays were performed as previously reported.[29] Cell or tissue proteomes were treated with either FP-TAMRA (1 µM or 500 nM final concentration), MB064 (0.25 µM final concentration), or DH379 (1 µM final concentration). For MB064 and DH379 labeled samples, 2 mg/mL of proteome was used to enhance endogenous DAGL signals; 1 mg/mL proteome was used for labeling with FP-TAMRA. Probe labeling was carried out for 30 min at r.t., followed by addition of 4X SDS-PAGE loading buffer to quench the reaction. After separation by SDS-PAGE (10% acrylamide), samples were visualized by in-gel fluorescence scanning using a ChemiDoc MP system.

Copper-catalyzed azide-alkyne cycloaddition (CuAAC or click) chemistry-ABPP

Mouse brain membrane proteomes from either naïve (*in vitro*) or inhibitor-treated (*in vivo*) mice were prepared for analysis as described in preparation of tissue proteome. Using previously developed methods[30], Cyanine 5-Azide (Cy5−N_3) was conjugated to each alkyne probe for in-gel analysis. Briefly, $CuSO_4$ (1.0 µL/reaction, 100 mM in H_2O), THPTA (0.2 µL/reaction, 100 mM in H_2O), sodium ascorbate (0.6 µL/reaction, 1 M in H_2O [freshly prepared]), and Cy5−N_3 (0.2 µL/reaction, 0.4 mM in DMSO) were premixed. This click reagent mixture (2.0 µL total volume) was immediately added to each proteome (18 µL), and the reaction was stirred by briefly vortexing. After 1 h at room temperature, reactions were diluted with 4× SDS loading buffer (10 µL) and resolved by SDS-PAGE.

***In vivo* target engagement studies of DH376**

The animal experiments were conducted in accordance with the ethical committee of Leiden University (DEC#14137). *In vivo* studies with DH376 were conducted in C57BL/6 mice. Mice were injected with DH376 (3 or 30 mg/kg) i.p. in 18:1:1 (v/v/v) solution of saline/ethanol/PEG40 (ethoxylated castor oil, 10 µL/g body weight of mouse). After 2h, mice were anesthetized with isoflurane, and euthanized by cervical dislocation. Mice were perfused with PBS and then brain, liver, spleen, heart, lung, pancreas, testis, muscle and kidney were collected. Tissue homogenates were prepared and competitive ABPP experiments were performed according to the previously described method.[8]

***In vivo* food intake studies with DH376, DO34 and DO53**

All animal experiments were approved by the Ethics Committee on Animal Care and Experimentation of the Leiden University Medical Center. 12-week-old male C57Bl/6J mice (Charles River, Saint-Germain-Nuelles, France) were single housed in metabolic cages (LabMaster System, TSE Systems, Bad Homburg, Germany) with a regular 12:12h light/dark cycle (6 a.m.- 6 p.m.) and free access to food and water unless noted otherwise. After 3 days of acclimatization, mice were fasted for 18h starting at midnight followed by an intraperitoneal injection with DH376 (50 mg/kg), DO34 (50

mg/kg), DO53 (50 mg/kg) or vehicle 30 min prior to refeeding. Solutions were prepared in mixture of saline/ethanol/PEG40 (18:1:1; v/v/v). Cumulative food intake, oxygen uptake ($V{\cdot}O_2$), carbon dioxide production ($V{\cdot}CO_2$) and physical activity (beam breaks) were monitored. Carbohydrate oxidation was calculated using the formula ((4.585* $V{\cdot}CO_2$)-(3.226* $V{\cdot}O_2$))*4, in which the 4 represents the conversion from mass per time unit to kcal per time unit. Similarly, fat oxidation was calculated using the formula ((1.695* $V{\cdot}O_2$)-(1.701* $V{\cdot}CO_2$))*9.

Supporting Figures

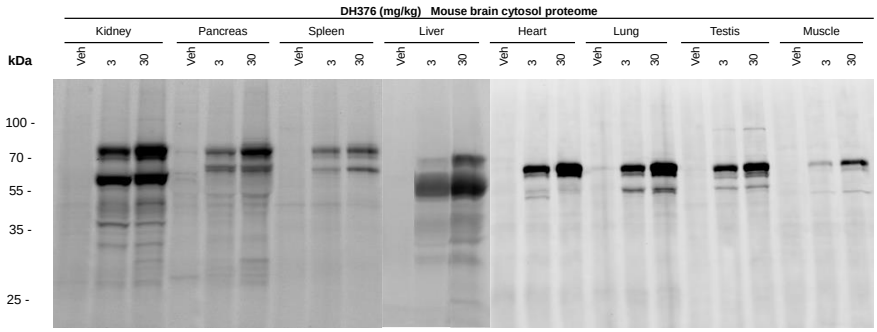

Figure S.1. Click chemistry (CuAAC) ABPP of tissue cytosols from DH376-treated mice. Tissue cytosol proteomes were conjugated with Cy5-azide for 1h followed by SDS-PAGE and in-gel fluorescence scanning. The protein bands (off-targets) in cytosol were directly visualized.

References

1. Di Marzo, V.; Matias, I. Endocannabinoid control of food intake and energy balance. *Nature Neuroscience* **2005,** 8, 585-589.
2. Boon, M. R.; Kooijman, S.; van Dam, A. D.; Pelgrom, L. R.; Berbee, J. F. P.; Visseren, C. A. R.; van Aggele, R. C.; van den Hoek, A. M.; Sips, H. C. M.; Lombes, M.; Havekes, L. M.; Tamsma, J. T.; Guigas, B.; Meijer, O. C.; Jukema, J. W.; Rensen, P. C. N. Peripheral cannabinoid 1 receptor blockade activates brown adipose tissue and diminishes dyslipidemia and obesity. *FASEB Journal* **2014,** 28, 5361-5375.
3. Bisogno, T.; Mahadevan, A.; Coccurello, R.; Chang, J. W.; Allara, M.; Chen, Y. G.; Giacovazzo, G.; Lichtman, A.; Cravatt, B.; Moles, A.; Di Marzo, V. A novel fluorophosphonate inhibitor of the biosynthesis of the endocannabinoid 2-arachidonoylglycerol with potential anti-obesity effects. *British Journal of Pharmacology* **2013,** 169, 784-793.
4. Janssen, F. J.; van der Stelt, M. Inhibitors of diacylglycerol lipases in neurodegenerative and metabolic disorders. *Bioorganic & Medicinal Chemistry Letters* **2016,** 26, 3831-3837.
5. Gruden, G.; Barutta, F.; Kunos, G.; Pacher, P. Role of the endocannabinoid system in diabetes and diabetic complications. *British Journal of Pharmacology* **2016,** 173, 1116-1127.
6. Powell, D. R.; Gay, J. P.; Wilganowski, N.; Doree, D.; Savelieva, K. V.; Lanthorn, T. H.; Read, R.; Vogel, P.; Hansen, G. M.; Brommage, R.; Ding, Z. M.; Desai, U.; Zambrowicz, B. Diacylglycerol lipase a knockout mice demonstrate metabolic and behavioral phenotypes similar to those of cannabinoid receptor 1 knockout mice. *Frontiers in Endocrinology* **2015,** 6, 86-91.
7. Jung, K. M.; Clapper, J. R.; Fu, J.; D'Agostino, G.; Guijarro, A.; Thongkham, D.; Avanesian, A.; Astarita, G.; DiPatrizio, N. V.; Frontini, A.; Cinti, S.; Diano, S.; Piomelli, D. 2-arachidonoylglycerol signaling in forebrain regulates systemic energy metabolism. *Cell Metabolism* **2012,** 15, 299-310.
8. Ogasawara, D.; Deng, H.; Viader, A.; Baggelaar, M. P.; Breman, A.; den Dulk, H.; van den Nieuwendijk, A. M.; Soethoudt, M.; van der Wel, T.; Zhou, J.; Overkleeft, H. S.; Sanchez-Alavez, M.; Mo, S.; Nguyen, W.; Conti, B.; Liu, X.; Chen, Y.; Liu, Q. S.; Cravatt, B. F.; van der Stelt, M. Rapid and profound rewiring of brain lipid signaling networks by acute diacylglycerol lipase inhibition. *Proceedings of the National Academy of Sciences of the United States of America* **2016,** 113, 26-33.
9. Bisogno, T.; Howell, F.; Williams, G.; Minassi, A.; Cascio, M. G.; Ligresti, A.; Matias, I.; Schiano-Moriello, A.; Paul, P.; Williams, E. J.; Gangadharan, U.; Hobbs, C.; Di Marzo, V.; Doherty, P. Cloning of the first sn1-DAG lipases points to the spatial and temporal regulation of endocannabinoid signaling in the brain. *Journal of Cell Biology* **2003,** 163, 463-468.
10. Gao, Y.; Vasilyev, D. V.; Goncalves, M. B.; Howell, F. V.; Hobbs, C.; Reisenberg, M.; Shen, R.; Zhang, M. Y.; Strassle, B. W.; Lu, P.; Mark, L.; Piesla, M. J.; Deng, K.; Kouranova, E. V.; Ring, R. H.; Whiteside, G. T.; Bates, B.; Walsh, F. S.; Williams, G.; Pangalos, M. N.; Samad, T. A.; Doherty, P. Loss of retrograde endocannabinoid signaling and reduced adult

neurogenesis in diacylglycerol lipase knock-out mice. *The Journal of neuroscience : the official journal of the Society for Neuroscience* **2010,** 30, 2017-2024.

11. Tanimura, A.; Yamazaki, M.; Hashimotodani, Y.; Uchigashima, M.; Kawata, S.; Abe, M.; Kita, Y.; Hashimoto, K.; Shimizu, T.; Watanabe, M.; Sakimura, K.; Kano, M. The Endocannabinoid 2-arachidonoylglycerol produced by diacylglycerol lipase alpha mediates retrograde suppression of synaptic transmission. *Neuron* **2010,** 65, 320-327.
12. Shonesy, B. C.; Bluett, R. J.; Ramikie, T. S.; Baldi, R.; Hermanson, D. J.; Kingsley, P. J.; Marnett, L. J.; Winder, D. G.; Colbran, R. J.; Patel, S. Genetic Disruption of 2-Arachidonoylglycerol Synthesis Reveals a Key Role for Endocannabinoid Signaling in Anxiety Modulation. *Cell Reports* **2014,** 9, 1644-1653.
13. Cota, D. Role of the endocannabinoid system in energy balance regulation and obesity. *Frontiers of Hormone Research* **2008,** 36, 135-145.
14. Bermudez-Silva, F. J.; Cardinal, P.; Cota, D. The role of the endocannabinoid system in the neuroendocrine regulation of energy balance. *Journal of Psychopharmacology* **2012,** 26, 114-124.
15. Baggelaar, M. P.; Janssen, F. J.; van Esbroeck, A. C.; den Dulk, H.; Allara, M.; Hoogendoorn, S.; McGuire, R.; Florea, B. I.; Meeuwenoord, N.; van den Elst, H.; van der Marel, G. A.; Brouwer, J.; Di Marzo, V.; Overkleeft, H. S.; van der Stelt, M. Development of an activity-based probe and in silico design reveal highly selective inhibitors for diacylglycerol lipase-alpha in brain. *Angewandte Chemie International Edition* **2013,** 52, 12081-12085.
16. Baggelaar, M. P.; Chameau, P. J. P.; Kantae, V.; Hummel, J.; Hsu, K. L.; Janssen, F.; van der Wel, T.; Soethoudt, M.; Deng, H.; den Dulk, H.; Allara, M.; Florea, B. I.; Di Marzo, V.; Wadman, W. J.; Kruse, C. G.; Overkleeft, H. S.; Hankemeier, T.; Werkman, T. R.; Cravatt, B. F.; van der Stelt, M. Highly selective, reversible inhibitor identified by comparative chemoproteomics modulates diacylglycerol lipase activity in neurons. *Journal of the American Chemical Society* **2015,** 137, 8851-8857.
17. Hsu, K. L.; Tsuboi, K.; Adibekian, A.; Pugh, H.; Masuda, K.; Cravatt, B. F. DAGLbeta inhibition perturbs a lipid network involved in macrophage inflammatory responses. *Nature Chemical Biology* **2012,** 8, 999-1007.
18. Bisogno, T.; Howell, F.; Williams, G.; Minassi, A.; Cascio, M. G.; Ligresti, A.; Matias, I.; Schiano-Moriello, A.; Paul, P.; Williams, E. J.; Gangadharan, U.; Hobbs, C.; Di Marzo, V.; Doherty, P. Cloning of the first sn1-DAG lipases points to the spatial and temporal regulation of endocannabinoid signaling in the brain. *The Journal of Cell Biology* **2003,** 163, 463-468.
19. Baggelaar, M. P.; Janssen, F. J.; van Esbroeck, A. C. M.; den Dulk, H.; Allara, M.; Hoogendoorn, S.; McGuire, R.; Florea, B. I.; Meeuwenoord, N.; van den Elst, H.; van der Marel, G. A.; Brouwer, J.; Di Marzo, V.; Overkleeft, H. S.; van der Stelt, M. Development of an Activity-Based Probe and In Silico Design Reveal Highly Selective Inhibitors for Diacylglycerol Lipase-alpha in Brain. *Angewandte Chemie International Edition* **2013,** 52, 12081-12085.
20. Marrs, W. R.; Blankman, J. L.; Horne, E. A.; Thomazeau, A.; Lin, Y. H.; Coy, J.; Bodor, A. L.; Muccioli, G. G.; Hu, S. S. J.; Woodruff, G.; Fung, S.; Lafourcade, M.; Alexander, J. P.; Long, J. Z.; Li, W. W.; Xu, C.; Moller, T.; Mackie, K.; Manzoni, O. J.; Cravatt, B. F.; Stella,

N. The serine hydrolase ABHD6 controls the accumulation and efficacy of 2-AG at cannabinoid receptors. *Nature Neuroscience* **2010,** 13, 951-967.

21. Pribasnig, M. A.; Mrak, I.; Grabner, G. F.; Taschler, U.; Knittelfelder, O.; Scherz, B.; Eichmann, T. O.; Heier, C.; Grumet, L.; Kowaliuk, J.; Romauch, M.; Holler, S.; Anderl, F.; Wolinski, H.; Lass, A.; Breinbauer, R.; Marsche, G.; Brown, J. M.; Zimmermann, R. alpha/beta Hydrolase Domain-containing 6 (ABHD6) Degrades the late endosomal/lysosomal lipid bis(monoacylglycero)phosphate. *Journal of Biological Chemistry* **2015,** 290, 29869-29881.
22. Hosokawa, M. Structure and catalytic properties of carboxylesterase isozymes involved in metabolic activation of prodrugs. *Molecules* **2008,** 13, 412-431.
23. Speers, A. E.; Adam, G. C.; Cravatt, B. F. Activity-based protein profiling in vivo using a copper(I)-catalyzed azide-alkyne [3+2] cycloaddition. *Journal of the American Chemical Society* **2003,** 125, 4686-4687.
24. Liu, Y.; Patricelli, M. P.; Cravatt, B. F. Activity-based protein profiling: the serine hydrolases. *Proceedings of the National Academy of Sciences of the United States of America* **1999,** 96, 14694-14699.
25. Kidd, D.; Liu, Y.; Cravatt, B. F. Profiling serine hydrolase activities in complex proteomes. *Biochemistry* **2001,** 40, 4005-4015.
26. Patricelli, M. P.; Giang, D. K.; Stamp, L. M.; Burbaum, J. J. Direct visualization of serine hydrolase activities in complex proteomes using fluorescent active site-directed probes. *Proteomics* **2001,** 1, 1067-1071.
27. Hsu, K.-L. L.; Tsuboi, K.; Adibekian, A.; Pugh, H.; Masuda, K.; Cravatt, B. F. DAGLβ inhibition perturbs a lipid network involved in macrophage inflammatory responses. *Nature Chemical Biology* **2012,** 8, 999-1007.
28. Baggelaar, M. P.; Janssen, F. J.; van Esbroeck, A. C.; den Dulk, H.; Allarà, M.; Hoogendoorn, S.; McGuire, R.; Florea, B. I.; Meeuwenoord, N.; van den Elst, H.; van der Marel, G. A.; Brouwer, J.; Di Marzo, V.; Overkleeft, H. S.; van der Stelt, M. Development of an Activity-Based Probe and In Silico Design Reveal Highly Selective Inhibitors for Diacylglycerol Lipase-α in Brain. *Angewandte Chemie International Edition* **2013,** 52, 12081-12085.
29. Bachovchin, D. A.; Ji, T.; Li, W.; Simon, G. M.; Blankman, J. L.; Adibekian, A.; Hoover, H.; Niessen, S.; Cravatt, B. F. Superfamily-wide portrait of serine hydrolase inhibition achieved by library-versus-library screening. *Proceedings of the National Academy of Sciences of the United States of America* **2010,** 107, 20941-20946.
30. Alexander, J. P.; Cravatt, B. F. Mechanism of carbamate inactivation of FAAH: implications for the design of covalent inhibitors and in vivo functional probes for enzymes. *Chemistry & Biology* **2005,** 12, 1179-1187.

5

[^{18}F]DH439, a positron emission tomography tracer for *in vivo* imaging of diacylglycerol lipases*

Introduction

The endocannabinoid system is a lipid signaling network that regulates several (patho)physiological processes, including anxiety, depression, pain, inflammation, hepatic steatosis, neurodegeneration and obesity.[1,2] 2-Arachidonoylglycerol (2-AG) and anandamide (AEA) are the most abundant endocannabinoids, and activate type-1 and type-2 G protein-coupled cannabinoid receptors (CB_1R and CB_2R), thereby modulating neurotransmission and immune responses.[3] Early efforts focused on direct pharmacological intervention of the endocannabinoid system by various CB receptor agonists and antagonists, such as the classical CB_1R/CB_2R agonist Δ^9-tetrahydrocannabinol (THC) and the synthetic CB_1R antagonist Rimonabant.[1,2,4,5] However, concomitant adverse effects have limited their use as therapeutic agents. To solve this problem, an indirect approach by targeting the enzymes that regulate endogenous endocannabinoid levels has emerged as an alternative drug discovery strategy.[6]

*This research was performed in collaboration with Future Chemistry, the Netherlands. Dion van der Born is kindly acknowledged.

Several inhibitors of monoacylglycerol lipase (MAGL) and fatty acid amide hydrolase (FAAH), which are the principal enzymes that degrade 2-AG and AEA, respectively,[7-9] are currently under clinical investigation as an alternative for THC.[6,8,10] By contrast, no inhibitors are available to reduce endocannabinoid formation in humans. Recently, compound **1** (DH376) was discovered as a brain active diacylglycerol lipase inhibitor (see Chapters 2-4). DH376 contains a 1,2,3-triazole urea and irreversibly inhibits DAGLs via carbamoylation of the active-site serine nucleophile. Pharmacological blockade of DAGLs by DH376 reduced 2-AG content in mouse brain as well as arachidonic acid (AA) and pro-inflammatory prostaglandins levels (Chapter 3). DH376 also reduced proinflammatory cytokines levels, prevented neuroinflammation in lipopolysaccharide-treated mice (Chapter 3) and reduced food intake in fasted mice (Chapter 4). This makes DH376 an interesting starting point for novel therapies aimed at treating the metabolic syndrome and/or neuroinflammatory disorders.

An important step in the translation of preclinical results from drug discovery towards the clinic is the demonstration of target engagement in animals and humans. Molecular imaging is the most frequently used technique to visualize inhibitor-target interactions in humans.[10-12] For example, positron emission tomography (PET) is a nuclear imaging technique that can be used to observe metabolic processes in the body.[13] Currently, no PET radiotracers for DAGL have been reported in the literature. A selective DAGL radiotracer will enable a more detailed assessment of DAGL distribution and DAGL activity in various tissues and will provide a tool for target engagement studies to guide dose selection in clinical trials. In this Chapter the first selective PET tracer for DAGL is described based on the structure of DH376.

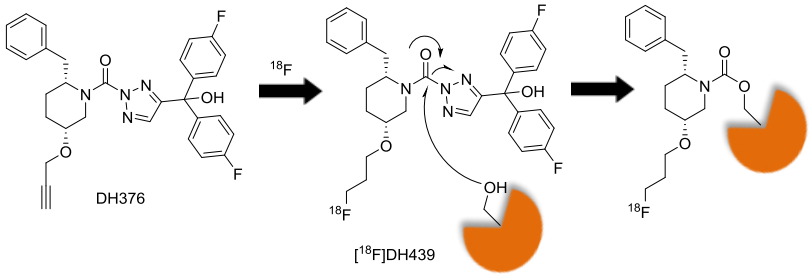

Figure 1. Design of PET radiotracer [^{18}F]DH439(2) for DAGL using the mechanism-based and irreversible *in vivo* active DAGL inhibitor DH376.

Results and Discussion

Design and profiling of DH439, a fluorinated analog of DH376

[^{18}F]DH439 was designed as a covalent DAGL PET tracer that retains the activity and selectivity profile of DH376, but will also allow the radioactive labeling of the enzyme (Figure 1). The propargyl ether of DH376 was replaced with a 3-fluoropropylether in DH439. The chemical synthesis of compound **3** (DH439) started with the chiral intermediate *tert*-butyl-(*2R,5R*)-2-benzyl-5-hydroxypiperidine-1-carboxylate **6**, which was synthesized using previously reported methods (Scheme 1).[14,15] Treatment of alcohol **6** with sodium hydride in the presence of 3-fluoropropyl 4-methylbenzenesulfonate **5**, obtained from the commercially available 3-fluoropropan-1-ol **4**, afforded ether **7**. Removal of the Boc-protecting group using 20% TFA in DCM (v/v) and subsequent triphosgene-mediated coupling with 1,2,3-triazole **9** (synthesized as described in Chapter 2) in the present of catalytic amount of DMAP provided the final compound **3** in 30% yield over the three steps.

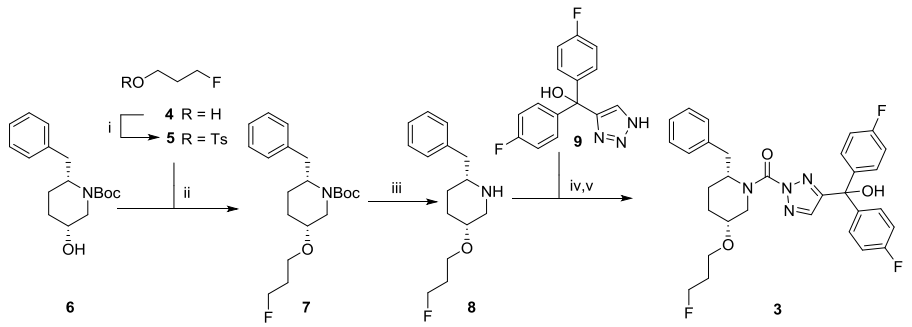

Scheme 1. Synthesis of compound **3** (DH439). Reagents and conditions: i) pTsCl, pyridine, DCM, r.t, 86%; ii) NaH, compound **5**, DMF, r.t., 19%; iii) 20% TFA, DCM, r.t.; iv) DIPEA, triphosgene, THF, 0 ^{o}C; v) DIPEA, DMAP, triazole **9**, THF, 60 ^{o}C, 30%.

Competitive activity-based protein profiling (ABPP) was employed to determine the activity and selectivity of fluorine-containing DH439 on endogenously expressed DAGL in mouse brain membrane proteome.[14] Briefly, DH439 was incubated for 20 min with mouse brain membrane homogenates, followed by two different activity-based probes (ABPs): DAGL-tailored ABP DH379 (described in Chapter 3) and broad-spectrum serine hydrolase ABP FP-TAMRA. DH379 provided target engagement assays for DAGLα and -β, and FP-TAMRA assessed selectivity over a broad array of brain serine hydrolases. DH439 potently inhibited DAGLα and DAGLβ labeling by DH379 with pIC_{50} values of 9.3±0.1 and 9.2±0.1, respectively (Figure 2). Furthermore, DH439 maintained good selectivity over other serine hydrolases with

minimal cross-reactivity against ABHD6 at high concentration (≥ 1 µM) (Figure 2a,b). In addition, DH439 showed negligible binding to cannabinoid CB_1 receptor, however, 64±14% displacement of [^{3}H]-CP55940 on the CB_2 receptor at concentrations ≥ 1 µM was observed (Figure 3).[16]

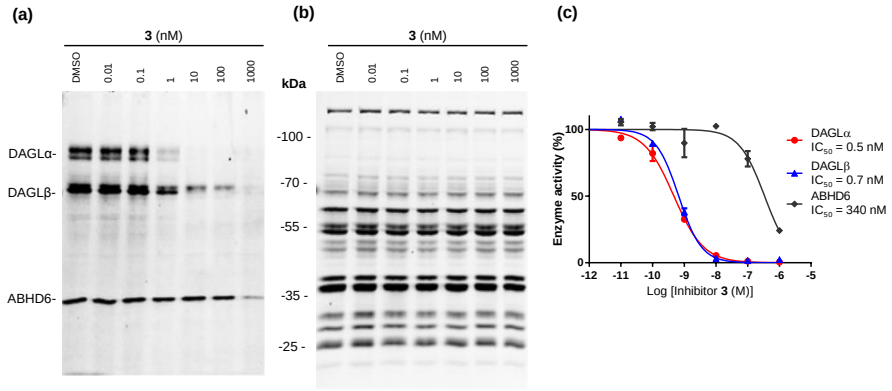

Figure 2. *In vitro* activity and selectivity profile of fluorine-containing DAGL inhibitor **3** (DH439) as measured by competitive ABPP. (a, b) Gel-based competitive ABPP of **3** using DH379 (a) and FP-TAMRA (b) as ABPs in mouse brain membrane proteome. (c) Concentration-inhibition curves for DAGLα, DAGLβ and ABHD6 as measured by competitive ABPP with ABP DH379 (1 µM). Data represent average ±SEM, n=3.

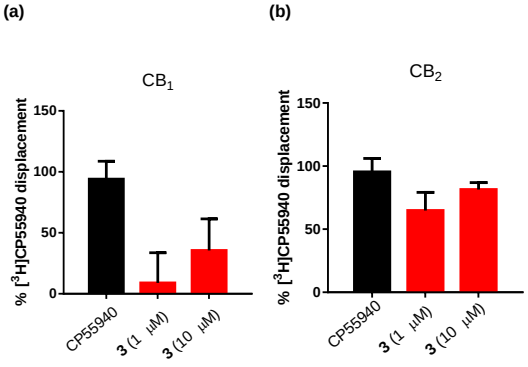

Figure 3. DAGL inhibitor **3** (DH439) shows variable interactions with CB_1 and CB_2. DH439 was tested for binding affinity to the CB_1 and CB_2 receptors using competition studies with radiolabeled CBR ligand [^{3}H]-CP55940 using membranes from recombinant human CB_1- and CB_2-overexpressing CHO cells. For CB_1, **3** was inactive at 1 µM and partial inhibition (35±25%) of ligand binding at 10 µM. For CB_2, **3** showed 64±14% and 81±5% inhibition of ligand binding at 1 µM and 10 µM, respectively. Data represent average ±SD, n=2.

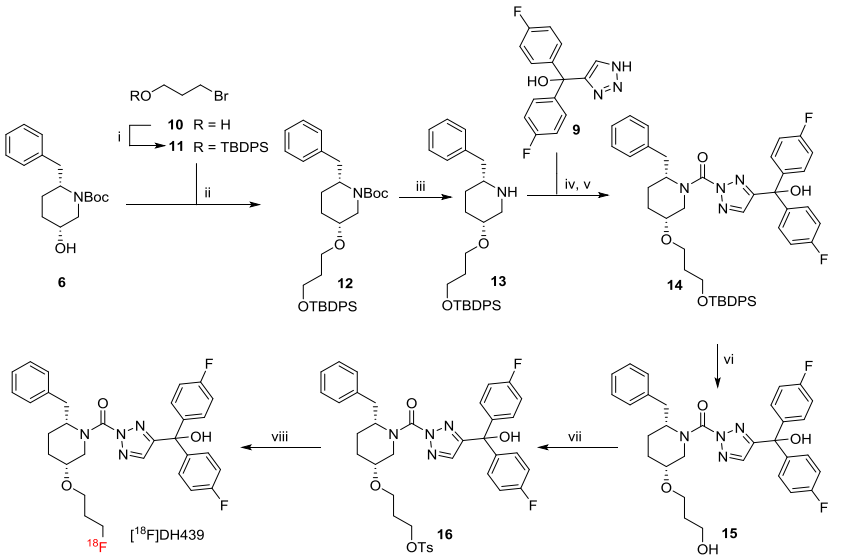

Scheme 2. Synthesis of PET radiotracer [^{18}F]DH439. Reagents and conditions: i) Imidazole, DMAP, TBDPS-Cl, DCM, r.t., 87%; ii) NaH, compound **11**, DMF, 87%; iii) 20% TFA, DCM, r.t.; iv) DIPEA, triphosgene, THF, 0 ^{o}C; v) DIPEA, DMAP, triazole **9**, THF, 60 ^{o}C; vi) HF-pyridine, THF : pyridine (1:1), 22% over 4 steps; vii) pTsCl, pyridine, DCM, r.t, 63%; viii) Micro reactor chip, K_2CO_3, TBA [^{18}F], CH_3CN, 95 min, 13-14%.

Synthesis of the fluorine-containing DAGL inhibitor and PET tracer, [^{18}F]DH439

Having established that DH439 retains a favorable activity and selectivity profile, compound **16** was prepared as an essential building block for the synthesis of [^{18}F]DH439 (Scheme 2), since it contains a tosylate required for the fluorination in the final step of the synthesis of **2** ([^{18}F]DH439). The synthesis of **16** commenced with the treatment of **6** with **11** prepared from commercially available 3-bromopropan-1-ol **10**, providing *O*-silyl protected intermediate **12**. *N*-Boc deprotection of **12** and subsequent coupling of the resulting product **13** to 1,2,3-triazole **9** furnished intermediate **14**, which was deprotected with HF-pyridine to provide alcohol **15** in 22% yield over four steps. Tosylation of **15** afforded the desired radiolabeling precursor **16** in 67% yield.

To substitute the tosylate of precursor **16** with the radiolabel (^{18}F), flow chemistry was employed by using a microreactor chip (FlowSafe - Future Chemistry). In brief, precursor **16** and [^{18}F]fluoride were transferred to a 110 µL microfluidic reactor chip and reacted in acetonitrile for 95 min. After a reversed-phase preparative HPLC purification, [^{18}F]DH439 was obtained in a radiochemical yield of 13-14% (decay corrected). The amount of activity obtained for the studies was 40-54 MBq. The

radiochemical purity of [^{18}F]DH439 as determined by analytical radio-HPLC was >98% (Figure 4).

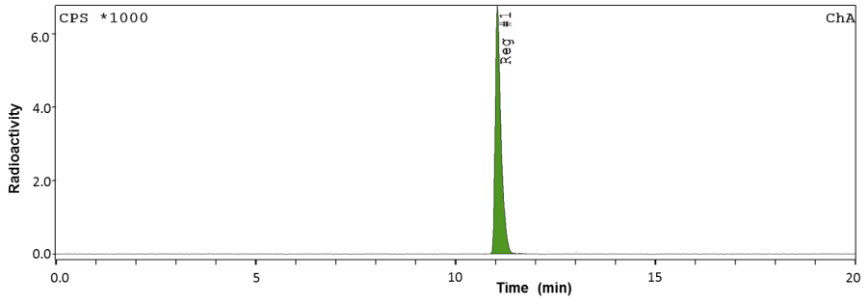

Figure 4. The radiochemical purity of [^{18}F]DH439 (**2**) was determined by analytical radio-HPLC (>98%).

In vivo biodistribution and PET imaging in a pilot mice study

Initial *in vivo* evaluation of [^{18}F]DH439 was conducted in male C57BL/6 (n = 3 per group) with intravenous injection. A bolus of 4-10 MBq [^{18}F]DH439 and DH439 (0.8 mg/kg) was injected intravenously using in saline/ethanol/tween-80 (18:1:1; v/v/v) as a vehicle. The additional injection of DH439 (0.8 mg/kg) was performed to reduce non-specific binding and metabolism of [^{18}F]DH439. Results of the biodistribution study in mice are presented in Figure 5. [^{18}F]DH439 displayed good uptake in several peripheral tissues after 140 min injection, and particularly in liver and kidney (Figure 5). Previously, DAGLα was found to be highly active in the brain (see Chapter 4), whereas DAGLβ activity was also found in heart, lung, kidney, pancreas, spleen and testis. In the PET-study only a trace amount of tracer uptake was observed in the brain. It could be that [^{18}F]DH439 has low blood-brain barrier (BBB) penetration, or, alternatively, [^{18}F]DH439 is not stable and quickly metabolized. The high amount of radioactivity in liver (Figure 5) might be an indication for the extensive metabolism of [^{18}F]DH439. Thus, it would be interesting to determine the rate of tracer metabolism by radio-metabolite analysis on blood samples and organs of interest with radio-HPLC. In addition, an important characteristic of a good PET tracer is the stability of the bond between the radionuclide and the molecule of interest. When the ^{18}F-C bond is unstable, the fluorine-18 atom could be cleaved and will accumulate in the bone. A slow accumulation of radioactivity was observed in the bone (Femur) (Figure 5), indicating some de-fluorination occurred. However, there was still sufficient amount of radioactivity in other organs, therefore de-fluorination does not seem to limit the application of the PET tracer [^{18}F]DH439 in mice.

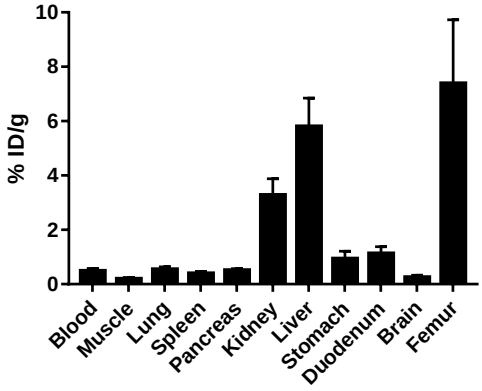

Figure 5. Bio-distribution (% ID/g) in mice (n=3; mean ± SEM) at 140 min after injection of radio tracer [^{18}F]DH439.

Next, an *in vivo* PET imaging was performed (Figure 6). This study generated comparable results to the biodistribution experiment. PET imaging showed the highest accumulation in liver and kidney. The representative dynamic PET images of [^{18}F]DH439 and time-activity curves at baseline with treatment of [^{18}F]DH439 are shown in Figure 6. [^{18}F]DH439 exhibited highly sustained binding in bladder, liver and kidney over 120 mins. PET-imaging showed that [^{18}F]DH439 accumulated slowly in the brain, which is in line with the biodistribution study. A dramatic increase in radioactivity in the kidney was also observed (Figure 6b). However, to confirm target engagement and to exclude non-specific binding of [^{18}F]DH439 further experiments are needed. For example, these experiments could include raising the dose of [^{18}F]DH439 to increase brain penetration; pretreat the mice with unlabeled DH439 to induce self-blockade, inject a specific ABHD6 inhibitor to exclude ABHD6 binding, or administer another selective DAGL inhibitor to confirm DAGL binding. Considering the low tracer uptake in the brain, further radiotracer optimization may also be required to improve brain penetration and *in vivo* stability.

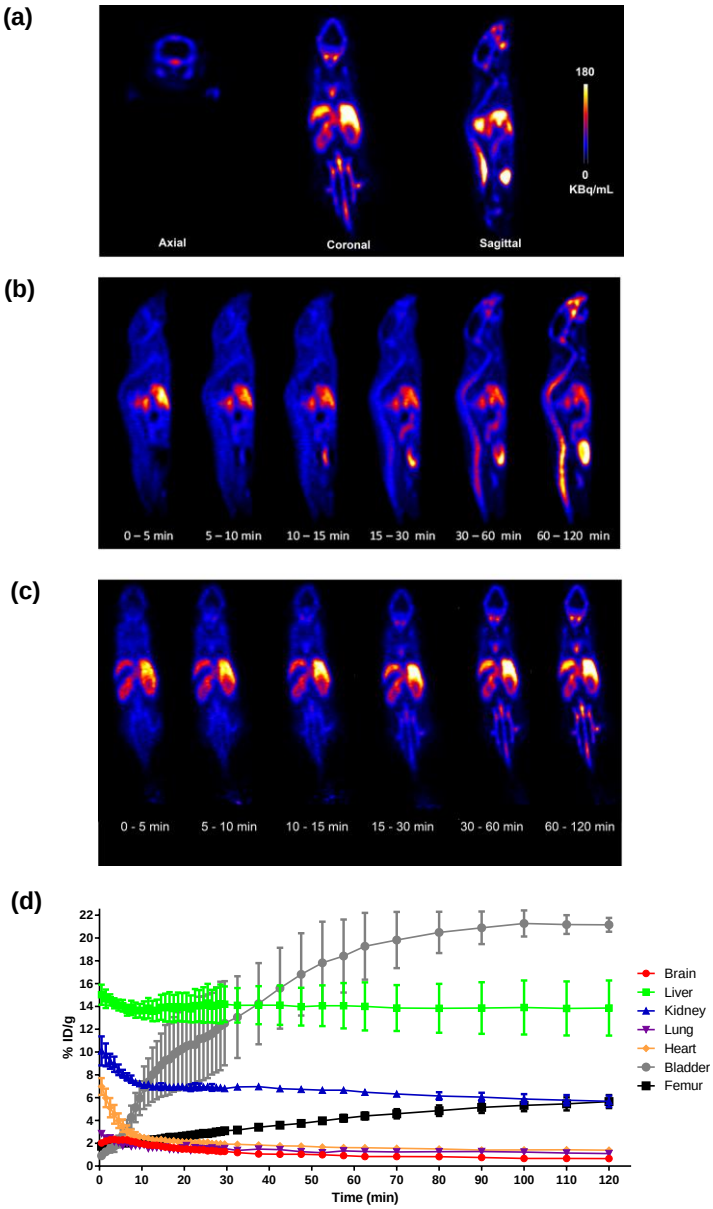

Figure 6. (a) Representative 2D reconstructed PET Images (0-120 min; axial, coronal and sagittal sections). (b-c) Representative 2D reconstructed dynamic PET images of [^{18}F]DH439-treated mice at various time frames (b for sagittal sections and c for coronal sections). (d) Time-activity curves from [^{18}F]DH439 at baseline in mice (n=3; mean ± SEM).

Conclusion

In summary, the first selective DAGL PET tracer [^{18}F]DH439 was designed and synthesized. As assessed by competitive ABPP and radioligand displacement assays, DH439 showed high potency and selectivity against DAGLs, but some minor affinity towards the cannabinoid CB_2 receptor was also identified. Biodistribution experiments of [^{18}F]DH439 in mice revealed low tracer uptake in the brain and high uptake in peripheral tissues such as liver and kidney. *In vivo* mouse PET imaging studies mirrored those of the biodistribution studies. Although this work was a pilot study, it demonstrated the feasibility of generating PET tracers from 1,2,3-triazole urea inhibitors for preclinical studies. These studies may pave the way for the development of clinical PET tracers of DAGL to study biodistribution and target engagement of DAGLs in humans and to guide dose selection for human clinical trials. An improvement in metabolic stability and brain penetration is required to obtain a suitable PET tracer to study target engagement of DAGL inhibitors in the brain.

Experimental section

Chemistry

General materials

All chemicals were obtained from commercial suppliers and were used without further purification. TLC analysis with Merck silica gel TLC plates (0.25 mm, 60/Kieselguhr F254) was used to monitor reactions. Flash chromatography was performed using SiliaFlash F60 silica gel (40–63 µm, 60 Å). NMR spectra were recorded at room temperature on Bruker AV 400 MHz spectrometer at 400 (^{1}H) and 101 (^{13}C) MHz using $CDCl_3$ as solvent. Chemical shifts are recorded in ppm relative to tetramethylsilane (TMS) with peaks being reported as follows: chemical shift, multiplicity (s = singlet, br = broad, d = doublet, t = triplet, q = quartet, m = multiplet), coupling constant (Hz). High-resolution mass spectra (HRMS) were recorded by direct injection (2 µL of a 2 µM solution in water/acetonitrile 50/50 (v/v) and 0.1% formic acid) on a mass spectrometer (Thermo Finnigan LTQ orbitrap) equipped with an electrospray ion source in positive mode (source voltage 3.5 kV, sheath gas flow 10, capillary temperature 250 ^{o}C) with resolution R = 60,000 at m/z 400 (mass range m/z = 150-2,000) and dioctylphthalate (m/z = 391.28428) as a “lock mass”. The high resolution mass spectrometer was calibrated prior to measurements with a calibration mixture (Thermo Finnigan). LC-MS analysis was performed on a Finnigan Surveyor HPLC system with a Gemmi C_{18} 50x4.60 mm column (detection at 200-600 nm), coupled to a Finnigan LCQ Adantage Max mass spectrometer with ESI. The applied buffers were H_2O, MeCN and 1.0% TFA in H_2O (0.1% TFA end concentration). Optical

rotations were measured on a Propol automatic polarimeter (Sodium D-line, λ = 589 nm).

Radiolabeling

Radiochemistry was performed using a flow reaction on a reactor chip in Future Chemistry's FlowSafe. [^{18}F]fluoride in acetonitrile was purchased from commercial sources. A reversed phase preparation HPLC method was setup to isolate [^{18}F]DH439 and a SPE procedure was applied to remove the acetonitrile from the pooled HPLC peak and to reformulate [^{18}F]DH439 in 80:10:10 NaCl (0.9%)/ethanol/Tween-80 (v/v/v). The identity of the labeled compound was confirmed by co-injection of the authentic on HPLC. The specific activity was determined by injection of an aliquot of the final solution with known radioactivity on the analytical HPLC system described above. The area of the UV peak measured at 254 nm corresponding to the carrier product was measured and compared to a standard curve relating mass to UV absorbance. Radioactivity was measured with a Capintec CRC-15 PET dose calibrator.

Synthesis

((*2R,5R*)-2-Benzyl-5-(3-fluoropropoxy)piperidin-1-yl)(4-(bis(4-fluorophenyl)(hydroxy)methyl)-*2H*-1,2,3-triazol-2-yl)methanone (3). A solution of compound **8** in THF was treated with DIPEA (0.38 mL, 2.19 mmol) and bis(trichloromethyl) carbonate (65.0 mg, 0.22 mmol). The reaction mixture was stirred for 30 min at 0 ^{o}C, then the mixture was poured into water and extracted with EtOAc (3 x 50 mL).The organic layer was washed with water, brine, dried over $MgSO_4$, filtered and concentrated under reduced pressure. The intermediate was dissolved in THF and DIPEA (0.38 mL, 2.19 mmol), DMAP (54 mg, 0.44 mmol) and compound **9** (126 mg, 0.438 mmol) were added to the solution. The mixture was stirred for 2 h at 60 ^{o}C and poured into saturated aqueous NH_4Cl solution. The mixture was extracted with EtOAc, washed with water, brine, dried over $MgSO_4$, filtered and concentrated under reduced pressure. The residue was purified by silica gel column chromatography with acetone/pentane (1%→10%) to yield the target compound DH439 (**3**) (74 mg, 0.13 mmol, 30% yield). HRMS calculated for $[C_{31}H_{32}F_3N_4O_3]^+$: 565.24210; found: 565.24218; ^{1}H NMR (400 MHz, $CDCl_3$) δ 7.52 (br, 1H), 7.34 – 7.24 (m, 6H), 7.18 (br, 2H), 7.05 – 7.00 (m, 4H), 6.89 (br, 1H), 4.79 – 4.24 (m, 4H), 3.71 (br, 1H), 3.53 – 3.43 (m, 2H), 3.16 – 2.85 (m, 3H), 2.10 – 1.84 (m, 3H), 1.77 – 1.62 (m, 3H); ^{13}C NMR (101 MHz, $CDCl_3$) δ 162.48 (d, *J* = 252.9 Hz), 157.74, 149.03, 140.71 (d, *J* = 3.0 Hz), 137.64, 135.32, 129.17 (d, *J* = 7.1 Hz), 129.05, 128.84, 126.95, 115.34 (d, *J* = 22.2 Hz), 81.02 (d, *J* = 170.7 Hz), 77.16, 76.60, 74.28, 64.36, 56.61, 44.47, 35.62, 31.14 (d, *J* = 20.2 Hz), 26.03, 25.97.

3-Fluoropropyl 4-methylbenzenesulfonate (5). To a solution of pyridine (0.725 mL, 8.96 mmol) in dry DCM was added 3-fluoropropan-1-ol (0.337 mL, 4.48 mmol) and *p*-toluenesulfonyl chloride (1.03 g, 5.38 mmol) at 0 °C. The reaction mixture was stirred for 24 h at r.t. The mixture was diluted with water and extracted with DCM. The organic layer was washed with brine, dried over $MgSO_4$, filtered and evaporated under

reduced pressure. The residue was purified by silica gel column chromatography with diethyl ether/pentane (1%→10%) to yield 3-fluoropropyl 4- methylbenzenesulfonate **5** (895 mg, 3.85 mmol, 86% yield). LC/MS calculated for $[C_{10}H_{13}FO_3S]^+$: 232.27; found: 233.02; ^{1}H NMR (400 MHz, $CDCl_3$) δ 7.79 (d, *J* = 8.3 Hz, 2H), 7.36 (d, *J* = 8.2 Hz, 2H), 4.54 (t, *J* = 5.7 Hz, 1H), 4.42 (t, *J* = 5.7 Hz, 1H), 4.15 (t, *J* = 6.2 Hz, 2H), 2.45 (s, 3H), 2.07 (p, *J* = 5.9 Hz, 1H), 2.00 (p, *J* = 5.9 Hz, 1H). ^{13}C NMR (101 MHz, $CDCl_3$) δ 145.06, 132.73, 129.98, 128.00, 79.58 (d, *J* = 166.7 Hz), 66.28, 30.00 (d, *J* = 20.2 Hz) 21.67.

***tert*-Butyl (*2R,5R*)-2-benzyl-5-(3-fluoropropoxy)piperidine-1-carboxylate (7).** To a solution of compound 6 (228 mg, 0.783 mmol) and NaH (78 mg, 1.96 mmol) in DMF (10 mL) at 0 ^{o}C, 3-fluoropropyl 4-methylbenzenesulfonate (200 mg, 0.86 mmol) was added dropwise with continuous stirring, and the mixture was allowed to stand at r.t. for 24 h. The mixture was diluted with water (50 mL), and extracted with EtOAc (80 mL x 3). The organic layers were washed with water, brine, dried over $MgSO_4$, filtered and concentrated under reduced pressure. The residue was then purified by silica gel column chromatography with diethyl ether/pentane (1%→20%) to yield *tert*-butyl (*2R,5R*)-2-benzyl-5-(3-fluoropropoxy)piperidine-1-carboxylate (53.0 mg, 0.151 mmol, 19% yield). LC/MS calculated for $[C_{20}H_{30}FNO_3]^+$: 351.46; found: 351.98; ^{1}H NMR (400 MHz, $CDCl_3$) δ 7.30 – 7.24 (m, 2H), 7.24 – 7.12 (m, 3H), 4.61 (t, *J* = 5.9 Hz, 1H), 4.49 (t, *J* = 5.9 Hz, 1H), 4.44 – 4.29 (m, 1H), 3.68 – 3.60 (m, 2H), 3.26 (br, 1H), 2.96 – 2.85 (m, 1H), 2.76 – 2.63 (m, 2H), 2.02 – 1.89 (m, 3H), 1.59 (d, *J* = 9.2 Hz, 3H), 1.27 (s, 9H); ^{13}C NMR (101 MHz, $CDCl_3$) δ 154.87, 139.14, 129.27, 128.52, 126.34, 81.15 (d, *J* = 164.6 Hz), 79.69, 74.83, 64.28, 52.21, 42.47, 35.97, 31.24 (d, *J* = 20.2 Hz), 28.28, 26.32, 26.10.

(*2R,5R*)-2-Benzyl-5-(3-fluoropropoxy)piperidine (8). To a solution of *tert*-butyl (*2R,5R*)-2- benzyl-5-(3-fluoropropoxy)piperidine-1-carboxylate **7** (351 mg, 0.597 mmol) in DCM was added TFA (20%, v/v), the reaction mixture was stirred at r.t. for 2.5 h until TLC showed the reaction was completed. The mixture was co-evaporated with toluene (3 x 20 mL), the residue was diluted with EtOAc and washed with 10% Na_2CO_3, water, brine, dried over $MgSO_4$, filtered and then concentrated under reduced pressure. The crude product was used for next step without further purification. ^{1}H NMR (400 MHz, $CDCl_3$) δ 7.31 – 7.22 (m, 3H), 7.17 (d, *J* = 7.0 Hz, 2H), 4.58 (t, *J* = 4.7 Hz, 1H), 4.47 (t, *J* = 4.6 Hz, 1H), 3.69 (s, 1H), 3.55 (q, *J* = 6.0 Hz, 2H), 3.45 (d, *J* = 12.2 Hz, 1H), 3.28 (s, 1H), 3.14 (d, *J* = 13.2 Hz, 1H), 3.05 (s, 1H), 2.89 – 2.79 (m, 1H), 2.06 (d, *J* = 12.8 Hz, 1H), 2.00 – 1.93 (m, 1H), 1.93 – 1.88 (m, 1H), 1.83 (d, *J* = 13.5 Hz, 1H), 1.64 (d, *J* = 13.1 Hz, 1H), 1.50 (d, *J* = 13.1 Hz, 1H). ^{13}C NMR (101 MHz, $CDCl_3$) δ 135.11, 129.48, 128.98, 127.46, 80.97 (d, *J* = 163.6 Hz), 69.04, 64.39, 58.19, 47.59, 39.60, 30.62 (d, *J* = 20.2 Hz), 26.07, 22.79.

(3-Bromopropoxy)(*tert*-butyl)diphenylsilane (11). *tert*-Butyl(chloro)diphenylsilane (4.62 mL, 18.0 mmol), DMAP (0.611 g, 5.0 mmol) and imidazole (1.40 g, 20.0 mmol) were added to a stirred solution of 3-bromopropan-1-ol (0.91 mL, 10.0 mmol) in DCM with ice cooling, and then stirred at r.t. for 2 h. The resulting mixture was quenched

with water, and extracted with EtOAc (3 x 80 mL). The combined organic layers were washed with water, brine, dried over $MgSO_4$, filtered and concentrated under reduced pressure. The residue was purified by silica gel column chromatography with diethyl ether/pentane (1%→10%) to yield compound **11** (3.28 g, 8.70 mmol, 87% yield). LC/MS calculated for $[C_{19}H_{25}BrOSi]^+$: 377.40; found: 378.12; ^{1}H NMR (400 MHz, $CDCl_3$) δ 7.76 – 7.57 (m, 4H), 7.52 – 7.25 (m, 6H), 3.77 (t, *J* = 5.7 Hz, 2H), 3.57 (t, *J* = 6.6 Hz, 2H), 2.08 – 2.03 (m, 2H), 1.06 (s, 9H). ^{13}C NMR (101 MHz, $CDCl_3$) δ 135.20, 134.95, 129.67, 127.76, 26.67, 19.06.

***tert*-Butyl (*2R,5R*)-2-benzyl-5-(3-((*tert*-butyldiphenylsilyl)oxy)propoxy)piperidine-1-carboxylate (12).** To a solution of compound **6** (200 mg, 0.69 mmol) and NaH (82.0 mg, 2.06 mmol) in DMF (4 mL) at 0 ^{o}C, compound **11** (777 mg, 2.06 mmol) was added dropwise under continuous stirring, and the mixture was allowed to stand at r.t. for 24 h. The mixture was diluted with water (20 mL), the residue of a product filtered off, washed with water, brine, dried over $MgSO_4$, filtered and concentrated under reduced pressure. The residue was purified by silica gel column chromatography with diethyl ether/pentane (1%→10%) to yield compound **12** (351 mg, 0.60 mmol, 87% yield). LC/MS calculated for $[C_{36}H_{49}NO_4Si]^+$: 587.88; found: 588.20; ^{1}H NMR (400 MHz, $CDCl_3$) δ 7.80 – 7.73 (m, 5H), 7.49 – 7.38 (m, 6H), 7.34 – 7.30 (m, 2H), 7.24 – 7.20 (m, 2H), 4.54 – 4.21 (m, 2H), 3.83 (t, *J* = 5.8 Hz, 2H), 3.79 – 3.64 (m, 2H), 3.29 (br, 1H), 3.05 – 2.91 (m, 1H), 2.73 – 2.69 (m, 2H), 2.02 – 1.76 (m, 3H), 1.62 (d, *J* = 10.0 Hz, 3H), 1.44 (s, 3H), 1.34 (s, 6H), 1.12 (s, 9H). ^{13}C NMR (101 MHz, $CDCl_3$) δ 154.79, 139.17, 135.62, 134.91, 133.97, 133.93, 129.64, 129.57, 129.25, 128.49, 127.71, 127.70, 126.29, 79.59, 74.54, 65.38, 60.69, 52.28, 42.53, 36.00, 33.18, 26.95, 26.67, 26.34, 26.12, 19.31.

((*2R,5R*)-2-Benzyl-5-(3-hydroxypropoxy)piperidin-1-yl)(4-(bis(4-fluorophenyl)(hydroxy)methyl)-2*H*-1,2,3-triazol-2-yl)methanone (15). To a solution of compound **12** (351 mg, 0.597 mmol) in DCM was added TFA (20%, v/v), the reaction mixture was stirred at room temperature for 2.5 h until TLC analysis showed that the reaction was completed. The mixture was co-evaporated with toluene (3 x 20 mL), the residue was diluted with EtOAc and washed with 10% Na_2CO_3, water, brine, dried over $MgSO_4$, filtered and then concentrated under reduced pressure. The crude product was used for next step without further purification. A solution of the crude product **13** in THF was treated with DIPEA (0.524 mL, 3.0 mmol) and bis(trichloromethyl) carbonate (89.0 mg, 0.30 mmol) and the reaction mixture was stirred for 30 min at 0 ^{o}C. The mixture was poured into water and extracted with EtOAc (40 mL x 3). The organic layer was washed with water, brine dried over $MgSO_4$, filtered and concentrated under reduced pressure. The intermediate was dissolved in THF and DIPEA (0.31 mL, 1.80 mmol), DMAP (74.0 mg, 0.60 mmol) and triazole **9** (172 mg, 0.60 mmol) were added to the solution. The mixture was stirred for 2 h at 60^{o}C and poured into saturated aqueous NH_4Cl solution and extracted with EtOAc, washed with water, brine, dried over $MgSO_4$, and concentrated under reduced pressure. The N2-carbamoyl triazole urea **14** was isolated by silica gel chromatography EtOAc/pentane (1%→10%). HF-pyridine (0.60 mL, 6.50 mmol) was subsequently added to a solution of N2-carbamoyl triazole urea in THF and pyridine (1:1; 2 mL) with ice cooling, and the reaction mixture was

stirred over night at r.t. The mixture was diluted with EtOAc (40 mL), and then washed with $NaHCO_3$, brine, dried with $MgSO_4$, and concentrated under reduced pressure. The residue was purified by silica gel column chromatography with EtOAc /pentane (1%→40%) to yield the title compound **15** (73 mg, 0.13 mmol, 22% yield) as a colorless oil. LC/MS calculated for $[C_{31}H_{32}F_2N_4O_4]^+$: 562.62; found: 567.13; ^{1}H NMR (400 MHz, $CDCl_3$) δ 7.52 (s, 1H), 7.41 – 7.15 (m, 8H), 7.07 – 6.84 (m, 5H), 4.54 (br, 1H), 4.31 (br, 1H), 3.80 – 3.58 (m, 4H), 3.50 – 3.44 (m, 1H), 3.17 – 2.86 (m, 3H), 2.04 (d, *J* = 7.9 Hz, 1H), 1.85 – 1.59 (m, 5H). ^{13}C NMR (101 MHz, $CDCl_3$) δ 162.36 (d, *J* = 252.5 Hz), 155.71, 149.27, 140.84 (d, *J* = 5.1 Hz), 137.57, 135.44, 129.13 (d, *J* = 9.1 Hz), 128.78, 126.89, 124.28, 115.20 (d, *J* = 22.4 Hz), 76.37, 74.41, 67.61, 61.39, 55.69, 46.06, 35.80, 32.22, 25.96, 25.06.

3-(((*3R,6R*)-6-Benzyl-1-(4-(bis(4-fluorophenyl)(hydroxy)methyl)-2*H*-1,2,3-triazole-2-carbonyl)piperidin-3-yl)oxy)propyl 4-methylbenzenesulfonate (16). To a solution of compound **15** (60.0 mg, 0.11 mmol) and pyridine (0.03 mL, 0.32 mmol) in dry DCM was added pTsCl (61.0 mg, 0.32 mmol) at 0 °C. The reaction mixture was stirred for 24 h at r.t. The mixture was quenched with water and extracted with DCM. The organic layer was washed with brine, dried over $MgSO_4$, filtered and co-evaporated under reduced pressure. The residue was purified by silica gel column chromatography EtOAc/pentane (1%→20%) to yield the title compound **16** (50 mg, 0.069 mmol, 63% yield). LC/MS calculated for $[C_{38}H_{38}F_2N_4O_6S]^+$: 716.80; found: 717.03; ^{1}H NMR (400 MHz, $CDCl_3$,, 60 °C) δ 7.76 (d, *J* = 7.9 Hz, 2H), 7.54 (s, 1H), 7.36 – 7.26 (m, 6H), 7.26 – 7.16 (m, 4H), 6.98 (t, *J* = 8.3 Hz, 5H), 4.48 (s, 1H), 4.13 (t, *J* = 4.0 Hz, 2H), 3.49 (br, 2H), 3.40 – 3.35 (m, 2H), 3.05 (dd, *J* = 13.4, 6.4 Hz, 1H), 2.90 (t, *J* = 12.0 Hz, 2H), 2.42 (s, 3H), 1.89 (d, *J* = 26.6 Hz, 3H), 1.65 (br, 3H); ^{13}C NMR (101 MHz, $CDCl_3$, 60 °C) δ 162.55 (d, *J* = 248.5 Hz), 155.74, 149.41, 144.87, 140.98 (d, *J* = 5.1 Hz), 137.76, 135.26, 133.72, 129.98, 129.20 (d, *J* = 8.1 Hz), 128.83, 128.01, 126.93, 115.26 (d, *J* = 21.2 Hz), 76.69, 74.39, 67.45, 64.29, 55.18, 45.62, 36.11, 29.71, 26.07, 25.14, 21.66.

Biological assays

Fluorophosphonate-TAMRA (FP-TAMRA), and DH379 were synthesized according to a previously described protocol.[17-21] FP-TAMRA is also commercially available at Thermo Fischer Scientific.

Preparation of tissue proteomes

Mouse tissues were dounce homogenized in lysis buffer (20 mM HEPES, 250 mM sucrose, 2 mM DTT, 1 mM $MgCl_2$ with or without 25 U/mL benzonase) and incubated in ice for 5 min, followed by a low-speed spin (1,400−2,500 x g, 3 min, 4 °C) to remove debris. The membrane and cytosolic fractions were separated by ultracentrifugation (100,000 x g, 45 min, 4 °C) of the resulting homogenate lysate. After removal of the soluble supernatant, the membrane pellet was washed 1x with cold HEPES buffer (20 mM, with or without 2 mM DTT) followed by resuspension in cold HEPES buffer (20

mM, with or without 2 mM DTT) by pipetting. Total protein concentrations in membrane and soluble fractions were determined using the Bio-Rad DC protein assay kit. Samples were stored at -80 °C until further use.

Tissue profiling by gel-based competitive ABPP

Gel-based ABPP assays were performed as previously described (Chapter 3). Cell or tissue proteomes were treated with either FP-TAMRA (1 µM or 500 nM final concentration), DH379 (1 µM final concentration). For DH379 labeled samples, 2 mg/mL of proteome was used to enhance endogenous DAGL signals; 1 mg/mL proteome was used for labeling with FP-TAMRA. Probe labeling was carried out for 30 min at r.t. followed by addition of 4X SDS-PAGE loading buffer to quench the reaction. After separation by SDS-PAGE (10% acrylamide), samples were visualized by in-gel fluorescence scanning using a ChemiDoc MP system.

ABPP inhibitor activity measurements

The percentage of activity remaining was determined by measuring the integrated optical intensity of the fluorescent protein bands using image lab 4.1. The relative intensity was compared to the vehicle treated proteins, which were set to 100%. IC_{50} and IC_{80} values were determined by plotting a log(inhibitor) vs. normalized response (Variable slope) dose-response curve generated using Prism software (GraphPad).

Radioligand binding assay

Materials: [^{3}H]CP55940 (specific activity 141.2 Ci/mmol) and GF-C filters were purchased from Perkin Elmer (Waltham, MA). Bicinchoninic acid (BCA) and BCA protein assay reagent were obtained from Pierce Chemical Company (Rochford, IL). The PathHunter® CHO-K1 CNR1 β-Arrestin Cell Line (catalog number 93-0959C2) and the PathHunter® CHO-K1 CNR2 β-Arrestin Cell Line (catalog number 93-0706C2), stably expressing the hCB_1 receptor ($CHOK1hCB_1$_bgal) or hCB_2 receptor ($CHOK1hCB_2$_bgal) respectively, was obtained from DiscoveRx.

Cell culture and membrane preparation: $CHOK1hCB_1$_bgal and $CHOK1hCB_2$_bgal cells were cultured in Ham's F12 Nutrient Mixture supplemented with 10% fetal calf serum, 1 mM glutamine, 50 µg/mL penicillin, 50 µg/mL streptomycin, 300 mg/mL hygromycin and 800 µg/mL geneticin in a humidified atmosphere at 37 °C and 5% CO_2. Cells were subcultured twice a week at a ratio of 1:20 on 10-cm diameter plates by trypsinization. For membrane preparation the cells were subcultured 1:10 and transferred to large 15-cm diameter plates. Membrane fractions were prepared exactly as described before.[22]

[^{3}H]CP55940 radioligand binding assay: [^{3}H]CP55940 binding assays to determine the cannabinoid CB_1 and CB_2 receptor binding affinity were performed as follows: ligands of interest were incubated at 30°C for 1h with membrane aliquots containing 5 µg $CHOK1hCB_1$_bgal membrane protein or 1 µg ($CHOK1hCB_2$_bgal) in 100 µL assay

buffer (50 mM Tris–HCl, 5 mM $MgCl_2$, 0.1% BSA, pH 7.4) with [^{3}H]CP55940 in a concentration of ~1.5 nM (CB_2 receptor) or ~3.5 nM (CB_1 receptor) per assay point. Non-specific binding was determined in the presence of 10 µM Rimonabant (CB_1 receptor) or 10 µM AM630 (CB_2 receptor). Filtration was performed on GF/C filters, presoaked for 30 min with 0.25% polyethylenimine, using a Brandel harvester. Filter-bound radioactivity was determined in a β-counter. The mean % of specific binding for CB_1 and CB_2 receptors were 36 ± 4% and 38 ± 42% for 6-12 experiments.

PET imaging study and Biodistribution studies in mice

Mice (C75Bl/6J, male, 32.0±0.4 gram) were used for the animal experiments. A cannula was inserted into the lateral tail vein and anesthesia was induced using 2% isoflurane. The mice were placed prone in an Inveon animal PET/CT scanner (Siemens Preclinical Solutions). Anesthesia was maintained using 1.5% isoflurane via a nose cone and their body temperature was maintained at 35 °C using a heating bed. A bolus of 4-10 MBq [^{18}F]DH439 and 25.6 µg of DH439 in 200 µL saline/ethanol/Tween-80 (18:1:1; v/v/v) was injected intravenously via the cannula. The additional 25.6 µg of DH439 was added to adjust the dose to 0.8 mg/kg. A 125 minute dynamic emission PET scan was acquired. For attenuation correction followed by a 10 minute transmission scan using the built-in 57Co source. The mice were euthanized by CO_2/O_2 asphyxiation directly after the transmission scan. Mouse was subsequently placed in the CT scanner of the Inveon PET/CT (spatial resolution, 110 µm; 80 kV, 500 µA; spatial resolution of PET is 1.5 mm) to obtain a CT scan for anatomic reference. Of all mice, tissues of interest (blood, muscle, lung, spleen, pancreas, kidney, liver, stomach, duodenum, brain and femur) were dissected, weighed and counted in a γ-counter. The percentage injected dose per gram of tissue (%ID/g) was calculated for each tissue on the basis of a dilution of the product for injection ([^{18}F]DH439).

PET images were reconstructed using Inveon Acquisition Workplace software using 3D-OSEM in the following frames: 30 x 60s , 7 x 300s and 6 x 600s. The images were analyzed using Siemens Inveon Research Workplace software. Regions of interest (ROIs) were manually drawn over the organs of interest (brain, liver, kidney, lung, heart, bladder, and femur). Quantification of [^{18}F]DH439 uptake in the ROIs of the attenuation-corrected slices was obtained by calculating the injected dose per gram of wet tissue (%ID/g).

References

1. Pacher, P.; Kunos, G. Modulating the endocannabinoid system in human health and disease successes and failures. *FEBS Journal* **2013,** 280, 1918-1943.
2. Pertwee, R. G. The pharmacology of cannabinoid receptors and their ligands: an overview. *International Journal of Obesity* **2006,** 30, S13-S18.
3. Katona, I.; Freund, T. F. Multiple functions of endocannabinoid signaling in the brain. *Annual Review of Neuroscience, 35* **2012,** 35, 529-558.
4. Janero, D. R.; Makriyannis, A. Cannabinoid receptor antagonists: pharmacological opportunities, clinical experience, and translational prognosis. *Expert Opinion on Emerging Drugs* **2009,** 14, 43-65.
5. Kirilly, E.; Gonda, X.; Bagdy, G. CB1 receptor antagonists: new discoveries leading to new perspectives. *Acta Physiologica* **2012,** 205, 41-60.
6. Blankman, J. L.; Cravatt, B. F. Chemical Probes of Endocannabinoid Metabolism. *Pharmacological Reviews* **2013,** 65, 849-871.
7. McKinney, M. K.; Cravatt, B. F. Structure and function of fatty acid amide hydrolase. *Annual Review of Biochemistry* **2005,** 74, 411-432.
8. Ahn, K.; McKinney, M. K.; Cravatt, B. F. Enzymatic pathways that regulate endocannabinoid signaling in the nervous system. *Chemical Reviews* **2008,** 108, 1687-1707.
9. Long, J. Z.; Cravatt, B. F. The Metabolic Serine Hydrolases and Their Functions in Mammalian Physiology and Disease. *Chemical Reviews* **2011,** 111, 6022-6063.
10. Hicks, J. W.; Parkes, J.; Tong, J.; Houle, S.; Vasdev, N.; Wilson, A. A. Radiosynthesis and ex vivo evaluation of [(11)C-carbonyl]carbamate- and urea-based monoacylglycerol lipase inhibitors. *Nuclear Medicine Biology* **2014,** 41, 688-94.
11. Cherry, S. R. Fundamentals of positron emission tomography and applications in preclinical drug development. *The Jouranl of Clinical Pharmacology* **2001,** 41, 482-491.
12. Patel, S.; Gibson, R. In vivo site-directed radiotracers: a mini-review. *Nuclear Medicine and Biology* **2008,** 35, 805-815.
13. Phelps, M. E. Positron emission tomography provides molecular imaging of biological processes. *Proceedings of the National Academy of Sciences of the United States of America* **2000,** 97, 9226-9233.
14. Ogasawara, D.; Deng, H.; Viader, A.; Baggelaar, M. P.; Breman, A.; den Dulk, H.; van den Nieuwendijk, A. M.; Soethoudt, M.; van der Wel, T.; Zhou, J.; Overkleeft, H. S.; Sanchez-Alavez, M.; Mo, S.; Nguyen, W.; Conti, B.; Liu, X.; Chen, Y.; Liu, Q. S.; Cravatt, B. F.; van der Stelt, M. Rapid and profound rewiring of brain lipid signaling networks by acute diacylglycerol lipase inhibition. *Proceedings of the National Academy of Sciences of the United States of America* **2016,** 113, 26-33.
15. van den Nieuwendijk, A. M.; Ruben, M.; Engelsma, S. E.; Risseeuw, M. D.; van den Berg, R. J.; Boot, R. G.; Aerts, J. M.; Brussee, J.; van der Marel, G. A.; Overkleeft, H. S. Synthesis of L-altro-1-deoxynojirimycin, D-allo-1-deoxynojirimycin, and D-galacto-1-deoxynojirimycin from a single chiral cyanohydrin. *Organic letters* **2010,** 12, 3957-3959.
16. Zweemer, A. J. M.; Nederpelt, I.; Vrieling, H.; Hafith, S.; Doornbos, M. L. J.; de Vries, H.; Abt, J.; Gross, R.; Stamos, D.; Saunders, J.; Smit, M. J.; IJzerman, A. P.; Heitman, L. H.

Multiple binding sites for small-molecule antagonists at the CC chemokine receptor 2. *Molecular Pharmacology* **2013,** 84, 551-561.

17. Liu, Y.; Patricelli, M. P.; Cravatt, B. F. Activity-based protein profiling: the serine hydrolases. *Proceedings of the National Academy of Sciences of the United States of America* **1999,** 96, 14694-14699.
18. Kidd, D.; Liu, Y.; Cravatt, B. F. Profiling serine hydrolase activities in complex proteomes. *Biochemistry* **2001,** 40, 4005-4015.
19. Patricelli, M. P.; Giang, D. K.; Stamp, L. M.; Burbaum, J. J. Direct visualization of serine hydrolase activities in complex proteomes using fluorescent active site-directed probes. *Proteomics* **2001,** 1, 1067-1071.
20. Hsu, K.-L. L.; Tsuboi, K.; Adibekian, A.; Pugh, H.; Masuda, K.; Cravatt, B. F. DAGLβ inhibition perturbs a lipid network involved in macrophage inflammatory responses. *Nature Chemical Biology* **2012,** 8, 999-1007.
21. Baggelaar, M. P.; Janssen, F. J.; van Esbroeck, A. C.; den Dulk, H.; Allarà, M.; Hoogendoorn, S.; McGuire, R.; Florea, B. I.; Meeuwenoord, N.; van den Elst, H.; van der Marel, G. A.; Brouwer, J.; Di Marzo, V.; Overkleeft, H. S.; van der Stelt, M. Development of an activity-based probe and in silico design reveal highly selective inhibitors for diacylglycerol lipase-α in brain. *Angewandte Chemie International Edition* **2013,** 52, 12081-12085.
22. Zweemer, A. J.; Nederpelt, I.; Vrieling, H.; Hafith, S.; Doornbos, M. L.; de Vries, H.; Abt, J.; Gross, R.; Stamos, D.; Saunders, J.; Smit, M. J.; Ijzerman, A. P.; Heitman, L. H. Multiple binding sites for small-molecule antagonists at the CC chemokine receptor 2. *Molecular pharmacology* **2013,** 84, 551-561.

6

Chiral disubstituted piperidinyl ureas: a class of dual diacylglycerol lipase-α and ABHD6 inhibitors

Based on
Hui Deng, Tom van der Wel, Richard J. B. H. N. van den Berg, Adrianus M.C.H. van den Nieuwendijk, Freek J. Janssen, Marc P. Baggelaar, Hermen S. Overkleeft , Mario van der Stelt;
manuscript submitted

Introduction

Diacylglycerol lipase α and diacylglycerol lipase β (DAGLα and DAGLβ) are intracellular, multi-domain, transmembrane serine hydrolases that employ a Ser-His-Asp catalytic triad to specifically hydrolyse arachidonate-containing diglycerides to form the endocannabinoid 2-arachidonoylglycerol (2-AG) in the brain and peripheral tissues.[1,2] Endocannabinoid signalling is involved in various neurophysiological functions, such as learning, memory, pain sensation, adult neurogenesis and regulation of the energy balance.[3-5] 2-AG is hydrolysed by monoacylglycerol lipase into arachidonic acid, which is a precursor for pro-inflammatory prostaglandins.[6-8] Consequently, the development of DAGL inhibitors that perturb 2-AG production is an emerging strategy for potential therapeutic intervention in various human diseases, including metabolic syndrome related diseases and neuroinflammation.[9,10]

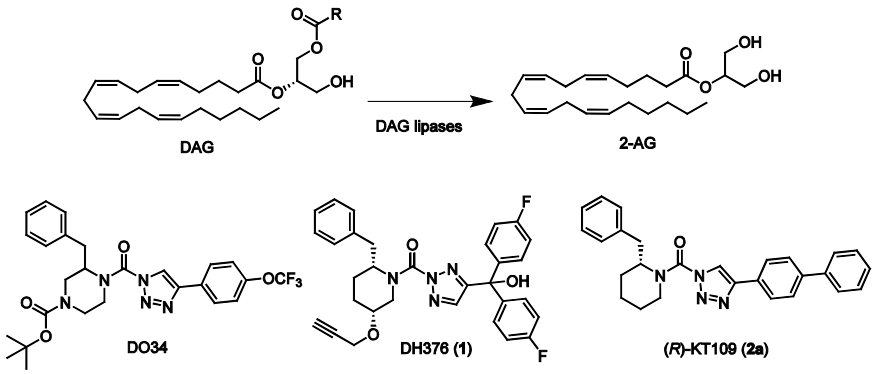

Figure 1. Conversion of DAG into 2-AG by DAG lipases and chemical structures of their inhibitors DO34, DH376 and (*R*)-KT109.

Previously, the discoveries of α-ketoheterocycles,[11-13] glycinesulfonamides[14] and triazole ureas (e.g. DO34 and DH376 (**1**))[15] were reported as selective DAGL inhibitors (Figure. 1). DH376 and DO34 are brain active DAGL inhibitors that reduce 2-AG levels in a time- and dose-dependent manner in mouse brain. They also reduce lipopolysaccharide-induced pro-inflammatory prostaglandin and cytokine levels in mouse brain, as well as anapyrexia and refeeding in fasted mice.[15] Of note, most DAGL inhibitors cross-react with α,β-hydrolase domain containing protein 6 (ABHD6), which has a minor role in the hydrolysis of 2-AG,[16] degrades bis(monoacylglycero)phosphate,[17] and acts as a lysophosphatidyl hydrolase.[18] Inhibition of ABHD6 produces neuroprotective, anti-obesity and anti-inflammatory effects in preclinical disease models.[19,20] Thus, dual inhibition of DAGLs and ABHD6 may actually be advantageous from a therapeutic point of view.

The design of DH376 and DO34 was inspired by (*R*)-KT109 (**2a**),[21,22] the first *in vivo* active DAGLα inhibitor. Both compounds are covalent irreversible inhibitors that feature a 2-benzylpiperidine moiety that confers selectivity and activity towards DAGLs and ABHD6. Previously, an enantioselective synthesis route for DH376 was described (Chapter 2) based on the experience with the synthesis of chiral piperidines from easily available starting materials following a strategy that encompasses enzyme-catalysed cyanohydrin synthesis followed by a transamination-reduction -ring-closing metathesis series of events.[23-25]

The strategy, as demonstrated earlier in the synthesis of polyhydroxylated piperidines (termed iminosugars), is especially suited for the construction of chiral, enantiopure 2-alkylpiperidines bearing one or more hydroxyl substituents. Therefore, in this way, piperidinylureas bearing multiple substituents, amongst which solubilizing hydroxyl groups, would be easy to accomplish. To demonstrate the validity of this reasoning, and to extend the panel of putative

serine hydrolase inactivators, a small library of chiral, disubstituted piperidinylureas **3**, **4a**-**7a**, **4b**-**7b, 6c**, **8** and **9**-**18** were made and the results are described in this chapter.

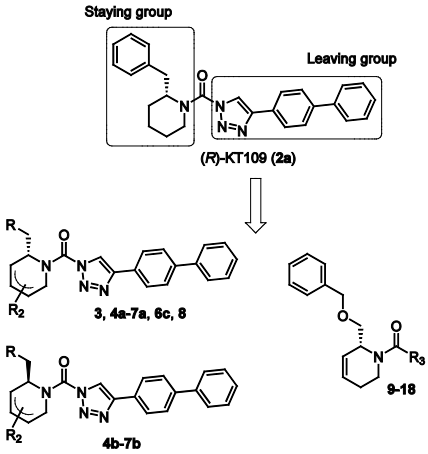

Figure 2. Design of compounds **3**, **4a**-**7a**, **4b**-**7b**, **6c**, **8** and **9**-**18** based on lead **2a**.

Results and discussion

Chemistry

To systematically investigate the structure-activity relationship of the covalent irreversible inhibitors, the attention was focused first on the modification of staying group, resulting 1,2,3-triazole ureas **3**, **4a**-**7a**, **4b**-**7b**, **6c**, **8** (Figure 2, Table 1 and 2). Next, the influence of electrophilicity of the leaving group (i.e. triazole scaffold) was explored by synthesizing compounds **9**-**18**. The synthesis started with compound **3**, as a close homologue of lead compound **2a** with a methyloxy moiety inserted into the benzylic position. The synthesis route commenced with *O*-TBDPS-protected intermediate **19** that was prepared according to the previously established procedure.[26] Treatment of **19** with 10% Pd/C in MeOH gave hydrogenated intermediate **20**, and ensuing desilylation and benzylation of the primary alcohol yielded Boc-protected intermediate **22** (Scheme 1). Removal of the Boc group using 25% (v/v) TFA in DCM gave amine **23** in near quantitative yield. Finally, triphosgene-mediated condensation of **23** with 4-([1,1'-biphenyl]-4-yl)-1*H*-1,2,3 -triazole and isolation of the 1,4-regioisomer by silica gel chromatography provided compound **3** in >95% ee as determined by chiral HPLC.

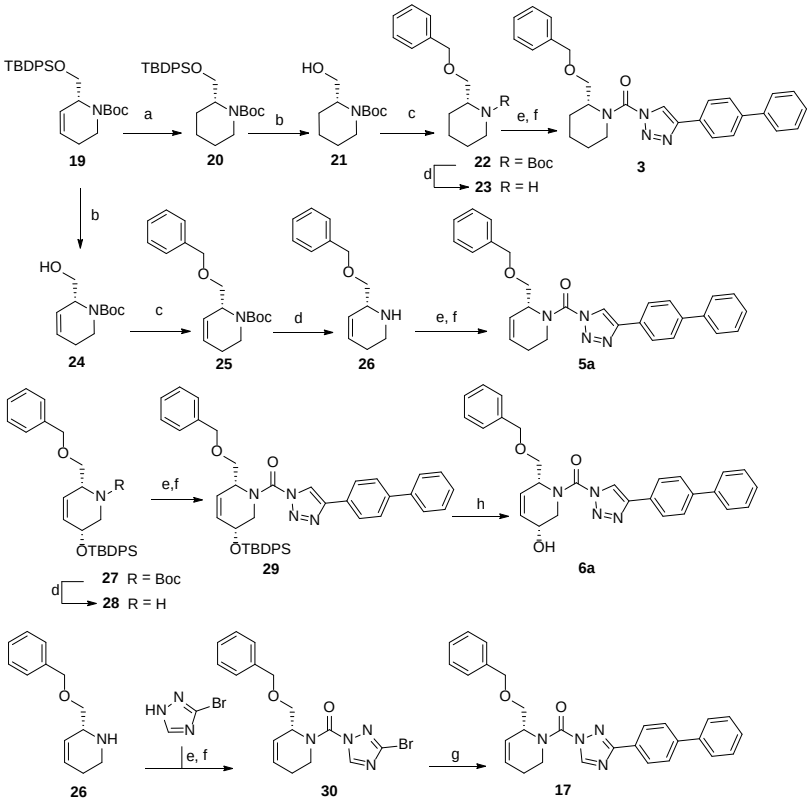

Scheme 1. Reagents and conditions: (a) 10% Pd/C, H_2, MeOH, 95%; (b) TBAF, THF, r.t., 98% (**21**), 92% (**24**); (c) BnBr, TBAI, NaH, DMF, 90% (**22**), 90% (**25**); (d) 25% TFA, DCM, 84% (**26**), 85% (**28**); (e) DIPEA, triphosgene, THF, 0 ^{o}C; (f) DIPEA, DMAP, 1,2,3-triazole, THF, 60 ^{o}C, 25% (**3**), 30% (**5a**), 40% (**30**) over 2 steps; (g) 1,4-dioxane: H_2O (2:1), biphenyl boronic acid, $PdCl_2$(dppf), 80 ^{o}C, 75%; (h) HF-pyridine, THF : pyridine = 1:1 (v/v), 20% over 3 steps (based on **28**).

Following a related sequence of events, but using TBAF for the desilylation step, compound **5a** was obtained (Scheme 1). Compound **5b** (the enantiomer of **5a**) was synthesized in the same fashion as described for **5a** (see experimental section, Scheme 3). For the synthesis of compound **6a**, key intermediate **27** was prepared by employing a previously reported method.[15,24] Subsequently, removal of the Boc group using 25% (v/v) TFA in DCM generated amine **28** that was directly coupled with 4-([1,1'-biphenyl]-4-yl)-1*H*-1,2,3-triazole. After silica gel chromatography, 1,4-regioisomer **29** was isolated and ensuing desilylation with HF-pyridine yielded target compound **6a** (Scheme 1). In a similar manner, compounds **4a**, **4b, 6b, 6c** and **8** with different stereochemistry and substitution pattern on the piperidine ring were prepared (see experimental

section). The synthesis of compound **7b** started with piperidene **33** that was previously prepared according to the reported method.[27,28] Deprotection of **33** with catalytic amount of *p*-TsOH yielded diol intermediate **34** that was then regioselectively benzylated using boronic amide as catalyst.[29] After *O*-silylation and *N*-Boc deprotection, free amine **37** was obtained via triphosgene coupling with triazole. Finally, desylilation (HF-pyridine) gave target compound **7b** (Scheme 2). Compound **7a** (being a diastereoisomer of **7b**) was obtained in the same fashion (see experimental section).

Compounds **9**-**17** were prepared by triphosgene-mediated condensation of free amine **26** with the appropriate heterocycle. As an example, heterocycle **17** (Scheme 1) synthesized by coupling of **26** with 3-bromo-*1H*-1,2,4-triazole followed by Suzuki coupling with 4-biphenylboronic acid (Scheme 1). Finally, the *para*-nitrophenyl carbamate derivative **18** was prepared following a strategy as followed for triazole derivative **5a** with 4-nitrophenol instead of 4-([1,1'-biphenyl]-4-yl)-1*H*-1,2,3-triazole (see experimental section).

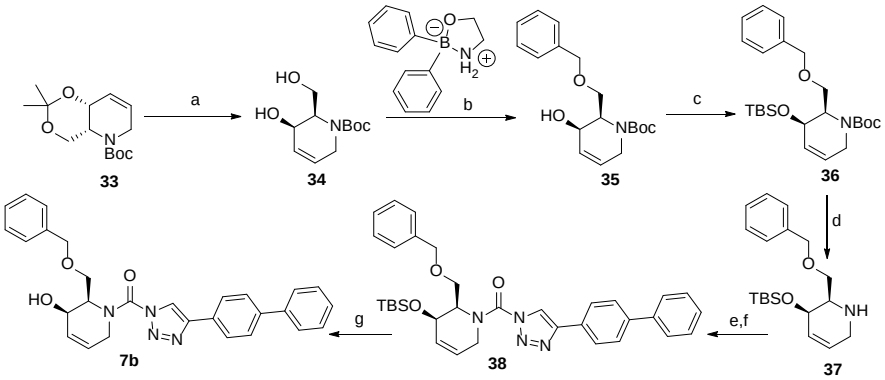

Scheme 2. Reagents and conditions: (a) cat. *p*-TsOH, MeOH, 86%; (b) BnBr, K_2CO_3, KI, MeCN, 60 °C, 89%; (c) TBS-Cl, imidazole, DMF, 95%; (d) 10% TFA, DCM, 0 °C, 69%. (e) DIPEA, triphosgene, THF, 0 °C; (f) DIPEA, DMAP, 1,2,3-triazole, THF, 60 °C; (g) HF-pyridine, THF : pyridine = 1:1 (v/v), 15% over 3 steps.

Biological evaluation

The potency of of **3**, **4a-7a**, **4b-7b**, **6c**, **8** and **9**-**18**, as DAGLα inhibitors was established in a colorimetric assay using *para*-nitrophenylbutyrate as a surrogate substrate and membrane fractions from HEK293T cells overexpressing recombinant human DAGLα. As a reference, the biochemical data of (*R*)-KT109 (**2a**) was shown. (*R*)-KT109 (**2a**) is more potent than its enantiomer, (*S*)-KT109 (**2b**), as described in Chapter 2. The same stereochemistry at the C-2 position was preferred for the compounds tested

(e.g. compare compounds **4a**-**6a** vs **4b**-**6b**). A 30-100-fold drop in potency of benzyloxy-containing compounds (**3** and **5**a was found. This may suggest that a lipophilic pocket in DAGLα, which accommodates the 2-benzylpiperidine moiety, is restricted in size or, alternatively, that a polar, flexible linker is less preferred. Introduction of polar hydroxyl groups at other positions in the unsaturated piperidines (e.g. **4a** vs **8**) also reduced the activity over 20-fold. Of note, introduction of a chiral hydroxyl group at the C-3 position of an unsaturated piperidine ring (compounds **7a** and **7b**) abolished the activity against DAGLα ($pIC_{50} < 5$), whereas a hydroxyl at the C-5 position (compounds **6a** and **6c**) was allowed. This suggests that the position of the chiral hydroxyl group plays an important role in the binding site of DAGLα. However, a change in conformation of the piperidine ring induced by the double bond can also not be excluded to be responsible for the decrease in potency. Of note, the stereochemistry of the chiral hydroxyl at the C-5 position in the ring (**6a** vs **6c**) is not important for DAGL activity, which may suggest that this functional group does not make any significant interaction in the binding pocket and may protrude into a solvent exposed region. Compounds **10**-**12** were equally potent as compound **5a**, but **9** showed ~10-fold less activity. The pyrazoles (**13** and **15**), imidazoles (**14** and **16**), 1,2,4-triazole (**17**) and carbamate (**18**) were inactive. This is in line with a reduced electrophilicity of their warhead imparted by the heterocycle.

To screen derivatives **3**, **4a**-**7a**, **4b**-**7b**, **6c**, **8** and **9**-**18** for ABHD6 inhibitory activity, a real-time, fluorescence-based natural substrate assay was employed with membranes from HEK293T cells expressing recombinant human ABHD6. In general, the inhibitory potency of the compounds followed the same trend as observed for DAGLα inhibition (Table 1 and 2). To compare the DAGLα and ABHD6 activities of the compounds, their pIC_{50} values against both targets was plotted (Figure 3). Most of the compounds were dual DAGLα /ABHD6 inhibitors and a linear relationship (r^2 =0.85) for the potency was observed. Compounds **6b**, **7a** and **7b** were inactive against DAGLα, but still showed inhibition against ABHD6 ($pIC_{50} > 6$). Therefore, these compounds could be interesting starting points for the discovery of selective ABHD6 inhibitors.

Table 1. Structure-activity relationship (SAR) of triazole ureas **3, 4a**-**7a, 4b**-**7b, 6c,** and **8**. Inhibition of recombinant human DAGLα or ABHD6 was measured by indicated assays. Data represent average values ± SEM; n = 4 per group.

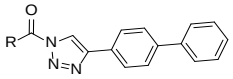

Entry	R	pIC_5 (DAGLα)	pIC_{50} (ABHD6)	Entry	R	pIC_{50} (DAGLα)	pIC_{50} (ABHD6)
2a	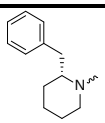	9.1±0.1	8.6±0.1	**2b**	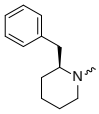	7.4±0.1	6.2±0.1
3	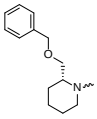	7.1±0.1	8.5±0.1	**8**	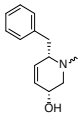	7.8±0.1	8.5±0.2
4a	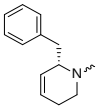	9.1±0.1	8.6±0.1	**4b**	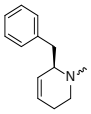	7.1±0.1	7.6±0.1
5a	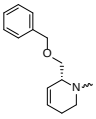	7.6±0.1	7.9±0.1	**5b**	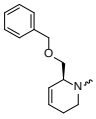	5.9±0.2	7.0±0.1
6a	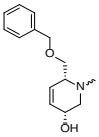	7.6±0.1	8.3±0.1	**6b**	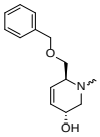	<5	6.5±0.1
6c	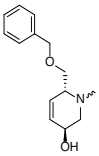	7.5±0.2	8.0±0.1				
7a	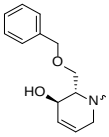	<5	6.1±0.1	**7b**	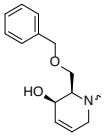	<5	6.6±0.1

Table 2. Structure-activity relationship (SAR) of compounds **9-18**. Inhibition of recombinant human DAGLα or ABHD6 was measured by indicated assays. Data represent average values ± SEM; n = 4 per group.

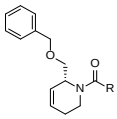

Entry	R	pIC_{50} (DAGLα)	pIC_{50} (ABHD6)
9	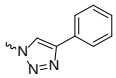	6.8±0.1	6.8±0.1
10	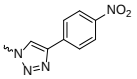	7.8±0.1	7.5±0.1
11	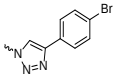	7.8±0.1	7.8±0.1
12	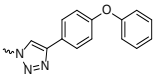	7.6±0.1	8.2±0.1
13	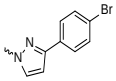	<5	<5
14	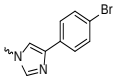	<5	<5
15	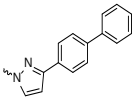	<5	<5
16	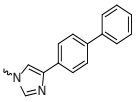	<5	<5
17	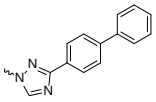	<5	<5
18	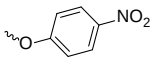	<5	<5

Finally, to evaluate the selectivity of compounds (**3**, **4a**-**7a**, **4b**-**7b**, **6c**, **8** and **9**-**18**) across a broad panel of serine hydrolases, activity-based protein profiling (ABPP) was applied using mouse brain membrane proteome. Fluorophosphonate (FP)-based probes are routinely used in competitive ABPP experiments to determine the selectivity of serine hydrolase inhibitors.[30,31] However, FP-based probes do not label DAGLα. MB064, a Bodipy-tagged tetrahydrolipstatin based β-lactone probe, was therefore previously developed, to detect endogenous DAGLα in brain proteomes[31]. Thus, both TAMRA-FP and MB064 were applied to assess the activity and selectivity of the dual DAGLα and ABHD6 inhibitors. In brief, inhibitors **3**, **4a**-**7a**, **4b**-**7b**, **6c**, **8** and **9**-**18** at 10 µM were incubated for 30 min with mouse brain membrane homogenates and performed a gel-based ABPP assay using MB064 (0.25 µM, 20 min) or TAMRA-FP (0.5 µM, 20 min). Almost complete blockade of DAGLα and ABHD6 was observed by compounds **3**, **4a**-**6a**, **4b**, **6c** and **8**-**12**, which is consistent with the results of the biochemical assay (Figure 4a and Table 3). Most compounds showed excellent selectivity over the other serine hydrolases (Figure 4). Compounds **3**, **5a**, **6c** and **9**-**12** did, however, reduce the labeling of DDHD2 (Figure 4a), while compounds **6c**, **9** and **10** were non-selective and prevented the labelling of several unknown off-targets (Figure 4a and 4b).

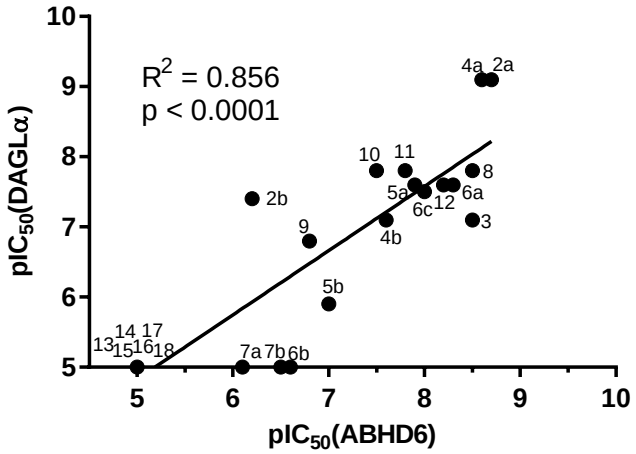

Figure 3. Graphical representation of DAGLα versus ABHD6 inhibition (pIC_{50}) compounds **2a**, **2b**, **3**, **4a**-**7a**, **4b**-**7b**, **6c**, **8** and **9**-**18**.

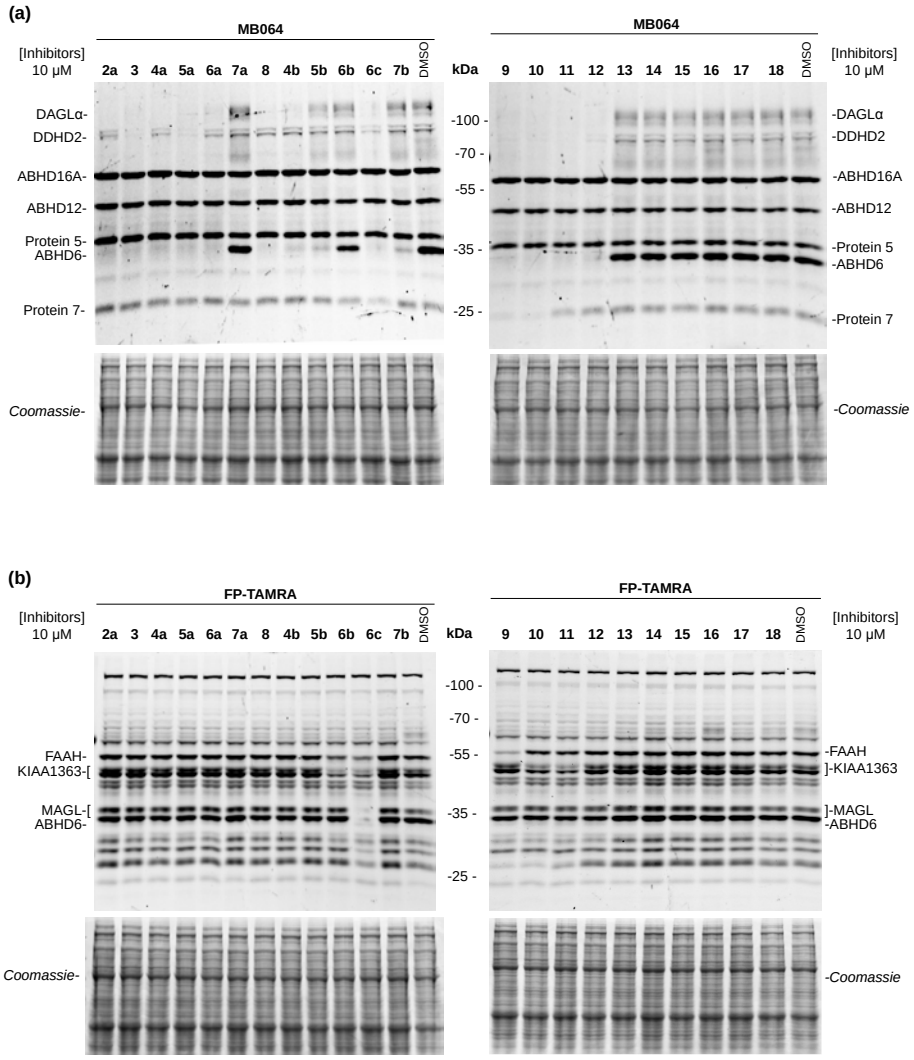

Figure 4. Selectivity profile of compounds **2a**, **3**, **4a**-**7a**, **4b**-**7b**, **6c**, **8** and **9**-**18** (10 µM, 30 min) across mouse brain membrane serine hydrolases as determined by competitive ABPP using two broad-spectrum probes MB064 (0.25 µM, 20 min) (a) and FP-TAMRA (0.5 µM, 20 min) (b). Coomassie staining gel were used as a loading control.

Table 3 . Inhibitory values for compounds **2a**, **3**, **4a**-**7a**, **4b**-**7b**, **6c**, **8** and **9**-**18** (10 µM, 30 min) against native DAGLα and ABHD6 using competitive activity–based protein profiling (ABPP) with probe MB064 (0.25 µM, 20 min). Data represent Means±SEM, n=3. Values are corrected for protein loading per lane as determined by coomassie staining.

Entry	Inhibition (%)		Entry	Inhibition (%)	
	DAGLα	ABHD6		DAGLα	ABHD6
2a	99±0	95±1	**7b**	18±11	83±2
3	96±1	96±0	**9**	89±5	89±2
4a	99±0	96±1	**10**	95±2	93±1
5a	94±2	96±0	**11**	93±3	94±1
6a	87±5	95±2	**12**	93±3	86±2
7a	6±13	18±9	**13**	-3±5	-3±4
8	92±2	96±2	**14**	-9±15	-15±15
4b	83±5	90±3	**15**	-14±18	-3±19
5b	30±12	84±5	**16**	-13±14	-28±15
6b	5±14	50±7	**17**	0±12	-16±9
6c	85±2	95±2	**18**	-11±12	-12±9

Conclusions

In summary, the enantioselective synthesis and structure–activity relationship studies of chiral, disubstituted piperidinylureas as dual inhibitors of DAGLα and ABHD6 were investigated in this chapter. The SAR studies revealed the stereochemistry of the C-2 substitution on the piperidine ring plays an important role. Incorporation of a hydroxyl group at the C-5 position on piperidine ring maintained the activity against DAGLα and ABHD6, whereas a hydroxyl at the C-3 position completely abolished all DAGLα activity. Competitive activity-based protein profiling confirmed the activity of the inhibitors against endogenous DAGLα and ABHD6 and revealed differences in the selectivity profile against other serine hydrolases.

Experimental section

Biological assays

Cloning Procedures

DAGLα and ABHD6 constructs were obtained as reported previously.[30] Plasmids were isolated from transformed XL-10 Z-competent cells (Maxi Prep,

Qiagen) and verified by Sanger sequencing (BaseClear). The sequences were confirmed by sequence analysis at the Leiden Genome Technology Centre.

Cell culture and membrane preparation

Cell culture was performed as previously reported.[30] In brief, HEK293T cells were grown in DMEM with stable glutamine and phenolred (PAA or Sigma) with 10% New Born Calf serum, penicillin and streptomycin. Cells were passaged every 2-3 days by resuspending in medium and seeding them to appropriate confluence. Membranes were prepared from transiently transfected HEK293T cells. One day prior to transfection 10^7 cells were seeded in a 15 cm petri dish. Cells were transfected by the addition of a 3:1 mixture of polyethyleneimine (60µg) and plasmid DNA (20µg) in 2 mL serum free medium. The medium was refreshed after 24 hours, and after 72 h the cells were harvested by suspending them in 20 mL medium. The suspension was centrifuged for 10 min at 1000 rpm, and the supernatant was removed. The cell pellet was stored at -80 ^{o}C until use.

Cell pellets were thawed on ice and suspended in lysis buffer A (20 mM Hepes, 2 mM DTT, 0.25 M sucrose, 1 mM $MgCl_2$, 25 U/mL Benzonase). The suspension was homogenized by polytrone (3 × 7 sec) and incubated for 30 min on ice. The suspension was subjected to ultracentrifugation (93.000 × g, 30 min, 4 ^{o}C, Beckman Coulter, Type Ti70 rotor) to yield the cytosolic fraction in the supernatant and the membrane fraction as a pellet. The pellet was resuspended in lysis buffer B (20 mM Hepes, 2 mM DTT). The protein concentration was determined with Quick Start Bradford reagent (BioRad) or Qubit™ fluorometric quantitation (Life Technologies). The protein fractions were diluted to a total protein concentration of 1 mg/mL and stored in small aliquots at -80 ^{o}C until use.

Biochemical DAGL activity assay

The biochemical hDAGLα assay was performed as reported previously.[30] In brief, the biochemical hDAGLα activity assay is based on the hydrolysis of para-nitrophenylbutyrate (PNP-butyrate) by membrane preparations from HEK293T cells transiently transfected with hDAGLα. Reactions were performed in 50 mM pH 7.2 HEPES buffer with 0.05 µg/µL final protein concentration hDAGLα transfected protein.

Natural substrate based fluorescence assay (ABHD6)

The natural substrate assay was performed as reported previously.[14,32] Standard assay conditions: 25 µM 2-AG, 0.2 U/mL glycerol kinase (GK), glycerol-3-phosphate oxidase (GPO) and horseradish peroxidase (HRP), 0.125 mM ATP, 10 µM Amplifu™Red, 5% DMSO and 0.5% acetonitrile in a total volume of 200 µL. The final protein (ABHD6) concentration is 40 µg/mL.

Preparation of mouse brain membrane proteome

Mouse brain membrane proteome preparation was performed as previously reported.[15,30] In brief, mouse brains were isolated according to guidelines approved by the ethical committee of Leiden University (DEC#10095). Mouse brains were Dounce homogenized in pH 7.2 lysis buffer A (20 mM HEPES pH 7.2, 2 mM DTT, 1 mM $MgCl_2$, 25 U/mL Benzonase) and incubated for 5 min on ice, followed by low speed spin (2,500 × g, 3 min, 4 ^{o}C) to remove debris. The supernatant was subjected to ultracentrifugation (100,000 × g, 45 min, 4 ^{o}C, Beckman Coulter, Type Ti70 rotor) to yield the cytosolic fraction in the supernatant and the membrane fraction as a pellet. The pellet was resuspended in storage buffer B (20 mM HEPES pH 7.2, 2 mM DTT). The total protein concentration was determined with Quick Start Bradford reagent (Bio-Rad) or QubitTM fluorometric quantitation (Life Technologies). Membranes and supernatant were flash frozen in liquid nitrogen and stored in aliquots at -80 ^{o}C until use.

Activity based protein profiling in mouse brain

Mouse brain proteome (2 mg/mL, 19.5 µL) was incubated with DMSO or inhibitor in 0.5 µL DMSO for 30 min at r.t. and subsequently incubated with 500 nM (final concentration) ABP FP-TAMRA for 20 min at r.t. before the reaction was quenched with standard 3x Laemmli sample buffer. The gels were scanned using a ChemiDoc MP system and analyzed using Image Lab 4.1.

Chemistry

General Synthetic Methods

Reagents were purchased from Sigma Aldrich, Acros or Merck and used without further purification unless noted otherwise. Some reactions were performed using oven or flame-dried glassware and dry solvents. All moisture sensitive reactions were performed under an argon atmosphere. Traces of water were removed from starting compounds by co-evaporation with toluene. ^{1}H-and ^{13}C-NMR spectra were recorded on a Bruker AV 400 MHz spectrometer at 400 (^{1}H) and 101 (^{13}C) MHz, or on a Bruker DMX-600 spectrometer 600 (^{1}H) and 150 (^{13}C) MHz using $CDCl_3$, or CD_3OD as solvent, unless stated otherwise. Chemical shift values are reported in ppm with tetramethylsilane or solvent resonance as the internal standard ($CDCl_3$, δ 7.26 for ^{1}H, δ 77.16 for ^{13}C; CD_3OD, δ 3.31 for ^{1}H, δ 49.00 for ^{13}C; $(CD_3)_2SO$, δ 2.50 for ^{1}H, δ 39.52 for ^{13}C). Data are reported as follows: chemical shifts (δ), multiplicity (s = singlet, d = doublet, dd = double doublet, td = triple doublet, t = triplet, q = quartet, m = multiplet, br = broad), coupling constants *J* (Hz), and integration. High-resolution mass spectra (HRMS) were recorded by direct injection (2 µL of a 2 µM solution in

water/acetonitrile 50/50 (v/v) and 0.1% formic acid) on a mass spectrometer (Thermo Finnigan LTQ orbitrap) equipped with an electrospray ion source in positive mode (source voltage 3.5 kV, sheath gas flow 10, capillary temperature 250 ^{o}C) with resolution R = 60,000 at m/z 400 (mass range m/z = 150-2,000) and dioctylphthalate (m/z = 391.28428) as a "lock mass". The high resolution mass spectrometer was calibrated prior to measurements with a calibration mixture (Thermo Finnigan). LC-MS analysis was performed on a Finnigan Surveyor HPLC system with a Gemmi C_{18} 50x4.60 mm column (detection at 200-600 nm), coupled to a Finnigan LCQ Adantage Max mass spectrometer with ESI. The applied buffers were H_2O, MeCN and 1.0% TFA in H_2O (0.1% TFA end concentration). IR spectra were recorded on a Shimadzu FTIR-8300 and are reported in cm^{-1}. Optical rotations were measured on a Propol automatic polarimeter (Sodium D-line, λ = 589 nm). Flash chromatography was performed using SiliCycle silica gel type SilicaFlash P60 (230 – 400 mesh). TLC analysis was performed on Merck silica gel 60/Kieselguhr F254, 0.25 mm. Compounds were visualized using either Seebach's reagent (a mixture of phosphomolybdic acid (25 g), cerium (IV) sulfate (7.5 g), H_2O (500 mL) and H_2SO_4 (25 mL)) or a $KMnO_4$ stain (K_2CO_3 (40 g), $KMnO_4$ (6 g), H_2O (600 mL) and 10% NaOH (5 mL)). All final compounds were determined to be above 90% pure by LC-MS analysis.

(*R*)-(4-([1,1'-Biphenyl]-4-yl)-1*H*-1,2,3-triazol-1-yl)(2-((benzyloxy)methyl)piperidin-1-yl)methanone (3). A solution of (*R*)-2-((benzyloxy)methyl)piperidine (50.0 mg, 0.244 mmol) in THF was treated with DIPEA (0.128 mL, 0.731 mmol) and bis(trichloromethyl) carbonate (36.1 mg, 0.122 mmol) and the reaction mixture was stirred for 30 min at 0 ^{o}C. After that the reaction mixture was poured into water and extracted with ethyl acetate (3 x 10 mL). The organic layer was washed with water, brine, dried over $MgSO_4$, filtered, and concentrated under reduced pressure. The intermediate was dissolved in THF and DIPEA (0.128 mL, 0.731 mmol), DMAP (29.8 mg, 0.244 mmol) and 4-([1,1'-biphenyl]-4-yl)-1*H*-1,2,3-triazole (48.5 mg, 0.219 mmol) were added to the solution. The mixture was stirred for 2h at 60 ^{o}C and poured into saturated aqueous NH_4Cl solution (20 mL). The mixture was extracted with ethyl acetate (3 x 20 mL), washed with water, brine, dried over $MgSO_4$ and filtered. The solvents are removed under reduced pressure to yield the crude triazole urea as a mixture of N1- and N2-carbamoylated regioisomers (2 to 1 ratio). The N1-carbamoyl triazole was isolated by silica gel chromatography (pentane/EtOAc 100:1 → 5:1) to afford compound **3** (27.6 mg, 0.061 mmol, 25% yield). $[\alpha]_D^{22}$ = +58.7 (*c* = 0.3, $CHCl_3$). HRMS calculated for $C_{28}H_{28}N_4O_2$ $[M+H]^+$ 453.2285, found: 453.2286. ^{1}H NMR (400 MHz, $CDCl_3$) δ 8.08 (br, 1H), 7.87 (d, *J* = 7.7 Hz, 2H), 7.69 – 7.59 (m, 4H), 7.49 – 7.43 (m, 2H), 7.41 – 7.23 (m, 6H), 4.83 (br, 1H), 4.46 (br, 2H), 4.25 (d, *J* = 6.0 Hz, 1H), 3.86 (t, *J* = 9.6 Hz, 1H), 3.44 (br, 1H), 3.15 (br, 1H), 1.98 – 1.53 (m, 6H). ^{13}C NMR (101 MHz, $CDCl_3$) δ 151.44, 146.48, 141.36, 140.63, 137.93, 128.98, 128.84, 128.59, 127.95, 127.86, 127.68, 127.65, 127.14, 126.37, 121.21, 73.30, 68.05, 53.34, 41.93, 25.67, 25.22, 19.58.

(*S*)-(4-([1,1'-Biphenyl]-4-yl)-1*H*-1,2,3-triazol-1-yl)(6-benzyl-3,6-dihydropyridin-1(2*H*)-yl)methanone (4a). The title compound was synthesized from (*S*)-6-benzyl-1,2,3,6-tetrahydropyridine (43.0 mg, 0.248 mmol) according to the

procedure described for compound **3**. This furnished compound **4a** (34.8 mg, 0.083 mmol, 33% yield). $[\alpha]_D^{22}$ = +59.6 (*c* = 0.4, $CHCl_3$). HRMS calculated for $C_{27}H_{25}N_4O$ $[M+H]^+$ 421.2023, found: 421.2021. ^{1}H NMR ($CDCl_3$, 600 MHz, mixture of two rotamers ratio A/B = 53/47) Major rotamer: δ 8.36 (br, 0.5H), 7.95 – 7.87 (m, 2H), 7.77 (br, 0.5H) 7.69 (d, *J* = 5.2 Hz, 2H), 7.64 (d, *J* = 4.8 Hz, 2H), 7.50 – 7.43 (m, 2H), 7.38 – 7.28 (m, 3H), 7.25 – 7.12 (m, 3H), 5.97 – 5.93 (m, 1H), 5.69 – 5.63 (m, 1H), 5.37 (br, 0.5H), 4.93 (br, 0.5H), 4.54 (dd, *J* = 4.0, 12.0 Hz, 1H), 3.29 – 3.26 (m, 1H), 3.23 – 3.18 (m, 1H), 3.05 – 2.90 (m, 1H), 2.65 – 2.51 (m, 1H), 2.23 – 2.11 (m, 1H). ^{13}C NMR ($CDCl_3$, 151 MHz) Major rotamer: δ 151.36, 148.86, 146.60, 141.58, 140.59, 137.18, 129.74, 129.01, 128.82, 128.66, 127.77, 127.69, 127.14, 126.94, 126.40, 125.75, 120.93, 57.43, 41.94, 40.95, 25.82.

(*R*)-(4-([1,1'-Biphenyl]-4-yl)-1*H*-1,2,3-triazol-1-yl)(6-((benzyloxy)methyl)-3,6-dihydropyridin-1(2*H*)-yl)methanone (5a). The title compound was synthesized from (*R*)-6-((benzyloxy)methyl)-1,2,3,6-tetrahydropyridine (50.0 mg, 0.246 mmol) according to the procedure described for compound **3**. This furnished compound **5a** (33.2 mg, 0.074 mmol, 30% yield). $[\alpha]_D^{22}$ = +146.5 (*c* = 0.4, $CHCl_3$). The enantiomeric purity was determined on a Daicel Chiralcel OD-H column (4.5 X 250 mm, 20:80 IPA/Hex, flow rate of 1 mL/min): 23.2 min, e.e.>96%. HRMS calculated for $C_{28}H_{26}N_4O_2$ $[M+H]^+$ 451.2129, found: 451.2130. ^{1}H NMR (400 MHz, $CDCl_3$) δ 8.23 (br, 1H), 7.87 (br, 2H), 7.87 – 7.62 (m, 4H), 7.48 – 7.44 (m, 2H), 7.40 – 7.34 (m, 1H), 7.34 – 7.24 (m, 5H), 6.05 (br, 1H), 5.71 (br, 1H), 5.34 (br, 0.5H), 4.96 (br, 0.5H), 4.51 (br, 3H), 3.86 – 3.32 (m, 3H), 2.59 (br, 1H), 2.16 (br, 1H). ^{13}C NMR (151 MHz, $CDCl_3$) δ 151.76, 146.42, 141.45, 140.58, 137.83, 128.98, 128.68, 128.56, 127.88, 127.79, 127.68, 127.61, 127.35, 127.13, 126.40, 124.90, 121.31, 73.39, 71.00, 55.65, 39.06, 25.77.

(4-([1,1'-Biphenyl]-4-yl)-1*H*-1,2,3-triazol-1-yl)(*(3R,6R)*-6-((benzyloxy)methyl)-3-hydroxy-3,6-dihydropyridin-1(2*H*)-yl)methanone (6a). A solution of (*3R*,*6R*)-6-((benzyloxy)methyl)-3-((*tert*-butyldiphenylsilyl)oxy)-1,2,3,6-tetrahydropyridine **37** (200 mg, 0.437 mmol) in THF was treated with DIPEA (0.229 mL, 1.31 mmol) and bis(trichloromethyl) carbonate (64.8 mg, 0.218 mmol) and the reaction mixture was stirred for 30 min at 0 ^{o}C. The mixture was poured into water and extracted with ethyl acetate (3 x 30 mL). The organic layer was washed with water, brine dried over $MgSO_4$, and concentrated under reduced pressure. The intermediate was dissolved in THF and DIPEA (0.229 mL, 1.31 mmol), DMAP (53.4 mg, 0.437 mmol) and 4-([1,1'-biphenyl]-4-yl)-1*H*-1,2,3-triazole (106 mg, 0.481 mmol) were added to the solution. The mixture was stirred for 2h at 60 ^{o}C and poured into saturated aqueous NH_4Cl solution. The mixture was extracted with ethyl acetate, washed with water, brine, dried over $MgSO_4$, and concentrated under reduced pressure. The N1-carbamoyl triazole urea **29** was isolated by silica gel chromatography (1-10% ethyl acetate/pentane) as top TLC spot. HF-pyridine (0.235 mL, 2.61 mmol) was subsequently added to a solution of N1-carbamoyl triazole urea in THF and pyridine (1:1; 2 mL) with ice cooling, and the reaction mixture was stirred over night at room temperature. The mixture was diluted with ethyl acetate (40 mL), and then washed with $NaHCO_3$, brine, dried with $MgSO_4$, and concentrated under reduced pressure.

Purification by flash chromatography to furnish compound **6a** (40 mg, 0.086 mmol, 20% yield). $[\alpha]_D^{22}$ = +7.2 (*c* = 1.4, $CHCl_3$). HRMS calculated for $C_{28}H_{26}N_4O_3$ $[M+H]^+$ 467.2078, found: 467.2078. ^{1}H NMR (400 MHz, $CDCl_3$) δ 8.26 (br, 1H), 7.88 (d, *J* = 4.8 Hz, 2H), 7.68 (d, *J* = 8.3 Hz, 2H), 7.66 – 7.59 (m, 2H), 7.48 – 7.43 (m, 2H), 7.39 – 7.34 (m, 1H), 7.34 – 7.23 (m, 5H), 6.04 (d, *J* = 10.4 Hz, 1H), 5.81 (br, 1H), 4.65 (d, *J* = 8.3 Hz, 2H), 4.51 (br, 2H), 3.76 (br, 2H), 3.24 (br, 1H), 2.51 (br, 1H). ^{13}C NMR (101 MHz, $CDCl_3$) δ 150.61, 146.51, 141.53, 140.41, 137.57, 132.51, 128.89, 128.50, 128.32, 127.88, 127.75, 127.65, 127.62, 127.03, 126.34, 125.55, 121.18, 73.40, 70.02, 63.86, 51.29, 36.61.

(4-([1,1'-Biphenyl]-4-yl)-1*H*-1,2,3-triazol-1-yl)(*(2S,3R)*-2-((benzyloxy)methyl)-3-hydroxy-3,6-dihydropyridin-1(2*H*)-yl)methanone (7a). The title compound was synthesized from (*2S,3R*)-2-((benzyloxy)methyl)-3-((*tert*-butyldimethylsilyl)oxy)-1,2,3,6-tetrahydropyridine (30.0 mg, 0.09 mmol) and 4-([1,1'-biphenyl]-4-yl)-1*H*-1,2,3-triazole (20.0 mg, 0.09 mmol), according to the procedure described for compound **6a**. This furnished compound **7a** (6.2 mg, 0.013 mmol, 15% yield). $[\alpha]_D^{22}$ = +8.13 (*c* = 0.2, $CHCl_3$). HRMS calculated for $C_{28}H_{26}N_4O_3$ $[M+H]^+$ 467.2078, found: 467.2077. ^{1}H NMR (600 MHz, $CDCl_3$) δ 8.15 (s, 1H), 7.94 (d, *J* = 8.3 Hz, 2H), 7.70 (d, *J* = 8.4 Hz, 2H), 7.64 (d, *J* = 7.1 Hz, 2H), 7.49 – 7.45 (m, 2H), 7.42 – 7.37 (m, 1H), 7.34 – 7.28 (m, 5H), 6.07 – 6.01 (m, 1H), 5.95 (br, 1H), 4.82 (br, 1H), 4.56 – 4.38 (m, 3H), 4.12 (br, 1H), 3.81 (br, 1H), 3.56 (br, 1H), 3.42 (br, 1H). ^{13}C NMR (151 MHz, $CDCl_3$) δ 151.24, 149.41, 142.62, 140.33, 137.56, 133.90, 129.05, 128.62, 128.02, 127.93, 127.89, 127.82, 127.65, 127.20, 127.11, 126.32, 126.27, 73.26, 67.00, 63.89, 59.94, 42.01.

(4-([1,1'-Biphenyl]-4-yl)-1*H*-1,2,3-triazol-1-yl)(*(3R,6S)*-6-benzyl-3-hydroxy-3,6-dihydropyridin-1(2*H*)-yl)methanone (8). The title compound was synthesized from (*3R,6S*)-6-benzyl-1,2,3,6-tetrahydropyridin-3-ol (80.0 mg, 0.187 mmol) and 4-([1,1'-biphenyl]-4-yl)-1*H*-1,2,3-triazole (41.4 mg, 0.187 mmol) according to the procedure described for compound **6a**. This furnished compound **8** (13.0 mg, 0.030 mmol, 16% yield). $[\alpha]_D^{20}$ = 3.70 (*c* = 1.0, $CHCl_3$). HRMS calculated for $C_{27}H_{24}N_4O_2$ $[M+H]^+$ 437.1972, found: 437.1971. ^{1}H NMR (400 MHz, $CDCl_3$) δ 8.38 (br, 1H), 7.90 (br, 2H), 7.70 (d, *J* = 8.3 Hz, 2H), 7.64 (d, *J* = 8.5 Hz, 2H), 7.50 – 7.45 (m, 2H), 7.41 – 7.14 (m, 6H), 5.93 (d, *J* = 11.7 Hz, 1H), 5.72 (dd, *J* = 10.4, 3.7 Hz, 1H), 5.41 (br, 0.4H), 4.86 (br, 0.6H), 4.70 (dd, *J* = 12.9, 5.1 Hz, 2H), 3.25 (dd, *J* = 13.0, 6.5 Hz, 1H), 3.12 – 2.93 (m, 2H). ^{13}C NMR (101 MHz, $CDCl_3$) δ 151.05, 146.48, 141.68, 140.52, 136.85, 131.10, 130.89, 129.58, 129.01, 128.85, 128.41, 127.81, 127.75, 127.16, 127.03, 126.43, 121.01, 64.19, 56.74, 47.83, 46.24.

(*R*)-(4-([1,1'-Biphenyl]-4-yl)-1*H*-1,2,3-triazol-1-yl)(6-benzyl-3,6-dihydropyridin-1(2*H*)-yl)methanone (4b). The title compound was synthesized from (*R*)-6-benzyl-1,2,3,6-tetrahydropyridine (75.0 mg, 0.433 mmol) according to the procedure described for compound **3**. This furnished compound **4b** (58.3 mg, 0.139 mmol, 32% yield). $[\alpha]_D^{22}$ = -75.20 (*c* = 0.5, $CHCl_3$). HRMS calculated for $C_{27}H_{24}N_4O$ $[M+H]^+$ 421.2023, found: 421.2021. ^{1}H NMR (500 MHz, $CDCl_3$, mixture of two

rotamers ratio A/B = 56/44) Major rotamer: δ 8.36 (br, 0.5H), 7.97 – 7.87 (m, 2H), 7.69 (d, *J* = 8.0 Hz, 2H), 7.64 (d, *J* = 4.0 Hz, 2H), 7.48 – 7.40 (m, 2H), 7.38 – 7.28 (m, 3H), 7.25 – 7.11 (m, 3H), 5.95 – 5.92 (m, 1H), 5.66 – 5.63 (m, 1H), 5.37 (br, 0.5H), 4.93 (br, 0.5H), 4.54 (dd, *J* = 4.0, 12.0 Hz, 1H), 3.30 – 3.26 (m, 1H), 3.23 – 3.18 (m, 1H), 3.06 – 2.98 (m, 1H), 2.61 – 2.49 (m, 1H), 2.22 – 2.11 (m, 1H). ^{13}C NMR (126 MHz, $CDCl_3$) Major rotamer: δ 151.55, 148.86, 146.59, 141. 63, 140.57, 137.21, 129.72, 128.98, 128.81, 128.64, 127.74, 127.68, 127.13, 126.67, 126.36, 125.73, 120.92, 57.39, 41.95, 39.73, 25.79.

(*S*)-(4-([1,1'-Biphenyl]-4-yl)-1*H*-1,2,3-triazol-1-yl)(6-((benzyloxy)methyl)-3,6-dihydropyridin-1(2*H*)-yl)methanone (5b). The title compound was synthesized from (*S*)-6-((benzyloxy)methyl)-1,2,3,6-tetrahydropyridine (50.0 mg, 0.251 mmol) according to the procedures described for compound **3**. This furnished compound **5b** (31.1 mg, 0.069 mmol, 28% yield). $[\alpha]_D^{22}$ = -154.0 (*c* = 0.8, $CHCl_3$). The enantiomeric purity was determined on a Daicel Chiralcel OD-H column (4.6 X 250 mm, 20:80 IPA/Hex, flow rate of 1 mL/min): 15.6 min, e.e.>95%. HRMS calculated for $C_{28}H_{26}N_4O_2$ $[M+H]^+$ 451.2129, found: 451.2128. ^{1}H NMR (400 MHz, $CDCl_3$): δ 8.37 (br, 1H), 7.87 (br, 2H), 7.69 – 7.63 (m, 4H), 7.48 – 7.44 (m, 2H), 7.40 – 7.32 (m, 1H), 7.32 – 7.15 (m, 5H), 6.11 – 5.97 (m, 1H), 5.71 (br, 1H), 5.32 (br, 0.5H), 4.96 (br, 0.5H), 4.49 (br, 3H), 3.73 (br, 2H), 3.32 (br, 1H), 2.56 (br, 1H), 2.15 (br, 1H). ^{13}C NMR (101 MHz, $CDCl_3$) δ 151.07, 146.41, 141.42, 140.55, 137.88, 128.96, 128.67, 128.53, 127.85, 127.77, 127.65, 127.56, 127.33, 127.11, 126.38, 124.88, 121.23, 73.37, 70.84, 55.16, 38.82, 24.95.

(4-([1,1'-Biphenyl]-4-yl)-1*H*-1,2,3-triazol-1-yl)((*3R,6S*)-6-((benzyloxy)methyl)-3-hydroxy-3,6-dihydropyridin-1(2*H*)-yl)methanone (**6b**). The title compound was synthesized from (*3R,6S*)-6-((benzyloxy)methyl)-3-((*tert*-butyldiphenylsilyl)oxy)-1,2,3,6-tetrahydropyridine (100 mg, 0.221 mmol) according to the procedure described for compound **6a**. This furnished compound **6b** (16.3 mg, 0.035 mmol, 16% yield). $[\alpha]_D^{22}$ = -144.2 (*c* = 0.7, $CHCl_3$). HRMS calculated for $C_{28}H_{26}N_4O_3$ $[M+H]^+$ 467.2078, found: 467.2077. ^{1}H NMR (400 MHz, $CDCl_3$) δ 8.38 (br, 0.5H), 8.05 (br, 0.5H), 7.85 (br, 2H), 7.71 – 7.56 (m, 4H), 7.50 – 7.44 (m, 2H), 7.41 – 7.15 (m, 6H), 6.23 – 6.16 (m, 1H), 5.90 (br, 1H), 5.41 (br, 0.4H), 5.07 (br, 0.6H), 4.70 – 4.35 (m, 3H), 4.26 (d, *J* = 5.4 Hz, 1H), 3.86 – 3.49 (m, 3H). ^{13}C NMR (101 MHz, $CDCl_3$) δ 150.99, 146.77, 141.67, 140.49, 137.70, 134.90, 129.03, 128.99, 128.61, 128.40, 127.98, 127.89, 127.71, 127.17, 127.12, 126.38, 121.31, 73.48, 69.80, 62.49, 54.20, 49.40.

(4-([1,1'-Biphenyl]-4-yl)-1*H*-1,2,3-triazol-1-yl)((*3S,6R*)-6-((benzyloxy)methyl)-3-hydroxy-3,6-dihydropyridin-1(2*H*)-yl)methanone (6c). The title compound was synthesized from (*3S,6R*)-6-((benzyloxy)methyl)-3-((*tert*-butyldimethylsilyl)oxy)-1,2,3,6-tetrahydropyridine (82.0 mg, 0.246 mmol) according to the procedure described for compound **6a**. This furnished compound **6c** (19.6 mg, 0.042 mmol, 17% yield). $[\alpha]_D^{22}$ = -142.7 (*c* = 0.2, $CHCl_3$). HRMS calculated for $C_{28}H_{26}N_4O_3$ $[M+H]^+$ 467.2078, found: 467.2079. ^{1}H NMR (400 MHz, $CDCl_3$) δ 8.39 (br, 1H), 7.94 – 7.78 (m, 2H), 7.71 – 7.60 (m, 4H), 7.48

– 7.42 (m, 2H), 7.41 – 7.23 (m, 6H), 6.25 – 6.16 (m, 1H), 5.90 (br, 1H), 5.41 (br, 0.4H), 5.05 (br, 0.6H), 4.62 (br, 2H), 4.40 (br, 1H), 4.27 (d, *J* = 5.4 Hz, 1H), 3.91 – 3.48 (m, 3H). ^{13}C NMR (101 MHz, $CDCl_3$) δ 151.91, 146.74, 141.64, 140.51, 137.69, 135.37, 133.11, 128.99, 128.62, 128.43, 128.35, 128.00, 127.79, 127.72, 127.13, 126.41, 121.35, 73.50, 69.80, 62.59, 54.33, 49.93.

(4-([1,1'-Biphenyl]-4-yl)-1*H*-1,2,3-triazol-1-yl)((*2R,3R*)-2-((benzyloxy)methyl)-3-hydroxy-3,6-dihydropyridin-1(2*H*)-yl)methanone (7b). The title compound was synthesized from (*2R,3R*)-2-((benzyloxy)methyl)-3-((*tert*-butyldimethylsilyl)oxy)-1,2,3,6-tetrahydropyridine **37** (30.0 mg, 0.090 mmol) according to the procedure described for compound **6a**. This furnished compound **7b** (6.6 mg, 0.014 mmol, 15% yield). $[\alpha]_D^{22}$ = -17.4 (*c* = 0.4, $CHCl_3$). HRMS calculated for $C_{28}H_{26}N_4O_3$ $[M+H]^+$ 467.2077, found: 467.2078. ^{1}H NMR (600 MHz, $CDCl_3$) δ 8.12 (s, 1H), 7.95 (d, *J* = 8.4 Hz, 2H), 7.70 (d, *J* = 8.4 Hz, 2H), 7.66 – 7.62 (m, 2H), 7.50 – 7.45 (m, 2H), 7.42 – 7.35 (m, 1H), 7.34 – 7.27 (m, 5H), 5.84 (d, *J* = 10.4 Hz, 1H), 5.74 (br, 1H), 5.10 – 4.85 (m, 2H), 4.52 (br, 2H), 4.29 (br, 1H), 3.90 – 3.76 (m, 3H). ^{13}C NMR (151 MHz, $CDCl_3$) δ 150.36, 149.33, 142.49, 140.36, 137.59, 133.79, 129.05, 128.96, 128.61, 127.98, 127.94, 127.91, 127.83, 127.82, 127.20, 127.10, 123.48, 73.46, 65.95, 65.83, 56.73, 42.07.

(*R*)-(6-((Benzyloxy)methyl)-3,6-dihydropyridin-1(2*H*)-yl)(4-phenyl-1*H*-1,2,3-triazol-1-yl)methanone (9). The title compound was synthesized from (*R*)-6-((benzyloxy)methyl)-1,2,3,6 -tetrahydropyridine (70.0 mg, 0.344 mmol) and 4-phenyl-1*H*-1,2,3-triazole (55.0 mg, 0.379 mmol) according to the procedure described for compound **3**. This furnished compound **9** (45.1 mg, 0.121 mmol, 35% yield). $[\alpha]_D^{20}$ = 125.1 (c = 1.0, $CHCl_3$). HRMS calculated for $C_{22}H_{22}N_4O_2$ $[M+H]^+$ 375.1816, found: 375.1815. ^{1}H NMR (400 MHz, $CDCl_3$) δ 8.20 (br, 1H), 7.80 (br, 2H), 7.46 – 7.40 (m, 2H), 7.35 – 7.17 (m, 6H), 6.03 (s, 1H), 5.68 (br, 1H), 5.30 (br, 0.5H), 4.96 (br, 0.5H), 4.67 – 4.30 (m, 3H), 3.85 – 3.20 (m, 3H), 2.53 (br, 1H), 2.16 (br, 1H). ^{13}C NMR (101 MHz, $CDCl_3$) δ 146.66, 137.81, 129.70, 128.98, 128.67, 128.49, 127.82, 127.74, 127.53, 125.96, 125.63, 124.86, 121.23, 73.33, 70.55, 55.37, 42.72, 24.87.

(*R*)-(6-((Benzyloxy)methyl)-3,6-dihydropyridin-1(2*H*)-yl)(4-(4-nitrophenyl)-1*H*-1,2,3-triazol-1-yl)methanone (10). The title compound was synthesized from (*R*)-6-((benzyloxy)methyl)- 1,2,3,6-tetrahydropyridine (70.0 mg, 0.344 mmol) and 4-(4-nitrophenyl)-1*H*-1,2,3-triazole (72.0 mg, 0.379 mmol) according to the procedure described for compound **3**. This furnished compound **10** (54.9 mg, 0.13 mmol, 38% yield). $[\alpha]_D^{22}$ = +123 (*c* = 0.9, $CHCl_3$). HRMS calculated for $C_{22}H_{21}N_5O_4$ $[M+H]^+$. 420.1666, found: 420.1666. ^{1}H NMR (400 MHz, $CDCl_3$) δ 8.38 – 8.21 (m, 2H), 8.18 – 7.81 (m, 3H), 7.36 - 7.21 (m, 5H), 6.08 – 6.04 (m, 1H), 5.67 (br, 1H), 5.28 (br, 0.5H), 4.97 (br, 0.5H), 4.71 – 4.32 (m, 3H), 3.85 – 3.20 (m, 3H), 2.54 (br, 1H), 2.22 (br, 1H). ^{13}C NMR (101 MHz, $CDCl_3$) δ 147.63, 144.67, 137.61, 135.98, 135.55, 128.54, 127.92, 127.66, 127.14, 126.51, 124.43, 124.38, 122.96, 73.44, 70.71, 55.84, 41.11, 24.42.

(*R*)-(6-((Benzyloxy)methyl)-3,6-dihydropyridin-1(2*H*)-yl)(4-(4-bromophenyl)-1*H*-1,2,3-triazol-1-yl)methanone (11). The title compound was synthesized from (*R*)-6-((benzyloxy)methyl)-1,2,3,6-tetrahydropyridine (50.0 mg, 0.246 mmol) according to the procedure described for compound **3**. This furnished compound **11** (35.7 mg, 0.079 mmol, 32% yield). $[\alpha]_D^{22}$ = +136.3 (*c* = 2.5, $CHCl_3$). The enantiomeric purity was determined on a Daicel Chiralcel OD-H column (4.6 X 250 mm, 20:80 IPA/Hex, flow rate of 1 mL/min): 17.4 min, e.e.>93%. HRMS calculated for $C_{22}H_{21}BrN_4O_2$ $[M+H]^+$. 453.0921, found: 453.0920. ^{1}H NMR ($(CD_3)_2SO$, 400 MHz, 100 ^oC): δ 8.82 (s, 1H), 7.85 (d, *J* = 6.8 Hz, 2H), 7.66 (d, *J* = 6.8 Hz, 2H), 7.31-7.26 (m, 5H), 6.05 - 6.01 (m, 1H), 5.80 – 5.76 (m, 1H), 4.92 (s, 1H), 4.50 (s, 2H), 4.12 (dd, *J* = 5.6 Hz, 13.2 Hz, 1H), 3.75-3.67 (m, 2H), 3.38 (t, *J* = 13.2 Hz, 1H), 2.49 – 2.40 (m, 1H), 2.18 – 2.16 (m, 1H). ^{13}C NMR ($CDCl_3$, 400MHz) δ 145.54, 137.70, 132.06, 129.60, 128.62, 128.44, 127.79, 127.71, 127.52, 127.40, 122.52, 121.39, 73.27, 70.71, 55.56, 38.87, 24.83.

(*R*)-(6-((Benzyloxy)methyl)-3,6-dihydropyridin-1(2*H*)-yl)(4-(4-phenoxyphenyl)-1*H*-1,2,3-triazol-1-yl)methanone (12). The title compound was synthesized from ((*R*)-6-((benzyloxy)methyl)-1,2,3,6-tetrahydropyridine (70.0 mg, 0.344 mmol) and 4-(4-phenoxyphenyl)-1*H*-1,2,3-triazole (90.0 mg, 0.443 mmol) according to the procedure described for compound **3**. This furnished compound **12** (52.0 mg, 0.112 mmol, 32% yield). $[\alpha]_D^{20}$ = 112.5 (c = 1.0, $CHCl_3$). HRMS calculated for $C_{28}H_{26}N_4O_3$ $[M+H]^+$. 467.2078, found: 467.2077. ^{1}H NMR (400 MHz, $CDCl_3$) δ 8.15 (br, 1H), 7.76 (br, 2H), 7.39 – 7.27 (m, 7H), 7.17 – 7.10 (m, 1H), 7.08 – 7.04 (m, 4H), 6.09 – 5.96 (m, 1H), 5.70 (br s, 1H), 5.31 (br, 0.5H), 4.95 (br, 0.5H), 4.48 (br, 3H), 3.90 – 3.21 (m, 3H), 2.55 (br, 1H), 2.16 (br, 1H). ^{13}C NMR (101 MHz, $CDCl_3$) δ 157.85, 156.84, 149.76, 146.23, 137.78, 129.95, 128.51, 127.83, 127.75, 127.55, 127.51, 126.15, 124.74, 123.74, 120.73, 119.30, 119.07, 73.34, 70.70, 55.57, 38.83, 24.83.

(*R*)-(6-((Benzyloxy)methyl)-3,6-dihydropyridin-1(2*H*)-yl)(3-(4-bromophenyl)-1*H*-pyrazol-1-yl)methanone (13). The title compound was synthesized from (*R*)-6-((benzyloxy)methyl)-1,2,3,6-tetrahydropyridine (63.0 mg, 0.310 mmol) and 3-(4-bromophenyl)-1H-pyrazole (76.0 mg, 0.341 mmol) according to the procedures described for compound **3**. This furnished compound **13** (119 mg, 0.263 mmol, 85% yield). $[\alpha]_D^{20}$ = 93.8 (c = 1.0, $CHCl_3$). HRMS calculated for $C_{23}H_{22}BrN_3O_2$ $[M+H]^+$. 452.0968, found: 452.0969. ^{1}H NMR (400 MHz, $CDCl_3$) δ 8.12 (d, *J* = 2.8 Hz, 1H), 7.68 (d, *J* = 8.5 Hz, 2H), 7.50 (d, *J* = 8.4 Hz, 2H), 7.36 – 7.20 (m, 5H), 6.61 (d, *J* = 2.4 Hz, 1H), 6.05 – 5.96 (m, 1H), 5.82 – 5.74 (m, 1H), 5.35 (br, 1H), 4.55 (br, 3H), 3.85 (br, 1H), 3.79 – 3.75 (m, 1H), 3.32 (br, 1H), 2.55 (br, 1H), 2.10 (dt, *J* = 17.4, 4.1 Hz, 1H). ^{13}C NMR (101 MHz, $CDCl_3$) δ 152.18, 138.12, 133.54, 131.88, 131.46, 128.40, 127.67, 127.62, 127.52, 127.10, 125.48, 122.66, 114.16, 104.49, 73.30, 71.24, 54.98, 41.93, 25.14.

(*R*)-(6-((Benzyloxy)methyl)-3,6-dihydropyridin-1(2*H*)-yl)(4-(4-bromophenyl)-1*H*-imidazol-1-yl)methanone (14). The title compound was synthesized from (*R*)-6-((benzyloxy)methyl)-1,2,3,6-tetrahydropyridine (68.0 mg, 0.335 mmol) and 4-(4-bromophenyl)-1*H*-imidazole (82.0 mg, 0.368 mmol) according to the procedure

described for compound **3**. This furnished compound **14** (129 mg, 0.284 mmol, 85% yield). $[\alpha]_D^{20}$ = 80.8 (c = 1.0, $CHCl_3$). HRMS calculated for $C_{23}H_{22}BrN_3O_2$ $[M+H]^+$. 452.0968, found: 452.0965. ^{1}H NMR (400 MHz, $CDCl_3$) δ 8.03 (s, 1H), 7.67 (s, 1H), 7.54 (d, *J* = 8.3 Hz, 2H), 7.45 (d, *J* = 8.4 Hz, 2H), 7.37 – 7.27 (m, 5H), 5.98 – 5.95 (m, 1H), 5.59 (d, *J* = 8.4 Hz, 1H), 4.66 (br, 1H), 4.54 (s, 2H), 4.17 – 4.05 (m, 1H), 3.67 – 3.61 (m, 2H), 3.29 – 3.19 (m, 1H), 2.53 – 2.36 (m, 1H), 2.10 (dt, *J* = 16.0, 4.0 Hz, 1H). ^{13}C NMR (101 MHz, $CDCl_3$) δ 151.50, 140.97, 137.57, 137.38, 132.18, 131.67, 128.59, 128.06, 127.92, 126.70, 126.66, 123.97, 121.01, 114.11, 73.48, 69.66, 55.31, 38.52, 24.66.

(*R*)-(3-([1,1'-Biphenyl]-4-yl)-1*H*-pyrazol-1-yl)(6-((benzyloxy)methyl)-3,6-dihydropyridin-1(2*H*)-yl)methanone (15). A solution of (*R*)-(6-((benzyloxy)methyl)-3,6-dihydropyridin-1(2*H*)-yl) (3-(4-bromophenyl)-1*H*-pyrazol-1-yl)methanone (40.0 mg, 0.088 mmol) in dioxane and water (2:1; 6 mL) was treated with phenylboronic acid (21.6 mg, 0.177 mmol), K_2CO_3 (36.7 mg, 0.265 mmol), $PdCl_2$(dppf) (9.71 mg, 0.013 mmol) and the reaction mixture was stirred for 6h at 80 ^{o}C under Ar. The mixture was poured into water and extracted with ethyl acetate (3 x 20 mL), the organic layer was washed with water and brine, dried over $MgSO_4$ and concentrated under reduced pressure. The residue was purified by flash chromatography to furnish compound **15** (30.6 mg, 0.068 mmol, 77% yield). $[\alpha]_D^{20}$ = 52.9 (c = 1.0, $CHCl_3$). HRMS calculated for $C_{29}H_{27}N_3O_2$ $[M+H]^+$. 450.2176, found: 450.2173. ^{1}H NMR (400 MHz, $CDCl_3$) δ 8.15 (d, *J* = 2.7 Hz, 1H), 7.91 (d, *J* = 8.3 Hz, 2H), 7.65 – 7.62 (m, 4H), 7.49 – 7.43 (m, 2H), 7.39 – 7.25 (m, 6H), 6.70 (d, *J* = 2.4 Hz, 1H), 6.08 – 5.98 (m, 1H), 5.81 (d, *J* = 8.2 Hz, 1H), 5.42 (br, 1H), 4.58 (s, 3H), 3.89 (br, 1H), 3.82 (dd, *J* = 8.0, 4.0 Hz, 1H), 3.35 (br s, 1H), 2.65 – 2.53 (m, 1H), 2.13 (dt, *J* = 17.4, 4.1 Hz, 1H). ^{13}C NMR (101 MHz, $CDCl_3$) δ 153.01, 141.46, 140.72, 138.27, 134.16, 133.47, 131.55, 128.97, 128.49, 127.72, 127.62, 127.53, 127.24, 127.13, 126.78, 126.58, 125.67, 104.73, 73.38, 71.73, 54.41, 41.64, 25.18.

(*R*)-(3-([1,1'-Biphenyl]-4-yl)-1*H*-pyrazol-1-yl)(6-((benzyloxy)methyl)-3,6-dihydropyridin-1(2*H*)-yl)methanone (16). The title compound was synthesized from compound **14** (40.0 mg, 0.088 mmol) according to the procedure described for compound **15**. This furnished compound **16** (27.8 mg, 0.062 mmol, 70% yield). $[\alpha]_D^{20}$ = 82.0 (c = 1.0, $CHCl_3$). HRMS calculated for $C_{29}H_{27}N_3O_2$ $[M+H]^+$. 450.2176, found: 450.2166. ^{1}H NMR (400 MHz, $CDCl_3$) δ 8.06 (s, 1H), 7.78 (d, *J* = 8.1 Hz, 2H), 7.70 (s, 1H), 7.68 – 7.60 (m, 4H), 7.46 – 7.42 (m, 2H), 7.39 – 7.31 (m, 6H), 6.01 – 5.97 (m, 1H), 5.61 (d, *J* = 8.0 Hz, 1H), 4.71 (br, 1H), 4.57 (d, *J* = 12.0 Hz, 2H), 4.18 – 4.03 (m, 1H), 3.69 – 3.60 (m, 2H), 3.28 (br, 1H), 2.46 (br, 1H), 2.11 (dt, *J* = 17.5, 4.0 Hz, 1H). ^{13}C NMR (101 MHz, $CDCl_3$) δ 151.76, 141.86, 140.88, 140.13, 137.62, 137.54, 132.27, 128.88, 128.70, 128.14, 128.00, 127.88, 127.41, 127.35, 127.03, 125.60, 124.21, 113.91, 73.58, 69.82, 55.37, 39.91, 24.85.

(*R*)-(3-([1,1'-Biphenyl]-4-yl)-1*H*-1,2,4-triazol-1-yl)(6-((benzyloxy)methyl)-3,6-dihydropyridin-1(2*H*)-yl)methanone (17). A solution of (*R*)-6-((benzyloxy)methyl)-1,2,3,6-tetrahydropyridine (60.0 mg, 0.295 mmol) in THF

was treated with DIPEA (0.155 mL, 0.885 mmol) and bis(trichloromethyl) carbonate (43.8 mg, 0.148 mmol) and the reaction mixture was stirred for 30 min at 0 ^{o}C. After that the reaction mixture was poured into water and extracted with ethyl acetate (3 x 10 mL).The organic layer was washed with water, brine and dried over $MgSO_4$, filtered, and concentrated under reduced pressure. The intermediate was dissolved in THF and DIPEA (0.155 mL, 0.885 mmol), DMAP (36.1 mg, 0.295 mmol) and 3-bromo-1*H*-1,2,4-triazole (48.0 mg, 0.325 mmol) were added to the solution. The mixture was stirred for 2h at 60 ^{o}C and poured into saturated aqueous NH_4Cl solution (20 mL). The mixture was extracted with ethyl acetate (3 x 20 mL), washed with water, brine, dried over $MgSO_4$ and filtered. The solvents were removed under reduced pressure to yield the crude 1,2,4-triazole urea, which was purified by silica gel chromatography (1-10% ethyl acetate/pentane). The purified 1,2,4-triazole urea (40.0 mg, 0.106 mmol) was subsequently reacted with [1,1'-biphenyl]-4-ylboronic acid (46.2 mg, 0.233 mmol) according to the same procedure described for compound **15**. This furnished compound **17** (35.8 mg, 0.080 mmol, 27% yield overall). $[\alpha]_D^{22}$ = +109.3 (*c* = 0.6, $CHCl_3$). HRMS calculated for $C_{28}H_{26}N_4O_2$ $[M+H]^+$. 451.2129, found: 451.2128. ^{1}H NMR (400 MHz, $CDCl_3$) δ 8.76 (s, 1H), 8.20 (d, *J* = 8.1 Hz, 2H), 7.69 (d, *J* = 8.2 Hz, 2H), 7.65 (d, *J* = 7.5 Hz, 2H), 7.50 – 7.43 (m, 2H), 7.39 – 7.25 (m, 6H), 6.08 – 6.01 (m, 1H), 5.76 (d, *J* = 8.1 Hz, 1H), 5.48 (br, 1H), 4.54 (br, 3H), 3.81 – 3.69 (m, 2H), 3.34 (br, 1H), 2.55 (br, 1H), 2.15 (dt, *J* = 16.0, 4.0 Hz, 1H). ^{13}C NMR (101 MHz, $CDCl_3$) δ 162.33, 147.48, 142.84, 140.56, 137.96, 129.06, 128.99, 128.94, 128.55, 127.88, 127.81, 127.67, 127.50, 127.36, 127.21, 124.84, 114.20, 73.41, 71.32, 55.34, 42.71, 25.68.

4-Nitrophenyl (*R*)-6-((benzyloxy)methyl)-3,6-dihydropyridine-1(2*H*)-carboxylate (18). To a stirred solution of 4-nitrophenol (38.3 mg, 0.275 mmol), pyridine (0.032 mL, 0.394 mmol) in dichloromethane, triphosgene (29.2 mg, 0.098 mmol) was added. After stirring at room temperature for 1h, TLC was used to confirm that reaction was complete. (*R*)-6-((benzyloxy)methyl)-1,2,3,6-tetrahydropyridine (40.0 mg, 0.197 mmol) and pyridine were then added to the mixture, and the reaction mixture was stirred for 12h at room temperature. Dichloromethane was removed *in vacuo* and the residual was extracted with ethyl acetate (3 x 20 mL). The organic layer was washed with water, brine, and dried over $MgSO_4$. The crude product was purified by column chromatography (2-20% ethyl acetate/pentane) to afford compound **18** (56.5 mg, 0.153 mmol, 78% yield). $[\alpha]_D^{20}$ = 87.2 (c = 1.0, $CHCl_3$). HRMS [ESI+] m/z: calculated for $C_{20}H_{20}N_2O_5$ $[M+H]^+$. 369.3914, found: 369.3915. ^{1}H NMR (400 MHz, $CDCl_3$) δ 8.24 (d, *J* = 8.0 Hz, 1H), 8.14 (d, *J* = 12 Hz, 1H), 7.37 – 7.27 (m, 6H), 7.12 (d, *J* = 8.8 Hz, 1H), 6.02 (br, 1H), 5.74 (t, *J* = 12.7 Hz, 1H), 4.77 (br, 1H), 4.64 – 4.52 (m, 2H), 4.27 (dd, *J* = 13.3, 5.9 Hz, 1H), 3.71 – 3.58 (m, 2H), 3.31 (t, *J* = 11.0 Hz, 0.4H), 3.10 (td, *J* = 12.7, 3.4 Hz, 0.6H), 2.39 – 2.30 (m, 1H), 2.10 (d, *J* = 17.3 Hz, 1H). ^{13}C NMR (101 MHz, $CDCl_3$) δ 156.50, 152.99, 144.84, 137.90, 128.60, 128.00, 127.76, 125.50, 125.09, 124.41, 122.42, 73.49, 70.93, 52.97, 37.91, 24.85.

***tert*-Butyl (*R*)-2-(((*tert*-butyldiphenylsilyl)oxy)methyl)piperidine-1-carboxylate (20)**. Compound **19** was prepared according to the reported method.[26] Obtained

tert-Butyl (*R*)-6-(((*tert*-butyldiphenylsilyl)oxy)methyl)-3,6-dihydropyridine-1(2*H*)-carboxylate **19** (800 mg, 1.77 mmol) was dissolved in MeOH (40 mL) and Pd/C (188 mg, 0.177 mmol) were added subsequently. The reaction was stirred overnight under a hydrogen atmosphere. After filtering over Celite and evaporation of the solvents the crude target compound was obtained. The residue was purified by flash chromatography (pentane/EtOAc = 99 : 1 → 90 : 10) to furnish the title compound (763 mg, 1.68 mmol, 95% yield) as a colorless oil. ^{1}H NMR (400 MHz, $CDCl_3$) δ 7.67 (d, *J* = 7.0 Hz, 4H), 7.43 – 7.37 (m, 6H), 4.36 (br, 1H), 3.95 (d, *J* = 11.2 Hz, 1H), 3.72-3.65 (m, 2H), 2.63 (t, *J* = 12.1 Hz, 1H), 1.92 (d, *J* = 12.0 Hz, 1H), 1.55 (d, *J* = 8.0 Hz, 3H), 1.43 (app. s, 11H), 1.05 (s, 9H). ^{13}C NMR (101 MHz, $CDCl_3$) δ 155.08, 135.56, 133.54, 129.66, 127.70, 79.10, 61.55, 51.84, 40.10, 28.47, 26.84, 25.31, 25.01, 19.20. LC-MS m/z: calculated for $C_{27}H_{39}NO_3Si$ $[M+H]^+$ 454.27, found: 454.06.

***tert*-Butyl (*R*)-2-(hydroxymethyl)piperidine-1-carboxylate (21)**. A solution of TBAF (3.17 mL, 3.17 mmol) was added to a solution of *tert*-butyl (*R*)-2-(((*tert*-butyldiphenylsilyl)oxy)methyl) piperidine-1-carboxylate **20** (960 mg, 2.12 mmol) in THF (30 mL) with ice cooling and the mixture was stirred at R.T. for 18h. After being diluted with water, the mixture was extracted with ethyl acetate (3 x 30 mL), the organic layer was washed with water and brine, dried over $MgSO_4$ and concentrated under reduced pressure. The residue was purified by flash chromatography (pentane/EtOAc = 10 : 1 → 3 : 1) to furnish title compound (446 mg, 2.07 mmol, 98% yield) as a colorless oil. ^{1}H NMR (400 MHz, $CDCl_3$) δ 4.33 – 4.17 (m, 1H), 3.90 (d, *J* = 12.2 Hz, 1H), 3.76 – 3.71 (m, 1H), 3.57 (dd, *J* = 11.0, 6.4 Hz, 1H), 2.81 (t, *J* = 12.2 Hz, 1H), 2.70 (br, 1H), 1.67 (d, *J* = 11.2 Hz, 1H), 1.62 – 1.50 (m, 3H), 1.41 (app. s, 11H). ^{13}C NMR (101MHz, $CDCl_3$) δ 155.23, 79.81, 61.25, 52.40, 39.93, 28.34, 25.31, 25.15, 19.56. LC-MS m/z: calculated for $C_{11}H_{21}NO_3$ $[M+H]^+$ 216.15, found: 216.52.

***tert*-Butyl (*R*)-2-((benzyloxy)methyl)piperidine-1-carboxylate (22)**. To a solution of **21** (217 mg, 1.01 mmol), BnBr (345 mg, 2.02 mmol), TBAI (14.9 mg, 0.040 mmol) in dry DMF 5 mL, was added NaH (81.0 mg, 2.02 mmol, 60% in mineral oil) with ice cooling. The reaction mixture was stirred overnight and quenched with saturated aqueous ammonium chloride. The mixture was diluted with DCM and washed with water, brine, dried over $MgSO_4$ and concentrated under reduced pressure. The residue was purified by flash chromatography (pentane/EtOAc = 10 : 1 → 3 : 1) to furnish title compound (277 mg, 0.907 mmol, 90% yield) as a colorless oil. ^{1}H NMR (400 MHz, $CDCl_3$) δ 7.36 – 7.29 (m, 4H), 7.28 – 7.25 (m, 1H), 4.53 (d, *J* = 12.0 Hz, 2H), 4.44 (br, 1H), 3.97 (d, *J* = 12.9 Hz, 1H), 3.53 (d, *J* = 7.3 Hz, 2H), 2.72 (t, *J* = 12.6 Hz, 1H), 1.86 (d, *J* = 12.0 Hz, 1H), 1.67 – 1.49 (m, 3H), 1.44 (app. s, 11H). ^{13}C NMR (101 MHz, $CDCl_3$) δ 155.22, 138.44, 128.32, 127.51, 79.25, 72.77, 67.87, 49.29, 40.01, 28.45, 25.32, 25.22, 19.24. LC-MS m/z: calculated for $C_{18}H_{27}NO_3$ $[M+H]^+$ 306.20, found: 306.01.

(*R*)-2-((Benzyloxy)methyl)piperidine (23). Compound **22** (264 mg, 0.864 mmol) was dissolved in a mixture of 25% TFA in DCM (5 mL). The reaction mixture was stirred at r.t. for 2.5h until TLC analysis showed the reaction was completely converted. The

mixture was co-evaporated with toluene (3 x 20 mL), the residue diluted with ethyl acetate and washed with 10% Na_2CO_3, water, brine and dried over $MgSO_4$, and concentrated under reduced pressure to afford the crude product that was used without further purification (151 mg, 0.735 mmol, 85% yield) as a colorless oil. ^{1}H NMR (400 MHz, $CDCl_3$) δ 7.35 – 7.30 (m, 4H), 7.28 – 7.23 (m, 1H), 4.50 (d, *J* = 12.0 Hz, 2H), 3.44 (dd, *J* = 9.0, 3.6 Hz, 1H), 3.31 (t, *J* = 8.8 Hz, 1H), 3.06 (d, *J* = 11.6 Hz, 1H), 3.00 (br, 1H), 2.80 – 2.74 (m, 1H), 2.61 (td, *J* = 11.7, 2.8 Hz, 1H), 1.78 (d, *J* = 11.8 Hz, 1H), 1.59 (d, *J* = 13.1 Hz, 1H), 1.52 (d, *J* = 13.0 Hz, 1H), 1.49 – 1.26 (m, 2H), 1.21 – 1.03 (m, 1H). ^{13}C NMR (101 MHz, $CDCl_3$) δ 138.27, 128.36, 127.73, 127.60, 75.16, 73.37, 56.27, 46.41, 28.63, 26.18, 24.37. LC-MS m/z: calculated for $C_{13}H_{19}NO$ $[M+H]^+$ 206.15, found: 206.43.

***tert*-Butyl (*R*)-6-(hydroxymethyl)-3,6-dihydropyridine-1(2*H*)-carboxylate (24)**. The title compound was synthesized from **19** (596 mg, 1.32 mmol) and TBAF (1.59 mL, 1.59 mmol) according to the procedures described for compound **21**. This furnished title compound (196 mg, 0.920 mmol, 92% yield) as a yellow oil. ^{1}H NMR ($CDCl_3$, 400 MHz,) δ 5.86 (br, 1H), 5.58 (dt, *J* = 10.2, 2.8 Hz, 1H), 4.43 (br, 1H), 3.99 (br, 1H), 3.57 (d, *J* = 6.6 Hz, 2H), 3.29 (br, 1H), 2.86 (br, 1H), 2.10 (br, 1H), 1.88 (dt, *J* = 17.2, 4.2 Hz, 1H), 1.38 (s, 9H). ^{13}C NMR ($CDCl_3$, 101 MHz,) δ 154.48, 127.35, 124.97, 79.97, 64.71, 54.01, 38.22, 28.37, 24.80. LC-MS m/z: calculated for $C_{11}H_{19}NO_3$ $[M+H]^+$ 214.28, found: 214.72.

***tert*-Butyl (*R*)-6-((benzyloxy)methyl)-3,6-dihydropyridine-1(2*H*)-carboxylate (25)**. The title compound was synthesized from compound **24** (520 mg, 2.44 mmol) according to the procedures described for compound **22**. This furnished title compound (666 mg, 2.19 mmol, 90% yield) as a yellow oil. ^{1}H NMR ($CDCl_3$, 400 MHz): δ 7.35 – 7.23 (m, 5H), 5.88 – 5.84 (m, 1H), 5.58 (dt, *J* =12.0, 4.0 Hz, 1H), 4.52 (s, 2H), 4.28 (br, 1H), 4.05 (br, 1H), 3.56 (br, 1H), 3.51 (br, 1H), 2.93 (br, 1H), 2.29 (br, 1H), 1.97 (d, *J* = 8.7 Hz, 1H), 1.38 (s, 9H). ^{13}C NMR ($CDCl_3$, 101MHz) δ 154.53, 138.32, 128.31, 128.25, 127.66, 127.53, 127.37, 79.40, 72.03, 71.26, 51.90, 37.06, 28.40, 25.00. LC-MS m/z: calculated for $C_{18}H_{25}NO_3$ $[M+H]^+$ 304.40, found: 303.99.

(*R*)-6-((Benzyloxy)methyl)-1,2,3,6-tetrahydropyridine (26). The title compound was synthesized from compound **25** (303 mg, 0.999 mmol) according to the procedures described for compound **23**. This furnished title compound (181 mg, 0.890 mmol, 89% yield) as a colorless oil. ^{1}H NMR (400 MHz, $CDCl_3$) δ 7.37 – 7.30 (m, 4H), 7.29 – 7.24 (m, 1H), 5.86 – 5.83 (m, 1H), 5.53 (dt, *J* = 10.2, 1.9 Hz, 1H), 4.54 (d, *J* = 12.0 Hz, 2H), 3.62 – 3.54 (m, 1H), 3.56 – 3.46 (m, 1H), 3.46 – 3.37 (m, 1H), 3.09 – 3.03 (m, 1H), 2.87 – 2.81 (m, 1H), 2.24 – 2.13 (m, 2H), 2.04 – 1.97 (m, 1H). ^{13}C NMR (101 MHz, $CDCl_3$) δ 138.26, 128.43, 127.78, 127.68, 126.81, 73.61, 73.38, 53.82, 41.32, 25.98. LC-MS m/z: calculated for $C_{13}H_{17}NO$ $[M+H]^+$ 204.29, found: 204.68.

(*R*)-(6-((Benzyloxy)methyl)-3,6-dihydropyridin-1(2*H*)-yl)(3-bromo-1*H*-1,2,4-triazol -1-yl)methanone (30). A solution of **26** (60.0 mg, 0.295 mmol) in THF was treated with DIPEA (0.155 mL, 0.885 mmol) and bis(trichloromethyl) carbonate (43.8 mg,

0.148 mmol) and the reaction mixture was stirred for 30 min at 0 ^{o}C. After that the reaction mixture was poured into water and extracted with ethyl acetate (3 x 10 mL). The organic layer was washed with water and brine, dried over $MgSO_4$, filtered, and concentrated under reduced pressure. The intermediate was dissolved in THF and DIPEA (0.155 mL, 0.885 mmol), DMAP (36.1 mg, 0.295 mmol) and 4-(4-bromophenyl)-1*H*-1,2,3-triazole (48.0 mg, 0.325 mmol) were added to the solution. The mixture was stirred for 2h at 60 ^{o}C and poured into saturated aqueous NH_4Cl solution (20 mL). The mixture was extracted with ethyl acetate (3 x 20 mL), washed with water, brine, dried over $MgSO_4$ and filtered. The solvents were removed under reduced pressure to yield the crude product. Purification by silica gel chromatography (pentane/EtOAc 100:1 → 5:1) afforded title compound (45.0 mg, 0.119 mmol, 40% yield). ^{1}H NMR (400 MHz, $CDCl_3$) δ 8.49 (s, 1H), 7.54 – 7.02 (m, 5H), 6.01 (dd, *J* = 10.3, 6.0 Hz, 1H), 5.69 (s, 1H), 5.51 – 4.79 (m, 1H), 4.70 – 4.21 (m, 3H), 3.65 (s, 2H), 3.26 (s, 1H), 2.43 (d, *J* = 14.4 Hz, 1H), 2.22 – 2.01 (m, 1H). ^{13}C NMR (101 MHz, $CDCl_3$) δ 155.54, 147.91, 141.23, 137.74, 128.56, 127.94, 127.69, 127.42, 124.86, 73.32, 70.52, 54.66, 29.80, 25.04. LC-MS m/z: calculated for $C_{16}H_{17}BrN_4O_2$ $[M+H]^+$ 378.24, found: 378.59.

(*3R,6R*)-6-((Benzyloxy)methyl)-3-((*tert*-butyldiphenylsilyl)oxy)-1,2,3,6-tetrahydro pyridine (28). The Boc-protected compound *tert*-butyl (*3R,6R*)-6-((benzyloxy)methyl)-3-((*tert*-butyldiphenylsilyl)oxy)-3,6-dihydropyridine-1(2*H*)-carboxylate **27** was prepared according the route reported.[23,24] The title compound was synthesized from **27** (500 mg, 0.896 mmol) according to the procedures described for compound **23** and furnished the free amine compound (347 mg, 0.758 mmol, 85% yield) as a light yellow oil. ^{1}H NMR (400 MHz, $CDCl_3$) δ 7.70 – 7.65 (m, 4H), 7.39 – 7.22 (m, 11H), 5.71 (s, 2H), 4.54 (s, 2H), 4.0 – 4.06 (m, 1H), 3.55 – 3.51 (m, 1H), 3.49 – 3.45 (m, 1H), 3.39 – 3.35(m, 1H), 2.98 (dd, *J* = 13.8, 4.2Hz, 1H), 2.77 (dd, *J* = 12.2, 4.0 Hz, 1H), 2.56 (br s, 1H), 1.07 (s, 9H). ^{13}C NMR (101 MHz, $CDCl_3$) δ 138.19, 135.80, 135.69, 134.15, 134.01, 130.67, 130.39, 129.65, 129.58, 128.33, 127.62, 127.54, 127.52, 127.51, 73.18, 71.82, 64.24, 53.71, 48.88, 26.96, 19.15.

(*3R,6S*)-6-((Benzyloxy)methyl)-3-((*tert*-butyldiphenylsilyl)oxy)-1,2,3,6-tetrahydro pyridine (31). The Boc-protected *tert*-butyl (*3R,6S*)-6-((benzyloxy)methyl)-3-((*tert*-butyldiphenylsilyl)oxy)-3,6-dihydropyridine-1(2*H*)-carboxylate was prepared according the route reported.[23,24] The target compound was synthesized from Boc-protected compound (500 mg, 0.896 mmol) according to the procedure described for compound **23**. This furnished title compound (357 mg, 0.781 mmol, 87% yield) as a light yellow oil. ^{1}H NMR (400 MHz, $CDCl_3$) δ 7.75 (br s, 1H), 7.69 – 7.63 (m, 4H), 7.43 – 7.34 (m, 6H), 7.32 – 7.23(m, 5H), 5.77 (d, *J* = 12.2 Hz, 1H), 5.57 (d, *J* = 11.8 Hz, 1H), 4.47 (s, 2H), 4.33 (s, 1H), 3.67 – 3.65(m, 1H), 3.50 (dd, *J* = 8.1, 3.7 Hz, 1H), 3.37 – 3.33 (m, 1H), 3.18 (dd, *J* = 12.3, 4.1 Hz, 1H), 2.81 – 2.79 (m, 1H), 1.06 (s, 9H). ^{13}C NMR (101 MHz, $CDCl_3$) δ 137.84, 135.93, 135.86, 135.80, 133.89, 133.77, 131.95, 129.88, 129.83, 128.46, 127.82, 127.79, 127.74, 127.48, 73.41, 71.89, 65.16, 53.34, 48.61, 27.01, 19.23.

(*3S,6R*)-6-((Benzyloxy)methyl)-3-((*tert*-butyldimethylsilyl)oxy)-1,2,3,6-tetrahydropyridine (32). The Boc-protected *tert*-butyl (*3S,6R*)-6-((benzyloxy)methyl)-3-((*tert*-butyldimethylsilyl)oxy)-3,6-dihydropyridine-1(2*H*)-carboxylate was prepared according the reported route.[23,24] To a solution of Boc-protected compound (210 mg, 0.480 mmol) was added 10% TFA in DCM (5 mL) with ice cooling, the reaction mixture was stirred at r.t. for 0.5h and subsequently co-evaporated with toluene (3x20 mL), the residue was diluted with ethyl acetate, washed with 10% Na_2CO_3, water, brine and dried over $MgSO_4$, and concentrated under reduced pressure, which afforded the crude product (97.0 mg, 0.291 mmol, 54% yield) as a light yellow oil. ^{1}H NMR (400 MHz, $CDCl_3$) δ 7.37 – 7.31 (m, 4H), 7.30 – 7.25 (m, 1H), 5.82 – 5.68 (m, 1H), 5.60 (dt, *J* = 10.3, 1.8 Hz, 1H), 4.60 – 4.45 (m, 2H), 4.35 – 4.29 (m, 1H), 3.62 – 3.54 (m, 1H), 3.50 (dd, *J* = 8.9, 4.0 Hz, 1H), 3.37 – 3.28 (m, 1H), 3.22 (dd, *J* = 12.1, 5.7 Hz, 1H), 2.64 (dd, *J* = 11.5, 8.5 Hz, 1H), 2.25 (br, 1H), 0.90 (s, 9H), 0.09 (s, 3H), 0.08 (s, 3H). ^{13}C NMR (101 MHz, $CDCl_3$) δ 138.14, 132.52, 128.49, 128.28, 127.84, 127.78, 73.83, 73.51, 65.84, 54.06, 50.44, 25.98, 18.31, -4.51, -4.62.

***tert*-Butyl (2*R*,3*R*)-3-hydroxy-2-(hydroxymethyl)-3,6-dihydropyridine-1(2*H*)-carboxylate (34).** Compound **33** was prepared according to the reported methods.[28] To a solution of compound **33** (790 mg, 2.92 mmol) in MeOH (25 mL) was added catalytic amount of *p*-TsOH (27.8 mg, 0.146 mmol). The reaction mixture was stirred at r.t. for 2.5h until TLC showed the reaction was completed. The reaction mixture was evaporated under reduced pressure and the residue was purified by flash chromatography to furnish title compound *tert*-butyl (*2R,3R*)-3-hydroxy-2-(hydroxymethyl)-3,6-dihydropyridine-1(2*H*)-carboxylate (576 mg, 2.51 mmol, 86% yield) as a light yellow oil. ^{1}H NMR (400 MHz, $CDCl_3$) δ 5.77 (br, *J* = 12.0 Hz, 1H), 5.69 (d, *J* = 12.0 Hz, 1H), 4.68 – 4.57 (m, 2H), 4.16 – 4.04 (m, 1H), 4.00 – 3.98 (m, 1H), 3.61 (dd, *J* = 11.3, 6.7 Hz, 1H), 3.51 (d, *J* = 16.5 Hz, 1H), 3.02 (br, 2H), 1.47 (s, 9H). ^{13}C NMR (101 MHz, $CDCl_3$) δ 155.03, 128.19, 124.16, 80.79, 66.91, 60.43, 53.37, 40.94, 28.50. LC-MS m/z: calculated for $C_{11}H_{19}NO_4$ $[M+H]^+$ 230.28, found: 230.86.

***tert*-Butyl (*2R,3R*)-2-((benzyloxy)methyl)-3-hydroxy-3,6-dihydropyridine-1(2*H*)-carboxylate (35)**. 2-Aminoethylborinate (10mol%), compound **34** (250 mg, 1.09 mmol), KI (217 mg, 1.31 mmol) and K_2CO_3 (181 mg, 1.31 mmol) were transferred to a 2-dram vial containing a magnetic stir bar. The vial was then sealed with a septum and purged with argon. Anhydrous acetonitrile was added to the flask, followed by benzyl bromide (0.233 mL, 1.96 mmol). The resulting mixture was stirred at 60 ^{o}C for 24h. The mixture was then transferred to a separation funnel containing water and ethyl acetate, the organic layer was separated, and the aqueous layer was extracted two more times with ethyl acetate. The combined organic layers were washed with brine, dried over $MgSO_4$, filtered, and concentrated in *vacuo*. The resulting crude material was purified by silica gel chromatography (pentane/EtOAc 10:1 → 2:1) to furnish title compound (310 mg, 0.972 mmol, 89% yield) as colorless oil. ^{1}H NMR (400 MHz, $CDCl_3$) δ 7.37 – 7.19 (m, 5H), 5.73 (d, *J* = 10.4 Hz, 1H), 5.65 (br, 1H), 4.91 (br, 1H), 4.59 – 4.49 (m, 1H), 4.44 (d, *J* = 11.9 Hz, 1H), 4.08 (br, 1H), 3.85 – 3.73 (m, 1H), 3.72

– 3.33 (m, 3H), 1.46 (s, 9H). ^{13}C NMR (101 MHz, $CDCl_3$) δ 155.11, 137.89, 128.68, 128.41, 127.73, 127.63, 123.92, 80.32, 73.08, 66.21, 65.93, 50.01, 40.73, 28.46. LC-MS m/z: calculated for $C_{18}H_{25}NO_4$ $[M+H]^+$ 320.40, found: 320.76.

***tert*-Butyl (*2R,3R*)-2-((benzyloxy)methyl)-3-((*tert*-butyldimethylsilyl)oxy)- 3,6-dihydropyridine-1(2*H*)-carboxylate (36).** Imidazole (243 mg, 3.57 mmol) and TBS-Cl (484 mg, 3.21 mmol) were added to a stirred solution of *tert*-butyl (*2S,3R*)-2-((benzyloxy)methyl)- 3-hydroxy-3,6-dihydropyridine-1(2*H*)-carboxylate **35** (570 mg, 1.79 mmol) in DMF with ice cooling, and stirred at room temperature for 2h. The reaction mixture was quenched with water, and extracted with EtOAc (3 x 50 mL). The organic layer was washed with water and brine, dried over $MgSO_4$, filtered, and concentrated *in vacuo*. The resulting crude material was purified by silica gel chromatography (pentane/EtOAc 100:1 →10:1) to furnish the title compound (735 mg, 1.70 mmol, 95% yield) as a colorless oil. ^{1}H NMR (400 MHz, $CDCl_3$) δ 7.39 – 7.28 (m, 5H), 5.70 – 5.57 (m, 2H), 5.03 – 4.84 (m, 1H), 4.79 – 4.41 (m, 3H), 4.32 – 4.22 (m, 0.5H), 4.12 – 4.03 (m, 0.5H), 3.77 – 3.70 (m, 1H), 3.64 – 3.52 (m, 1H), 3.53 – 3.41 (m, 1H), 1.53 (s, 9H), 0.94 (s, 9H), 0.15 (s, 6H). ^{13}C NMR (101 MHz, $CDCl_3$) δ 155.34, 138.63, 129.08, 128.34, 127.73, 127.52, 124.54, 79.86, 72.60, 66.18, 65.12, 53.81, 40.48, 28.47, 25.85, 18.11, -4.69, -4.84. LC-MS m/z: calculated for $C_{24}H_{39}NO_4$ Si $[M+H]^+$ 434.66, found: 434.12.

(*2R,3R*)-2-((Benzyloxy)methyl)-3-((*tert*-butyldimethylsilyl)oxy)-1,2,3,6-tetrahydro pyridine (37). To a solution of compound **36** (540 mg, 1.25 mmol) was added 10% TFA in DCM (5mL) in DCM with ice cooling. The reaction mixture was stirred at r.t. for 0.5h. The reaction mixture was co-evaporated with toluene (3 x 20 mL), the residue was diluted with ethyl acetate and washed with 10% Na_2CO_3, water, brine and dried over $MgSO_4$. Concentration under reduced pressure afforded the crude product (290 mg, 0.871 mmol, 69% yield). ^{1}H NMR (400 MHz, $CDCl_3$): δ 7.40 – 7.34 (m, 4H), 7.30 – 7.28 (m, 1H), 5.88 – 5.79 (m, 2H), 4.53 (s, 2H), 4.14 – 4.07 (m, 1H), 3.54 – 3.51 (m, 2H), 3.38 – 3.34 (m, 1H), 3.32 (d, *J* = 4.0 Hz, 1H), 2.99 (dt, *J* = 4.0 Hz, 8.0 Hz, 1H), 2.94 – 2.87 (m, 1H), 0.87 (s, 9H), 0.06 (s, 3H), 0.05 (s, 3H). ^{13}C NMR (101 MHz, $CDCl_3$) δ 138.39, 130.42, 128.48, 128.18, 128.01, 127.74, 73.58, 70.37, 63.46, 57.38, 44.90, 26.01, 18.21, -3.89, -4.72. LC-MS m/z: calculated for $C_{19}H_{31}NO_2Si$ $[M+H]^+$ 334.55, found: 334.92.

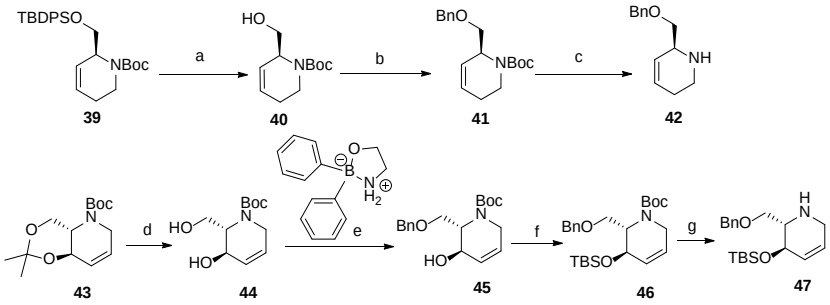

Scheme 3. Synthesis of key intermediates **42** and **47**. Reagents and conditions: (a) TBAF, THF, r.t. 92%; (b) BnBr, TBAI, NaH, DMF, 87%; (c) 25% TFA (v/v), DCM, r.t., 82%; (d) cat. *p*-TsOH, MeOH, 84%; (e) BnBr, KI, MeCN, 60 °C, 90%; (f) TBSCl, imidazole, DMF, 95%; (g) 10% TFA, DCM, 0 °C, 71%.

***tert*-Butyl (*S*)-6-(hydroxymethyl)-3,6-dihydropyridine-1(2*H*)-carboxylate (40)**. The title compound was synthesized from compound **39** (596 mg, 1.32 mmol) according to the procedures described for compound **21**. This furnished title compound (196 mg, 0.920 mmol, 92% yield) as a yellow oil. ^{1}H NMR ($CDCl_3$, 400 MHz): δ 5.89 – 5.77 (m, 1H), 5.57 (dt, *J* = 10.2, 2.8 Hz, 1H), 4.39 (br s, 1H), 3.96 (br s, 1H), 3.54 (d, *J* = 6.4 Hz, 2H), 3.33 (br s, 1H), 2.84 (br s, 1H), 2.08 (br s, 1H) 1.86 (dt, *J* = 16.0 Hz, 4.0Hz, 1H), 1.36 (s, 9H). ^{13}C NMR ($CDCl_3$, 101 MHz) δ 158.67, 127.20, 125.01, 79.87, 64.33, 53.93, 38.13, 28.32, 24.75. LC-MS m/z: calculated for $C_{11}H_{19}NO_3$ $[M+H]^+$ 214.28, found: 214.65.

***tert*-Butyl (*S*)-6-((benzyloxy)methyl)-3,6-dihydropyridine-1(2*H*)-carboxylate (41)**. The title compound was synthesized from alcohol **40** (360 mg, 1.69 mmol) according to the procedures described for compound **22**. This furnished title compound (446 mg, 1.47 mmol, 87% yield) as a yellow oil. ^{1}H NMR ($CDCl_3$, 400 MHz): δ 7.37 – 7.21 (m, 5H), 5.93 (br, 1H), 5.74 (d, *J* = 12.0 Hz, 1H), 4.58 – 4.50 (m, 3H), 4.19 – 4.06 (m, 1H), 3.56 (br, 2H), 3.04 – 2.83 (m, 1H), 2.19 (br, 1H), 1.97 (d, *J* = 12.0 Hz, 1H), 1.44 (s, 9H). ^{13}C NMR ($CDCl_3$, 101 MHz,) δ 154.74, 138.53, 128.43, 127.60, 127.55, 126.92, 125.99, 79.74, 73.14, 71.43, 51.96, 37.17, 28.56, 25.03. LC-MS m/z: calculated for $C_{18}H_{25}NO_3$ $[M+H]^+$ 304.40, found: 303.89.

(*S*)-6-((Benzyloxy)methyl)-1,2,3,6-tetrahydropyridine (42). The title compound was synthesized from **41** (500 mg, 1.65 mmol) according to the procedures described for compound **23**. This furnished (*S*)-6-((benzyloxy)methyl)-1,2,3,6-tetrahydropyridine (275 mg, 1.35 mmol, 82% yield) as a yellow oil. ^{1}H NMR (400 MHz, $CDCl_3$): δ 7.34 – 7.29 (m, 4H), 7.19 – 7.23 (m, 1H), 5.86 - 5.81 (m, 1H), 5.54 – 5.50 (m, 1H), 4.52 (d, *J* = 8.0 Hz, 2H), 3.59 – 3.55 (m, 1H), 3.46 (dd, *J* = 12.0, 4.0 Hz, 1H), 3.38 (app. t, *J* = 8.0 Hz, 1H), 3.07 – 3.01 (m, 1H), 2.86 – 2.79 (m, 1H), 2.36 (br s, 1H), 2.21 – 2.11(m, 1H), 2.06 – 1.91 (m, 1H). ^{13}C NMR (101 MHz, $CDCl_3$) δ 138.10, 128.25, 127.59, 127.49, 127.47, 126.66, 73.42, 73.19, 53.64, 41.15, 25.81. LC-MS m/z: calculated for $C_{13}H_{17}NO$ $[M+H]^+$ 204.29, found: 204.88.

***tert*-Butyl (*2S,3R*)-3-hydroxy-2-(hydroxymethyl)-3,6-dihydropyridine-1(2*H*)-carboxylate (44)**. Compound **43** was prepared according to the literature reported method.[28] The title compound was synthesized from **43** (280 mg, 1.1 mmol) and *p*-TsOH (28.0 mg, 0.15 mmol), according to the procedures described for compound **34**. This furnished title compound (200 mg, 0.87 mmol, 84% yield) as a light yellow oil. ^{1}H NMR (400 MHz, $CDCl_3$) δ 5.87 – 5.81 (m, 1H), 5.77 (br, 1H), 4.38 – 4.28 (m, 1H), 4.12 (br, 2H), 3.89 (br, 2H), 3.53 – 3.33 (m, 3H), 1.37 (s, 9H). ^{13}C NMR (101 MHz, $CDCl_3$) δ 156.28, 127.16, 124.51, 80.31, 62.76, 60.64, 57.79, 41.08, 28.33. LC-MS m/z: calculated for $C_{11}H_{19}NO_4$ $[M+H]^+$ 230.28, found: 230.59.

***tert*-Butyl (*2S,3R*)-2-((benzyloxy)methyl)-3-hydroxy-3,6-dihydropyridine-1(2*H*)-carboxylate (45)**. Title compound was synthesized from compound **44** (280 mg, 1.22 mmol), benzyl bromide (0.140 mL, 1.18 mmol), KI (130 mg, 0.79 mmol) and K_2CO_3 (109 mg, 0.79 mmol), according to the procedures described for the preparation of compound **35**. This furnished title compound (188 mg, 0.590 mmol, 90% yield) as yellow oil. ^{1}H NMR (400 MHz, $CDCl_3$) δ 7.47 – 7.13 (m, 5H), 5.89 (br, 1H), 5.84 (br, 1H), 4.80 – 4.38 (m, 3H), 4.24 (br, 1H), 4.09 (br, 1H), 3.49 – 3.31 (m, 3H), 1.45 (s, 9H). ^{13}C NMR (101 MHz, $CDCl_3$) δ 155.72, 138.10, 128.30, 127.93, 127.56, 127.49, 124.72, 80.09, 72.73, 67.80, 63.56, 56.46, 40.19, 28.36. LC-MS m/z: calculated for $C_{18}H_{25}NO_4$ $[M+H]^+$ 320.40, found: 320.08.

***tert*-Butyl (*2S,3R*)-2-((benzyloxy)methyl)-3-((*tert*-butyldimethylsilyl)oxy)-3,6-dihydro pyridine-1(2*H*)-carboxylate (46)**. The title compound was synthesized from compound **45** (570 mg, 1.78 mmol), and TBS-Cl (480 mg, 3.21 mmol), according to the procedures described for compound **36**. This furnished title compound (740 mg, 1.70 mmol, 95% yield) as a light yellow oil. ^{1}H NMR (400 MHz, $CDCl_3$) δ 7.34 – 7.25 (m, 5H), 5.79 (d, *J* = 11.4 Hz, 2H), 4.66 – 4.47 (m, 3H), 4.34 (br d, *J* = 20.0 Hz 1H), 4.19 (br, 1H), 3.37 (m, 3H), 1.46 (s, 9H), 0.90 (s, 9H), 0.11 (s, 3H), 0.08 (s, 3H). ^{13}C NMR (101 MHz, $CDCl_3$) δ 155.40, 138.29, 128.32, 127.56, 127.38, 127.20, 124.66, 79.58, 72.72, 68.21, 64.35, 56.50, 39.94, 28.41, 25.91, 18.26, -4.36, -4.54. LC-MS m/z: calculated for $C_{24}H_{39}NO_4Si$ $[M+H]^+$ 434.66, found: 434.89.

(*2S,3R*)-2-((Benzyloxy)methyl)-3-((*tert*-butyldimethylsilyl)oxy)-1,2,3,6-tetrahydro pyridine (47). The title compound was synthesized from compound **46** (210 mg, 0.484 mmol) according to the procedures described for compound **37**. This furnished crude product (120 mg, 0.344 mmol, 71% yield) as a light yellow oil. ^{1}H NMR (400 MHz, $CDCl_3$) δ 7.43 – 7.39 (m, 4H), 7.38 – 7.32 (m, 1H), 5.85 – 5.80 (m, 1H), 5.71 (dd, *J* = 10.2, 2.1 Hz, 1H), 4.70 – 4.53 (m, 2H), 4.18 (d, *J* = 8.2 Hz, 1H), 3.80 (dd, *J* = 9.0, 2.8 Hz, 1H), 3.60 (dd, *J* = 9.0, 6.8 Hz, 1H), 3.53 – 3.45 (m, 1H), 3.37 – 3.31 (m, 1H), 2.85 – 2.81 (m, 1H), 2.61 (br, 1H), 0.95 (s, 9H), 0.15 (s, 3H), 0.11 (s, 3H). ^{13}C NMR (101 MHz, $CDCl_3$) δ 138.17, 130.30, 128.44, 127.89, 127.84, 127.73, 73.47, 71.06, 66.61, 59.02, 44.66, 29.72, 25.87, -4.09, -4.76. LC-MS m/z: calculated for $C_{19}H_{31}NO_2Si$ $[M+H]^+$ 334.55, found: 334.68.

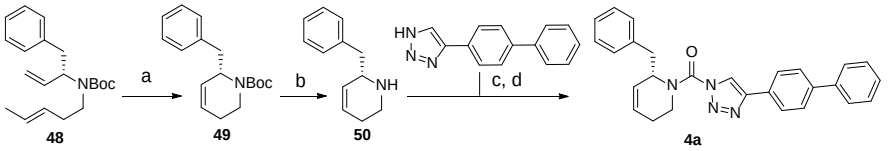

Scheme 4. Enantioselective synthesis of compound **4a**. Reagents and conditions: (a) Grubbs I cat. 4 mol %, DCM, reflux, 48h; (b) 25% TFA, DCM; (c) DIPEA, Triphosgene, THF, 0 °C; (d) DIPEA, DMAP, triazole , THF, 60 °C.

***tert*-Butyl (*S*)-6-benzyl-3,6-dihydropyridine-1(2*H*)-carboxylate (49)**. The title compound was prepared according to the literature reported method as depicted in S.Scheme 2. In brief, the diene **48** (425 mg, 1.35 mmol) was dissolved in DCM (10 mL) and purged with argon. After the addition of Grubb's 1st generation catalyst (42.0 mg, 0.050 mmol, 3.6 mol%) and refluxing overnight TLC analysis confirmed complete conversion. The solvent was evaporated and the crude product purified by silica gel column chromatography using pentane : EtOAc = 97 : 3 as the eluent to afford the title compound (252 mg, 0.920 mmol, 68% yield). $[\alpha]_D^{21}$ = +161 (c = 1.0, $CHCl_3$). HRMS calculated for $C_{17}H_{23}NO_2$ $[M+H]^+$: 274.1802; found: 274.1802. ^{1}H NMR (400 MHz, $CDCl_3$, 60 °C) δ 7.28 – 7.21 (m, 2H), 7.20 – 7.14 (m, 3H), 5.79 (dd, *J* = 10.3, 6.1 Hz, 1H), 5.54 (dt, *J* = 10.3, 3.3 Hz, 1H), 4.54 (s, 1H), 4.11 (s, 1H), 2.89 (dd, *J* = 13.0, 6.2 Hz, 1H), 2.83 – 2.67 (m, 2H), 2.15 (m, 1H), 1.88 (m, 1H), 1.39 (s, 9H). ^{13}C NMR (101 MHz, $CDCl_3$, 60 °C) δ 154.28, 138.23, 129.36, 128.10, 127.94, 126.06, 125.38, 79.17, 53.47, 40.20, 36.30, 28.29, 24.85.

(*S*)-6-Benzyl-1,2,3,6-tetrahydropyridine (50). Boc-protected compound **49** (100 mg, 0.366 mmol) was added 25% TFA in DCM (5 mL), the reaction mixture was stirred at r.t. for 0.5h. The reaction mixture was co-evaporated with toluene (3 x 20 mL). The residue was diluted with ethyl acetate, washed with 10% Na_2CO_3, water, brine, dried over $MgSO_4$ and concentrated under reduced pressure. The crude product **50** was used without further purification. ^{1}H NMR (400 MHz, $CDCl_3$) δ 7.33 – 7.26 (m, 2H), 7.25 – 7.18 (m, 3H), 5.85 – 5.74 (m, 1H), 5.70 – 5.54 (m, 1H), 3.56 – 3.53 (m, 1H), 3.07 – 3.03 (m, 1H), 2.85 – 2.73 (m, 2H), 2.71 – 2.65 (m, 1H), 2.27 – 2.13 (m, 1H), 2.03 (br, 1H), 1.99 – 1.89 (m, 1H). ^{13}C NMR (101 MHz, $CDCl_3$) δ 138.99, 130.34, 129.30, 128.47, 126.32, 126.13, 55.46, 42.61, 42.15, 25.91.

***tert*-Butyl (*R*)-6-benzyl-3,6-dihydropyridine-1(2*H*)-carboxylate (51)**. The title compound was prepared as described for the preparation of **49**, and afforded compound **51** (491 mg, 1.80 mmol). $[\alpha]_D^{21}$ = -172 (c =1.0 $CHCl_3$). HRMS calculated for $C_{17}H_{23}NO_2$ $[M+H]^+$: 274.1802; found: 274.1803. IR 2974, 2926, 1690, 1454, 1416, 1391, 1364, 1337, 1279, 1250, 1171, 1107. ^{1}H NMR (400 MHz, $CDCl_3$) δ 7.38 – 7.08 (m, 5H), 5.81 (s, 1H), 5.63 – 5.48 (m, 1H), 4.68 – 4.42 (m, 1H), 4.33 – 3.94 (m, 1H), 2.99 – 2.82 (m, 1H), 2.84 – 2.67 (m, 2H), 2.19 (m, 1H), 2.02 – 1.83 (m, 1H), 1.36 (s, 9H). ^{13}C NMR (101 MHz, $CDCl_3$) δ 154.34, 138.25, 129.40, 128.22, 127.70, 126.15, 125.63, 79.33, 53.84, 40.27, 35.87, 28.29, 24.85.

(*R*)-6-Benzyl-1,2,3,6-tetrahydropyridine (52). The title compound was prepared as described for **50** from *tert*-butyl (*R*)-6-benzyl-3,6-dihydropyridine-1(2*H*)-carboxylate (130 mg, 0.476 mmol). The crude product was obtained that was used without further purification. ^{1}H NMR (400 MHz, $CDCl_3$) δ 7.33 – 7.25 (m, 2H), 7.25 – 7.15 (m, 3H), 5.81 – 5.76 (m, 1H), 5.65 – 5.61 (m, 1H), 3.56 – 3.50 (m, 1H), 3.06 - 3.01 (m, 1H), 2.85 – 2.72 (m, 2H), 2.72 – 2.49 (m, 1H), 2.28 – 2.07 (m, 1H), 1.99 – 1.90 (m, 1H), 1.88 (br, 1H). ^{13}C NMR (101 MHz, $CDCl_3$) δ 138.95, 130.32, 129.22, 128.39, 126.24, 126.05, 55.40, 42.58, 42.10, 25.88.

References

1. Bisogno, T.; Howell, F.; Williams, G.; Minassi, A.; Cascio, M. G.; Ligresti, A.; Matias, I.; Schiano-Moriello, A.; Paul, P.; Williams, E. J.; Gangadharan, U.; Hobbs, C.; Di Marzo, V.; Doherty, P. Cloning of the first sn1-DAG lipases points to the spatial and temporal regulation of endocannabinoid signaling in the brain. *The Journal of Cell Biology* **2003,** 163, 463-468.
2. Reisenberg, M.; Singh, P. K.; Williams, G.; Doherty, P. The diacylglycerol lipases: structure, regulation and roles in and beyond endocannabinoid signalling. *Philosophical transactions of the Royal Society of London. Series B, Biological sciences* **2012,** 367, 3264-3275.
3. Katona, I.; Freund, T. F. Multiple functions of endocannabinoid signaling in the brain. *Annual Review of Neuroscience* **2012,** 35, 529-558.
4. Gao, Y.; Vasilyev, D. V.; Goncalves, M. B.; Howell, F. V.; Hobbs, C.; Reisenberg, M.; Shen, R.; Zhang, M. Y.; Strassle, B. W.; Lu, P.; Mark, L.; Piesla, M. J.; Deng, K.; Kouranova, E. V.; Ring, R. H.; Whiteside, G. T.; Bates, B.; Walsh, F. S.; Williams, G.; Pangalos, M. N.; Samad, T. A.; Doherty, P. Loss of retrograde endocannabinoid signaling and reduced adult neurogenesis in diacylglycerol lipase knock-out mice. *The Journal of Neuroscience : the official journal of the Society for Neuroscience* **2010,** 30, 2017-2024.
5. Tanimura, A.; Yamazaki, M.; Hashimotodani, Y.; Uchigashima, M.; Kawata, S.; Abe, M.; Kita, Y.; Hashimoto, K.; Shimizu, T.; Watanabe, M.; Sakimura, K.; Kano, M. The endocannabinoid 2-arachidonoylglycerol produced by diacylglycerol lipase alpha mediates retrograde suppression of synaptic transmission. *Neuron* **2010,** 65, 320-327.
6. Nomura, D. K.; Morrison, B. E.; Blankman, J. L.; Long, J. Z.; Kinsey, S. G.; Marcondes, M. C. G.; Ward, A. M.; Hahn, Y. K.; Lichtman, A. H.; Conti, B.; Cravatt, B. F. Endocannabinoid hydrolysis generates brain prostaglandins that promote neuroinflammation. *Science* **2011,** 334, 809-813.
7. Kohnz, R. A.; Nomura, D. K. Chemical approaches to therapeutically target the metabolism and signaling of the endocannabinoid 2-AG and eicosanoids. *Chemical Society Reviews* **2014,** 43, 6859-6869.
8. Rouzer, C. A.; Marnett, L. J. Endocannabinoid oxygenation by cyclooxygenases, lipoxygenases, and cytochromes P450: cross-talk between the eicosanoid and endocannabinoid signaling pathways. *Chemical Review* **2011,** 111, 5899-5921.

9. Kohnz, R. A.; Nomura, D. K. Chemical approaches to therapeutically target the metabolism and signaling of the endocannabinoid 2-AG and eicosanoids. *Chemical Society reviews* **2014,** 43, 6859-6869.
10. Muccioli, G. G. Endocannabinoid biosynthesis and inactivation, from simple to complex. *Drug Discovery Today* **2010,** 15, 474-483.
11. Baggelaar, M. P.; Janssen, F. J.; van Esbroeck, A. C. M.; den Dulk, H.; Allara, M.; Hoogendoorn, S.; McGuire, R.; Florea, B. I.; Meeuwenoord, N.; van den Elst, H.; van der Marel, G. A.; Brouwer, J.; Di Marzo, V.; Overkleeft, H. S.; van der Stelt, M. Development of an activity-based probe and in silico design reveal highly selective inhibitors for diacylglycerol lipase-alpha in brain. *Angewandte Chemie International Edition* **2013,** 52, 12081-12085.
12. Baggelaar, M. P.; Chameau, P. J. P.; Kantae, V.; Hummel, J.; Hsu, K. L.; Janssen, F.; van der Wel, T.; Soethoudt, M.; Deng, H.; den Dulk, H.; Allara, M.; Florea, B. I.; Di Marzo, V.; Wadman, W. J.; Kruse, C. G.; Overkleeft, H. S.; Hankemeier, T.; Werkman, T. R.; Cravatt, B. F.; van der Stelt, M. Highly selective, reversible inhibitor identified by comparative chemoproteomics modulates diacylglycerol lipase activity in neurons. *Journal of the American Chemical Society* **2015,** 137, 8851-8857.
13. Janssen, F. J.; Baggelaar, M. P.; Hummel, J. J. A.; Overkleeft, H. S.; Cravatt, B. F.; Boger, D. L.; van der Stelt, M. Comprehensive analysis of structure-activity relationships of alpha-ketoheterocycles as sn-1-diacylglycerol lipase alpha inhibitors. *Journal of Medicinal Chemistry* **2015,** 58, 9742-9753.
14. Janssen, F. J.; Deng, H.; Baggelaar, M. P.; Allara, M.; van der Wel, T.; den Dulk, H.; Ligresti, A.; van Esbroeck, A. C.; McGuire, R.; Di Marzo, V.; Overkleeft, H. S.; van der Stelt, M. Discovery of glycine sulfonamides as dual inhibitors of sn-1-diacylglycerol lipase alpha and alpha/beta-hydrolase domain 6. *Journal of Medicinal Chemistry* **2014,** 57, 6610-6622.
15. Ogasawara, D.; Deng, H.; Viader, A.; Baggelaar, M. P.; Breman, A.; den Dulk, H.; van den Nieuwendijk, A. M.; Soethoudt, M.; van der Wel, T.; Zhou, J.; Overkleeft, H. S.; Sanchez-Alavez, M.; Mo, S.; Nguyen, W.; Conti, B.; Liu, X.; Chen, Y.; Liu, Q. S.; Cravatt, B. F.; van der Stelt, M. Rapid and profound rewiring of brain lipid signaling networks by acute diacylglycerol lipase inhibition. *Proceedings of the National Academy of Sciences of the United States of America* **2016,** 113, 26-33.
16. Marrs, W. R.; Blankman, J. L.; Horne, E. A.; Thomazeau, A.; Lin, Y. H.; Coy, J.; Bodor, A. L.; Muccioli, G. G.; Hu, S. S. J.; Woodruff, G.; Fung, S.; Lafourcade, M.; Alexander, J. P.; Long, J. Z.; Li, W. W.; Xu, C.; Moller, T.; Mackie, K.; Manzoni, O. J.; Cravatt, B. F.; Stella, N. The serine hydrolase ABHD6 controls the accumulation and efficacy of 2-AG at cannabinoid receptors. *Nature Neuroscience* **2010,** 13, 951-967.
17. Pribasnig, M. A.; Mrak, I.; Grabner, G. F.; Taschler, U.; Knittelfelder, O.; Scherz, B.; Eichmann, T. O.; Heier, C.; Grumet, L.; Kowaliuk, J.; Romauch, M.; Holler, S.; Anderl, F.; Wolinski, H.; Lass, A.; Breinbauer, R.; Marsche, G.; Brown, J. M.; Zimmermann, R. alpha/beta Hydrolase domain-containing 6 (ABHD6) degrades the late endosomal/lysosomal lipid bis(monoacylglycero)phosphate. *Journal of Biological Chemistry* **2015,** 290, 29869-29881.
18. Thomas, G.; Betters, J. L.; Lord, C. C.; Brown, A. L.; Marshall, S.; Ferguson, D.; Sawyer, J.; Davis, M. A.; Melchior, J. T.; Blume, L. C.; Howlett, A. C.; Ivanova, P. T.; Milne, S. B.; Myers, D. S.; Mrak, I.; Leber, V.; Heier, C.; Taschler, U.; Blankman, J. L.; Cravatt, B. F.; Lee, R. G.;

Crooke, R. M.; Graham, M. J.; Zimmermann, R.; Brown, H. A.; Brown, J. M. The serine hydrolase ABHD6 is a critical regulator of the metabolic syndrome. *Cell Reports* **2013,** 5, 508-520.

19. Fisette, A.; Tobin, S.; Decarie-Spain, L.; Bouyakdan, K.; Peyot, M. L.; Madiraju, S. R.; Prentki, M.; Fulton, S.; Alquier, T. alpha/beta-Hydrolase domain 6 in the ventromedial hypothalamus controls energy metabolism flexibility. *Cell Reports* **2016,** 17, 1217-1226.
20. Tchantchou, F.; Zhang, Y. M. Selective Inhibition of Alpha/Beta-Hydrolase Domain 6 attenuates neurodegeneration, alleviates blood brain barrier breakdown, and improves functional recovery in a mouse model of traumatic brain injury. *Journal of Neurotraum* **2013,** 30, 565-579.
21. Hsu, K. L.; Tsuboi, K.; Adibekian, A.; Pugh, H.; Masuda, K.; Cravatt, B. F. DAGLbeta inhibition perturbs a lipid network involved in macrophage inflammatory responses. *Nature Chemical Biology* **2012,** 8, 999-1007.
22. Hsu, K. L.; Tsuboi, K.; Whitby, L. R.; Speers, A. E.; Pugh, H.; Inloes, J.; Cravatt, B. F. Development and optimization of piperidyl-1,2,3-triazole ureas as selective chemical probes of endocannabinoid biosynthesis. *Journal of Medicinal Chemistry* **2013,** 56, 8257-8269.
23. van den Nieuwendijk, A. M.; Ruben, M.; Engelsma, S. E.; Risseeuw, M. D.; van den Berg, R. J.; Boot, R. G.; Aerts, J. M.; Brussee, J.; van der Marel, G. A.; Overkleeft, H. S. Synthesis of L-altro-1-deoxynojirimycin, D-allo-1-deoxynojirimycin, and D-galacto-1-deoxynojirimycin from a single chiral cyanohydrin. *Organic letters* **2010,** 12, 3957-3959.
24. van den Nieuwendijk, A. M. C. H.; van den Berg, R. J. B. H. N.; Ruben, M.; Witte, M. D.; Brussee, J.; Boot, R. G.; van der Marel, G. A.; Aerts, J. M. F. G.; Overkleeft, H. S. Synthesis of eight 1-deoxynojirimycin isomers from a single chiral cyanohydrin. *European Journal of Organic Chemistry* **2012**, 3437-3446.
25. Jiang, J. B.; Artola, M.; Beenakker, T. J. M.; Schroder, S. P.; Petracca, R.; de Boer, C.; Aerts, J. M. F. G.; van der Marel, G. A.; Codee, J. D. C.; Overkleeft, H. S. The synthesis of cyclophellitol-aziridine and its configurational and functional isomers. *European Journal of Organic Chemistry* **2016**, 3671-3678.
26. Banba, Y.; Abe, C.; Nemoto, H.; Kato, A.; Adachi, I.; Takahata, H. Asymmetric synthesis of fagomine and its congeners. *Tetrahedron-Asymmetry* **2001,** 12, 817-819.
27. Garner, P.; Park, J. M.; Malecki, E. A Stereodivergent synthesis of D-Erythro-sphingosine and D-Threo-sphingosine from L-serine. *Journal of Organic Chemistry* **1988,** 53, 4395-4398.
28. Takahata, H.; Banba, Y.; Ouchi, H.; Nemoto, H. Concise and highly stereocontrolled synthesis of 1-deoxygalactonojirimycin and its congeners using dioxanylpiperidene, a promising chiral building block. *Organic letters* **2003,** 5, 2527-2529.
29. Lee, D.; Williamson, C. L.; Chan, L. N.; Taylor, M. S. Regioselective, borinic acid-catalyzed monoacylation, sulfonylation and alkylation of diols and carbohydrates: expansion of substrate scope and mechanistic studies. *Journal of the American Chemical Society* **2012,** 134, 8260-8267.
30. Baggelaar, M. P.; Janssen, F. J.; van Esbroeck, A. C.; den Dulk, H.; Allara, M.; Hoogendoorn, S.; McGuire, R.; Florea, B. I.; Meeuwenoord, N.; van den Elst, H.; van der Marel, G. A.; Brouwer, J.; Di Marzo, V.; Overkleeft, H. S.; van der Stelt, M. Development of an activity-based probe and in silico design reveal highly selective inhibitors for

diacylglycerol lipase-alpha in brain. *Angewandte Chemie International Edition* **2013,** 52, 12081-12085.

31. Cravatt, B. F.; Wright, A. T.; Kozarich, J. W. Activity-based protein profiling: from enzyme chemistry to proteomic chemistry. *Annual Review of Biochemistry* **2008,** 77, 383-414.
32. van der Wel, T.; Janssen, F. J.; Baggelaar, M. P.; Deng, H.; den Dulk, H.; Overkleeft, H. S.; van der Stelt, M. A natural substrate-based fluorescence assay for inhibitor screening on diacylglycerol lipase alpha. *Journal of Lipid Research* **2015,** 56, 927-935.

7

Activity-based protein profiling reveals the mitochondrial localization of monoacylglycerol lipase

Based on
H. Deng, D. M. van Elsland, A. C. M. van Esbroeck, T. van der Wel, H. den Dulk, H. S. Overkleeft, S. I. van Kasteren, M. van der Stelt; *manuscript in preparation*

Introduction

Activity-based probes (ABPs) are versatile chemical tools to monitor enzyme function in a wide range of biological systems.[1] ABPs are small molecules that covalently and irreversibly inhibit enzymes and that are equipped with a tag (e.g., fluorophore or biotin) through which the target enzyme, or enzyme family, is visualized in living systems by fluorescence microscopy, or enriched to enable identification and characterization using chemical proteomics methodology by mass spectrometers. To date, various ABPs have been designed to target a number of enzyme families, such as serine hydrolases,[2,3] cysteine proteases,[4] phosphatases,[5] kinases,[6] glycosidases,[7] metalloproteases[8] and various oxidoreductases.[9] These ABPs can been used for various applications, including target discovery, (sub)cellular target localization, characterization of enzyme active sites, inhibitor discovery, lead optimization and target engagement.[10] Most of the existing ABPs target numerous enzymes within a family, enabling the global profiling of many enzymes in parallel. Thus, those ABPs

provide a robust method to evaluate the potency and proteome-wide selectivity of inhibitors in a single experiment. Tailor-made ABPs, on the other hand, target only a single enzyme. This provides additional advantages, including visualization of active enzymes in cells, tissues and even animals. The development of such selective tailor-made ABPs poses substantial challenges. Excellent physico-chemical and biological properties, such as solubility, selectivity, cell permeability and pharmacokinetics, are important criteria to apply tailor-made ABPs to living biological systems. Currently, there are only a limited number of tailor-made ABPs available to study enzyme activity in cellular imaging studies.[9,11,12]

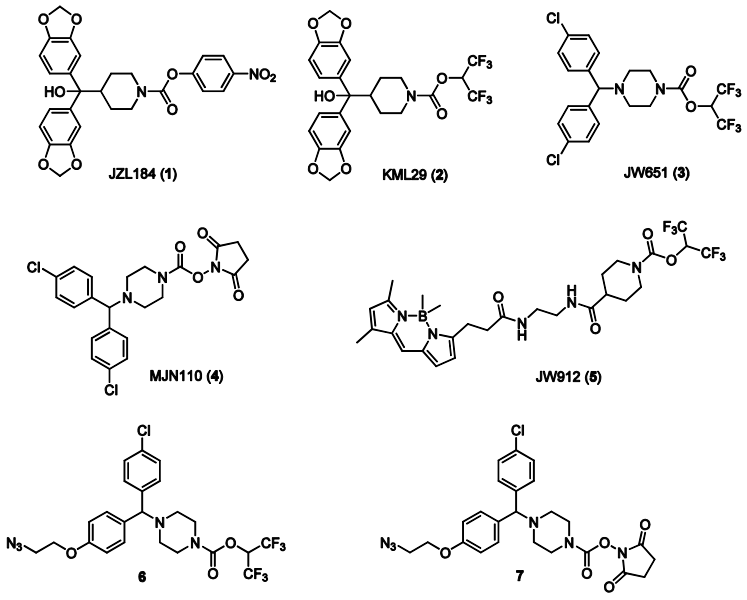

Figure 1. Chemical structures of known MAGL inhibitors **1**-**4** and ABP **5**, and clickable probes **6** and **7** described in this chapter.

Monoacylglycerol lipase (MAGL) is a membrane-associated serine hydrolase, which exists in two splice forms with molecular weight of 33 and 35 kDa, respectively.[13] MAGL links endocannabinoid and eicosanoid biology via hydrolysis of the endocannabinoid 2-arachidonoylglycerol (2-AG), thereby releasing glycerol and arachidonic acid (AA). The latter is the precursor of pro-inflammatory eicosanoids.[14] Additionally, Nomura *et al.* found that MAGL is highly expressed in aggressive human cancer cell lines and primary tumours,[10] where it regulates an oncogenic signaling network of lipids that promotes cancer cell migration, invasion, survival and tumor growth. Consequently, inhibitors of MAGL are proposed to have therapeutic potential as anti-cancer drugs. Several covalent, irreversible MAGL inhibitors (**1**-**4**) and an ABP (**5**) have been reported in the literature (Figure 1). These agents are, however, not

completely selective, which hampers the interpretation of the biological results obtained with these compounds. A common off-target of these inhibitors is the serine hydrolase α,β-hydrolase domain 6 (ABHD6), a lipase that metabolizes various classes of lysophospholipids involved in oncogenic signaling. Of note, ABHD6 has also been reported to act as the principle lipase responsible for 2-AG hydrolysis in cells lacking MAGL.[15] Thus, it would be of value to have a tailored-ABP to study the role of MAGL activity in oncogenic lipid signaling in cancer cells. This chapter reports on the discovery of a new ABP for MAGL that does not label ABHD6 and is used to visualize the subcellular localization of MAGL in MCF7 breast cancer cells and can be applied *in vivo*.

Results and discussion

Development of a highly selective activity-based probe for MAGL

Chemical probes **6** and **7** targeting MAGL were designed, based on compounds **4** and **5**, in which a para-chlorine substituent of the phenyl ring was replaced by a 2-azidoethanol group to enable ligation to an alkyne-containing fluorophore at a late stage. Compounds **6** and **7** were synthesized in 8 steps starting from commercially available building blocks (Scheme 1). In brief, treatment of **8** with sodium azide, subsequent mesylation of azido alcohol **9** and alkylation of 4-hydroxybenzaldehyde with **10** afforded intermediate **11**. Treatment of aldehyde **11** with *p*-chlorophenylmagnesiumbromide, followed by thionyl chloride treatment provided compound **13**, which was coupled to *tert*-butyl piperazine-1-carboxylate. Removal of Boc-protecting group using HCl in 1,4-dioxane gave the free amine **15** in quantitative yield. Finally, direct coupling with the corresponding alcohols of 1,1,1,3,3,3-hexafluoroisopropanol or *N*-hydroxysuccinimide yielded azide probes **6** and **7**.

The activity of compounds **6** and **7** was assessed in a real time, fluorescence-based natural substrate assay using membrane fractions of HEK293T cells transiently transfected with recombinant human MAGL.[16] JZL184 (**1**), which was used as a positive control, displayed a pIC_{50} of 7.7 ± 0.1 (Figure 2a). Compounds **6** and **7** were also potent inhibitors with pIC_{50} values of 8.0±0.1 and 7.2±0.2, respectively. Competitive ABPP, using the broad-spectrum serine hydrolase ABP FP-TAMRA, was employed to analyze the inhibitor activity and selectivity on endogenously expressed serine hydrolases in mouse brain (Figure 2b-d). Compounds **6** and **7** inhibited the labeling of MAGL with a pIC_{50} of 6.7±0.1 and 6.8±0.1, respectively (Figure 2b-d). ABHD6 was detected as the only off-target for compound **6** at 10 µM, while compound **7** inhibited labeling of ABHD6 and an additional unidentified off-target (Figure 2c, indicated by the arrow). Reaction of mouse

proteome treated with compounds **6** or **7** to a fluorophore (Cy5-alkyne) using click chemistry demonstrated labeling of the two MAGL splice forms.

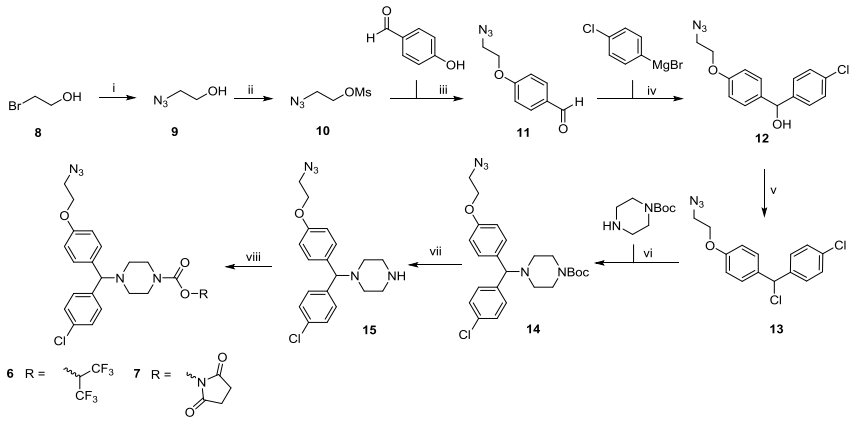

Scheme 1. Reagents and conditions: i) NaN_3, H_2O, 80 °C, 96%; ii) MsCl, TEA, DCM; iii) 4-hydroxybenzaldehyde, K_2CO_3, DMF, 80 °C, 86%; iv) 4-chlorophenyl magnesium bromide, THF, -78 °C, 89%; v) $SOCl_2$, DCM, 40 °C; vi) *tert*-butyl piperazine-1-carboxylate, K_2CO_3, DCM, 40 °C, 89%; vii) HCl in 1,4-dioxane, ethyl acetate; viii) corresponding alcohol, triphosgene, DIPEA, DCM, 54% (**6**), 87% (**7**).

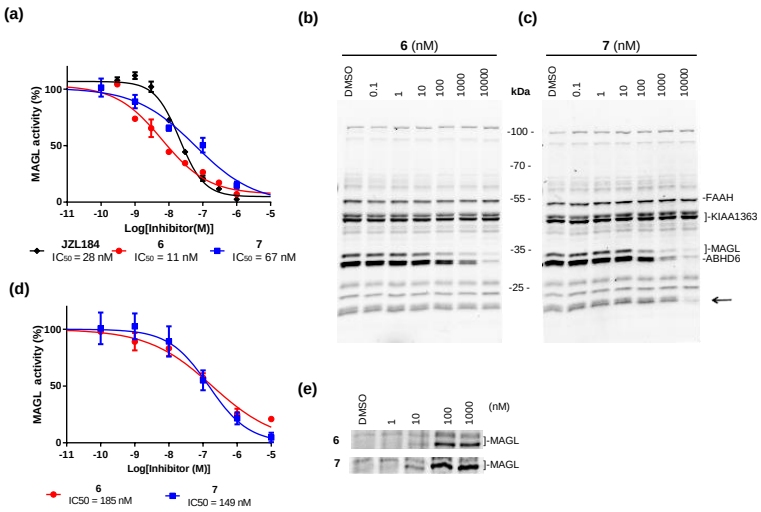

Figure 2. Activity and selectivity profile of MAGL inhibitors **6** and **7**. (a) Concentration-dependent inhibition curves of **6**, **7** and JZL184 (positive control) against hMAGL as determined with a natural substrate fluorescence assay (±SEM, n = 4); (b-c) Competitive ABPP with **6** (b) and **7** (c) (0.1 nM – 10000 nM) or vehicle (DMSO) in mouse brain membrane proteome using a broad-spectrum probe FP-TAMRA (500 nM, 20 min); (d) Concentration-dependent inhibition curves of **6** and **7** against endogenous MAGL as measured from gel (b) and (c) (±SEM, n = 3); (e) Two-step labeling of MAGL in mouse brain membrane proteome using **6** or **7** (1 – 1000 nM) followed by CuAAC reaction with alkyne-Cy5 tag (5 µM).

In view of its high selectivity profile, inhibitor **6** was conjugated to three different fluorophores: BODIPY-red, BODIPY-green and Cy5, which resulted in three different ABPs (**16**, **17** and **18,** respectively) (Figure 3a). All three probes were tested in the natural substrate assay and displayed a pIC_{50} of 5.5±0.4, 7.0±0.3 and 8.0±0.2, respectively (Figure 3b). The gel-based ABPP confirmed that probe **18** selectively and concentration-dependently labeled endogenous MAGL in mouse and rat brain proteomes (Figure 3c and 3d). MAGL activity was already visualized at low nanomolar concentrations and could be prevented by preincubation with JZL184 (Figure 4a). Surprisingly, competitive ABPP with FP-TAMRA and MB064 did not reveal any off-target activity for ABP **18**, including ABHD6 (Figure 4b,c). To further confirm the selectivity profile of ABP **18** over ABHD6, a real-time, fluorescence-based natural substrate assay was performed. Indeed, compound **18** did not inhibit ABHD6 up to 10 µM concentrations (Figure 4d). Collectively, these data show that ABP **18** serves as a potent and highly selective fluorescent probe for MAGL and is termed **LEI-463**.

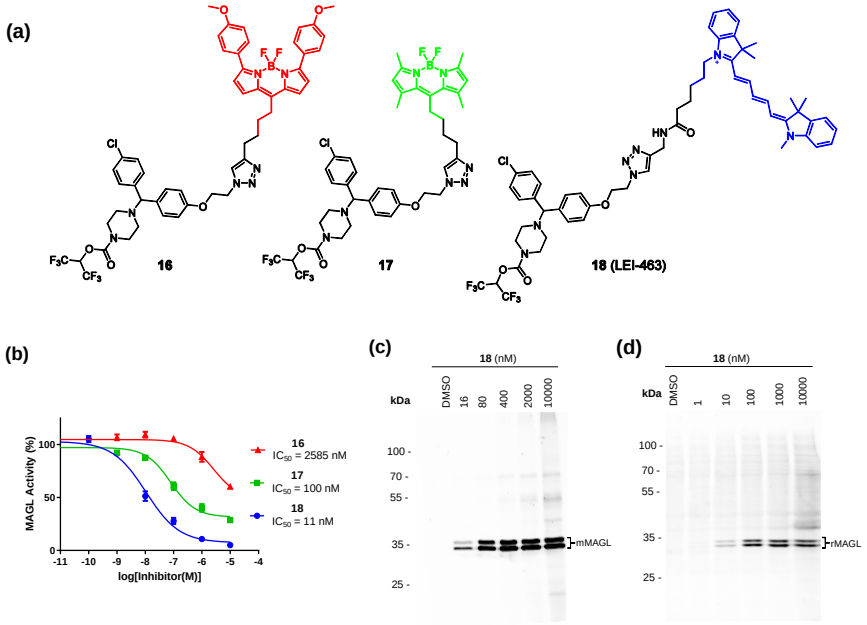

Figure 3. Development and characterization of fluorescent activity-based probes **16**-**18**. (a) Chemical structures of tailored-MAGL activity-based probes **16-18**; (b) Concentration-dependent inhibition curves of ABPs **16**-**18** against hMAGL as determined with 2-AG substrate assay, (±SEM, n=4); (c,d) Concentration-dependent labeling of MAGL activity with probe **18** (LEI-463) (30 min) in mouse (c) or rat (d) brain membrane proteome.

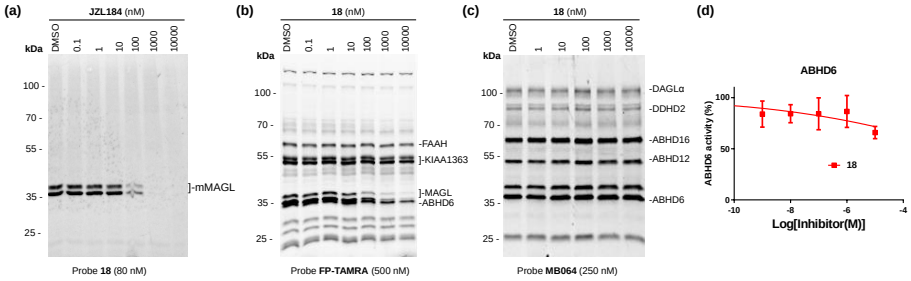

Figure 4. Selectivity profile of ABP **18** (LEI-463): (a) Competitive ABPP with MAGL inhibitor JZL184 (0.1-10000 nM) in mouse brain membrane proteome using **18** (80 nM; 30 min); (b,c) Competitive ABPP with **18** (0.1-10000 nM) in mouse brain proteome using probe FP-TAMRA (b) (500 nM, 20 min) or MB064 (c) (250 nM, 20 min); Of note, MB064 labels ABHD6 but not MAGL; (d) Concentration-dependent inhibition against hABHD6 by **18** as measured by 2-AG natural substrate assay (±SEM, n = 4).

Imaging of MAGL activity in cancer cells using LEI-463

Next, it was investigated whether LEI-463 can label MAGL in living cells. To this end, mouse neuroblastoma Neuro2A cells, which do not have endogenous MAGL activity,[17,18] were transiently transfected with a pcDNA3.1-construct in which MAGL is fused to Green Fluorescent Protein (eGFP). The cells were preincubated, 24h after transfection, with vehicle (DMSO), MAGL inhibitor JZL184 (10 µM) or ABHD6 inhibitor KT195 (10 µM) for 2h, and subsequently treated with LEI-463 (100 nM, 2h). Fluorescence microscopy was performed to study the co-localization of MAGL-eGFP (green colour) and LEI-463 labeling (red colour). Clear co-localization was observed in vehicle-treated cells, whereas JZL184, but not KT195, abolished MAGL labeling by LEI-463 (Figure 5a). Target engagement and selectivity of LEI-463 was confirmed in a gel-based ABPP experiment (Figure 5b-d). Together, these results indicate that LEI-463 is cell penetrable and selectively labels MAGL in living cells.

Next, it was assessed whether endogenous MAGL activity could be visualized by LEI-463 in breast cancer MCF7 cells.[10] Confocal fluorescent microscopy of MCF7 cells treated with LEI-463 (100 nM) showed a time-dependent increase in labeling of intracellular compartments, which could be prevented by pre-treatment of the cells with compound **6** (Figure 6a-b). Gel-based ABPP studies confirmed target engagement and selectivity of the probe in *in situ*-treated MCF7 cells (Figure 6c-e). Interestingly, prolonged incubation times (> 2h) at high concencentrations (> 100 nM) revealed an additional unidentified off-target with a molecular weight of 25 kDa, which could not be outcompeted by JZL184 or KT195.

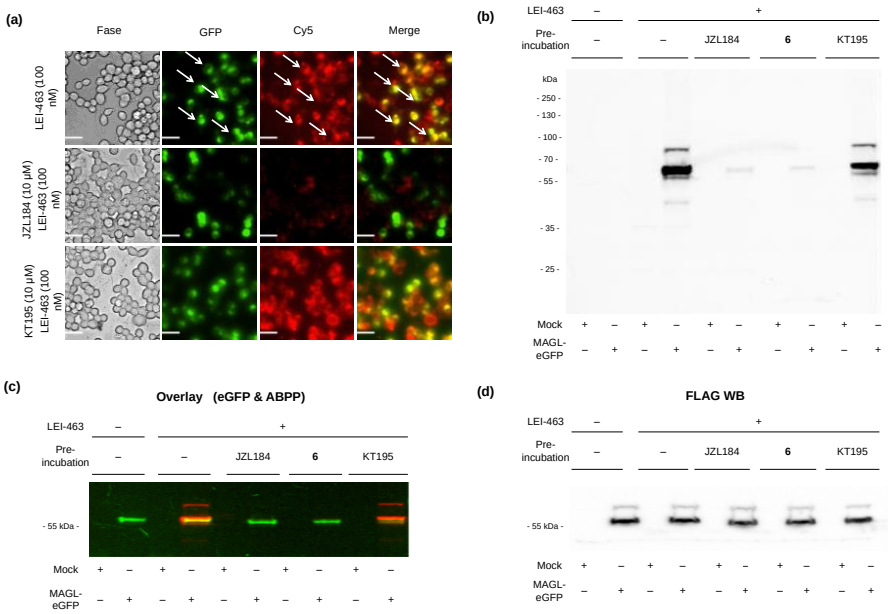

Figure 5. Imaging and labeling of recombinant MAGL-eGFP with probe LEI-463 in Neuro 2A cells. (a) Neuro2A cells transiently transfected with MAGL-eGFP were pre-incubated with vehicle (DMSO), JZL184 (10 µM) or ABHD6 inhibitor KT195 (10 µM) for 2h, followed by incubation with ABP LEI-463 (100 nM, 2h). Cells were washed with PBS (3x), and then used for fluorescent microscopy imaging. Arrows indicate representative examples of co-localization of MAGL-eGFP and probe labeled-MAGL. Scale bars: 50 µm; (b-c) MAGL-eGFP- or mock-transfected Neuro2A cells were pre-treated with MAGL inhibitors JZL184 or **6** (10 µM, 2h), KT195 (10 µM, 2h) or vehicle (DMSO), followed by treatment with probe LEI-463 (100 nM, 2h). After washing with PBS (3 x), cells were harvested and analyzed by gel-based ABPP. Scanning of the gel on Cy5 fluorescence shows probe labeling (b), and scanning on GFP fuorescence shows recombinant MAGL-eGFP signal (c); (d) MAGL-FLAG-eGFP expression levels in transfected Neuro2A cells as determined by anti-FLAG western blot.

To determine the subcellular membrane structures that contain MAGL activity in MCF7 cells, counterstaining experiments for LEI463-treated cells were performed with markers of various subcellular organelles, such as lyso-tracker that specifically stains acidic lysomosomes,[19-21] mito-tracker that contains a mildly thiol-reactive chloromethyl moiety for labeling mitochondria[22,23] and an ER-tracker that labels the endoplasmic reticulum.[24,25] Confocal imaging of LEI-463-treated cells on wavelengths specific to each marker revealed significant colocalization of MAGL activity with mitochondria and partial overlap with the ER, whereas very little co-localization with the punctate signals of lysosomes was found (Figure 7).

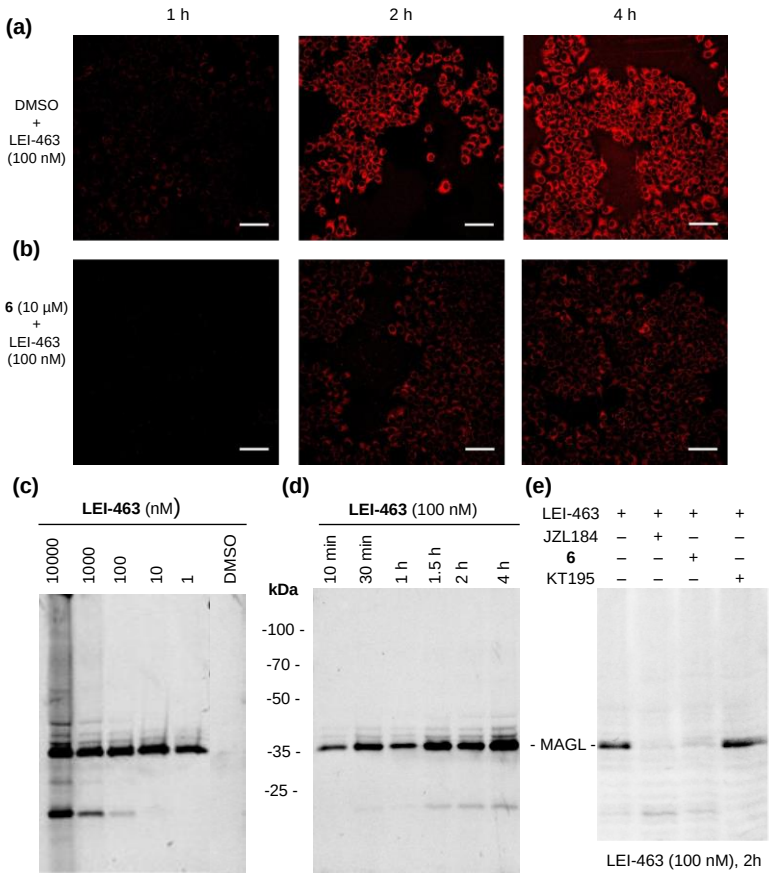

Figure 6. Detecting MAGL activity in cancer cells with probe LEI-463. (a,b) Confocal imaging of LEI-463-treated (100 nM) MCF7 cells with or without competitor **6** (10 µM); Laser setting: 20x lens; Cy5 channel: Gain: 754v, 18% intensity, excitation: 635 nm, emission: 660-700 nm; scale bar: 20 µm; (c,d) Gel analysis of LEI-463-treated MCF7 cells with various concentrations (c), and indicated incubation time (d); (e) Gel analysis of MCF7 cells treated with LEI-463 (100 nM, 2h) in presence or absence of following inhibitors: MAGL inhibitors JZL184 (10 µM, 2h), **6** (10 µM, 2h), or ABHD6 inhibitor KT195 (10 µM, 2h);

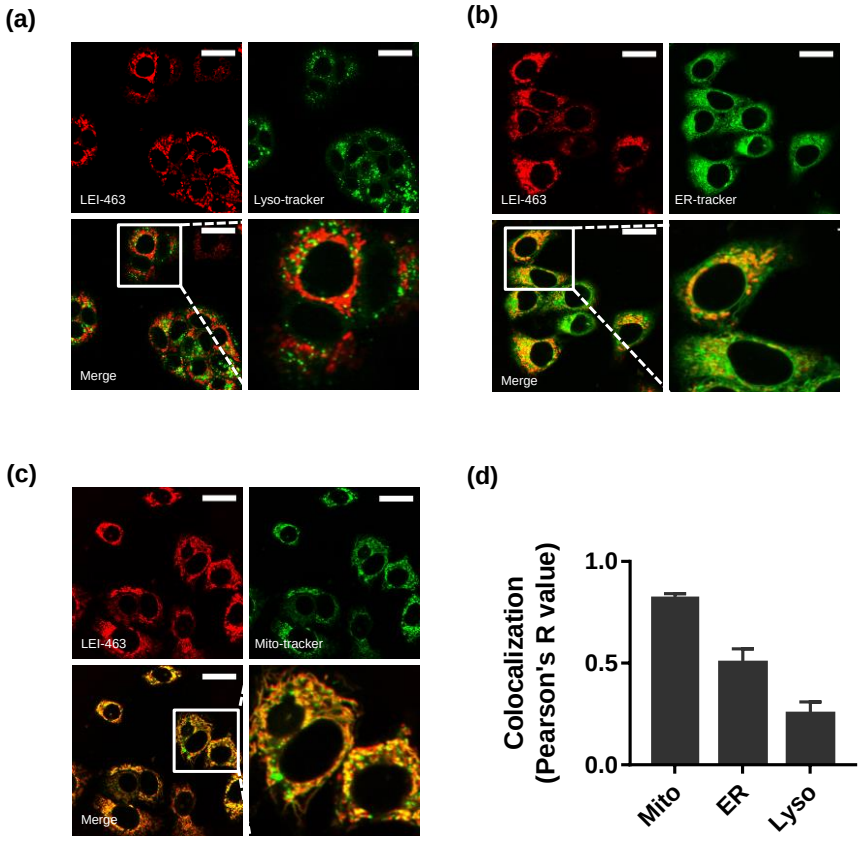

Figure 7. Subcellular localization of active MAGL in MCF7 cells with probe LEI-463 and various markers of subcellular organelles. MCF7 cells were treated with LEI-463 (100 nM, 2h), and stained with either lyso-tracker (a), ER-tracker (b), or mito-tracker (c) to visualize lysosomes, mitochondria and the endoplasmic reticulum respectively. After a PBS washing, the cells were used for confocal microscopy. Images show each fluorescence channel separately and the overlay of probe (Cy5, red) channel with lyso-marker (eGFP, green), ER-marker (DAPI, blue, false colored in image) or mito-marker channel (eGFP, green). Scale bar: 20 µm. (d) Colocalization of LEI-463 with lyso-, ER- or mito-marker was analyzed by Image J software (Coloc 2 plugin) using Pearson's R value (above threshold) as a measure; data represent average values ± SD; each experiment was repeated 3 times.

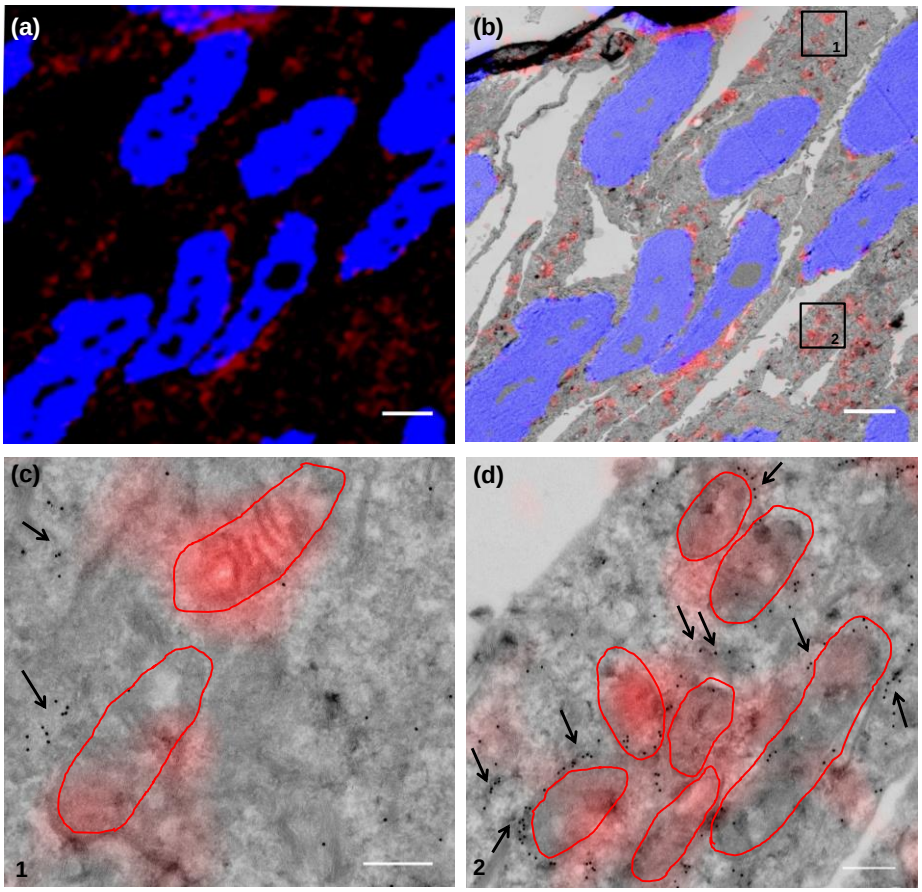

Figure 8. Correlative light-electron microscopy (CLEM) imaging of LEI-463 labeled MAGL in MCF7 cells. Cells were treated with LEI-463 (100 nM, 2 h) in 10 cm dish, followed by a PBS wash and immediate fixation. The fixed cells were harvested, subjected to Tokuyasu sample preparation, and cryosectioned into 75 nm sections. Sections were reacted with ER marker (anti-PDI) containing 15 nm gold particles (black dots in EM images, indicated with black arrows in c and d) and DAPI (blue) for nucleus. (a) Confocal microscopy images; (b) CLEM image obtained from overlay confocal microscopy and electron microscopy; (c) CLEM details from (b, region 1); (d) CLEM details from (b, region 2). Scale bar: 20 µm (a-b); 200 nm (c-d). Red circles in c and d indicate the locations of mitochondria from EM-images.

To confirm the subcellular localisation of MAGL activity at higher resolution, correlative light electron microscopy (CLEM) was performed. ABP-CLEM is a novel technology that allows one to correlate the activity of enzymes with the ultrastructural localisation of organelles as determined by electron microscopy (EM). LEI-463-treated MCF7 cells (100 nM, 2h) were fixated, cryosectioned according to the Tokuyasu-like sample preparation[26] and imaged. Confocal microscopy showed intracellular

fluorescence staining (Figure 8a) and subsequent correlation with EM-images of the same section revealed that MAGL activity resided to a large extent in mitochondria (indicated with red circles in Figure 8c-d). Considering the difficulty of visualizing ER structures in the cultured cells, an ER marker (anti-PDI with 15 nm gold particles) was used to detect the ER. The black dots indicated by the arrows in Figure 8c-d showed the subcellular localisation of the ER. The MAGL activity in the ER could not, however, unequivocally be established, due to the diffuse fluorescent signal and the close proximity of the ER and mitochondrial membranes (Figure 8d). Altogether, these experiments point towards the mitocondria as the principle subcellular compartment where MAGL activity resides in MCF7 cells.

LEI-463 labels MAGL *in vivo*

LEI-463 was further profiled *in vivo* to obtain tissue-wide MAGL activity and selectivity profile. LEI-463 (30 mg/kg, i.p.) or vehicle (saline/ethanol/PEG40, 18:1:1 (v/v/v)) was administrated to male C57BL/6 mice. After 2h or 4h, the animals were sacrificed and perfused with PBS and the organs (brain, heart, lung, liver, spleen, kidney, pancreas and testis) were isolated. Membrane and soluble proteomes of each tissue were prepared and analyzed by gel-based ABPP. No fluorescent bands were detected in any tissue after 2h of administration. At 4h a fluorescent band, corresponding to the molecular weight of MAGL (at ~33 kDa), was detected in all tissues except the brain (Figure 9), which indicated that LEI-463 is not brain penetrable. In testis, an additional band at ~35kDa was observed, which could represent the alternative splice variant of MAGL. Competitive ABPP with FP-TAMRA was performed to label residual MAGL activity. Near-complete blockade of MAGL activity was observed in all tissues, except the testis and the brain, indicating that almost full target engagement was obtained in heart, lung, liver, spleen, kidney and pancreas (Figure 9). LEI-463 maintained good selectivity for MAGL in most of the tissues, but several off-targets were detected in liver and pancreas (Figure 9b and 9g). The major off-targets of LEI-463 are around 50-65 kDa, which might correspond to carboxylesterases (CES), a subfamily of serine hydrolases that are commonly targeted by carbamate inhibitors. These in vivo studies, taken together, indicate that LEI-463 can be used to detect MAGL activity in intact animals and could function as a biomarker for target engagement.

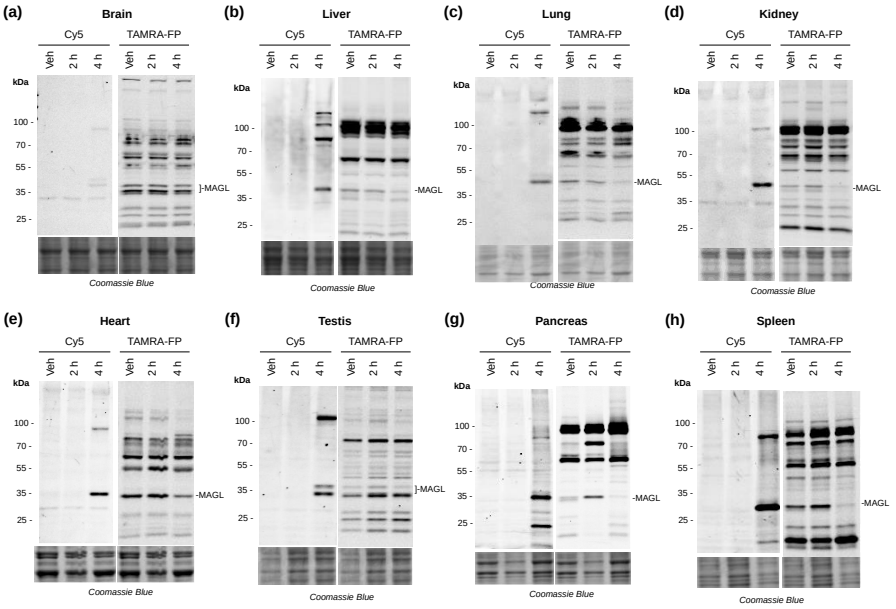

Figure 9. *In vivo* labeling of MAGL activity in mice. (a-h) C57Bl/6J mice were treated with LEI-463 (30 mg/kg) through intrapheritoneal injection for indicated time (2h or 4h), after which the animals were sacrificed and tissues, including brain (a), liver (b), lung (c), kidney (d), heart (e), testis (f), pancreas (g) and spleen (h), were harvested and analyzed for LEI-463-labeled proteins by gel-based fluorescence scanning. Scanning on Cy5 (left) and FP-TAMRA (*ex vivo*, 500 nM, 30 min) (right) channel confirmed the labeling of MAGL by LEI-463 *in vivo*.

Conclusion

This chapter describes the design, synthesis and application of a novel, highly selective and potent activity-based probe LEI-463 that visualizes MAGL activity in cell and tissue lysates as well as in living cells. It was discovered that MAGL activity is mainly localized in mitochondria of MCF7 cells. In addition, MAGL activity was detected in most mouse tissues, except the brain, after in vivo adminstration. It is envisioned that LEI-463 may serve as a valuable tailored ABP to study MAGL activity and distribution during (patho)physiological processes and may serve as a biomarker for target engagement studies to guide drug development.

Experimental section

Chemistry

All of reactions were performed using oven or flame-dried glassware and dry solvents. Reagents were purchased from Sigma Aldrich, Acros and Merck and used without further purification unless noted otherwise. All moisture sensitive reactions were performed under an argon atmosphere. Traces of water were removed from starting compounds by co-evaporation with toluene. ^{1}H-and ^{13}C-NMR spectra were recorded on a Bruker AV 400 MHz spectrometer at 400 (^{1}H) and 101 (^{13}C) MHz, or on a Bruker DMX-600 spectrometer 600 (^{1}H) and 150 (^{13}C) MHz using $CDCl_3$, or CD_3OD solvent, unless stated otherwise. Chemical shift values are reported in ppm with tetramethylsilane or solvent resonance as the internal standard ($CHCl_3$, δ 7.26 for ^{1}H, δ 77.16 for ^{13}C). Data are reported as follows: chemical shifts (δ), multiplicity (s = singlet, d = doublet, dd = double doublet, td = triple doublet, t = triplet, m = multiplet, br = broad), coupling constants *J* (Hz), and integration. High-resolution mass spectra (HRMS) were recorded by direct injection (2 µL of a 2 µM solution in water/acetonitrile 50/50 (v/v) and 0.1% formic acid) on a mass spectrometer (Thermo Finnigan LTQ orbitrap) equipped with an electrospray ion source in positive mode (source voltage 3.5 kV, sheath gas flow 10, capillary temperature 250 ^{o}C) with resolution R = 60,000 at m/z 400 (mass range m/z = 150-2,000) and dioctylphthalate (m/z = 391.28428) as a "lock mass". The high resolution mass spectrometer was calibrated prior to measurements with a calibration mixture (Thermo Finnigan). LC-MS analysis was performed on a Finnigan Surveyor HPLC system with a Gemmi C_{18} 50x4.60 mm column (detection at 200-600 nm), coupled to a Finnigan LCQ Adantage Max mass spectrometer with ESI. The applied buffers were H_2O, MeCN and 1.0% TFA in H_2O (0.1% TFA end concentration). Optical rotations were measured on a Propol automatic polarimeter (Sodium D-line, λ = 589 nm). Flash chromatography was performed using SiliCycle silica gel type SilicaFlash P60 (230 – 400 mesh). TLC analysis was performed on Merck silica gel 60/Kieselguhr F254, 0.25 mm. Compounds were visualized using either Seebach's reagent (a mixture of phosphomolybdic acid (25 g), cerium (IV) sulfate (7.5 g), H_2O (500 mL) and H_2SO_4 (25 mL)) or a $KMnO_4$ stain (K_2CO_3 (40 g), $KMnO_4$ (6 g), H_2O (600 mL) and 10% NaOH (5 mL)).

2-Azidoethan-1-ol (9). To a stirred solution of 2-bromoethan-1-ol (2 g, 16 mmol) in water (15 mL) was added sodium azide (2.6 g, 40 mmol), and the mixture was heated to 80 ^{o}C. After 15 h, KOH in pellets was added to basify the solution, followed by extraction with diethyl ether (3 x 20 mL). The combined organic phases were dried over $MgSO_4$. After filtration and removal of the solvent, 2-azidoethanol **9** was obtained as colorless liquid (1.34 g, 16 mmol, 96% yield). ^{1}H NMR (400 MHz, $CDCl_3$) δ 3.84 – 3.52 (m, 2H), 3.41 – 3.22 (m, 2H), 2.21 (br, 1H); ^{13}C NMR (101 MHz, $CDCl_3$) δ 61.51, 53.60.

2-Azidoethyl methanesulfonate (10). A solution of Ms-Cl (1.6 mL, 20.7 mmol) in DCM (5 mL) was added dropwise to a stirred solution of **9** (1.2 g, 13.8 mmol) and triethylamine (3.8 mL, 27.6 mmol) in DCM (15 mL) at 0 °C. After 2 h stirring at room temperature the reaction mixture was washed with water, dried over $MgSO_4$, filtered and evaporated to dryness to give title compound **10** as yellow oil, which was used directly without further purification. LC/MS calculated for $[C_3H_7N_3O_3S]^+$: 165.17, found: 165.92; ^{1}H NMR (400 MHz, $CDCl_3$) δ 4.39 – 4.11 (m, 1H), 3.52 (s, 1H), 3.00 (s, 1H); ^{13}C NMR (101 MHz, $CDCl_3$) δ 67.92, 49.60, 37.31.

4-(2-Azidoethoxy)benzaldehyde (11). 4-Hydroxybenzaldehyde (1.4 g, 11.6 mmol) and K_2CO_3 (2.4 g, 17.5 mmol) were added to a solution of 2-azidoethyl methanesulfonate (2.5 g, 15.1 mmol) in DMF (30 mL) at room temperature and the reaction mixture was stirred for 12 h at 80 ^oC. The resulting mixture was poured into water (30 mL) and extracted with diethyl ether (3 times). The combined organic layers were washed with brine (2 mL), dried over $MgSO_4$, filtered, and concentrated under reduced pressure. The residue was purified by flash column chromatography on silica gel with ethyl acetate/pentane (5−25%) as an eluent to yield **11** (1.9 g, 10 mmol, 86% yield). LC/MS calculated for $[C_9H_9N_3O_2]^+$: 191.19, found: 191.87; ^{1}H NMR (400 MHz, $CDCl_3$) δ 9.91 (s, 1H), 7.87 (d, *J* = 9.6 Hz, 2H), 7.04 (d, *J* = 8.4 Hz, 2H), 4.25 (t, *J* = 4.9 Hz, 2H), 3.67 (t, *J* = 4.8 Hz, 2H); ^{13}C NMR (101 MHz, $CDCl_3$) δ 190.85, 163.19, 132.09,130.48,114.88, 67.29, 50.03.

(4-(2-Azidoethoxy)phenyl)(4-chlorophenyl)methanol (12). To a stirring solution of **11** (1.2 g, 6.28 mmol) in dry THF (25 mL) at −78 °C under argon atmosphere was added (4-chlorophenyl)magnesium bromide (12.55 mL, 12.55 mmol) (1.0 M in diethyl ether). After 4 h, the reaction was quenched with saturated aqueous $NaHCO_3$ (5 mL) and the aqueous layer extracted with DCM (3 x 80 mL). The combined organic layers were dried over $MgSO_4$ and concentrated under reduced pressure. The residue was purified by flash chromatography (5−15% EtOAc/pentane) to give product **12** (1.7 g, 5.60 mmol, 89% yield). LC/MS calculated for $[C_{15}H_{14}ClN_3O_2]^+$: 303.75, found: 304.12; ^{1}H NMR (400 MHz, $CDCl_3$) δ 7.30 (s, 4H), 7.28 – 7.22 (m, 2H), 6.89 (d, *J* = 8.7 Hz, 2H), 5.77 (s, 1H), 4.13 (t, *J* = 5.0 Hz, 2H), 3.58 (t, *J* = 4.9 Hz, 2H), 2.22 (br, 1H). ^{13}C NMR (101 MHz, $CDCl_3$) δ 157.64, 142.40, 136.35, 132.88, 128.39, 127.87, 127.71, 114.50, 77.16, 74.79, 66.90, 49.98.

***tert*-Butyl**
4-((4-(2-azidoethoxy)phenyl)(4-chlorophenyl)methyl)piperazine-1-carboxylate
(14). To a stirring solution of **12** (800 mg, 2.63 mmol) in dry DCM (5 mL) at room temperature under argon atmosphere was added thionyl chloride (2.1 mL, 29 mmol). After stirred at 40 °C for overnight, the reaction was quenched with saturated aqueous $NaHCO_3$ (20 mL) and the aqueous layer extracted with DCM (3 × 10 mL). The combined organic layers were dried over $MgSO_4$, filtered and concentrated under reduced pressure to give crude product **13**, which was used for next step without further purification. To a solution of **13** (850 mg, 2.64 mmol) in DCM (12 mL) was added *tert*-butyl piperazine-1-carboxylate (1.5 g, 7.9 mmol) and K_2CO_3 (1.9 g, 13.7

mmol) at room temperature. After stirred at 40 °C for overnight, the reaction was quenched with saturated aqueous $NaHCO_3$ (20 mL) and the aqueous layer extracted with CH_2Cl_2 (3 × 10 mL). The combined organic layers were dried over Na_2SO_4 and concentrated under reduced pressure. The mixture was purified by flash chromatography (5−15% EtOAc/pentane) to give title compound **14** (1.2 g, 2.4 mmol, 89% yield). LC/MS calculated for $[C_{24}H_{30}ClN_5O_3]^+$: 471.99, found: 472.52; ^{1}H NMR (400 MHz, $CDCl_3$) δ 7.33 (d, *J* = 8.5 Hz, 2H), 7.29 – 7.21 (m, 4H), 6.84 (d, *J* = 8.7 Hz, 2H), 4.17 (s, 1H), 4.10 (t, *J* = 4.0 Hz, 2H) 3.56 (t, *J* = 5.0 Hz, 2H), 3.44 – 3.36 (m, 4H), 2.31 (br, 4H), 1.43 (s, 9H); ^{13}C NMR (101 MHz, $CDCl_3$) δ 157.51, 154.90, 141.39, 134.77, 132.71, 129.13, 129.09, 128.86, 114.81, 79.68, 74.69, 67.08, 51.72, 50.23, 44.38, 28.54.

1-((4-(2-Azidoethoxy)phenyl)(4-chlorophenyl)methyl)piperazine (15). To a solution of compound **14** (300 mg, 0.64 mmol) in ethyl acetate (2 mL) was added HCl (0.8 mL, 3.2 mmol) in 1,4-dioaxe. After TLC analysis indicated complete consumption of starting material, the mixture was poured into a saturated solution of $NaHCO_3$ and the product was extracted with DCM (3 x 20 mL). The combined organic layers were dried over $MgSO_4$, filtered and concentrated under reduced pressure to provide crude product **15**, which was used in the next step without further purification. LC/MS calculated for $[C_{19}H_{22}ClN_5O]^+$: 371.87, found: 372.64; ^{1}H NMR (400 MHz, $CDCl_3$) δ 7.63 – 7.09 (m, 6H), 6.84 (d, *J* = 8.6 Hz, 2H), 4.61 (br, 1H), 4.20 (s, 1H), 4.10 (t, *J* = 5.0 Hz, 2H), 3.55 (t, *J* = 8.0 Hz, 2H), 2.97 (t, *J* = 4.5 Hz, 4H), 2.44 (br, 4H); ^{13}C NMR (101 MHz, $CDCl_3$) δ 173.00, 157.42, 141.20, 134.55, 132.61, 129.04, 128.98, 128.76, 114.74, 74.87, 66.98, 51.85, 50.12, 45.53.

1,1,1,3,3,3-Hexafluoropropan-2-yl 4-((4-(2-azidoethoxy)phenyl)(4-chlorophenyl)methyl) piperazine-1-carboxylate (6). To a stirring solution of triphosgene (80 mg, 0.3 mmol) in CH_2Cl_2 (4 mL) at 0 ^{o}C was added the 1,1,1,3,3,3-hexafluoropropan-2-ol (0.062 mL, 0.59 mmol) followed by DIPEA (0.28 mL, 1.6 mmol). After stirring for 2h at room temperature, **15** (200 mg, 0.54 mmol) was added as a solution in CH_2Cl_2 (1 mL) and stirred for another 2 h. The mixture was concentrated under reduced pressure and purified by flash chromatography on silica gel (1−20% EtOAc/pentane) to provide the title compound **6** (165 mg, 0.29 mmol, 54% yield). HRMS calculated for $[C_{23}H_{22}ClF_6N_5O_3]^+$: 566.13881, found: 566.13875; ^{1}H NMR (400 MHz, $CDCl_3$) δ 7.33 (d, *J* = 8.4 Hz, 2H), 7.30 – 7.20 (m, 4H), 6.84 (d, *J* = 8.6 Hz, 2H), 5.74 (septet, *J* = 6.4 Hz, 1H), 4.20 (s, 1H), 4.09 (t, *J* = 4.9 Hz, 2H), 3.59 – 3.48 (m, 6H), 2.38 (dt, *J* = 14.2, 4.1 Hz, 4H); ^{13}C NMR (101 MHz, $CDCl_3$) δ 157.64, 151.44, 140.95, 134.27, 132.91, 129.02, 129.00, 128.95, 114.90, 74.46, 68.87 (q, *J* = 228 Hz), 68.08 (p, *J* = 35.4 Hz), 67.08, 51.36, 51.20, 50.18, 44.92, 44.56.

2,5-Dioxopyrrolidin-1-yl 4-((4-(2-azidoethoxy)phenyl)(4-chlorophenyl)methyl)piperazine-1- carboxylate (7). To a stirring solution of triphosgene (40 mg, 0.13 mmol) in DCM (5 mL) at 0 ^{o}C was added *N*-Hydroxysuccinimide (37 mg, 0.32 mmol) followed by DIPEA (0.14 mL,

0.81 mmol). After stirring for 2 h at room temperature, **15** (100 mg, 0.27 mmol) was added as a solution in DCM (1 mL) and stirred for another 2 h. The mixture was concentrated under reduced pressure and purified by flash chromatography on silica gel (1−20% EtOAc/pentane) to provide the title compound **7** (120 mg, 0.23 mmol, 87% yield). HRMS calculated for $[C_{24}H_{25}ClN_6O_5]^+$: 513.16477, found: 513.16478; ^{1}H NMR (400 MHz, $CDCl_3$) δ 7.34 (d, *J* = 8.4 Hz, 2H), 7.30 – 7.21 (m, 4H), 6.84 (d, *J* = 8.5 Hz, 2H), 4.22 (s, 1H), 4.18 – 4.01 (m, 2H), 3.68 – 3.44 (m, 6H), 2.78 (s, 4H), 2.42 (s, 4H); ^{13}C NMR (101 MHz, $CDCl_3$) δ 169.84, 157.59, 150.36, 140.94, 134.25, 132.85, 129.01, 128.99, 128.92, 114.88, 74.37, 67.04, 51.09, 51.03, 50.15, 45.25, 44.73, 25.54.

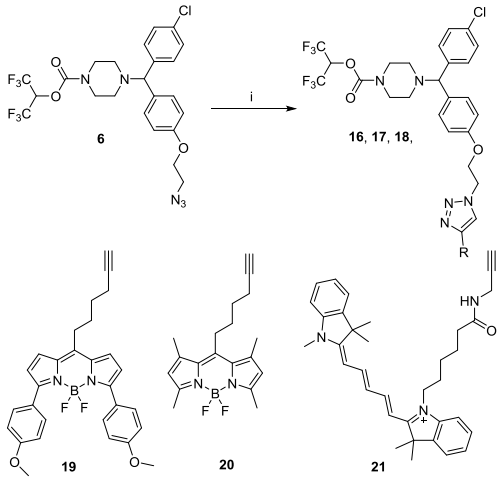

Scheme S.1. Synthesis of activity-based probe **16**-**18**. Reagents and conditions: (a) **19**, **20** or **21**, $CuSO_4$, sodium ascorbate, DCM/H_2O, r.t., 24 h, 69% (**16**), 61% (**17**) and 38% (**18**).

1,1,1,3,3,3-Hexafluoropropan-2-yl 4-((4-chlorophenyl)(4-(2-(4-(4-(5,5-difluoro-3,7-bis(4-methoxyphenyl)-*5H*-4l4,5l4-dipyrrolo[1,2-c:2',1'-f][1,3,2]diazaborinin-10-yl)butyl)-*1H*-1,2,3-triazol-1-yl)ethoxy)phenyl)methyl)piperazine-1-carboxylate (16). Compound **6** (38 mg, 0.07 mmol) and **19** (35 mg, 0.07 mmol) were dissolved in degassed DCM/H_2O (2 mL, 1:1, v/v) and aqueous solutions of sodium ascorbate (15.8 mg, 0.08 mmol) and copper(II) sulfate pentahydrate (8.3 mg, 0.03 mmol) were added. The resulting mixture was stirred vigorously for 2 h, after which TLC indicated completed conversion of the reaction. The solvents were evaporated *in vacuo*, and the residue was taken up in DCM and purified by silica column chromatography (1−5% DCM/MeOH) to give the desired product **16** (48 mg, 0.05 mmol, 69% yield). HRMS calculated for $[C_{52}H_{49}BClF_8N_7O_5]^+$ 1050.3522, found: 1050.3537; ^{1}H NMR (400 MHz, $CDCl_3$) δ 7.83 (d, *J* = 8.8 Hz, 4H), 7.33 – 7.14 (m, 9H), 6.93 (d, *J* = 8.9 Hz, 4H), 6.75 (d, *J* = 8.2 Hz, 2H), 6.58 (s, 2H), 5.72 (septet, *J* = 6.4 Hz, 1H), 4.71 (s, 2H), 4.31 (s,

2H), 4.15 (s, 1H), 3.83 (s, 6H), 3.52 (d, *J* = 5.0 Hz, 4H), 2.96 (s, 2H), 2.78 (br, 1H), 2.34 (dt, *J* = 12.2, 4.5 Hz, 4H), 1.87 (br, 4H). ^{13}C NMR (101 MHz, $CDCl_3$) δ 160.67, 157.66, 157.21, 151.42, 144.87, 140.81, 136.26, 134.68, 132.95, 131.14, 131.09,131.04, 129.05, 128.98, 128.97, 125.29, 122.17, 120.12, 114.87, 113.84, 74.35, 69.08 (q, *J* = 224.2 Hz), 68.09 (p, *J* = 35.35 Hz), 66.42, 55.36, 51.32, 51.16, 50.29, 44.88, 44.53, 33.12, 31.70, 30.52.

1,1,1,3,3,3-Hexafluoropropan-2-yl 4-((4-chlorophenyl)(4-(2-(4-(4-(5,5-difluoro-1,3,7,9-tetramethyl-*5H*-4l4,5l4-dipyrrolo[1,2-c:2',1'-f][1,3,2]diazaborinin-10-yl)butyl)-*1H*-1,2,3-triazol-1-yl)ethoxy)phenyl)methyl)piperazine-1-carboxylate (17). The title compound was synthesized from compound **6** (33 mg, 0.06 mmol), **20** (21 mg, 0.06 mmol), sodium ascorbate (13.9 mg, 0.07 mmol) and copper(II) sulfate pentahydrate (7.3 mg, 0.03 mmol) according to the procedure described for compound **16**. This furnished the title compound **17** (32 mg, 0.04 mmol, 61% yield). HRMS calculated for $[C_{42}H_{45}BClF_8N_7O_3]^+$ 894.33105, found: 894.33253; ^{1}H NMR (400 MHz, $CDCl_3$) δ 7.45 (s, 1H), 7.31 (d, *J* = 8.4 Hz, 2H), 7.29 – 7.20 (m, 5H), 6.77 (d, *J* = 8.5 Hz, 2H), 6.02 (s, 2H), 5.72 (septet, *J* = 6.4 Hz, 1H), 4.70 (s, 2H), 4.29 (s, 2H), 4.19 (s, 1H), 3.63 – 3.42 (m, 4H), 2.97 (br, 2H), 2.77 (s, 2H), 2.50 (s, 6H), 2.37 (s, 10H), 1.91 (s, 2H), 1.68 (br, 4H). ^{13}C NMR (101 MHz, $CDCl_3$) δ 157.24, 153.98, 153.95, 151.46, 146.18, 140.84, 140.46, 140.45, 134.76, 133.02, 129.08, 129.02, 129.00, 121.81, 121.76, 114.90, 74.41, 68.66 (q, *J* = 244.4 Hz), 68.12 (p, *J* = 34.34 Hz), 66.54, 51.38, 51.21, 49.89, 44.91, 44.55, 31.48, 29.49, 28.25, 25.52, 16.48, 14.55.

1-(6-(((1-(2-(4-((4-Chlorophenyl)(4-(((1,1,1,3,3,3-hexafluoropropan-2-yl)oxy)carbonyl)piperazin-1-yl)methyl)phenoxy)ethyl)-*1H*-1,2,3-triazol-4-yl)methyl)amino)-6-oxohexyl)-3,3-dimethyl-2-((1*E*,3*E*)-5-((*E*)-1,3,3-trimethylindolin-2-ylidene)penta-1,3-dien-1-yl)-*3H*-indol-1-ium chloride (18, LEI-463). The title compound was synthesized from compound **6** (10 mg, 0.018 mmol), **21** (9.8 mg, 0.018 mmol), sodium ascorbate (4.20 mg, 0.021 mmol) and copper(II) sulfate pentahydrate (2.2 mg, 8.8 µmol) according to the procedure described for compound **16**. This furnished the title compound **18** (7.6 mg, 0.007 mmol, 38% yield). HRMS calculated for $[C_{58}H_{64}ClF_6N_8O_4]^+$ 1085.46378, found: 1085.46335; ^{1}H NMR (600 MHz, $CDCl_3$) δ 7.86 (d, *J* = 10.1 Hz, 2H), 7.42 – 7.32 (m, 4H), 7.26 (s, 8H), 7.10 – 7.08 (m, 2H), 6.99 – 6.72 (m, 4H), 6.38 (br d, *J* = 45.0 Hz, 2H), 5.76 – 5.65 (m, 1H), 4.76 (br, 4H), 4.34 (br, 3H), 4.04 (s, 3H), 3.78 – 3.44 (m, 6H), 2.53 – 2.23 (m, 4H), 1.83 – 1.54 (m, 18H), 1.25 (s, 2H). ^{13}C NMR (151 MHz, $CDCl_3$) δ 173.02, 158.94, 153.36, 152.92, 151.35, 142.86, 142.03, 141.16, 140.88, 128.96, 128.85, 125.48, 125.24, 122.32, 122.23, 110.96, 110.48, 70.29 (q, *J* = 285.4 Hz), 68.13 (p, *J* = 36.2 Hz), 67.92, 66.38, 64.35, 51.47, 51.34, 49.44, 49.20, 45.11, 29.85, 28.30, 28.25, 27.35.

Biological assays

Cloning Procedures

For the preparation of the different constructs, full length human cDNA was purchased from Source Bioscience and cloned into mammalian expression vector pcDNA3.1, containing genes for ampicillin and neomycin resistance. MAGL constructs were obtained as reported previously [27]. Plasmids were isolated from transformed XL-10 Z-competent cells (Maxi Prep, Qiagen) and verified by Sanger sequencing (BaseClear). The sequences were confirmed by sequence analysis at the Leiden Genome Technology Centre.

Cell culture and membrane preparation

Cells (HEK293T, Neuro2A) were grown in DMEM with stable glutamine and phenolred (PAA or Sigma) with 10% New Born Calf serum, penicillin and streptomycin. Cells were passaged every 2-3 days by resuspending (HEK293T, Neuro2A) in medium and seeding them to appropriate confluence. Membranes were prepared from transiently transfected cells. One day prior to transfection 10^7 cells were seeded in a 15 cm petri dish. Cells were transfected by the addition of a 3:1 mixture of polyethyleneimine (60 µg) and plasmid DNA (20 µg) in 2 mL serum free medium. The medium was refreshed after 24 h, and after 72 h the cells were harvested by suspending them in 20 mL medium. The suspension was centrifuged for 10 min at 1000 rpm, and the supernatant was removed. The cell pellet was stored at -80 ^{o}C until use. Of note, Neuro2A cells were transfected by the addition of a 5:1 mixture of polyethyleneimine (5 µg) and plasmid DNA (1 µg) in serum free medium in 6-well plate.

Cell pellets were thawed on ice and suspended in lysis buffer A (20 mM HEPES, 2 mM DTT, 0.25 M sucrose, 1 mM $MgCl_2$, 25 U/mL Benzonase). The suspension was homogenized by polytrone (3 × 7 sec) and incubated for 30 min on ice. The suspension was subjected to ultracentrifugation (93.000 × g, 30 min, 4 ^{o}C, Beckman Coulter, Type Ti70 rotor) to yield the cytosolic fraction in the supernatant and the membrane fraction as a pellet. The pellet was resuspended in lysis buffer B (20 mM HEPES, 2 mM DTT). The protein concentration was determined with Quick Start Bradford reagent (BioRad) or Qubit^{TM} fluorometric quantitation (Life Technologies). The protein fractions were diluted to 1 mg/mL and stored in small aliquots at -80 ^{o}C until use.

Live-cell microscopy

Experiments were conducted on a Leica TCS SPE confocal microscope, using Cy5 filter setting (λex: 633 nm, λem: 660-700 nM). MCF7 cells (1-2 x 10^4) were seeded onto sterile µ-Slide 8 well coverglass (I bidi). Stock solutions of probes and other reagents in DMSO (0.1%) were diluted with medium without serum. Cells were incubated with probe LEI-463 for 2 h and then subsequently washed with PBS (3x), fixed (4% formaldehyde in PBS; 15 min at r.t.), washed again with PBS (3x). Fixed

cells were then used for fluorescent imaging. For the competition experiments, MAGL inhibitors JZL184 or ABHD6 inhibitor KT195 were *in situ* pre-incubated for 2 h prior and then co-incubated with probe LEI-463 for another 2 h. For the co-localization experiments, after treatment with probe LEI-463 for 2 h, cells were washed with PBS (3x), and then stained with lyso-tracker Green DND26 (Thermo Fisher; 1 µM), Mito-tracker Green FM (Thermo Fisher; 200 nM) or ER-tracker Blue-White DPX (Thermo Fisher 1 µM) according to manufacturer's recommendations for 30 min at 25 ^{o}C. For the co-localization studies, Pearson's correlation coefficient was measured by Image J software with Coloc 2 plugin. Each staining experiment was repeated 3 times.

Correlation of light-electron microscopy (CLEM)

The CLEM approach used was adapted from Van Elsland et. al.[28] Samples were prepared for cryo sectioning as described elsewhere.[29] MCF-7 cells were incubated with the LEI-463 probe for 2 h. After the probe incubation cells were washed with PBS (3x) and were then fixed for 24h in freshly prepared 2% PFA in 0.1 M phosphate buffer. Fixed cells were embedded in 12% gelatin (type A, bloom 300, Sigma) and cut with a razor blade into 0.5 mm^3 cubes. The sample blocks were infiltrated in phosphate buffer containing 2.3 M sucrose for 3h. Sucrose-infiltrated sample blocks were mounted on aluminum pins and plunged in liquid nitrogen. The frozen samples were stored under liquid nitrogen.

Ultrathin cell sections of 75 nm were obtained as described elsewhere.[28] Briefly, the frozen sample was mounted in a cryo-ultramicrotome (Leica). The sample was trimmed to yield a squared block with a front face of about 300 x 250 µm (Diatome trimming tool). Using a diamond knife (Diatome) and antistatic devise (Leica) a ribbon of 75 nm thick sections was produced that was retrieved from the cryo-chamber with a droplet of 2.3 M sucrose. Obtained sections were transferred to a specimen grid previously coated with formvar and carbon Grids were additionally coated as indicated with either 100 nm TetraSpeck beads or 100 nm FluoroSpheres (blue) carboxylate-modified (350/440) (Life Technologies).

Obtained sample sections were subsequently immunogold-labeled with 15 nm gold particles using a rabbit anti-protein disulfide isomerase (PDI) polyclonal antibody.[30] Sections were labeled as follows; thawed cryo sections on an EM grid were left for 30 minutes on the surface of 2% gelatin in phosphate buffer at 37 °C. Grids were washed 5 times with PBS/glycine and blocked with PBS/Glycine containing 1% BSA after which the grids were incubated for 1h with PBS/Glycine 1% BSA supplemented with anti-PDI.[30] Grids were then washed 5 times with PBS/glycine and blocked with PBS/Glycine 0.1% BSA, grids were incubated for 20 min on PBS/Glycine 1% BSA supplemented with protein A coated 15 nm gold particles (CMC, Utrecht University). Grids were then washed with PBS, labeled with DAPI (1:5000 in PBS for 5 min), and additionally washed with PBS and aquadest.

Grids containing the sample sections were then washed with 50% glycerol and

placed on glass slides (pre- cleaned with 100% ethanol). Grids were then covered with a small drop of 50% glycerol after which a coverslip was mounted over the grid. Coverslips were fixed using Scotch Pressure Sensitive Tape. Samples were imaged with a Leica TCS SP8 confocal microscope (63x oil lens, N.A.=1.4). Confocal microscopy was used as it allowed to make image stacks from the sections at different focus planes, this was convenient as the sections were found to be in different focus planes whilst placed between the glass slides and coverslip. After fluorescence microscopy the EM grid with the sections was remove from the glass slide, rinsed in distilled water and incubated for 5' on droplets of unranylacetate/methylcellulose. Excess of uranylacetate/methylcellulose was blotted away and grids were air-dried. EM imaging was performed with an Tecnai 12 Biotwin transmission electron microscope (FEI) at 120 kV acceleration voltage. Correlation of confocal and EM images was performed in Adobe Photoshop CS6. In Adobe Photoshop, the LM image was copied as a layer into the EM image and made 50% transparent. Transformation of the LM image was necessary to match it to the larger scale of the EM image. This was performed via isotropic scaling and rotation. Interpolation settings; bicubic smoother. Alignment at low magnification was carried out with the aid of nuclear DAPI staining in combination with the shape of the cells, at high magnification alignment was performed using the fiducial beads.

Natural substrate based fluorescence assay (MAGL and ABHD6)

The natural substrate assays were performed as reported previously.[27, 31] Standard assay conditions: 0.2 U/mL glycerol kinase (GK), glycerol-3-phosphate oxidase (GPO) and horseradish peroxidase (HRP), 0.125 mM ATP, 10 µM Amplifu™Red, 5% DMSO in a total volume of 200 µL. For ABHD6, the assay additionally contained 25 µM 2-AG and 0.5% acetonitrile, with a final protein concentration of 40 µg/mL.

Preparation of mouse tissue membrane proteome

Mouse tissues were isolated according to guidelines approved by the ethical committee of Leiden University (DEC#13191), frozen in liquid nitrogen and stored at -80 °C until use. Mouse tissues were thawed on ice and homogenized by polytrone (3 x 5 seconds, 20,000 rpm) in lysis buffer A (20 mM HEPES pH 7.2, 2 mM DTT, 250 mM sucrose, 1 mM $MgCl_2$ and 25 U/mL benzonase). The suspension was incubated on ice for 15 min, followed by low speed centrifugation (2500 g, 3 min. at 4 °C) to remove debris. The supernatant was subjected to ultracentrifugation (93,000 g, 45 min at 4 °C) to yield the mouse tissue membrane proteome as a pellet. The pellet was resuspended in storage buffer B (20 mM HEPES, pH 7.2, 2 mM DTT) and homogenized by polytrone (1 x 7 seconds, 20,000 rpm). Protein concentrations were determined and membranes preparations were stored as described above.

Activity based protein profiling in mouse brain.

Mouse brain proteome (2 mg/mL, 19.5 µL) was incubated with DMSO or inhibitor in 0.5 µL DMSO for 30 min at r.t. and subsequently incubated with 500 nM (final

concentration) ABP FP-TAMRA, or 250 nM (final concentration) ABP MB064 for 20 min at r.t. before the reaction was quenched with standard 3x Laemmli sample buffer. The gels were scanned using a ChemiDoc MP system and analyzed using Image Lab 4.1.

Activity-based protein profiling in living cells

Breast cancer cell MCF7 were grown in DMEM with stable glutamine and phenolred (PAA), 10% New Born Calf serum, penicillin and streptomycin. Cells were passaged every 2-3 days by resuspension (trypsinization) in medium and seeing them to appropriate confluence. Before inhibitor treatment, the culture medium was removed and the cells were washed with warm (37 ^{o}C) serum-free medium (3x). For labeling experiments, cells were treated with DMSO or various concentrations of probe LEI-463 (1000x DMSO stock; final DMSO concentration 0.1%), incubated for 2 h (37 ^{o}C; 5% CO_2), washed with PBS (3x) and harvested (trypsinization). Cell pellets were flash frozen in liquid nitrogen before ABPP analysis. Experiments that required pre-treatment were conducted as follows: the cells were incubated with DMSO or inhibitor (1000x DMSO stock; final DMSO concentration 0.1%) in serum-free medium for 2 h. The medium was removed and the cells were washed with PBS (3x). Probe LEI-463 (100 nM) was added directly to the medium and incubated for 2 h. After washing with PBS (3x), the cells were suspended in PBS and the cells were pelleted by centrifugation. Cell pellets were flash frozen in liquid nitrogen before analysis by ABPP.

***In vivo* target engagement studies of LEI-463**

The animal experiments were conducted in accordance with the ethical committee of Leiden University (DEC#14137). *In vivo* studies with LEI-463 were conducted in C57BL/6 mice. Mice were injected with LEI-463 (30 mg/kg) i.p. in 18:1:1 (v/v/v) solution of saline/ethanol/PEG40 (ethoxylated castor oil, 10 µL/g body weight of mouse). After 2 h or 4 h, mice were anesthetized with isoflurane, and euthanized by cervical dislocation. Mice were perfused with PBS and then brain, liver, spleen, heart, lung, pancreas, testis, muscle and kidney were collected. Tissue homogenates were prepared and competitive ABPP experiments were performed according to the previously described method.

References

1. Niphakis, M. J.; Cravatt, B. F. Enzyme inhibitor discovery by activity-based protein profiling. *Annual Review Biochemistry* **2014,** 83, 341-377.
2. Liu, Y. S.; Patricelli, M. P.; Cravatt, B. F. Activity-based protein profiling: The serine hydrolases. *Proceedings of the National Academy of Sciences of the United States of America* **1999,** 96, 14694-14699.
3. Adam, G. C.; Sorensen, E. J.; Cravatt, B. F. Proteomic profiling of mechanistically distinct enzyme classes using a common chemotype. *Nature Biotechnology* **2002,** 20, 805-809.
4. Greenbaum, D.; Baruch, A.; Hayrapetian, L.; Darula, Z.; Burlingame, A.; Medzihradszky, K. F.; Bogyo, M. Chemical approaches for functionally probing the proteome. *Molecular & Cellular Proteomics* **2002,** 1, 60-68.
5. Kumar, S.; Zhou, B.; Liang, F. B.; Wang, W. Q.; Huang, Z. H.; Zhang, Z. Y. Activity-based probes for protein tyrosine phosphatases. *Proceedings of the National Academy of Sciences of the United States of America* **2004,** 101, 7943-7948.
6. Patricelli, M. P.; Szardenings, A. K.; Liyanage, M.; Nomanbhoy, T. K.; Wu, M.; Weissig, H.; Aban, A.; Chun, D.; Tanner, S.; Kozarich, J. W. Functional interrogation of the kinome using nucleotide acyl phosphates. *Biochemistry* **2007,** 46, 350-358.
7. Vocadlo, D. J.; Bertozzi, C. R. A strategy for functional proteomic analysis of glycosidase activity from cell lysates. *Angewandte Chemie International Edition* **2004,** 43, 5338-5342.
8. Sieber, S. A.; Niessen, S.; Hoover, H. S.; Cravatt, B. F. Proteomic profiling of metalloprotease activities with cocktails of active-site probes. *Nature Chemical Biology* **2006,** 2, 274-281.
9. Niphakis, M. J.; Cravatt, B. F. Enzyme inhibitor discovery by activity-based protein profiling. *Annual Review of Biochemistry,* **2014,** 83, 341-377.
10. Nomura, D. K.; Long, J. Z.; Niessen, S.; Hoover, H. S.; Ng, S. W.; Cravatt, B. F. Monoacylglycerol lipase regulates a fatty acid network that promotes cancer pathogenesis. *Cell* **2010,** 140, 49-61.
11. Verdoes, M.; Florea, B. I.; Menendez-Benito, V.; Maynard, C. J.; Witte, M. D.; Van der Linden, W. A.; Van den Nieuwendijk, A. M. C. H.; Hofmann, T.; Berkers, C. R.; van Leeuwen, F. W. B.; Groothuis, T. A.; Leeuwenburgh, M. A.; Ovaa, H.; Neefjes, J. J.; Filippov, D. V.; Van der Marel, G. A.; Dantuma, N. P.; Overkleeft, H. S. A fluorescent broad-spectrum proteasome inhibitor for labeling proteasomes in vitro and in vivo. *Chemistry & Biology* **2006,** 13, 1217-1226.
12. Chang, J. W.; Moellering, R. E.; Cravatt, B. F. An activity-based imaging probe for the integral membrane hydrolase KIAA1363. *Angewandte Chemie International Edition* **2012,** 51, 966-970.
13. Dinh, T. P.; Carpenter, D.; Leslie, F. M.; Freund, T. F.; Katona, I.; Sensi, S. L.; Kathuria, S.; Piomelli, D. Brain monoglyceride lipase participating in endocannabinoid inactivation. *Proceedings of the National Academy of Sciences of the United States of America* **2002,** 99, 10819-10824.
14. Nomura, D. K.; Morrison, B. E.; Blankman, J. L.; Long, J. Z.; Kinsey, S. G.; Marcondes, M. C. G.; Ward, A. M.; Hahn, Y. K.; Lichtman, A. H.; Conti, B.; Cravatt, B. F. Endocannabinoid

hydrolysis generates brain prostaglandins that promote neuroinflammation. *Science* **2011,** 334, 809-813.

15. Marrs, W. R.; Blankman, J. L.; Horne, E. A.; Thomazeau, A.; Lin, Y. H.; Coy, J.; Bodor, A. L.; Muccioli, G. G.; Hu, S. S. J.; Woodruff, G.; Fung, S.; Lafourcade, M.; Alexander, J. P.; Long, J. Z.; Li, W. W.; Xu, C.; Moller, T.; Mackie, K.; Manzoni, O. J.; Cravatt, B. F.; Stella, N. The serine hydrolase ABHD6 controls the accumulation and efficacy of 2-AG at cannabinoid receptors. *Nature Neuroscience* **2010,** 13, 951-967.
16. Navia-Paldanius, D.; Savinainen, J. R.; Laitinen, J. T. Biochemical and pharmacological characterization of human alpha/beta-hydrolase domain containing 6 (ABHD6) and 12 (ABHD12). *Journal of Lipid Research* **2012,** 53, 2413-2424.
17. Shankavaram, U. T.; Reinhold, W. C.; Nishizuka, S.; Major, S.; Morita, D.; Chary, K. K.; Reimers, M. A.; Scherf, U.; Kahn, A.; Dolginow, D.; Cossman, J.; Kaldjian, E. P.; Scudiero, D. A.; Petricoin, E.; Liotta, L.; Lee, J. K.; Weinstein, J. N. Transcript and protein expression profiles of the NCI-60 cancer cell panel: an integromic microarray study. *Molecular Cancer Therapeutics* **2007,** 6, 820-832.
18. Hsu, K. L.; Tsuboi, K.; Adibekian, A.; Pugh, H.; Masuda, K.; Cravatt, B. F. DAGLbeta inhibition perturbs a lipid network involved in macrophage inflammatory responses. *Nature Chemical Biology* **2012,** 8, 999-1007.
19. Anderson, R. G. W.; Orci, L. A view of acidic intracellular compartments. *Journal of Cell Biology* **1988,** 106, 539-543.
20. Dolman, N. J.; Kilgore, J. A.; Davidson, M. W. A review of reagents for fluorescence microscopy of cellular compartments and structures, part I: BacMam labeling and reagents for vesicular structures. *Current Protocols in Cytometry* **2013,** Chapter 12, Unit 12 30.
21. Li, Y.; Zhang, Q.; Tian, R.; Wang, Q.; Zhao, J. J.; Iglehart, J. D.; Wang, Z. C.; Richardson, A. L. Lysosomal transmembrane protein LAPTM4B promotes autophagy and tolerance to metabolic stress in cancer cells. *Cancer Research* **2011,** 71, 7481-7489.
22. Buckman, J. F.; Hernandez, H.; Kress, G. J.; Votyakova, T. V.; Pal, S.; Reynolds, I. J. MitoTracker labeling in primary neuronal and astrocytic cultures: influence of mitochondrial membrane potential and oxidants. *Journal of Neuroscience Methods* **2001,** 104, 165-176.
23. Peng, T.; Bonamy, G. M. C.; Glory-Afshar, E.; Rines, D. R.; Chanda, S. K.; Murphy, R. F. Determining the distribution of probes between different subcellular locations through automated unmixing of subcellular patterns. *Proceedings of the National Academy of Sciences of the United States of America* **2010,** 107, 2944-2949.
24. Abodeely, M.; DuBois, K. N.; Hehl, A.; Stefanic, S.; Sajid, M.; deSouza, W.; Attias, M.; Engel, J. C.; Hsieh, I.; Fetter, R. D.; McKerrow, J. H. A contiguous compartment functions as endoplasmic reticulum and endosome/lysosome in Giardia lamblia. *Eukaryotic Cell* **2009,** 8, 1665-1676.
25. Mironov, S. L.; Ivannikov, M. V.; Johansson, M. [Ca2+](i) signaling between mitochondria and endoplasmic reticulum in neurons is regulated by microtubules - From mitochondrial permeability transition pore to Ca2+-induced Ca2+ release. *Journal of Biological Chemistry* **2005,** 280, 715-721.
26. Maranto, A. R. Neuronal mapping: a photooxidation reaction makes Lucifer yellow useful for electron microscopy. *Science* **1982,** 217, 953-955.

27. van der Wel, T.; Janssen, F. J.; Baggelaar, M. P.; Deng, H.; den Dulk, H.; Overkleeft, H. S.; van der Stelt, M. A natural substrate-based fluorescence assay for inhibitor screening on diacylglycerol lipase alpha. *Journal of Lipid Research* **2015,** 56, 927-935.
28. van Elsland, D. M.; Bos, E.; de Boer, W.; Overkleeft, H. S.; Koster, A. J.; van Kasteren, S. I. Detection of bioorthogonal groups by correlative light and electron microscopy allows imaging of degraded bacteria in phagocytes. *Chemical Science* **2016,** 7, 752-758.
29. Peters, P. J.; Hunziker, W. Subcellular localization of Rab17 by cryo-immunogold electron microscopy in epithelial cells grown on polycarbonate filters. *Regulators and Effectors of Small Gtpases, Pt E* **2001,** 329, 210-225.
30. McGehee, A. M.; Dougan, S. K.; Klemm, E. J.; Shui, G. H.; Park, B.; Kim, Y. M.; Watson, N.; Wenk, M. R.; Ploegh, H. L.; Hu, C. C. A. XBP-1-Deficient plasmablasts show normal protein folding but altered glycosylation and lipid synthesis. *Journal of Immunology* **2009,** 183, 3690-3699.
31. Janssen, F. J.; Deng, H.; Baggelaar, M. P.; Allara, M.; van der Wel, T.; den Dulk, H.; Ligresti, A.; van Esbroeck, A. C.; McGuire, R.; Di Marzo, V.; Overkleeft, H. S.; van der Stelt, M. Discovery of glycine sulfonamides as dual inhibitors of sn-1-diacylglycerol lipase alpha and alpha/beta-hydrolase domain 6. *Journal of Medicinal Chemistry* **2014,** 57, 6610-6622.

8

Summary and future prospects

In **Chapter 1**, the endocannabinoid system is introduced. Endocannabinoids are endogenous signaling lipids that activate cannabinoid CB_1 and CB_2 receptors.[1,2] Endocannabinoids can be considered as the body's own marijuana, because CB receptors are also targeted by Δ^9-tetrahydrocannabinol, the psychoactive principle of marijuana.[3] Endocannabinoids play an essential role in human health and disease, regulating processes, such as immunomodulation, energy balance, neurotransmission, mood, appetite, pain sensation and reward.[4-9] Endocannabinoids are also involved in pathophysiological conditions. Continuous stimulation of the CB_1 receptor by endocannabinoids is associated with nicotine addiction, obesity and the metabolic syndrome (all major risk factors for illness and death in Europe).[8] The CB_1 receptor blocker Rimonabant was effective in obese patients, but was withdrawn from the European market due to unacceptable psychiatric side effects (i.e. depression, anxiety and suicidal ideation in some individuals).[10,11] This highlights the medical need to modulate the endocannabinoid system in a more controlled manner.

There are two main endocannabinoids: anandamide and 2-arachidonoylglycerol (2-AG).[12] Both endocannabinoids have an arachidonic acid backbone, but vary in their polar head group. Both endocannabinoids are often found together, but their levels vary between species, tissue, developmental stage and pathological condition. Although, selective inhibitors of their metabolic pathways have provided information about the biological function of the endocannabinoids, it is still unclear to a large extent which endocannabinoid is responsible for specific cannabinoid CB_1 and CB_2 receptor dependent (patho)physiological effects.[13] Selective inhibition of the formation of anandamide and 2-AG would be instrumental to determine which endocannabinoid is responsible for specific CB_1-mediated physiological effects. However, pathway-selective and *in vivo* active inhibitors for 2-AG and anandamide biosynthesis are currently lacking.

Endocannabinoids are produced “on demand” upon different biological stimuli via different biosynthetic pathways. 2-AG is mainly formed by the action of two diacylglycerol lipases (DAGL-α and DAGL-β).[14] Studies with DAGL-KO mice have shown that DAGL-α controls to a large extent the formation of 2-AG in the central nervous system, whereas DAGL-β appears to partake in 2-AG production in the periphery (Table 1).[15-17] Selective DAGL-α inhibition has been hypothesized to be an alternative for Rimonabant, whereas selective DAGL-β inhibitors are envisioned to have protective properties by reducing neuroinflammation.[18]

Table 1. Reductions of 2-AG levels in DAGL$\alpha^{-/-}$ and DAGL$\beta^{-/-}$ mouse tissues.

	DAGL$\alpha^{-/-}$	DAGL$\beta^{-/-}$
Brain	~80%	~50%
Spinal cord	~80%	0%
Liver	~60%	~90%
Adipose	~50%	0%

The discovery of DAGL inhibitors has, however, been hindered by a lack of DAGL crystal structures and a dearth of functional assays to evaluate endogenous DAGL activity. Currently, several classes of DAGL inhibitors have been discovered. Among them are bis-oximino-carbamates (RHC-80267), β-lactones (THL) and fluorophosphonates (MAFP, O-3640, O-3841 and O-5596), which are the first-generation of covalent (ir)reversible DAGL inhibitors.[19,20] Most of these inhibitors are lipid-based molecules that are not selective over other lipases and/or lack *in vivo* activity on DAGL. In 2012, the triazole ureas KT109 and KT172 were reported as the first specific and *in vivo* active DAGLβ inhibitors.[18] Hsu *et al.* discovered that inhibition of DAGLβ reduced 2-arachidonolyglycerol (2-AG), arachidonic acid and eicosanoids levels in peritoneal macrophages of lipopolysaccharide (LPS)-treated mice and significantly decreased pro-inflammatory cytokines.[18] Yet, these inhibitors were not

brain-penetrable and did not inhibit DAGLα, thus, the main aim of this thesis was to develop highly selective and *in vivo* CNS-active DAGL inhibitors to study DAGL function in the brain.

In **Chapter 2** the enantioselective synthesis and structure-activity-relationship (SAR) studies of 2,4-regioisomer of 1,2,3-triazole ureas as a novel chemotype of DAGLα inhibitors is described. It was found that (*R*)-benzylpiperidine substituted triazole ureas constitute the active enantiomer for DAGLα inhibition as measured in biochemical assays and activity-based protein profiling. It was shown that (*R*)-KT109 was the eutomer. The investigations culminated in the discovery of DH376, as a highly potent, cellular active DAGL inhibitor.

In **Chapter 3**, DAGL inhibitors DH376 and DO34 (Figure 1) as well as a structurally related control compound DO53 (see structure in Chapter 3) were further characterized and used, in combination with chemical proteomics and lipidomics, to determine the impact of acute DAGL blockade on brain lipid networks in mice. Within two hours, DAGL inhibition produced a striking reorganization of bioactive lipids, including elevations in DAGs and reductions in endocannabinoids and eicosanoids. It was also found that DAGLα is a short half-life protein, and the inactivation of DAGLs disrupts cannabinoid receptor-dependent synaptic plasticity and impairs neuroinflammatory responses, including lipopolysaccharide-induced anapyrexia. These findings illuminated the highly interconnected and dynamic nature of lipid signaling pathways in the brain and the central role that DAGL enzymes play in regulating this network.

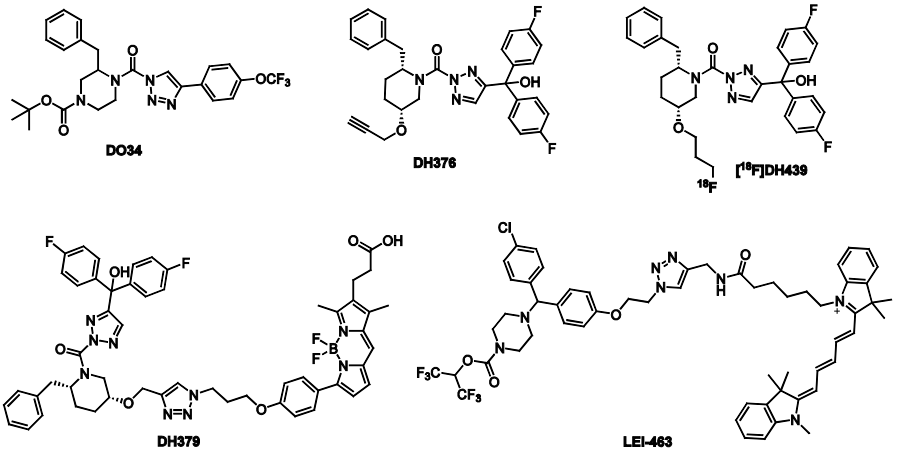

Figure 1. Structures of chemical probes described in the thesis. DO34 and DH376 are *in vivo* CNS-active DAGL inhibitors; [^{18}F]DH439 is a potential PET tracer candidate for DAGL; LEI-463 is a highly selective and potent activity-based imaging probe for MAGL.

In **Chapter 4** the therapeutic efficacy of DAGL inhibitors as a potential anti-obesity treatment was investigated.[17,21] DH376 temporarily reduced fasting-induced refeeding of mice, emulating the effects of cannabinoid CB_1-receptor inverse agonists. As a consequence of reduced food intake, increased fat oxidation and lowered carbohydrate metabolism was observed in DH376-treated mice. Moreover, DH376 did not affect locomotion. These effects were mirrored by DO34, but also by negative control compound DO53, which indicated that the triazole ureas may affect the energy balance in mice through multiple molecular targets. Further selectivity studies were performed to assess the selectivity profile of DH376 in peripheral tissues.

In **Chapter 5**, the design, synthesis and application of [^{18}F]DH439 as a positron emission tracer for DAGL is described. Activity-based protein profiling (ABPP) and radioligand displacement assays demonstrated that DH439 maintained good potency and selectivity against DAGLs, but did show some affinity towards CB_2 receptor. Biodistribution and PET-imaging experiments using [^{18}F]DH439 in mice showed good uptake in peripheral tissues, but low tracer uptake in the brain.

To improve physico-chemical properties of triazole ureas, the structure-activity-relationship of triazole ureas featuring chiral, hydroxylated disubstituted piperidines as dual inhibitors of DAGLα and ABHD6 were investigated in **Chapter 6**. The chirality of the carbon bearing the C2 substituent, as well as the position of the hydroxyl (tolerated at C5, but not at C3) had profound influence on the inhibitory activity of both DAGLα and ABHD6, as established using biochemical assays and competitive activity-based protein profiling on mouse brain extracts (Figure 2). Inhibition of ABHD6 has been reported to produce neuroprotective, anti-obesity and anti-inflammatory effects in preclinical disease models.[22,23] Thus, dual inhibitors of DAGLs and ABHD6 are potential leads for the development of therapeutic agents for metabolic and neurodegenerative disorders.

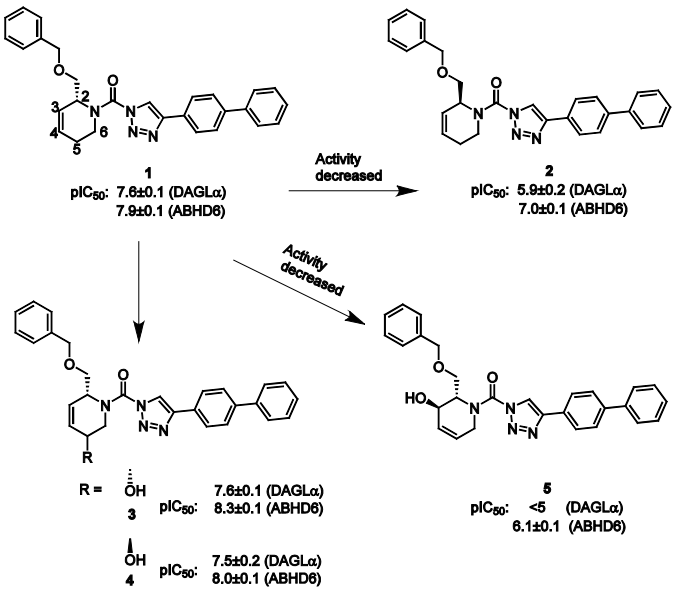

Figure 2. Structure-activity relationships (SAR) of disubstituted piperidinylureas as dual inhibitors of DAGLα and ABHD6.

Monoacylglycerol lipase (MAGL) activity is tightly regulated in both normal and disease conditions. For example, MAGL is highly expressed in aggressive human cancer cells and primary tumors, where it regulates a set of pro-tumorigenic signals.[24] Specific chemical probes that target MAGL are required to monitor the dynamic nature of lipid signaling in living cells or whole organism, but are currently not available. To address this limitation, a potent, selective and cell-permeable activity-based probe LEI-463 (Figure 1) was developed in **Chapter 7**. LEI-463 showed high selectivity over other serine hydrolases, including ABHD6, a common off-target for most MAGL inhibitors and probes. LEI-463 was used to visualize MAGL activity in MCF7 cells by fluorescence confocal microscopy and correlative light electron microscopy. Mitochondria were identified as the principle subcellular compartment where MAGL resides. It is envisioned that LEI463 may serve as a valuable tailored ABP to study MAGL activity and distribution during (patho)physiological processes and may serve as a biomarker for target engagement studies to guide drug development.

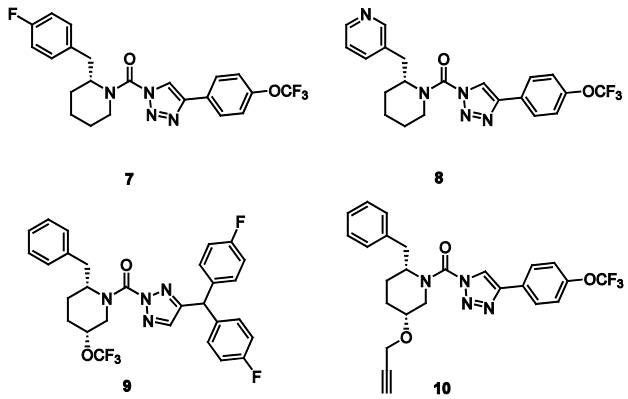

Figure 3. Proposed DAGLs inhibitors for improving pharmacokinetic properties.

Future prospects

In this thesis, a set of chemical probes is described to modulate and visualize 2-AG production via acute inhibition of DAGLs. These chemical probes are not specific for each isoform, therefore the development of inhibitors that can selectively inhibit DAGLα or DAGLβ would be of value to investigate the physiological roles of each isoform.Since high doses (50 mg/kg, i.p.) are required to maintain complete target engagement over a prolonged period of time (> 8 h), improvement of the pharmacokinetic properties of DH376 is desired to lower the effective dose required for *in vivo* studies. There are multiple possibilities to improve the pharmacokinetic properties of the DAGL inhibitors. In general, the lipophilicity of the inhibitors should be further reduced and metabolite identification could be performed to identify metabolic hot spots. Potential metabolic sites may include the propargylether, the benzylic position of the 2-benzylpiperidine and the para-position on the phenyl ring of DH376. It is envisioned that compounds **7-9** and hybrid molecules of DH376 and DO34 (e.g. (**10**)) may represent selective DAGL inhibitors with improved physicochemical properties and improved metabolic stability. DH376 is a substrate of the PgP-transporter (unpublished data), therefore the number of H-bond donors and acceptors should be lowered to reduce its interaction with the transporter protein and to improve its brain penetration. These new compounds may also serve as leads for the development of new PET tracers for in vivo target engagement studies.

In sharp contrast to the 2-AG biosynthetic pathway, the biosynthesis of the other endocannabinoid anandamide is still poorly understood due to the lack of molecular tools to modulate and detect the proteins responsible for anandamide biosynthesis. Anandamide belongs to the class of *N*-acylethanolamines (NAEs), which is an important family of bioactive lipids in the central nervous system.[1,2] A calcium-dependent *N*-acyltransferase (NAT) that generates *N*-acyl

phosphatidylethanolamines (NAPEs) is the rate-limiting step in the biosynthesis of NAEs in the brain.[12,25,26] Recently, the poorly characterized serine hydrolase PLA2G4E was discovered to act as a mouse brain Ca^{2+}-dependent NAT by Ogura *et. al*.[27] They showed that this enzyme generates NAPEs and NAEs in mammalian cells. Thus, PLA2G4E is an interesting target to modulate and study the *in vivo* functions of NAPEs and NAEs, including anandamide. To this end, potent and selective PLA2G4E inhibitors and activity-based probes are required.

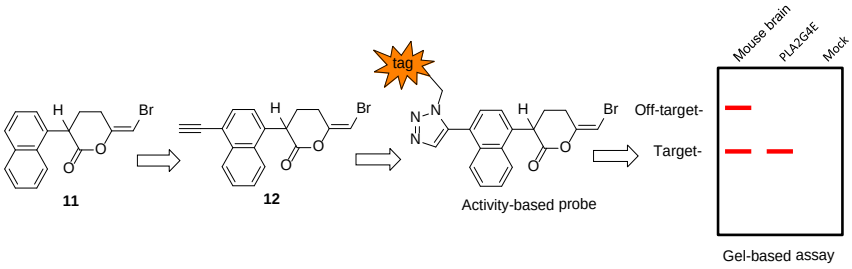

Figure 4. Proposed strategy to design and identify activity-based probe for PLA2G4E.

Previously, (*E*)-6-(bromomethylene)-3-(naphthalen-1-yl)tetrahydro-*2H*-pyran-2-one (**11**) (Figure 4) has been shown to non-selectively covalently inhibit NAT activity with an IC_{50} of 2 µM.[28] Compound **11** may, therefore, represent as an excellent starting point for the development of PLA2G4E inhibitors and activity-based probes. An alkyne or azide can be introduced at various positions of the naphtyl moiety to serve as a ligation handle to introduce fluorophores or a biotin. As an example, probe **12** (Figure 4) was synthesized according to the route depicted in Scheme 1. Subsequent introduction of a fluorescent reporter tag by copper-catalyzed azide-alkyne cycloaddition (CuAAC, or "click") chemistry generated a direct activity-based probe **13** for future target engagement studies of PLA2G4E. To validate the activity of probe **13** against PLA2G4E, gel-based ABPP assay with recombinant PLA2G4E (using Mock as a negative control) or mouse brain proteome should be performed.

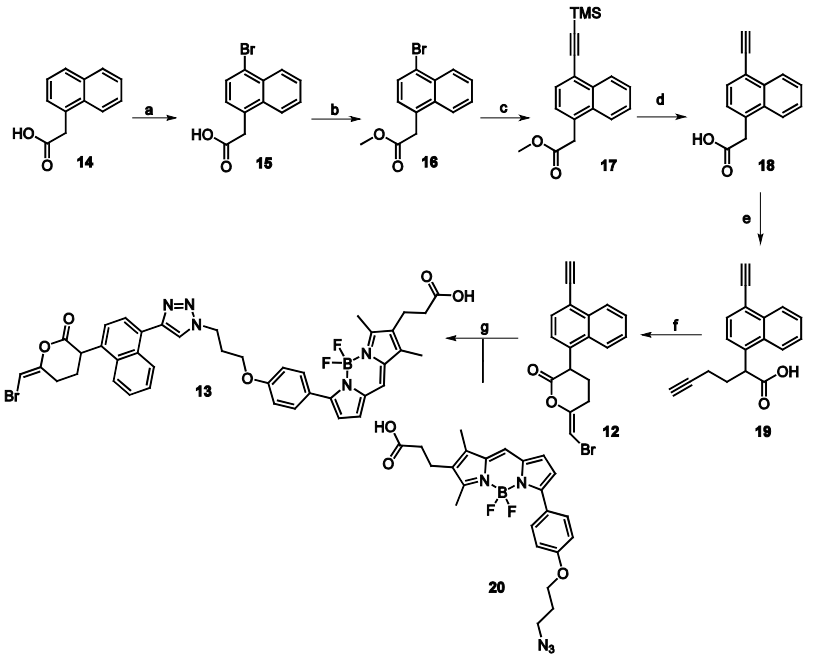

Scheme 1. Synthesis route of proposed activity-based probe for PLA2G4E. Reagents and conditions: (a) Br_2, AcOH, 50-60 ^{o}C, 50%; (b) MeOH, H_2SO_4, 65 ^{o}C, 95%; (c) Ethynyltrimethylsilane, triethylamine, CuI, $PdCl_2(PPh_3)_2$, DMF:1,4-dioxane (1:2.5), reflux, 31%; (d) LiOH, MeOH:H_2O (3:1), r.t., 73%; (e) 4-Bromobut-1-yne, LDA, HMPA, THF, -20 ^{o}C, 62%; (f) NBS, $KHCO_3$, H_2O, DCM, r.t., 8%; (g) $CuSO_4$, sodium ascorbate, DCM/H_2O (1:1), r.t., 38%.

Experimental section

Chemistry

General materials: All of reactions were performed using oven or flame-dried glassware and dry solvents. Reagents were purchased from Sigma Aldrich, Acros and Merck and used without further purification unless noted otherwise. All moisture sensitive reactions were performed under an argon atmosphere. Traces of water were removed from starting compounds by co-evaporation with toluene. ^{1}H-and ^{13}C-NMR spectra were recorded on a Bruker AV 400 MHz spectrometer at 400 (^{1}H) and 101 (^{13}C) MHz, or on a Bruker DMX-600 spectrometer 600 (^{1}H) and 150 (^{13}C) MHz using $CDCl_3$, or CD_3OD solvent, unless stated otherwise. Chemical shift values are reported in ppm with tetramethylsilane or solvent resonance as the internal standard ($CDCl_3$, δ 7.26 for ^{1}H, δ 77.16 for ^{13}C; CD_3OD, δ 3.31 for ^{1}H, δ 49.00 for ^{13}C). Data are reported as follows: chemical shifts (δ), multiplicity (s = singlet, d = doublet, dd = double doublet, td = triple doublet, t = triplet, m = multiplet, br = broad), coupling constants *J*

(Hz), and integration. High-resolution mass spectra (HRMS) were recorded by direct injection (2 µL of a 2 µM solution in water/acetonitrile 50/50 (v/v) and 0.1% formic acid) on a mass spectrometer (Thermo Finnigan LTQ orbitrap) equipped with an electrospray ion source in positive mode (source voltage 3.5 kV, sheath gas flow 10, capillary temperature 250 ^{o}C) with resolution R = 60,000 at m/z 400 (mass range m/z = 150-2,000) and dioctylphthalate (m/z = 391.28428) as a "lock mass". The high resolution mass spectrometer was calibrated prior to measurements with a calibration mixture (Thermo Finnigan). LC-MS analysis was performed on a Finnigan Surveyor HPLC system with a Gemmi C_{18} 50x4.60 mm column (detection at 200-600 nm), coupled to a Finnigan LCQ Adantage Max mass spectrometer with ESI. The applied buffers were H_2O, MeCN and 1.0% TFA in H_2O (0.1% TFA end concentration). Flash chromatography was performed using SiliCycle silica gel type SilicaFlash P60 (230 – 400 mesh). TLC analysis was performed on Merck silica gel 60/Kieselguhr F254, 0.25 mm. Compounds were visualized using either Seebach's reagent (a mixture of phosphomolybdic acid (25 g), cerium (IV) sulfate (7.5 g), H_2O (500 mL) and H_2SO_4 (25 mL)) or a $KMnO_4$ stain (K_2CO_3 (40 g), $KMnO_4$ (6 g), H_2O (600 mL) and 10% NaOH (5 mL)).

2-(4-Bromonaphthalen-1-yl)acetic acid (15). A solution of compound **14** (6.0 g, 32 mmol) in 3mL glacial acetic acid was added bromine (1.63 mL, 31.6 mmol) dropwise with stirring, and then the mixture was heated at 50-60 ^{o}C for 2h. After that the mixture was allowed to stand at 20 ^{o}C for 6h, the resulting precipitate was collected by filtration and washed with aqueous acetic acid to afford the crude product that was recrystallized from chloroform to afford pure product (4.24 g, 15.99 mmol, 50% yield). ^{1}H NMR (400 MHz, $CDCl_3$) δ 8.34 – 8.23 (m, 1H), 7.94 (dd, *J* = 7.3, 1.9 Hz, 1H), 7.74 (d, *J* = 7.6 Hz, 1H), 7.65 – 7.55 (m, 2H), 7.29 – 7.19 (m, 1H), 4.05 (s, 2H). ^{13}C NMR (101 MHz, $CDCl_3$) δ 176.98, 133.28, 132.29, 129.96, 129.68, 128.70, 128.22, 127.50, 127.46, 124.29, 123.25, 38.70.

Methyl 2-(4-bromonaphthalen-1-yl)acetate (16) A solution of compound **15** (4.2 g, 15.8 mmol) in MeOH and sulfuric acid (5.91 mL, 111 mmol) was heated at reflux overnight. The reaction mixture was concentrated and extracted with EtOAc and $NaHCO_3$, washed with water, brine and dried over $MgSO_4$, filter. After concentration under reduced pressure, the residue was purified by silica gel chromatography (pentane/ EtOAc = 1%-10%) to afford title compound (4.2 g, 15 mmol, 95% yield). ^{1}H NMR (400 MHz, $CDCl_3$) δ 8.20 – 8.13 (m, 1H), 7.87 – 7.77 (m, 1H), 7.57 (d, *J* = 7.6 Hz, 1H), 7.48 – 7.39 (m, 2H), 7.04 (d, *J* = 7.6 Hz, 1H), 3.85 (s, 2H), 3.53 (s, 3H). ^{13}C NMR (101 MHz, $CDCl_3$) δ 171.11, 132.96, 131.77, 130.46, 129.28, 128.09, 127.60, 126.94, 126.93, 124.02, 122.41, 51.90, 38.45.

Methyl 2-(4-((trimethylsilyl)ethynyl)naphthalen-1-yl)acetate (17). To a solution of ethynyltrimethylsilane (1.82 mL, 12.9 mmol), compound **16** (1.80 g, 6.45 mmol), $PdCl_2(PPh_3)_2$ (679 mg, 0.97 mmol) and CuI (184 mg, 0.97 mmol) were suspended in the mixture of dry DMF (20 mL), 1,4-dioxane (8.0 mL) and triethylamine (9.0 mL, 64.5 mmol). The mixture was refluxed for 24h, and then diluted with DCM, washed with

brine, water, dried over $MgSO_4$ and filtered. After concentration, the residue was purified by silica gel chromatography (pentane/Et_2O = 1%-10%) to afford title compound (600 mg, 2.02 mmol, 31% yield). ^{1}H NMR (400 MHz, $CDCl_3$) δ 8.51 (d, *J* = 8.0 Hz, 1H), 8.04 (d, *J* = 7.7 Hz, 1H), 7.74 (d, *J* = 7.9 Hz, 1H), 7.71 – 7.56 (m, 2H), 7.37 (d, *J* = 7.3 Hz, 1H), 4.09 (s, 2H), 3.71 (s, 3H), 0.45 (s, 9H). ^{13}C NMR (101 MHz, $CDCl_3$) δ 171.52, 133.64, 131.78, 131.71, 130.40, 127.37, 127.01, 126.88, 126.71, 124.08, 120.78, 103.25, 99.66, 52.10, 39.06, 0.16.

2-(4-Ethynylnaphthalen-1-yl)acetic acid (18). Compound **17** (200 mg, 0.675 mmol) was dissolved in a mixture of MeOH-H_2O (3:1, 4 mL), and LiOH (22.62 mg, 0.945 mmol) was added. After 20h at room temperature, the reaction mixture was concentrated, diluted with water and acidified with concentrated HCl to pH4. The resultant mixture was extracted with ethyl acetate (3 X 20 mL), the combined extracts dried over $MgSO_4$, and the solvent was evaporated to give the crude acid without further purification (104 mg, 0.495 mmol, 73% yield). ^{1}H NMR (400 MHz, $CDCl_3$) δ 9.95 (br, 1H), 8.52 – 8.39 (m, 1H), 8.05 – 7.91 (m, 1H), 7.69 (d, *J* = 7.3 Hz, 1H), 7.64 – 7.49 (m, 2H), 7.36 (d, *J* = 7.3 Hz, 1H), 4.08 (s, 2H), 3.49 (s, 1H). ^{13}C NMR (101 MHz, $CDCl_3$) δ 177.48, 133.89, 131.84, 131.34, 130.91, 127.66, 127.22, 127.08, 127.03, 124.15, 120.27, 82.46, 81.73, 38.99.

2-(4-Ethynylnaphthalen-1-yl)hex-5-ynoic acid (19). A solution of compound **18** (358 mg, 1.7 mmol) in dry THF (3 mL) was added to a solution of LDA (3.4 mL, 6.8 mmol) in THF at -20 ^{o}C. The resulting deep orange solution was stirred at 0 ^{o}C for 2h and the precipitate that formed was dissolved by the addition of HMPA (0.3 mL, 1.7 mmol). To this orange solution, a solution of 4-bromobut-1-yne (0.18 mL, 1.9 mmol) in THF was added dropwise at -20 ^{o}C. The mixture was stirred at 0 ^{o}C for 2h and at 25 ^{o}C for 12h. The reaction was acidified with 3 M HCl, extracted with ether, washed with water, brine and dried with $MgSO_4$, filtered and concentrated under reduced pressure. The residue was purified by silica gel chromatography (pentane/EtOAc = 1:1) and afforded title compound (275 mg, 1.05 mmol, 62% yield). ^{1}H NMR (400 MHz, $CDCl_3$) δ 11.32 (br, 1H), 8.46 – 8.34 (m, 1H), 8.16 – 8.06 (m, 1H), 7.68 (d, *J* = 7.5 Hz, 1H), 7.57 – 7.51 (m, 2H), 7.43 (d, *J* = 7.6 Hz, 1H), 5.10 (t, *J* = 6.7 Hz, 1H), 4.66 – 4.62 (m, 2H), 4.53 (dd, *J* = 8.6, 6.1 Hz, 1H), 3.45 (s, 1H), 2.95 – 2.84 (m, 1H), 2.58 – 2.50 (m, 1H). ^{13}C NMR (101 MHz, $CDCl_3$) δ 179.64, 135.62, 133.98, 131.29, 130.89, 127.16, 126.88, 126.58, 124.41, 123.51, 119.97, 87.41, 82.64, 81.71, 76.30, 46.43, 31.27, 31.14.

(*E*)-6-(bromomethylene)-3-(4-ethynylnaphthalen-1-yl)tetrahydro-2*H*-pyran-2-one (12). To $KHCO_3$ (25 mg, 0.25 mmol) was added compound **19** (65 mg, 0.248 mmol) and DCM (3 mL) with stirring at r.t. After 10 mins, NBS (44 mg, 0.25 mmol) was added followed by addition of H_2O (18 µL, 0.99 mmol). The solution was then washed with 5% NaS_2O_3, water, brine and dried over $MgSO_4$, filtered and concentrated under reduced pressure. The residue was purified by silica gel chromatography (pentane/ EtOAc = 1%-10%) to afford title compound (8 mg, 0.023 mmol, 8% yield). ^{1}H NMR (400 MHz, $CDCl_3$) δ 8.24 – 8.13 (m, 1H), 8.03 – 7.96 (m, 1H), 7.76 – 7.71 (m, 1H), 7.63 – 7.55 (m, 2H), 7.49 (dd, *J* = 7.5, 2.5 Hz, 1H), 7.06 (s, 1H), 5.75 – 5.68 (m, 1H), 2.62 – 2.53 (m,

1H), 2.45 – 2.39 (m, 1H), 2.22 – 2.13 (m, 1H), 2.10 (d, *J* = 2.8 Hz, 1H), 2.07 – 1.96 (m, 1H). ^{13}C NMR (101 MHz, $CDCl_3$) δ 142.10, 134.84, 130.47, 129.67, 126.70, 126.58, 125.79, 123.60, 123.46, 122.45, 119.62, 106.78, 69.80, 69.48, 69.34, 36.76, 15.51.

(*E*)-3-(7-(4-(3-(4-(4-(6-(bromomethylene)-2-oxotetrahydro-2*H*-pyran-3-yl)naphthalen-1-yl)-1*H*-1,2,3-triazol-1-yl)propoxy)phenyl)-5,5-difluoro-1,3-dimethyl-5*H*-4l4,5l4-dipyrrolo[1,2-c:2',1'-f][1,3,2]diazaborinin-2-yl)propanoic acid (13) Compound **12** (6.0 mg, 0.018 mmol) and compound **20** (9.86 mg, 0.021 mmol) were dissolved in degassed DCM/H_2O (2 mL, 1:1, v/v) and aqueous solutions of sodium ascorbate (2.61 mg, 0.013 mmol) and $CuSO_4 \cdot 5H_2O$(2.20 mg, 8.79 µmol) (20%mol) were added. The resulting mixture was stirred vigorously for 2h, after which TLC indicated completed conversion of the reaction. The solvents were evaporated under reduced pressure, and the residue was taken up in DCM and purified by silica column chromatography (DCM/MeOH = 0.5%-5%). The pure final product was obtained (5.4 mg, 6.68 µmol, 38% yield). ^{1}H NMR (600 MHz, $CDCl_3$) δ 8.13 – 7.94 (m, 2H), 7.86 – 7.62 (m, 3H), 7.59 – 7.41 (m, 3H), 7.09 (s, 1H), 7.04 (s, 1H), 6.94 (d, *J* = 4.0 Hz, 1H), 6.89 (d, *J* = 8.1 Hz, 2H), 6.48 (dd, *J* = 6.6, 3.9 Hz, 1H), 5.60 (br, 1H), 4.83 – 4.39 (m, 2H), 4.03 – 3.87 (m, 2H), 2.74 (s, 2H), 2.51 – 2.45 (m, 6H), 2.21 (s, 4H), 1.29 – 1.22 (m, 5H). ^{13}C NMR (151 MHz, $CDCl_3$) δ 159.58, 159.23, 155.44, 140.06, 135.10, 134.65, 134.58, 134.48, 130.91, 130.65, 130.57, 129.98, 129.74, 129.70, 128.13, 126.91, 126.72, 126.54, 126.09, 126.08, 125.82, 123.18, 119.94, 119.90, 118.48, 114.24, 106.89, 106.79, 64.06, 54.00, 32.07, 29.85, 29.81, 29.52, 22.85, 14.29, 13.33, 9.82, 0.15.

References

1. Devane, W. A.; Hanus, L.; Breuer, A.; Pertwee, R. G.; Stevenson, L. A.; Griffin, G.; Gibson, D.; Mandelbaum, A.; Etinger, A.; Mechoulam, R. Isolation and structure of a brain constituent that binds to the cannabinoid receptor. *Science* **1992,** 258, 1946-1949.
2. Di Marzo, V. Endocannabinoid signaling in the brain: biosynthetic mechanisms in the limelight. *Nauture Neuroscience* **2011,** 14, 9-15.
3. Gaoni, Y.; Mechoulam, R. Isolation, structure, and partial synthesis of an active constituent of hashish. *Journal of the American Chemical Society* **1964,** 86, 1646-1647.
4. Di Marzo, V.; Bifulco, M.; De Petrocellis, L. The endocannabinoid system and its therapeutic exploitation. *Nature Reviews. Drug Discovery* **2004,** 3, 771-784.
5. Di Marzo, V.; Stella, N.; Zimmer, A. Endocannabinoid signalling and the deteriorating brain. *Nature Reviews Neuroscience* **2015,** 16, 30-42.
6. Lutz, B.; Marsicano, G.; Maldonado, R.; Hillard, C. J. The endocannabinoid system in guarding against fear, anxiety and stress. *Nature Reviews Neuroscience* **2015,** 16, 705-718.
7. Mendizabal, V. E.; Adler-Graschinsky, E. Cannabinoids as therapeutic agents in cardiovascular disease: a tale of passions and illusions. *British Journal Pharmacology* **2007,** 151, 427-440.
8. Parsons, L. H.; Hurd, Y. L. Endocannabinoid signalling in reward and addiction. *Nature Reviews Neuroscience* **2015,** 16, 579-594.

9. Di Marzo, V.; Matias, I. Endocannabinoid control of food intake and energy balance. *Nature Neuroscience* **2005,** 8, 585-589.
10. Moreira, F. A.; Crippa, J. A. S. The psychiatric side-effects of rimonabant. *Revista Brasileira de Psiquiatria* **2009,** 31, 145-153.
11. Van Gaal, L. F.; Rissanen, A. M.; Scheen, A. J.; Ziegler, O.; Rossner, S.; Group, R. I.-E. S. Effects of the cannabinoid-1 receptor blocker rimonabant on weight reduction and cardiovascular risk factors in overweight patients: 1-year experience from the RIO-Europe study. *Lancet* **2005,** 365, 1389-1397.
12. Di Marzo, V.; Fontana, A.; Cadas, H.; Schinelli, S.; Cimino, G.; Schwartz, J. C.; Piomelli, D. Formation and inactivation of endogenous cannabinoid anandamide in central neurons. *Nature* **1994,** 372, 686-91.
13. Iannotti, F. A.; Di Marzo, V.; Petrosino, S. Endocannabinoids and endocannabinoid-related mediators: Targets, metabolism and role in neurological disorders. *Progress in Lipid Research* **2016,** 62, 107-128.
14. Reisenberg, M.; Singh, P. K.; Williams, G.; Doherty, P. The diacylglycerol lipases: structure, regulation and roles in and beyond endocannabinoid signalling. *Philosophical transactions of the Royal Society of London. Series B, Biological sciences* **2012,** 367, 3264-3275.
15. Tanimura, A.; Yamazaki, M.; Hashimotodani, Y.; Uchigashima, M.; Kawata, S.; Abe, M.; Kita, Y.; Hashimoto, K.; Shimizu, T.; Watanabe, M.; Sakimura, K.; Kano, M. The endocannabinoid 2-arachidonoylglycerol produced by diacylglycerol lipase alpha mediates retrograde suppression of synaptic transmission. *Neuron* **2010,** 65, 320-327.
16. Gao, Y.; Vasilyev, D. V.; Goncalves, M. B.; Howell, F. V.; Hobbs, C.; Reisenberg, M.; Shen, R.; Zhang, M. Y.; Strassle, B. W.; Lu, P.; Mark, L.; Piesla, M. J.; Deng, K.; Kouranova, E. V.; Ring, R. H.; Whiteside, G. T.; Bates, B.; Walsh, F. S.; Williams, G.; Pangalos, M. N.; Samad, T. A.; Doherty, P. Loss of retrograde endocannabinoid signaling and reduced adult neurogenesis in diacylglycerol lipase knock-out mice. *The Journal of Neuroscience : the official Journal of the Society for Neuroscience* **2010,** 30, 2017-2024.
17. Powell, D. R.; Gay, J. P.; Wilganowski, N.; Doree, D.; Savelieva, K. V.; Lanthorn, T. H.; Read, R.; Vogel, P.; Hansen, G. M.; Brommage, R.; Ding, Z. M.; Desai, U.; Zambrowicz, B. Diacylglycerol lipase a knockout mice demonstrate metabolic and behavioral phenotypes similar to those of cannabinoid receptor 1 knockout mice. *Frontiers in Endocrinology* **2015,** 6.
18. Hsu, K. L.; Tsuboi, K.; Adibekian, A.; Pugh, H.; Masuda, K.; Cravatt, B. F. DAGLbeta inhibition perturbs a lipid network involved in macrophage inflammatory responses. *Nature Chemical Biology* **2012,** 8, 999-1007.
19. Kohnz, R. A.; Nomura, D. K. Chemical approaches to therapeutically target the metabolism and signaling of the endocannabinoid 2-AG and eicosanoids. *Chemical Society reviews* **2014,** 43, 6859-6869.
20. Bisogno, T.; Burston, J. J.; Rai, R.; Allara, M.; Saha, B.; Mahadevan, A.; Razdan, R. K.; Wiley, J. L.; Di Marzo, V. Synthesis and pharmacological activity of a potent inhibitor of the biosynthesis of the endocannabinoid 2-arachidonoylglycerol. *ChemMedChem* **2009,** 4, 946-950.
21. Di Marzo, V.; Goparaju, S. K.; Wang, L.; Liu, J.; Batkai, S.; Jarai, Z.; Fezza, F.; Miura, G. I.; Palmiter, R. D.; Sugiura, T.; Kunos, G. Leptin-regulated endocannabinoids are involved in maintaining food intake. *Nature* **2001,** 410, 822-825.

22. Fisette, A.; Tobin, S.; Decarie-Spain, L.; Bouyakdan, K.; Peyot, M. L.; Madiraju, S. R.; Prentki, M.; Fulton, S.; Alquier, T. alpha/beta-Hydrolase domain 6 in the ventromedial hypothalamus controls energy metabolism flexibility. *Cell Reports* **2016,** 17, 1217-1226.
23. Tchantchou, F.; Zhang, Y. M. Selective Inhibition of alpha/beta-Hydrolase domain 6 attenuates neurodegeneration, alleviates blood brain barrier breakdown, and improves functional recovery in a mouse model of traumatic brain injury. *Journal of Neurotrauma* **2013,** 30, 565-579.
24. Nomura, D. K.; Long, J. Z.; Niessen, S.; Hoover, H. S.; Ng, S. W.; Cravatt, B. F. Monoacylglycerol lipase regulates a fatty acid network that promotes cancer pathogenesis. *Cell* **2010,** 140, 49-61.
25. Ahn, K.; McKinney, M. K.; Cravatt, B. F. Enzymatic pathways that regulate endocannabinoid signaling in the nervous system. *Chemical Reviews* **2008,** 108, 1687-1707.
26. Jin, X. H.; Okamoto, Y.; Morishita, J.; Tsuboi, K.; Tonai, T.; Ueda, N. Discovery and characterization of a Ca2+-independent phosphatidylethanolamine N-acyltransferase generating the anandamide precursor and its congeners. *The Journal of Biological Chemistry* **2007,** 282, 3614-3623.
27. Ogura, Y.; Parsons, W. H.; Kamat, S. S.; Cravatt, B. F. A calcium-dependent acyltransferase that produces N-acyl phosphatidylethanolamines. *Nature Chemical Biology* **2016,** 12, 669-671.
28. Cadas, H.; diTomaso, E.; Piomelli, D. Occurrence and biosynthesis of endogenous cannabinoid precursor, N-arachidonoyl phosphatidylethanolamine, in rat brain. *Journal of Neuroscience* **1997,** 17, 1226-1242.

List of publications

1. **Triazole ureas act as diacylglycerol lipase inhibitors and prevent fasting-induced refeeding**
   H. Deng, S. Kooijman, A. M.C.H. van den Nieuwendijk, D. Ogasawara, T. van der Wel, F. van Dalen, M. P. Baggelaar, F. J. Janssen, R. J.B.H.N. van den Berg, H. den Dulk, B. F. Cravatt, H. S. Overkleeft, P. C.N. Rensen, M. van der Stelt, *Journal of Medicinal Chemistry*, **2017**, 60, 428-440.
2. **Rapid and profound rewiring of brain lipid signaling networks by acute diacylglyerol lipase inhibition**
   D. Ogasawara[1], H. Deng[1] (co-first author), A. Viader, M. P. Baggelaar, A. C. Breman, H. den D. ,A. M.C.H. van den Nieuwendijk, M. Soethoudt,T. van der Wel, J.Zhou, H. S. Overkleeft, M. Sanchez-Alavez, S. M., W. Nguyen, B. Conti, X.J. Liu, Y. Chen, Q.S. Liu, B. F. Cravat, M. van der Stelt; *Proceedings of the National Academy of Sciences of the United States of America*, **2016**, 113, 26-33.
3. **Chiral disubstituted piperidinyl ureas: a class of dual diacylglycerol lipase-α and ABHD6 inhibitors**
   H. Deng, T. van der Wel, R. J. B. H. N. van den Berg, A. M.C.H. van den Nieuwendijk, F. J. Janssen, M. P. Baggelaar, H. S. Overkleeft, M. van der Stelt; *manuscript submitted.*
4. **Activity-based protein profiling reveals the mitochondrial localization of monoacylglycerol lipase**
   H. Deng, D. M. van Elsland, A. C. M. van Esbroeck, T. van der Wel, H. den Dulk, H. S. Overkleeft, S. I. van Kasteren, M. van der Stelt; *manuscript in preparation.*
5. **A natural substrate-based fluorescence assay for inhibitor screening on diacylglycerol lipase alpha**
   T. van der Wel, F. J. Janssen, M. P. Baggelaar, H. Deng, H. den Dulk, H. S. Overkleeft, M. van der Stelt; *Journal of Lipid Research* 2015, 56, 927.
6. **Highly selective, reversible inhibitor identified by comparative chemoproteomics modulates diacylglycerol lipase activity in neurons**
   M. P Baggelaar, P. J. P. Chameau, V. Kantae, J. Hummel, K. L. Hsu, F. Janssen, T. van der Wel, M. Soethoudt, H. Deng, H. den Dulk, M. Allara, B. I. Florea, V. Di Marzo, W. J. Wadman., C. G. Kruse, H. S. Overkleeft, T. Hankemeier, T. R. Werkman, B. F. Cravatt, M. van der Stelt, *Journal of the American Chemical Society* **2015**, 137, 8851-8857.
7. **Discovery of glycine sulfonamides as dual inhibitors of sn-1-diacylglycerol lipase alpha and alpha/beta-hydrolase domain 6**
   F. J. Janssen, H. Deng, M. P. Baggelaar, M. Allara, T. van der Wel, H. den Dulk, A. Ligresti, A. C. M. van Esbroeck, R. McGuire, V. Di Marzo, H. S. Overkleeft, M. van der Stelt, *Journal of Medicinal Chemistry.* **2014**, 57, 6610-6622.
8. **Design, synthesis and in vitro antifungal evaluation of 1,3,5-trisubstituted-2-pyrazoline derivatives**
   H. Deng, Z. Y. Yu, G.Y. Shi, M.J. Chen, K. Tao, T. P. Hou, *Chemical Biology & Drug Design* **2012**, 79, 279-289.

9. **Isolation of an antifungal compound from Anaphalis sinica Hance**
   L. Y. Yang, Z. Y. Yu, X. G Zhang, J. Y. Fan, M.J. Chen, H. Deng, T. P. Hou, K. Tao, *Asian Journal of Chemistry*. **2013**, 25 446-468.
10. **Cannabinoid CB_2 receptor ligand profiling reveals biased signalling and off-target activity**
    M. Soethoudt, U. Grether, J. Fingerle, T. W. Grim, F. Fezza, L. de Petrocellis, C. Ullmer, B. Rothenhäusler, C. Perret, N. van Gils, D. Finlay, C. MacDonald, A. Chicca, M. D. Gens, J. Stuart, H. de Vries, N. Mastrangelo, L. Z. Xia, G. Alachouzos, M. P. Baggelaar, A. Martella, E. D. Mock, H. Deng, L. H. Heitman, M. Connor, V. Di Marzo, J. Gertsch, A. H. Lichtman, M. Maccarrone, P. Pacher, M. Glass, M. van der Stelt, *Nature Communications*, **2017**, 8, 13958.
11. **BIA 10-2474 is a non-selective FAAH inhibitor that disrupts lipid metabolism**
    A. C.M. van Esbroeck[1], A. P.A. Janssen[1], A. B. Cognetta[2], D. Ogasawara[2], G. Shpak, M. van der Kroeg, V. Kantae, M. P. Baggelaar, F. M.S. de Vrij, H. Deng, M. Allarà, F. Fezza, Z.M. Lin, T. van der Wel, M. Soethoudt, E. D. Mock, H. den Dulk, I. L. Baak, B. I. Florea, G. Hendriks, L. De Petrocellis, H. S. Overkleeft, T. Hankemeier, B. F. Cravatt, C. I. De Zeeuw, V. Di Marzo, M. Maccarrone, S. A. Kushner, M. van der Stelt; *manuscript submitted.*
12. **Discovery of in vivo active and selective sn-1 daiacylglycerol lipase α inhibitors**
    A.P.A. Janssen, F. J. Janssen, M. P. Baggellar, A. C. M. van Esbroeck, H. den Dulk, H. Deng, E. van Doornmalen, N. Smits, A. Morrison, E. Russell, J. Schulz, L. Brown, J. Hewitt, F. Macleod, J. Robinson, P. P. Geurink, H. Ovaa, B. I. Florea, H. S. Overkleeft, S. P. I. Mcelroy, C. A. A. van Boeckel, H. Rutjes, P. S. Jones, M. van der Stelt; *manuscript in preparation.*

中文总结

化学小分子探针调控内源性大麻素的生物合成

本书主要讨论了如何设计，合成以及发现能够调控内源性大麻素(endocannabinoids)合成的化学小分子探针。基于活性的蛋白质组学分析(activity-based protein profiling, ABPP)作为一种新型的，非常有效的化学生物学手段是成功发现这些化学小分子探针的关键。

第一章简述了内源性大麻素系统的生物学功能。内源性大麻素作为一种脂类信号分子能够激活大麻素受体（CB1 和 CB2），CB1 和 CB2 均属于 G-蛋白偶联受体。内源性大麻素在人类健康和疾病中具有非常重要的作用，其中包括免疫调控，能量平衡，神经传递，食欲等。曾上市的 CB1 受体的拮抗剂 Rimonabant 对于肥胖病患者具有很好的疗效，然而由于其严重的副作用（比如产生抑郁，焦虑，甚至自杀）被迫下市。因此，适度调控内源性大麻素的产生在医药领域仍然是一个亟待解决的问题。目前有两种主要的内源性大麻素，AEA（anandamide）和 2-AG(2-arachidonoylglycerol)。2-AG 和 AEA 体内的表达水平因不同的物种、组织、病理状况等具有一定差异。近年来，虽然已有特异性的抑制剂能够控制 2-AG 和 AEA 的代谢水平， 然而究竟是哪个内源性大麻素负责激活相应的 CB1 或 CB2 受体以调控相应的（病）生理效应仍属于未知。因此，如果能发现特异性的抑制剂来分别调控 2-AG 和 AEA 的生成将非常有助于研究大麻素受体调节的生理学效应。

据报道，内源性大麻素是根据不同的生物学刺激而“按需”生成的。2-AG 的生成主要依靠于二酰基甘油酯酶（DAGLα 和 DAGLβ）。遗传学研究表明，DAGLα 主要负责中枢神经系统中 2-AG 的生成，而 DAGLβ 则主要负责免疫系统中 2-AG 的生成。特异性的 DAGLα 抑制剂被认为是 Rimonabant 的替代品，而特异性的 DAGLβ 抑制剂则被认为具有降低神经炎症的作用。

第二章主要简述了对映选择性合成 1,2,3-三氮唑尿素类化合物，并采用了相应的生物化学测试和活性蛋白质组学的分析方法对 DAGLα 的抑制作用进行了评估。测试结果显示（*R*）-苄基哌啶取代的三氮唑尿素对 DAGLα 的抑制作用优于相应的（*S*）型异构体。通过相关的 SAR 研究最终发现了具有高活性、选择性、以及细胞活性的 DAGL 抑制剂——DH376。

第三章主要利用了三氮唑尿素类 DAGL 的抑制剂 DH376 和 DO34, 以及结构类似的对照化合物 DO53, 化学蛋白质组学和脂质学的分析方法通过体内急性抑制 DAGL 来研究了其对小鼠大脑内活性脂类的影响。结果显示，两个小时的体内抑制 DAGL 诱导了小鼠大脑内活性脂质的迅速重组，其中包括二酰基甘油（DAGs）的升高，内源性大麻素和类花生酸的降低。另外，结果显示 DAGLα 是一个具有较短半寿期（2-4 h）的蛋白。此外，DAGL 的抑制也中断了大麻素受体调节的相关电生理作用，并减弱了相应的神经炎症作用，其中包括脂多糖在小鼠体内诱导的炎症。这些发现表明，

小鼠大脑内这些脂质类信号分子通路具有高度的互联性以及动态性，并表明 DAGL 对这些活性脂类具有重要作用。

第四章主要研究了 DAGL 抑制剂作为一种潜在减肥药的治疗功效。DAGL 抑制剂 DH376 能够暂时降低小鼠空腹后的摄食量，这一效应与大麻素受体 CB1 的拮抗剂 Rimonabant 具有相似性。注射了小分子探针 DH376 的小鼠，其摄食量降低，同时伴随着体内脂质氧化水平的升高和碳水化合物代谢水平的降低。重要的是，DH376 并没有影响到小鼠的正常运动。DO34 作为 DAGL 的抑制剂具有类似的效应，然而 DO53 做为阴性对照化合物（不抑制 DAGL）也产生了相似的效应。这表明，三氮唑尿素类化合物能够通过抑制多个分子靶点来影响小鼠的能量平衡。本章进一步评估了 DAGL 的抑制剂 DH376 在小鼠其他组织（非中枢神经系统）中的特异性。

第五章主要描述了正电子发射断层扫描（PET）的标记物[^{18}F]-DH439 的设计，合成和应用。活性蛋白质组学分析和放射性配体置换的生物测试表明，DH439 对于 DAGL 保留了很好的抑制作用和特异性，但对 CB2 受体具有一定的结合作用。对于[^{18}F]−DH439 静脉注射的小鼠进行相关的生物分布测试和 PET−成像实验，结果显示 ^{18}F 的标记物在非大脑组织中具有很好的吸收，而在大脑里仅发现少量的 ^{18}F 的标记物。

第六章是关于对映选择性合成含有手型双取代基的哌啶三氮唑尿素类化合物作为 DAGLα 和 ABHD6 的双重抑制剂，以及对该类化合物的相关结构优化。通过生物学活性测试发现，哌啶环上 C2 位置取代基的手型类型和哌啶环上羟基的取代位置（C3 取代活性降低，C5 取代活性不变）对 DAGLα 和 ABHD6 的抑制有很重要的作用。据报道，抑制丝氨酸水解酶 ABHD6 具有一定的减肥、抗炎以及神经保护等作用。因此，同时抑制 DAGLs 和 ABHD6 的化合物对治疗代谢以及神经降解类疾病有一定的作用。

第七章介绍了设计，合成以及发现对单酰基甘油酯酶（MAGL）具有特异选择性的荧光小分子探针。MAGL 的活性在生理和病理中具有很重要的作用。据报道，MAGL 高度表达于癌细胞中，可控制一系列的促肿瘤信号的产生。研究 MAGL 在活细胞或体内的脂质信号中所扮演的重要作用，设计合成一种能够特异性结合 MAGL 的化学探针将有重要作用。本章设计合成了对 MAGL 具有高度选择性的化学荧光探针 LEI463。并利用激光共聚焦技术（confocal microscopy）和 correlative light electron microscopy（CLEM）技术发现，MAGL 的活性主要表达在癌细胞（MCF7）的线粒体里。该探针 LEI463 将会成为一种非常有用的生物标记物，可用来研究具有活性的 MAGL 在生理和病理过程中的分布情况，对新药的研发具有很重要的作用。

第八章对本论文的的实验工作进行了归纳和总结，并对未来的研究方向进行了展望。

Curriculum Vitae

Hui Deng was born on September 23th 1987 in Lanzhou, China. After graduating from the affiliated High School of Northwest Normal University in 2005, she started her Bachelor of Science in Sichuan University with a major in chemistry. In 2009, she completed her Bachelor degree with honor and was recommended to the Master in chemistry at Sichuan University. She did a Master research project in the group of prof. dr. Taiping Hou, which focused on the discovery of potent antifungal compounds against several plant pathogenic fungi.

In 2012, she obtained her Master degree and started as a PhD candidate in the Bio-Organic Synthesis group at Leiden Institute of Chemistry (Leiden University, The Netherlands). She was supported by the China Scholarship Council (No. 201206240055). Hui performed her research under the supervision of dr. M. van der Stelt and prof. dr. H.S. Overkleeft. After two years, she continued her research in the newly created department of Molecular Physiology led by dr. Mario van der Stelt. During her research, she developed several chemical tools to modulate endocannabinoid production activity-based protein profiling. She presented her work at several (inter)national conferences, including the International Cannabinoid Research Society (ICRS) symposium (Poland, Bukovina, 2016), where she received the award for best oral presentation, FIGON Dutch Medicine Days (The Netherlands, Ede, 2016), Endocannabinoid Pharmacology Meeting (Switzerland, Bern, 2016), Wageningen International Symposium on Organic Chemistry (The Netherlands, Wageningen, 2016) and CHAINS-Dutch Chemistry conference (The Netherlands, Veldhoven, 2016). Furthermore, she was awarded a poster presentation prize at the COST Chemical Proteomics Meeting (United Kingdom, Oxford, 2015).